



# Fundamental investigation of the drilling of multi-material aerospace stacks to aid adaptive drilling

A thesis submitted to the University of Manchester for the degree of Doctor of Philosophy in the Faculty of Science and Engineering

**Andrea Pardo**

Department of Mechanical, Aerospace and Civil Engineering

2021

# List of contents

List of figures.....	5
List of tables.....	9
List of abbreviations .....	10
Abstract.....	11
Declaration.....	12
Copyright Statement .....	13
Acknowledgements.....	14
Publications.....	15
Conferences.....	15
Chapter 1: Introduction .....	16
1.1    Background .....	16
1.2    Motivation.....	18
1.3    Aim and objectives.....	18
1.4    Outline of the Thesis .....	19
Chapter 2: Literature Review.....	20
2.1    Drilling of aerospace materials .....	20
2.1.1    Aluminium.....	20
2.1.2    Titanium.....	21
2.1.3    Carbon fibre reinforced polymers.....	23
2.1.4    Multi-materials stacks.....	26
2.2    Process monitoring.....	30
2.2.1    Signal acquisition.....	31
2.2.2    Signal processing and feature extraction .....	43
2.2.3    Decision-making.....	48
2.3    Process monitoring applications.....	52

2.3.1	Tool Condition Monitoring (TCM) .....	52
2.3.2	Process monitoring in drilling of aerospace stacks.....	54
2.3.3	Tool position monitoring .....	57
2.3.4	Monitoring of workpiece damage .....	62
2.3.5	Other relevant applications .....	63
2.4	Systems available on the market .....	65
2.5	Conclusions .....	67
Chapter 3: Experimental setup.....		70
3.1	Workpiece material and clamping jig .....	70
3.2	Tools and cutting parameters .....	72
3.3	Machine tools .....	74
3.4	Borehole quality inspection.....	79
3.5	Equipment used for process signals acquisition.....	80
3.6	Validation of the bespoke modification on the portable drilling unit .....	85
Chapter 4: Influence of interlayer gap width on interlayer burr formation .....		93
4.1	Correlation between interlayer gap width and clamping load.....	93
4.2	Interlayer burr formation investigation .....	95
4.3	Summary .....	102
Chapter 5: Influence of tool point angle and interlayer gap width on interface quality .....		104
5.1	Influence of tool point angle on CFRP interface quality .....	104
5.2	Influence of tool point angle on titanium interface quality .....	112
5.3	Influence of interlayer gap size on interface quality .....	115
5.4	Summary .....	117
Chapter 6: Influence of parameter changeover position on interface quality .....		119
6.1	Parameter changeover positions.....	119
6.2	Borehole diameter .....	120
6.3	Interlayer damage factor.....	121

6.4	Interlayer burr formation.....	123
6.5	Summary .....	124
Chapter 7: Process signals characterisation .....		125
7.1	Process signals characterisation at different tool life stages .....	126
7.1.1	Thrust force and torque.....	127
7.1.2	Acoustic emission .....	129
7.1.3	Acceleration .....	132
7.2	Investigating the effect of different machine tools on process signals .....	133
7.3	Summary .....	138
Chapter 8: Investigation on the feed and spindle current signals .....		140
8.1	Impact of the utilisation of industrial parameters on process signals .....	140
8.2	Assessment of feed and spindle current signals .....	145
8.3	Significant feature assessment .....	152
8.4	Summary .....	163
Chapter 9: Decision-making strategy design and assessment.....		164
9.1	Decision-making strategies design.....	164
9.2	Assessment of decision-making algorithms.....	166
9.3	Impact of lower sampling rates on the responsiveness of the decision-making strategies.....	173
9.4	Summary .....	175
Chapter 10: Conclusions and suggestions for future work .....		177
10.1	Conclusions .....	177
10.2	Suggestions for further research.....	179
List of references.....		183

Word count: 50159



## List of figures

Figure 1: Example of an automated drilling unit .....	17
Figure 2: Influence of cutting parameters on interlayer burr formation when drilling aluminium .....	21
Figure 3: Temperature distribution on the tool during drilling of titanium at various tool wear states .....	22
Figure 4: Delamination classification .....	24
Figure 5: Delamination factor definition .....	24
Figure 6: Delamination at borehole exit with and without backing plate .....	28
Figure 7: Process monitoring stages. ....	31
Figure 8: Triaxle force sensor integrated in milling tool holder .....	33
Figure 9: AE sources in machining processes .....	35
Figure 10: Schematic assembly of AE sensor .....	36
Figure 11: Workpiece design to allow for separation of tool features engagement .....	38
Figure 12: Comparison of process signals for new and worn tool .....	42
Figure 13: Signal processing stages .....	43
Figure 14: Signal segmentation .....	45
Figure 15: Examples of stable and dynamic thresholds .....	49
Figure 16: Fuzzy logic membership functions for tool condition monitoring system .....	50
Figure 17: Back propagation learning mechanism in neural networks .....	51
Figure 18: AE signal in drilling of CFRP/Al stacks .....	56
Figure 19: AE RMS and AE band pass filtered, together with the actual time of process incidences, for one drilling cycle .....	59
Figure 20: TC-USB unit and power consumption monitoring example .....	66
Figure 21: Stack clamping jig. ....	72
Figure 22: Takisawa MAC-V3. ....	75
Figure 23: Machining centre auxiliary equipment .....	75
Figure 24: Fives Light-eADU electric drilling unit. ....	76
Figure 25: Fives eADU communication software. ....	77
Figure 26: Seti-tec éVo Light EDU electric drilling unit .....	77
Figure 27: EVO V2.0.14 software interface. ....	78
Figure 28: Bespoke experimental rig for testing with portable drilling units .....	79

Figure 29: Equipment used for borehole quality measurements .....	80
Figure 30: Sensor mounting locations. ....	81
Figure 31: Data acquisition chain. ....	82
Figure 32: Feed and spindle current processed signal from Seti-tec software. ....	83
Figure 33: Modification to éVo Light EDU control board. ....	84
Figure 34: Additional connectors implemented on the control unit to output spindle and feed current signals. ....	84
Figure 35: UoM raw feed and spindle current signals. ....	85
Figure 36: UoM processed feed and spindle current signals. ....	86
Figure 37: UoM feed and spindle currents plotted against Seti-tec outputs. ....	87
Figure 38: Scaled UoM feed and spindle currents compared to Seti-tec signals. ....	87
Figure 39: Feed and spindle currents with average linear scaling. ....	89
Figure 40: UoM feed and spindle current plotted against dynamometer thrust force and torque. ....	91
Figure 41: UoM indirectly measured thrust force and torque compared to dynamometer reference thrust force and torque. ....	91
Figure 42: Thrust and torque current with averaged linear scaling. ....	92
Figure 43: Stack composition. ....	93
Figure 44: Vice with load cells and pressure ring used to clamp the stack with pre-set clamping forces. ....	94
Figure 45: Interlayer gap width of stack with sealant in relation to clamping force. ....	95
Figure 46: Typical borehole edge profiles when drilling stacks with different interlayer gap widths. ....	97
Figure 47: Average maximum surface level with different pre-set interlayer gap widths. ....	97
Figure 48: Accumulation of swarf around the borehole on the bottom surface of the top layer ....	98
Figure 49: Surface damage of the material adjacent to the borehole for both interlayer surfaces. ....	99
Figure 50: Profiles of the interlayer surfaces in close proximity to the borehole. ....	100
Figure 51: Thrust and torque recorded when drilling a stack with different pre-set interlayer gap widths ....	100
Figure 52: Burr height measurements for drilling of top stack layer plus initial engagement with bottom stack layer at different interface conditions. ....	102
Figure 53: Tip geometries of the tools used in the drilling tests. ....	105

Figure 54: CFRP interface damage of the holes drilled using tools with different geometries. ....	107
Figure 55: Titanium chips formed by different tool geometries.....	107
Figure 56: Accumulation of cutting heat at CFRP interface and heat migration from the titanium layer into the CFRP layer. ....	108
Figure 57: Interface damage on the top layer of CFRP/CFRP stack. ....	109
Figure 58: Thrust force and torque generated by the assessed tool geometries.....	112
Figure 59: Thrust force signal frequency domain analysis.....	112
Figure 60: Average entry interlayer burr on the top surface of the bottom titanium layer....	113
Figure 61: Borehole quality measurements of titanium layer for different tool geometries .	114
Figure 62: CFRP interface damage for different interlayer gaps.....	115
Figure 63: Variation in CFRP interlayer surface damage within two boreholes drilled with the same parameters.....	116
Figure 64: Entry interlayer burr height in titanium for different pre-set interlayer gaps.....	117
Figure 65: Changeover positions investigated.....	120
Figure 66: CFRP and aluminium borehole diameters in relation to parameter changeover position.....	121
Figure 67: Interlayer damage factor at CFRP interface in relation to cutting parameter changeover position. ....	122
Figure 68: CFRP interface surface for different changeover positions. ....	123
Figure 69: Interlayer burr height at entry of aluminium layer. ....	123
Figure 70: Investigated process incidences.....	125
Figure 71: Comparison of wear for different tools. ....	126
Figure 72: Tool tip aging after 111 holes.....	126
Figure 73: Recorded thrust force and torque during a drilling cycle. ....	128
Figure 74: Progression of thrust force and torque with tool wear. ....	129
Figure 75: Recorded AE during a drilling cycle.....	130
Figure 76: AE RMS signal during drilling of the CFRP layer with increasing tool wear. ....	131
Figure 77: Progression of the average AE RMS signal during drilling of the CFRP layer with an increase of the number of holes drilled (extended drilling tests). ....	131
Figure 78: Recorded acceleration during a drilling cycle.....	133
Figure 79: Progression of the average acceleration RMS signal during drilling of the CFRP layer with an increase of the number of holes drilled.....	133

Figure 80: Recorded thrust force and torque using portable drilling unit and machining centre.	136
Figure 81: Recorded AE RMS using portable drilling unit and machining centre.	137
Figure 82: Recorded z-acceleration RMS using portable drilling unit and machining centre.	138
Figure 83: Raw and smoothened thrust and torque signal.	141
Figure 84: Acoustic emission RMS signal.	142
Figure 85: Progression of average AE during cutting of the CFRP layer with tool wear. ....	143
Figure 86: Comparison of the percentage variation from the mean value of the AE RMS signal between the drilling tests carried out with the sensor placed on the tool and on the workpiece.	144
Figure 87: X and Z acceleration RMS signals.	145
Figure 88: Progression of average acceleration in X and Z directions during cutting of the CFRP layer with tool wear. ....	145
Figure 89: Feed and spindle current signal, raw and processed. ....	146
Figure 90: Progression of feed and spindle current with tool wear. ....	148
Figure 91: Spectrogram for current signals ....	150
Figure 92: Gearbox schematic with the rotating speed of the different components during cutting of the workpiece.....	151
Figure 93: Feed and spindle current range.....	153
Figure 94: Feed and spindle current range using different time windows.....	154
Figure 95: Feed and spindle current gradient .....	156
Figure 96: Gradient features extracted from the motor current signals. ....	157
Figure 97: Tool engagement SF 1-4 .....	160
Figure 98: Material transition SF 1-4.....	161
Figure 99: Tool disengagement SF 1-4.....	162
Figure 100: Impact of sampling rate on cutting force signals. ....	168
Figure 101: Variation between incidence detection and occurrence (machining centre). ....	171
Figure 102: Thrust magnitude and gradient with decision-making thresholds.....	172
Figure 103: Variation between incidence detection and occurrence (electric drilling unit). .	173
Figure 104: Variation in incidence detection (machining centre tests, signals under-sampled at 100 Hz).....	174
Figure 105: Variation in incidence detection (machining centre tests, signals-under sampled at 10 Hz).....	175

## List of tables

Table 1: Commonly employed time domain features.....	46
Table 2: Al 7010, Ti-6Al-4V and CFRP specifications.....	70
Table 3: Workpiece and tooling details for the experimental work.....	73
Table 4: Seti-tec éVo Light EDU and Fives Light-eADU specifications.....	78
Table 5: Linear coefficients for each borehole and RMSE for both ad hoc and average linear scaling (Seti-tec/UoM).....	88
Table 6: Linear coefficients for each borehole and RMSE for both ad hoc and average linear scaling (Dynamometer/UoM). ....	91
Table 7: Workpiece and tooling details. ....	106
Table 8: Workpiece and tooling details. ....	120
Table 9: Workpiece and tooling details ....	127
Table 10: Tool wear assessment. ....	134
Table 11: List of selected parameters for the decision-making algorithms. ....	169

## List of abbreviations

<i>Abbreviation</i>	<i>Description</i>
ADU	Automated Drilling Unit
AE	Acoustic Emission
CFRP	Carbon Fibre Reinforced Polymer
NN	Neural Network
RMS	Root-mean-square
RMSE	Root-mean-square error
SF	Significant Figure
TCM	Tool Condition Monitoring

# Abstract

Drilling multi-material aerospace stacks is a challenging task due to the different properties of each stack layer material. Carrying out adaptive drilling, i.e. automatically making adjustments to the drilling process in response to information extracted from process signals, would allow for the utilisation of the optimal parameters throughout the drilling cycle, thereby resulting in improved borehole quality and tool life. To aid the development of adaptive drilling, this thesis deals with gaining a fundamental understanding of the drilling of multi-material aerospace stacks in view of, firstly, the effect of different parameters on the cutting process and, secondly, the relationships between process signals and process incidences.

In the first part of the thesis, the impact of the interlayer gap width, tool point angle and parameter changeover on the resulting borehole quality is investigated. Adapting the cutting parameters and cooling strategy based on the material being machined was found to result in a stable cutting process and generate boreholes exhibiting small interface damage. Introducing an interlayer gap to a stack comprising aluminium layers resulted in an increase in interlayer burr formation, as opposed to drilling a stack with no interlayer gap. However, the presence of an interlayer gap can ultimately limit the final burr size, due to the sliding action of the upwards-travelling chips over the borehole edges. When drilling stacks comprising a composite layer above a titanium one, the damage on the composite interlayer surface was caused by the drilling of the metal layer below, as a result of the upwards-travelling metal chips and heat accumulation in the tool and stack interface. The wider the interlayer gap, the easier it becomes for metal chips to penetrate the interface and damage the composite surface.

The second part of the thesis deals with establishing relationships between signals recorded from different sensors and process incidences, using both a machining centre and examples of the latest generation of aerospace portable drilling units. Thrust force and torque, motor current, acoustic emission and acceleration were found to be suitable process signals for the detection of tool engagement, material transition and tool disengagement, with the thrust force being the most responsive signal to the occurrence of these incidences. Based on the gained knowledge, a decision-making strategy was designed. Its performance was tested and compared to the strategies used in the drilling units available on the market. The proposed strategy, based on gradient monitoring, yields substantial improvements in terms of both reliability and responsiveness when compared to the currently used magnitude-based approaches.

## Declaration

No portion of the work referred to in the dissertation has been submitted in support of an application for another degree or qualification of this or any other university or other institute of learning.



## Copyright Statement

- i. The author of this thesis (including any appendices and/or schedules to this thesis) owns certain copyright or related rights in it (the “Copyright”) and s/he has given The University of Manchester certain rights to use such Copyright, including for administrative purposes.
- ii. Copies of this thesis, either in full or in extracts and whether in hard or electronic copy, may be made only in accordance with the Copyright, Designs and Patents Act 1988 (as amended) and regulations issued under it or, where appropriate, in accordance with licensing agreements which the University has from time to time. This page must form part of any such copies made.
- iii. The ownership of certain Copyright, patents, designs, trademarks and other intellectual property (the “Intellectual Property”) and any reproductions of copyright works in the thesis, for example graphs and tables (“Reproductions”), which may be described in this thesis, may not be owned by the author and may be owned by third parties. Such Intellectual Property and Reproductions cannot and must not be made available for use without the prior written permission of the owner(s) of the relevant Intellectual Property and/or Reproductions.
- iv. Further information on the conditions under which disclosure, publication and commercialisation of this thesis, the Copyright and any Intellectual Property and/or Reproductions described in it may take place is available in the University IP Policy (see <http://documents.manchester.ac.uk/DocuInfo.aspx?DocID=24420>), in any relevant Thesis restriction declarations deposited in the University Library, The University Library’s regulations (see <http://www.library.manchester.ac.uk/about/regulations/>) and in The University’s policy on Presentation of Theses.

## Acknowledgements

Taking a moment to reflect on the last 44 months, I am grateful for all the professional and personal support I have received throughout the duration of the project, making all of this possible. While there are too many names to list them all, my sincere gratitude goes out to everyone who contributed time or thought.

Undoubtedly this work could not have been done without the encouragement, support and guidance of my main supervisor Dr. Robert Heinemann. Thank you for all the effort you have invested, your availability and the motivating discussions, which have inspired me to continue investigating and dig even deeper. I would also like to thank my co-supervisor Dr. Kali Babu Katnam, for his direction and valuable advice.

I am thankful to the industrial collaborator, Airbus, who supported this project. Special thanks to Luke Bagshaw, Phil Edwards, Glenn Ford, Amer Liaqat and Robert Whiffen, to name a few key people.

My appreciation goes out to the University workshop for their expertise and assistance in creating the various components required for the research, particularly to: Alexander Williams, Brian Clancy, Dave Jones, Eddie Whitehouse, Robert Brown, Stewart McIntyre and Tom Lawton.

Thanks to my PhD colleagues and friends Becan Lawless, Nuno Nobre, Robert Crawford and Vasco Zeferina, for providing valuable ideas and empathising with the challenges of PhD life. I would also like to thank Alice, whose encouragement and assistance cannot be overestimated.

Lastly I would like to thank my parents, my sister and my brother for their unconditional support throughout the years. Even from far away, you have always been there when I needed.

## Publications

Pardo, A., Cseke, A., Heinemann, R., Whiffen, R., 2019. The effect of interlayer gap width on burr formation in drilling of aluminium-aluminium aerospace stacks. *International Journal of Advanced Manufacturing Technology*. 104, 3035–3043.

Pardo, A., Majeed, M., Heinemann, R., 2020. Process signals characterisation to enable adaptive drilling of aerospace stacks. *Procedia CIRP*. 88, 479–484.

Pardo, A., Le Gall, J., Heinemann, R., Bagshaw, L., 2021. The impact of tool point angle and interlayer gap width on interface borehole quality in drilling CFRP/Titanium stacks. *International Journal of Advanced Manufacturing Technology*. 114, 159-171.

Pardo, A., Heinemann, R., Nobre, N., Bagshaw, L., 2021 Assessment of decision-making algorithms for adaptive drilling of aerospace stacks. *Procedia CIRP*. 99, 392-397.

Pardo, A., Heinemann, R., Chen, C., The effect of cutting parameter changeover position on interface borehole quality in drilling of aerospace CFRP/Al stacks. *Procedia CIRP*. [accepted, in press].

## Conferences

Pardo, A., Majeed, M., Heinemann, R., July 2019. *13th CIRP Conference on Intelligent Computation in Manufacturing Engineering (ICME)*. Presented paper ‘Process signals characterisation to enable adaptive drilling of aerospace stacks’.

Pardo, A., Heinemann, R., Nobre, N., Bagshaw, L., July 2020. *14th CIRP Conference on Intelligent Computation in Manufacturing Engineering (ICME)*. Presented paper ‘Assessment of decision-making algorithms for adaptive drilling of aerospace stacks’.

Pardo, A., Heinemann, R., Chen, C., May 2021. *9th CIRP Conference on High Performance Cutting (HPC)*. Presented paper ‘The effect of cutting parameter changeover position on interface borehole quality in drilling of aerospace CFRP/Al stacks’.

# Chapter 1: Introduction

## 1.1 Background

Drilling is considered to be the standard process for producing boreholes, and it is amongst the most common metal cutting operations (Stephenson and Agapiou, 2016). It is typically one of the last processes performed on a workpiece, meaning that a considerable amount of resources have already been employed for the manufacturing of the component (Sharman et al., 2008). Therefore, it is crucial that drilling operations are carried out with satisfactory reliability to avoid expensive waste resulting from tool failures and workpiece damages. The fact that more than 100 million boreholes are drilled within Airbus production facilities each year (Whiffen, 2018) provides evidence for the importance of drilling as a machining process in the aerospace sector. As a result, considerable effort is put into the improvement and optimisation of drilling operations.

In both commercial and military aircraft manufacturing, multi-material stacked structures comprising carbon fibre reinforced polymers (CFRPs) and metal alloys, most commonly aluminium and titanium, have become increasingly common. By stacking different materials, it is possible to take advantage of the differing and complementary material properties of each layer, resulting in improved combined assembly strength and toughness whilst reducing overall weight. The typical assembly method for such stacked structures is riveting and bolting, which offers a suitable assembly solution for constrained designs. The drilling of stacked structures to provide the necessary boreholes to accommodate any rivet or bolt is referred to as stack drilling. To reduce positional errors, the various stack layers are usually clamped together and drilled in a single shot, which requires the tool having to cut through a series of different layers (Xu et al., 2016). In the case of multi-material stacked structures, this is a challenging task due to the different material properties, and thus machinability, of each of the stack layers (Krishnaraj et al., 2010).

In aerospace assembly processes, a great number of boreholes are drilled with portable automated drilling units (ADUs). An example of such a unit is shown in Figure 1. Traditionally, drilling of stacked structures has been mainly achieved by conventional drilling, i.e. pre-set parameters are used throughout the drilling cycle. When drilling multi-material stacks, the parameters selected are often those appropriate for the layer which is considered more

challenging to machine, or a compromise between the optimal parameters for each of the layers (Bagshaw, 2018). Alternatively, the parameters are switched over between layers based on pre-set timers. Given the variations in thickness of aerospace structures, the use of these timers often leads to a mismatch between the times set and the actual machining time for a stack layer at a particular location. Furthermore, every time a change to the drilling application is made, as for example a change in stack configuration, the system has to be taken out of operation and re-programmed, all of which adds significant costs to the assembly machining process.



**Figure 1: Example of an automated drilling unit (Desoutter Industrial Tools, 2020).**

If, however, a process monitoring system is integrated within the machining equipment, it is possible to recognise the occurrence of relevant process incidences and automatically make adjustments to the drilling process. For example, the cutting parameters could be adjusted as the tool transitions between two stack layers made of different materials, in response to information extracted from sensors integrated into the drilling device. This approach is referred to as adaptive drilling, and it allows for continuous employment of the optimal cutting parameters depending on factors such as workpiece material, tool position and wear, thereby resulting in substantial improvements in terms of borehole quality and tool life. An increase in tool life would result in a reduced number of tool changes, whereas improved borehole quality would make time-consuming post-processing obsolete and consequently reduce the assembly manufacturing time. For this reason, Airbus considers adaptive drilling as a key element for enhancing its manufacturing capabilities and is developing this technology in its new generation of electric portable drilling units (Bagshaw, 2020).

## 1.2 Motivation

The most recent generation of drilling units includes some basic adaptive drilling capability, which in its current form however exhibit three major shortcomings. Firstly, the impact of certain process parameters on the resulting borehole quality is still unclear. The use of adequate cutting parameters is crucial for maximising the effectiveness of adaptive drilling and, consequently, improving borehole quality and reducing manufacturing time. Thus, certain issues related to multi-material stack drilling still need addressing to allow for a fundamental understanding of the stack drilling process and the identification of appropriate adaptive process parameters. Secondly, there is a lack of understanding of the impact of the various stages of a stack drilling cycle on the monitored process signals. This hinders the development of more effective and reliable strategies to enable adaptive drilling, which would allow manufacturers to move beyond the current state-of-the-art where decision-making algorithms that are strongly dependent on the operator's input are used. Thirdly, the understanding of the relationship between tool wear and the monitored process signals is still rather limited, meaning that the typical system is ill suited for coping with changes in the signals due to tool wear but instead is tuned for a tool in a particular wear condition. This restricts the adaptive drilling system's ability to make a reliable decision irrespective of the extent of tool wear, resulting in poor reliability and effectiveness.

Addressing these three fundamental limitations would result in major improvements to the effectiveness and reliability of adaptive drilling and, as a result, the quality of boreholes drilled. Furthermore, it would also allow for a reduction in the overall machining costs and improvement of the work environment, through improved tool utilisation and reduced wastage of cutting fluid.

## 1.3 Aim and objectives

The aim of this project was to make a significant contribution to the reliability and effectiveness of adaptive drilling of aerospace stacks, by providing a fundamental understanding of the impact of process and tool parameters on the cutting process and by establishing relationships between process incidences, process signals and tool wear.

To achieve this aim, the following objectives were addressed:

- Gain a fundamental engineering understanding of the impact of critical process conditions (stack clamping force, interlayer gap width, tool point angle, cutting parameter changeover position) on borehole quality. This not only allows for the determination of appropriate parameters for the aerospace stack drilling process, but also for the identification of appropriate reactions to the occurrence of different process incidences.
- Identify features and feature patterns from signals acquired from the drilling process that are related to key process incidences within a stack drilling cycle.
- Analyse the impact of tool wear on the signal features and patterns identified and establish a means of making an adaptive system robust against the effect of tool wear on signals.
- Design and develop a decision-making strategy capable of identifying process incidences when drilling multi-material stacks via monitoring of process signals. Assess and benchmark the strategy's responsiveness and reliability.

## 1.4 Outline of the Thesis

Following on from this introduction, Chapter 2 is a review of the relevant literature. Chapter 3 describes the setup used for the experimental work, which can broadly be divided in two groups: Chapters 4 to 6 and Chapters 7 to 9. Chapters 4 to 6 focus on gaining a fundamental understanding of the stack drilling process, investigating the effect of different parameters on the resulting borehole quality. Chapters 7 to 9 instead focus on establishing relationships between process signals and the occurrence of certain incidences in the drilling process, as well as on the development and testing of strategies to detect the occurrence of these incidences. The majority of the research work reported on in this thesis, i.e. Chapters 4, 5, 6, 7 and 9, is based on the accepted journal publications that are listed on page 15. In order to ensure that the flow of the thesis was not distorted, some modifications were made to both the text and the figures. Finally, the main conclusions that can be drawn from the project are presented in Chapter 10, together with suggestions for future research.

## Chapter 2: Literature Review

In this chapter, a literature review on topics which were considered to be highly relevant to the project is presented. Publications related to the drilling of aerospace materials commonly used in stacked structures (aluminium, titanium and CFRP) are first analysed. Then, the main stages common to most process monitoring systems are outlined and discussed. Finally, a review on studies carried out on monitoring applications relevant to the PhD project, together with a summary of the systems currently available on the market, is presented.

### 2.1 Drilling of aerospace materials

#### 2.1.1 Aluminium

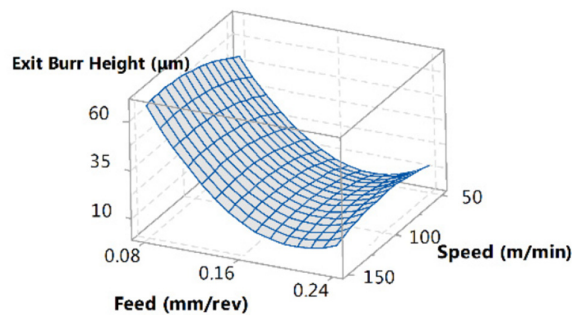
Historically, aluminium alloys have been employed as the main material used for aerospace structures. Today, even though titanium and CFRP have gradually gained popularity, aluminium alloys are still very common due to their relatively high strength-to-weight ratio and corrosion resistance, as well as their relatively low cost resulting from being one of the most easily fabricated high performance materials (Rambabu et al., 2017).

When drilling aluminium alloys, the majority of manufacturing challenges encountered are due to their particularly high softness and ductility, which result in adhesion being the dominant tool wear mechanism (Klocke, 2011). Moreover, the generation of long continuous chips and the formation of burrs are of particular concern during drilling of aerospace stacked assemblies, as they require time-expensive unclamping of the stack layers and deburring to be carried out at the stack interface.

The selection of cutting parameters has been found to significantly influence both chip and burr formation, in different ways depending on the grade of aluminium being machined. For example, according to Sakurai et al. (2000), in the case of A2017 and A6016, drilling with high feed rates is recommended. In contrast, when cutting softer alloys with a smaller percentage of alloying elements, lower feed rates should be employed. High speed drilling is also often found to be beneficial to improve surface finish. This is because adhesion, which through the formation of built-up edges leads to poor surface finish, is mostly dominant at lower cutting speeds (Klocke, 2011). With regards to burr formation during stack drilling, various studies (Abdelhafeez et al., 2015; Hellstern, 2009; Melkote et al., 2010; Tian et al., 2016) agree that an increase in feed rate results in an increase in thrust force, which in turn leads to larger plastic



deformation, thereby increasing the exit interlayer burr height. Moreover, Abdelhafeez et al. (2015) observed that using too low feed rates can also lead to an increase in interlayer burr height, as shown in Figure 2. When feed rate is reduced to values close to the cutting edge radius, ploughing occurs, resulting in increased plastic deformation of the material and, thus, a more pronounced exit interlayer burr formation (Abdelhafeez et al., 2015). According to both Melkote et al. (2010) and Abdelhafeez et al. (2015) cutting speed does not influence significantly burr formation, as shown in Figure 2.



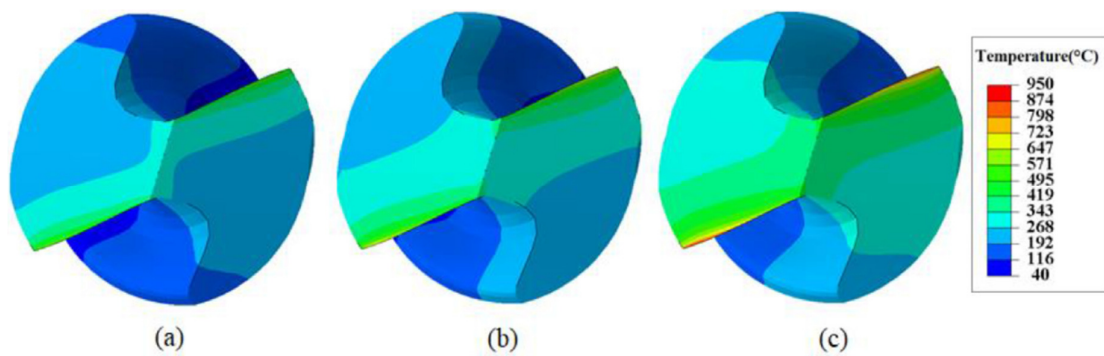
**Figure 2: Influence of cutting parameters on interlayer burr formation when drilling aluminium (Abdelhafeez et al., 2015).**

The effect of lubrication on drilling of aluminium has been assessed by Chatha et al. (2016). The authors carried out experiments using high speed steel tools in combination with dry machining, minimal quantity lubrication and flood cooling. According to their analysis, dry cutting results in particularly high thrust force and torque, which in turn leads to poor surface finish and short tool life when compared to the other lubrication strategies. Minimal quantity lubrication was found to yield lower tool wear rates than flood cooling, while the results obtained in terms of surface roughness were comparable. These findings are in agreement with the observations made by other researchers (Braga et al., 2002; Kao et al., 2017; Kelly and Cotterell, 2002; Nandi and Davim, 2009).

### 2.1.2 Titanium

Titanium is widely used in the aerospace industry due to its mechanical, thermal and chemical properties. Titanium alloys exhibit a higher strength-to-weight ratio than aluminium and steel, as well as being corrosion resistant and unaffected by ductile-to-brittle transitions even at extremely low temperatures (ASM International, 1990). However, they are renowned to be particularly cumbersome to machine, mainly due to their resistance to deformation at elevated temperatures, low thermal conductivity, strong chemical affinity to almost all tool materials and small chip-tool contact area, which results in high cutting pressures (Malchado and

Wallbank, 1990). These, in combination with high cutting temperatures, typically lead to tool wear characterised by edge chipping and flank wear (Qiu et al., 2014; Sharif and Rahim, 2007). The most commonly used titanium alloy is Ti-6Al-4V, part of the ( $\alpha + \beta$ ) alloy group (Klocke, 2011; Lazoglu et al., 2017; Sharif and Rahim, 2007), which is significantly stronger than pure titanium, whilst having the same stiffness, albeit even lower thermal conductivity. For this reason, during machining of Ti-6Al-4V the majority of the heat is conducted into the tool and only a small portion flows into the workpiece (Ezugwu and Wang, 1997). According to the research carried out by both Patne et al. (2017) and Lazoglu et al. (2017), the temperatures recorded during drilling of titanium (using a 6.35 mm and a 12 mm uncoated tungsten carbide (WC/Co) drill) exceed 500°C on the periphery of the cutting edges, where the generated cutting speed is highest. At these temperatures, the chemical affinity of titanium with the tool material drastically reduces the tool life. Moreover, as shown in Figure 3, tool wear results in a further increase in the heat generated, leading to peak temperatures in excess of 800°C (Patne et al., 2017).



**Figure 3: Temperature distribution on the tool during drilling of titanium at various tool wear states; (a) sharp cutting edge, (b) 50 µm cutting edge radius, (c) 100 µm cutting edge radius (Patne et al., 2017).**

Extensive research has been carried out on identifying the optimal machining parameters when drilling titanium alloys, as for example by Matsumura and Tamura (2015), Chatterjee, Mahapatra and Abhishek (2016) and Lukyanov, Onoyko and Najafabadi (2017). These clearly vary depending on workpiece grade and thickness, as well as on tool size and geometry. Nonetheless, it is possible to identify some general trends, one of which is that the cutting speed has a major influence on tool life. According to both Balaji et al. (2018) and Patne et al. (2017), drilling with high speeds leads to the development of particularly high frictional shear stresses, resulting in further heat generation in the machining area. Heat dissipation through the tool enhances tool wear by adhesion and diffusion (Balaji et al., 2018). In addition, burr formation was found to decrease with low cutting speeds (Shetty et al., 2014). Thus, although high speed

drilling was found to improve borehole roundness and surface finish due to workpiece material softening (Shetty et al., 2014; Zhu et al., 2017), low cutting speeds are often preferred due to the resulting significant improvements in tool life and reduction in burr formation. In the drilling cycle, the feed rate determines the duration over which the tool and the workpiece are in contact and consequently produce heat. High feed rates are thus preferred when drilling titanium to minimise the amount of heat generated (Ramulu et al., 2001). In addition, the use of higher feed rates facilitates chip breakage (Xu and El Mansori, 2016) and increases productivity (Ezugwu and Wang, 1997).

Due to high cutting temperatures being the main concern when drilling titanium, cutting fluid is found to greatly increase tool life and reduce thrust force and torque. Li et al. (2007) reported a 10-fold increase in tool life when using coolant applied through the drill in comparison to the results obtained without cutting fluid. Various coolants have been studied, such as water (Mathew and Vijayaraghavan, 2016), oil (Nandgaonkar et al., 2016), liquid nitrogen (Hong and Ding, 2001) and graphene oxide-suspended fluid (Yi et al., 2017). Minimum quantity lubrication in drilling of titanium has also been investigated, and was found to be significantly more effective when supplied through internal cooling channels rather than by an external nozzle (Klocke, 2011; Zeilmann and Weingaertner, 2006). However, due to the relatively limited cooling improvements achieved by minimal quantity lubrication when compared to flood cooling, its rate of adoption in industry has been slow (Kao et al., 2017).

### 2.1.3 Carbon fibre reinforced polymers

During the last few decades, carbon fibre reinforced polymers (CFRPs) have been increasingly implemented in the aerospace industry as structural materials, owing to their particularly high strength-to-weight ratio as well as their resistance to fatigue, creep, wear and corrosion (Caggiano et al., 2019b; Geng et al., 2019). However, as a result of the CFRP's abrasiveness, inhomogeneity and anisotropic properties, drilling of CFRP is rather challenging, as the inherently high tool wear rates lead to high thrust force and torque and are detrimental to the workpiece surface quality (Fleischer et al., 2018; Teti, 2002). The hard and abrasive nature of the reinforcement fibres results in the main tool wear mechanism being abrasive wear (Isbilar and Ghassemieh, 2012; Wang et al., 2014), whilst the fluctuation of the thrust force and torque due to the material inhomogeneity can result in edge chipping (Fernández-Pérez et al., 2017). Additionally, drilling of CFRPs may result in the formation of specific defects which are not

observed during cutting of metallic materials, including delamination, fibre pull-out and matrix thermal degradation.

Layers of fibres detaching from adjacent layers results in a phenomenon known as delamination of the composite (Krishnamoorthy et al., 2015). Delamination is regarded as the most common and critical damage when drilling CFRP (Abrão et al., 2007), and according to Xu et al. (2014) it accounts for 60% of all part rejections. Delamination mechanisms are classified into two types: peel-up delamination and push-down delamination. As shown in Figure 4, peel-up delamination occurs at borehole entry, while push-down delamination occurs at hole exit (Faraz et al., 2009). Delamination is known to negatively affect surface finish and workpiece strength, often compromising the suitability of a component for its intended use (Xu et al., 2016). To quantify the extent of delamination in drilling CFRP, the ‘delamination factor’ ( $F_D$ ) has been defined by Chen (1997) as the ratio between the maximum diameter of the delaminated zone, and the borehole’s nominal diameter, see in Figure 5.

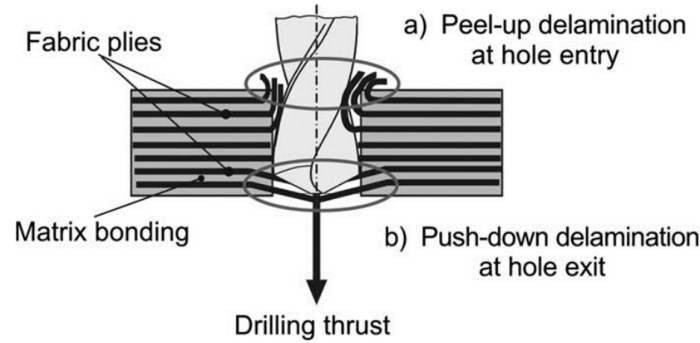


Figure 4: Delamination classification (Faraz et al., 2009).

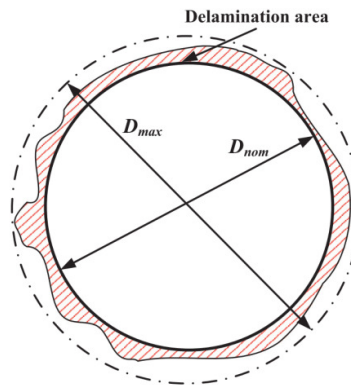


Figure 5: Delamination factor definition (Xu et al., 2014).

Fibre pull-out occurs when bundles of fibres are pulled away from the workpiece by fibre-matrix de-bonding and matrix stripping (Ashrafi et al., 2016). It is considered to be responsible for fatigue cracking of the CFRP layer and subsequent catastrophic failure of the structure (Lang et al., 1987). Another common defect resulting from cutting of CFRP is matrix thermal degradation. The hard and abrasive nature of fibres results in strong friction between the tool and the workpiece. This, in combination with the low thermal conductivity of the matrix, leads to rises in temperatures in the machining area (Sorrentino et al., 2016). If the cutting temperature exceeds the degradation temperature of the resin, thermal damage of the matrix in proximity to the borehole will occur, resulting in critical strength loss of the composite (Sorrentino et al., 2017). This is of particular concern for the composite materials used in the aerospace industry whose matrix is constituted by thermoset resins, such as epoxy, which exhibit a degradation temperature above which the cross-links between the polymer chains are permanently damaged.

When drilling CFRP, the selection of cutting parameters has a major impact on the resulting borehole quality. The feed rate was found to have a strong influence on delamination; various studies (Feito et al., 2018; Karimi et al., 2012; Qiu et al., 2014; Xu et al., 2014) report on increased delamination factors even with small increments in feed rate. This is due to the strong correlation between thrust force, which according to the authors is directly affected by feed rate, and delamination damage. For this reason, the delamination factor rises gradually with tool wear, which is known to result in an increase in thrust force and torque (Chen, 1997). As research indicates that there is no strong correlation between cutting speed and thrust force (Iliescu et al., 2010), the correlation between cutting speed and delamination is also rather weak (Geier and Szalay, 2017). Instead, according to both Shunmugesh and Panneerselvam (2016) and Fernández-Pérez et al. (2017), increasing the cutting speed results in improved surface finish, as well as in a reduction of cutting torque and tool wear rate, which are all desirable effects. However, high cutting speeds also result in a rise in cutting temperatures (Brinksmeier et al., 2011), potentially leading to thermal damage of the matrix. Overall, authors agree that as long as the cutting temperature does not approach the matrix degradation temperature, low feed rates and high cutting speeds are the preferred cutting parameter combination for drilling CFRP (Isbilir and Ghassemieh, 2012; Phadnis et al., 2013; Shunmugesh and Panneerselvam, 2016).

With regards to the use of coolant, there are two main conflicting effects that have to be taken into account when drilling CFRP for aerospace applications. On the one hand, using coolant

decreases cutting temperatures, thereby reducing the chances of temperature-related defects occurring (Weinert and Kempmann, 2004). On the other hand, during machining, minuscule amounts of the cutting fluid can get trapped in small cavities inside the workpiece material. In aerospace components, which are periodically subjected to temperatures well below zero during flight, freeze-thaw of these small amounts of cutting fluid can result in substantial cyclic stressing, which may compromise the fatigue life of the part (Mouritz, 2012). Furthermore, mixing of the coolant with the powder-like CFRP chips results in the formation of sludge which is cumbersome to remove and hinders the assembly operation (Bagshaw, 2017). For this reason, drilling of CFRP is often carried out dry, i.e. without coolant (Feito et al., 2018).

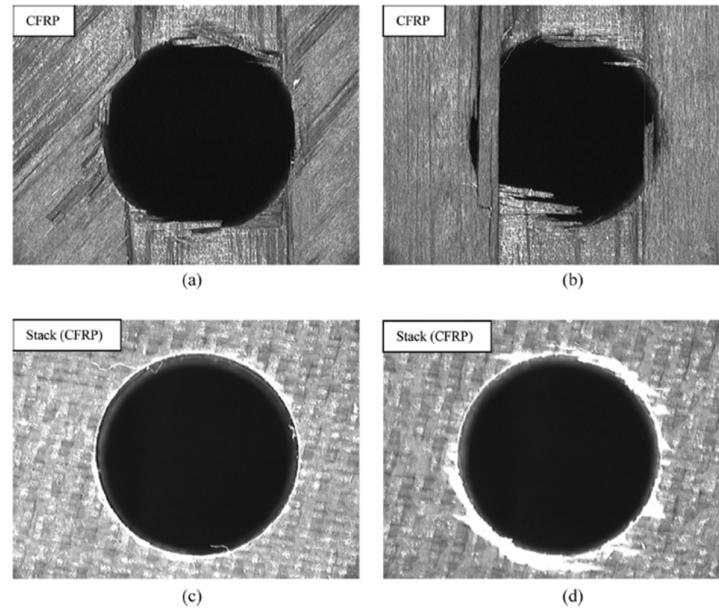
#### 2.1.4 Multi-materials stacks

Stacking of the three aforementioned materials, titanium, aluminium and CFRP, in various combinations, is commonly carried out in aerospace applications as an assembly solution in complex designs to take advantage of their different and complementary material properties. The purpose of this section is to provide an insight into the findings of the most relevant studies investigating the main challenges related to drilling of aerospace stacks.

Drilling stacks comprising metallic layers results in burrs created at the interface between two adjacent layers. These so-called interlayer burrs are of great concern as they require time-expensive unclamping (i.e. separation) of the stack layers and the deburring of the boreholes at the stack interface. Various studies have focused on the reduction of these interlayer burrs through the optimisation of process parameters. Zhu et al. (2018) investigated the impact of tool geometry on burr formation in dry drilling of Aluminium/Titanium stacks. The authors observed that double cone drills produce significantly smaller burrs when compared to drills with multipoint and step geometries. Melkote et al. (2010) and Tian et al. (2016) established relationships between feed rate and burr height and thickness, which can be explained by the strong correlation between feed rate and thrust force observed by Pande and Relekar (1986). Besides the tool geometry, the influence of interlayer gap width on burr formation has also been the subject of extensive research. By using an analytical model and experiments, Jie (2013) found that applying a pre-load clamping force in the proximity of the drilling site when drilling Aluminium/Titanium stacks reduces the interlayer gap width, thereby resulting in smaller interlayer burrs. This observation is in agreement with the findings made by Li et al. (2012) and Yin et al. (2015), who focused on Aluminium/Aluminium stacks. Gao et al. (2015) however pointed out that increasing the pre-load clamping force beyond a certain threshold

does not lead to a further reduction in the interlayer gap. Melkote et al. (2010), who assessed the effect of various clamping methods on interlayer burr formation in drilling of Aluminium/Aluminium stacks, observed an increase in interlayer burr height with an increase in the distance between drilling site and clamping location, which the authors attribute to the corresponding increase in interlayer gap width.

When drilling stacks comprising a combination of composite and metallic layers (e.g. CFRP/Aluminium, CFRP/Titanium), the recommended stacking sequence depends on what workpiece defect is of most concern. If composite deterioration is the main concern, the preferred stacking sequence is to place the CFRP layer on top. This allows the metal layer to act as a backing plate for the CFRP during machining, thus preventing laminate inflection, limiting workpiece dynamics and, ultimately, drastically reducing the occurrence of push-down delamination (Jia et al., 2020; Ramulu et al., 2001; Xu and El Mansori, 2016) and fibre pull-out (Isbilir and Ghassemieh, 2013; Zitoune et al., 2016). The impact of the presence of a metal layer underneath the CFRP is illustrated by the differences in borehole exit shown in Figure 6, clearly indicating a reduction in damage of the CFRP when drilled as part of a stack rather than as an individual layer. However, a major disadvantage of such a stacking sequence is that the hot chips formed when drilling the metal layer need to be disposed of through the upper CFRP layer, which results in a deterioration in the quality of the CFRP borehole. This is particularly the case when drilling CFRP/Titanium stacks (Xu et al., 2020; Zitoune et al., 2016). To alleviate this, Xu et al. (2016) suggest avoiding the use of low cutting speeds and feed rates, which would lead to the formation of continuous chips and, consequently, a more pronounced abrasion of the borehole wall in the CFRP layer. If burr formation tends to be the most problematic phenomenon, having the metal layer on top was found to significantly reduce the generated burr size (Xu and El Mansori, 2016), due to a reduction in the available space for the burr to protrude. However, it is worth noting that in the case of one-way assembly, which typically employs one-shot drilling, the presence of a burr at the exit of a borehole poses less of a problem than a burr at the interface, as the former can be removed without having to separate the stack. This is beneficial as it would avoid having to separate the stack layers after drilling. It is also pertinent to note that placing the CFRP layer underneath the metallic layer results in a stronger heat input in the composite layer as the cutting of the upper metallic alloy result in the preheating of the cutting tool, which is of particular concern when the stack comprises a titanium layer (Xu et al., 2020).



**Figure 6: Delamination at borehole exit with and without backing plate;  
(a) and (c): first hole, (b) and (d): 56th hole (Isbilir and Ghassemieh, 2013).**

Xu and El Mansori (2016) carried out experiments to determine factors affecting the drilling of CFRP/Titanium stacks. They observed that tool features such as chisel edge length, point angle and helix angle play a more dominant role in the resulting borehole quality and tool life than tool substrate and coating. Wang et al. (2014) compared the tool life recorded when drilling CFRP and titanium layers separately to that obtained when drilling stacks comprising both the materials. The authors observed that tool life increases substantially when drilling stacks compared to when drilling single layers of titanium, which they attribute to titanium material adhesions to the tool surface being brushed away by the hard carbon fibres, thereby significantly reducing edge chipping of the tool. When drilling Titanium/CFRP/Aluminium stacks, Kuo et al. (2018) found uncoated carbide drills to exhibit a longer tool life than TiAlN/TiN coated drills, which they attributed to the pronounced rounding of the cutting edges (i.e. duller cutting edges) as a result of the presence of the coating. However, the uncoated drills were found to produce boreholes of less accurate diameter as they started to wear out. According to the authors, this is a result of the more extensive wear at the tool periphery of the uncoated tools. When Li et al. (2019) investigated the impact of low frequency vibration-assisted drilling and chip suction when cutting CFRP/Titanium stacks, they observed a major reduction in cutting temperatures and improvement in chip evacuation, which the authors attributed to the smaller chips being produced and the forced air flow. The authors however also observed an increase in oxidation wear, which they believed to be caused by the enhanced



air flow through the chip flutes. Alonso et al. (2019) assessed the impact of stepped tool geometries when drilling CFRP/Titanium stacks and reported a positive correlation between tool wear and the resulting exit burr height in the titanium layer. This is due to the increasing roundness of the outer cutting edges, which the authors argue affects both the heat generation and shearing of the titanium material, promoting material flow.

The traditional approach when drilling multi-material aerospace stacks is to use a fixed set of parameters (i.e. cutting speed, feed rate and cooling strategy) throughout the drilling cycle. In the case of drilling stacks comprising CFRP and metals, this approach is not ideal due to the significantly different cutting mechanism occurring in the two layers. According to Xu et al. (2016), because of the composite's brittleness and heterogeneity, material removal when cutting CFRP occurs through a series of successive brittle fractures aided by uneven load shearing between the matrix and fibre, which is in contrast to the characteristic plastic flow of metal cutting. For this reason, the chips produced when drilling CFRP are often in the form of dust. The authors also believe that, due to the different cutting mechanisms characterising drilling of CFRP on one side and metals such as aluminium or titanium on the other, the interface between the composite and metal layer is the area most vulnerable to severe damage. At the interface, where the drill transitions from one layer to the next, the tool's cutting edges are simultaneously engaged in both the composite and metal layer, resulting in an unstable cutting process characterised by substantial fluctuations of the thrust force and torque and variable chip separation modes. This can in turn lead to various defects, such as delamination and fibre pull-out, which in some cases can result in cracking during the assembly process. In addition, the drill suffers from increased wear, due to the cutting edges experiencing two different wear patterns whilst progressing from one layer to the next. The authors speculate that increasing the feed velocity should limit interface damage, as it would reduce the duration during which the tool tip is engaged in cutting at the interface. However, they acknowledge that, due to the difficulty in inspecting the complex tool-work interaction, little research has been carried out on the physics governing interface drilling.

Two factors directly affecting interface drilling are the tool's point angle and the interlayer gap width, as these determine the distance over which the drill's cutting edges are simultaneously engaged in both the materials. Heisel and Pfeifroth (2012) assessed carbide tools with point angles ranging from  $155^{\circ}$  to  $185^{\circ}$  when drilling single-layer CFRP, and they observed that larger point angles resulted in more extensive exit delamination. However, Xu and El Mansori (2016) observed that the presence of a metallic layer can affect the resulting composite

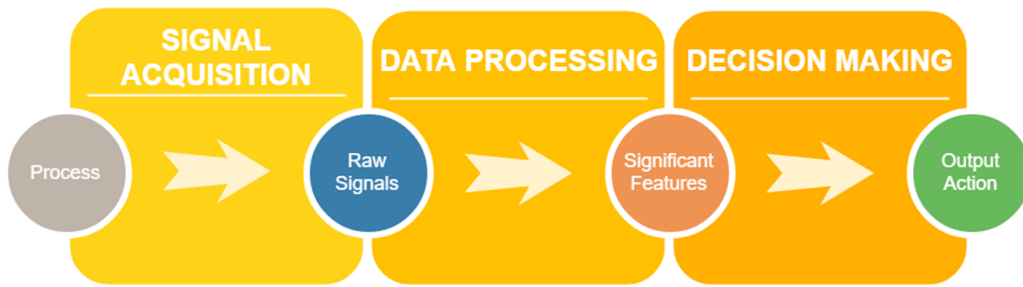
borehole quality, to different extents depending on the stacking order, which suggests that the observations made by Heisel and Pfeifroth (2012) may not be directly applicable to the drilling of CFRP/Titanium stacks. With regards to the interlayer gap width, although its impact on the formation of burrs protruding from metal layers into the stack interface has been researched (Gao et al., 2015; Jie, 2013; Melkote et al., 2010; Tian et al., 2016; Yin et al., 2015), its influence on other important borehole quality indicators, such as edge condition, surface roughness and borehole diameter, is still not understood.

Research indicates that using cutting parameters tailored for individual stack layers appears to be beneficial to borehole quality. Research conducted by Shyha et al. (2010) and Kuo et al. (2014), who studied the influence of cutting speed and feed rate on borehole quality when drilling Titanium/CFRP/Aluminium stacks, revealed that low feed rates lead to longer tool life and better surface finish. Shyha et al. also noticed that high pressure (~70 bar) through-spindle coolant supply improved the cooling of the process due to the improved access of the coolant to the cutting zone as compared to external spray mist, resulting in significantly longer tool life. Fernández-Pérez et al. (2019) assessed the impact of flow rate of minimal quantity lubrication on borehole quality and tool wear when drilling Titanium/CFRP/Aluminium stacks and observed an increase in tool wear rate due to workpiece adhesion when using smaller flow rates. What these three aforementioned studies have in common is that the cutting speed was changed depending on the material the tool was engaged in, whilst the feed rate was kept constant. Unfortunately the authors failed to specify the position (i.e. depth) at which the parameters were changed over. Due to the conical geometry of the drilling tools employed, the change in cutting parameters could have occurred at any point during the interface drilling phase, where the cutting edges are engaged with two different layers simultaneously. As previously discussed, this region is considered to be most vulnerable to severe damage, thus it is reasonable to assume that the position where the change in cutting parameters occurs has a major impact on the resulting quality of the borehole at the stack interface.

## 2.2 Process monitoring

In general, process monitoring systems comprise of three main parts: signal acquisition, data processing and decision-making, see Figure 7. In machining operations, process monitoring systems operate by measuring, through the use of suitable sensors, one or more process characteristics that are influenced by the process state, such as thrust force, torque, temperature, acoustic emission, surface finish and vibration. The signals recorded by the sensors are then

conditioned and processed in order to extract functional significant features (SFs) that are related to certain process conditions, such as tool position and wear, as well as possible defects on the workpiece as a result of the machining process. These significant features are then used by a decision-making system to initiate appropriate countermeasures, for example raising an alarm or executing adaptive actions. The following subchapters allude to the three stages in greater detail.



**Figure 7: Process monitoring stages.**

### 2.2.1 Signal acquisition

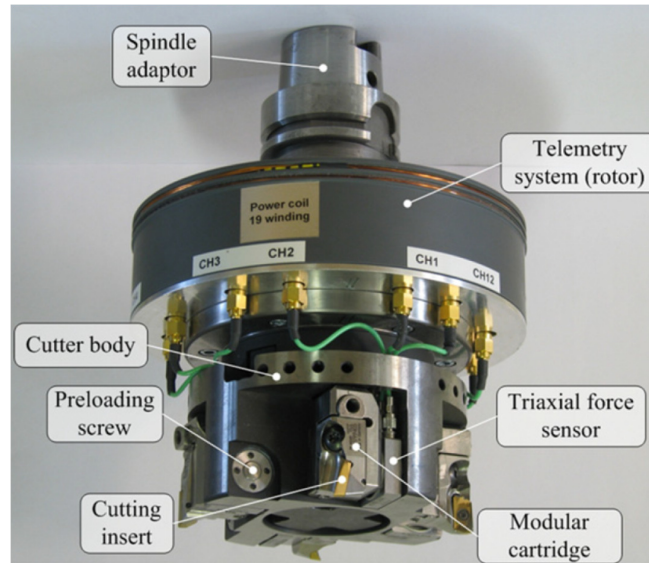
Signal acquisition can be carried out through direct or indirect measuring methods. In direct methods, the variable quantity is directly measured. For example, it is possible to directly measure tool wear by using cameras for visual inspection and radioactive isotopes. The information gathered, e.g. a photo of the cutting tool, can be used to directly quantify the geometric changes arising from tool wear (Teti et al., 2010). Although these methods are usually highly accurate, their application is often limited to off-line laboratory experiments (Siddhpura and Paurobally, 2013). This is because direct measurements, due to their intrusive nature, often interfere with the machining process as well as being usually incompatible with cutting fluids (Ambhore et al., 2015). In the case of indirect methods, an auxiliary quantity is measured in order to deduce the actual variable via empirically determined correlations (Teti et al., 2010). If, for example, it is required to indirectly monitor tool wear, it is possible to measure acoustic emission or vibration and to subsequently find correlations between particular features of the recorded signals and the magnitude of tool wear, thereby estimating the tool wear state. Indirect methods, albeit being less accurate than direct ones, are less intrusive and more suitable for on-line monitoring, because of which they are often preferred in industrial applications (Teti et al., 2010). Sensing techniques applicable for on-line monitoring are reviewed in the following sections.

### *Thrust force and torque*

Cutting operations require a certain amount of force to remove workpiece material. The components of this force are known as thrust force and torque, and their magnitudes are highly sensitive and reactive to variations in the cutting process (Teti et al., 2010). For this reason, the monitoring of thrust force and torque has historically been employed to gain an understanding of the phenomena that take place during machining. More recently, it has also been used for process monitoring applications, such as determining tool wear (Teti et al., 2020) or detecting material transition (Fang et al., 2015). To measure thrust force and torque, piezoelectric sensors are commonly used. Within these sensors, the applied load deforms a piezoelectric crystal lattice, which in turn generates an electrical dipole moment. This charge transfer, with the help of a charge amplifier, can be converted into a voltage that is proportional to the magnitude of the applied load (Klocke, 2011). To measure loads in different directions, e.g. along the x, y and z-axis, piezo electric sensors utilise arrangements of piezo crystals in different orientations (Kistler, 2015). Various studies (Denkena et al., 2016; Jun et al., 2002; Korkut, 2003; Park, 2003) have integrated force and torque sensors into the motor spindle. Even though this arrangement allows the sensor to be contained within the machine, these concepts have rarely been introduced in industrial applications, as they require complex strategies to isolate process signals from noise generated from spindle and machine dynamics. Totis et al. (2010) and Xie et al. (2017) instead developed systems where the cutting force sensors are integrated within the tool holder. The system proposed by Totis et al., shown in Figure 8, comprises four tri-axial force sensors fixed in proximity of each of the four cutting edges of a face mill, thereby allowing individual force measurements for each cutting edge. When compared to the studies that propose cutting force sensors integrated to the spindle, this configuration resulted in sensors being located closer to the signal source, i.e. the machining area, and further away from the noise source, i.e. the machine spindle, thereby significantly increasing the signal-to-noise ratio.

Turrini et al. (2009) patented a method intended for detecting and quantifying drilling anomalies, through the monitoring of thrust force and torque. Anomalies are detected by the proposed method when the thrust force or torque exceeds a set threshold. The authors also claim that by measuring for how long and by how much the threshold is exceeded, their proposed method is also capable of identifying the anomaly type and its severity. From the patent it is not clear what workpiece material the invention would be compatible with, as well as whether the analysis is carried out online or after a hole is drilled. Despite this lack of

information, a downside of the proposed method originates from Jantunen's (2002) verdict, which is that the direct monitoring of thrust force and torque is not believed to be suitable for industrial applications, as it requires the employment of expensive and fragile dynamometers.



**Figure 8: Triaxle force sensor integrated in milling tool holder (Totis et al., 2010).**

### *Motor power*

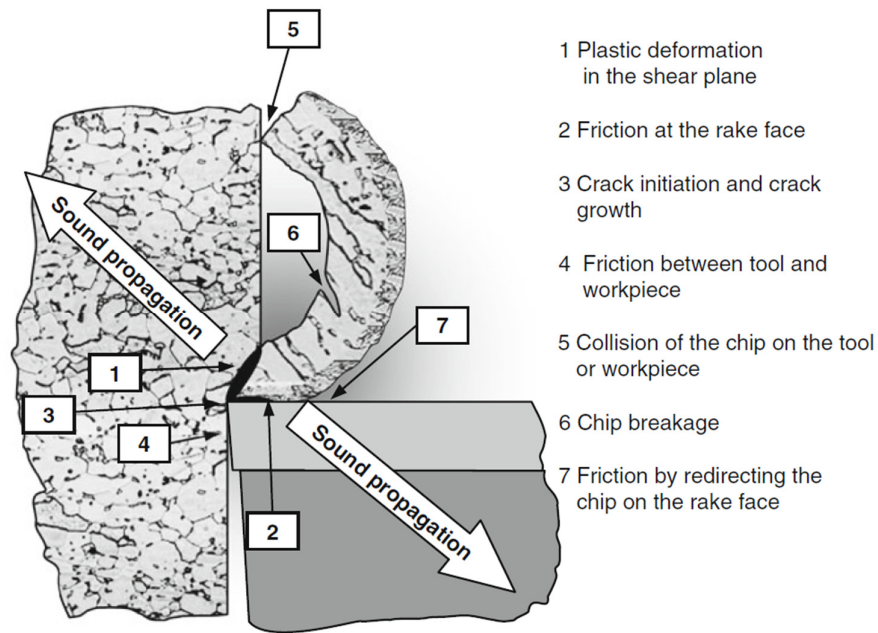
An alternative to directly measuring thrust force and torque using force sensors is the monitoring of the power provided to the various machine tool elements (e.g. feed drives and spindles) that, by providing a cutting motion between the workpiece and cutting tool, achieve material to be removed. In order for a certain cutting force to be provided, power needs to be supplied to the motor. Thus, it is possible to indirectly measure thrust force and torque through the power consumed by the spindle and feed drive elements (Teti et al., 2010). The most common way of determining these signals is by using a so-called Hall effect sensor (or Hall sensor), which is a coil that can measure the current passing through a wire placed inside of it. When an electric current flows through the wire, a magnetic field is created, which in turn produces a proportional current within the Hall sensor coil. Because Hall sensors are incorporated into the electrical cabinet and, thus, do not disturb the machining process, they are suitable for use in production environments (Heinemann and Hinduja, 2012). An alternative to the use of Hall sensors employed in modern machine tools with open control systems is to directly acquire the motor power signals from the numerical controller (Corne et al., 2017).

The total power required to run feed drives and spindles is composed of an idle component, which refers to the power required to keep the drives rotating and translating in air, and an effective component, which refers to the power required to achieve material removal (Klocke, 2011). As only the effective power is representative of the thrust force and torque, the suitability of power sensing as a process monitoring tool is strongly dependant on the ratio between effective and total power. As this ratio diminishes, i.e. the power required for material removal becomes insignificant compared to the total power (e.g. using a small diameter tool on a relatively large spindle), distinguishing variations in the thrust force and torque becomes increasingly difficult (Klocke, 2011). Al-Sulaiman et al. (2005) claim to have circumvented this problem by designing a ‘differential power detector box’, which nullifies the spindle and feed motor idle powers prior to measuring. To achieve this, the device resets the current signal to zero after the spindle has reached its operating speed but before the tool engages in any cutting. Consequently, once the cutting of the workpiece begins, only the effective power is recorded. By using the differential power detector box, Al-Sulaiman et al. claim to be able to detect variations in drilling power of less than one Watt even on a machine tool using a 10 kW main spindle. The authors however fail to allude how the system can cope with fluctuations in the spindle power that are inherent to the spindle unit and its power supply. In addition to these fluctuations in power supply, according to Byrne et al. (1995) and Teti et al. (2010), two further issues are often problematic when trying to correlate motor power to thrust force and torque. Firstly, power consumption is influenced by temperature rises inherent in electrical motors, meaning that an error is introduced when comparing signals obtained at different motor temperatures. Secondly, variations in lubrication and general wear conditions influence significantly the static and dynamic behaviour of both rotary and translation axes and, thus, the power characteristics of the electrical drives involved.

#### *Acoustic emission*

Acoustic emission (AE) consists of transient elastic ultrasonic waves generated by sudden movements within a material under stress (Miller and McIntire, 1987). When a component undergoes deformation it releases AE energy, which travels in the form of high frequency stress waves with frequencies between approximately 16 kHz and 30 MHz, depending on the type and magnitude of the AE source (Klocke, 2011). Extensive studies (Dornfeld and Kannatey-Asibu, 1980; Emel and Kannatey-Asibu, 1989; Frederick and Felbeck, 1972; Liang and Dornfeld, 1989; Moriwaki, 1983; Teti, 1988; Teti and Dornfeld, 1989; Teti and La Commare, 1992; Teti and Micheletti, 1989) have been carried out to identify the various AE sources in

metal cutting processes. Figure 9 shows a diagram of the possible sources of AE during machining.

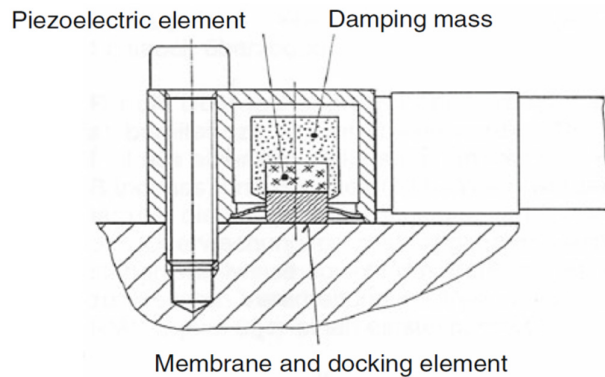


**Figure 9: AE sources in machining processes (Klocke, 2011).**

There are two distinct types of acoustic emission: continuous and burst, the latter also referred to as transient (Gómez et al., 2010). Continuous waves are commonly due to shearing in the primary zone and wear on the tool face and flank, whereas burst signals are associated with discrete events such as tool fracture or chip breakage (Li, 2002). Given that plastic deformation and chip breakage are a primary source of AE, material deformation-based manufacturing processes, such as drilling, have the greatest potential for being monitored using AE as one of the input signals (Lee et al., 2006).

A cross section of a typical AE sensor is shown in Figure 10. The AE wave reaches the piezoelectric element through a thin membrane surrounded by a damping mass. The inertia of the sensor itself is sufficient to produce measurable charge transfers at frequencies typically between 50 kHz and 2 MHz (Klocke, 2011). Mounting an AE sensor requires the use of couplant between the sensor and the measurement surface to remove any air from the interface, as air exhibits an extremely low acoustic impedance (Higo and Inaba, 1991). The influence of different couplants on AE sensor performance was studied by Theobald et al. (2008). According to the authors, the use of couplant was found to be particularly beneficial for AE frequencies above 400 kHz. At these frequencies, when compared to high performance

ultrasonic couplants, such as propylene glycol, the widely used silicone grease was found to reduce the sensor sensitivity by up to 65%. However, it is improbable that an online monitoring system would operate at sampling frequencies above 400 kHz due to the associated requirements in terms of computing resources. Hence, the use of high performance couplant is not deemed necessary for such applications.



**Figure 10: Schematic assembly of AE sensor (Klocke, 2011).**

In their study on initial contact detection in micromachining, Min et al. (2008, 2011) noticed that stainless steel produces much clearer AE signals than aluminium. According to the authors, this is because of the magnitude of the recorded AE signals depends on the material where the elastic waves are generated and propagate. When compared to materials with a lower elastic modulus, stiff materials generate more elastic energy, hence AE, for the same amount of impact (Min et al., 2011, 2008). Based on the authors' observations, AE could be used to identify material transition during drilling of multi-material aerospace stacks, as successfully attempted by certain studies (Neugebauer et al., 2012; Renganathan et al., 2015; Wertheim et al., 2012).

In addition to what has been presented before, related to metallic material, the literature agrees that AE can also be used to characterise damage and fracture of fibre reinforced polymers. Barré and Benzeggagh (1994) correlated the magnitude of the recorded AE signal to damage mechanisms occurring in glass fibre reinforced polymers. In their study, AE amplitudes were identified for matrix cracking (40-55 dB), interface fracture (60-65 dB), fibre pull-out (65-85 dB) and fibre fracture (85-95 dB). The results obtained by the authors highlight how AE is mainly influenced by damage mechanisms related to the fibres, whereas matrix damage represents a secondary AE source. Similar findings were reported by Kim and Lee (1997), who carried out their analysis on CFRP.



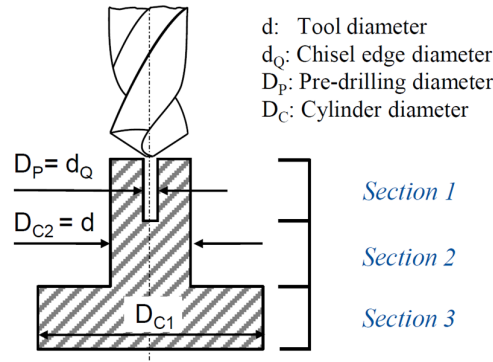
A major advantage of using AE in process monitoring is that elastic waves propagate through the entire workpiece and tool, meaning that the sensor does not need to be placed in close proximity to the machining area, unlike thermocouples or pressure sensors (Elbestawi et al., 2006). Furthermore, according to Inasaki (1998), because of the high frequency and low amplitude nature of AE, the coolant stream can also be used as a medium for transmitting the AE waves. This greatly enhances the ease of implementation in industrial manufacturing processes. In addition, according to both Li (2002) and Elbestawi et al. (2006), AE signals cannot be misinterpreted for vibration generated by drilling, as the frequency range of AE signals is significantly higher than that of machine vibrations and environmental noises and thus, can be easily separated.

As AE contains a multitude of information from various sources, post-processing is vital in order to extract significant data that can be related to various phenomena associated with material removal occurring during machining of the workpiece (Karimi et al., 2015). In view of the high frequency components characterising AE signals, a strong demand is placed on the data acquisition and processing equipment, particularly in the case of online analysis (Patra, 2011). To ease the load on the computing equipment, filters have been used in various process monitoring studies (amongst others Patra, 2011; Neugebauer et al., 2012; Pv et al., 2015; Renganathan et al., 2015) to select the appropriate frequency range to be analysed.

Petueli (2001) assessed the impact of AE sensor positioning in process monitoring of thread forming, finding that the further the sensor is located from the machining point, the greater the signal attenuation. However, according to the author it should also be considered that tool wear can result in substantial increases in AE, potentially leading to oversaturation of the signal. Furthermore, Shuaib (2018) and Teti et al. (2010) agree that if the sensor is fixed on the workpiece or on the vice, the varying distance between the sensor and the machining point influences the signal recording. For this reason, Shuaib recommends fitting the AE sensor at a fixed distance to the source of AE of interest, thereby ensuring constant distance between the sensor and the machining point.

Klocke et al. (2019) assessed how the drill's chisel edge, primary and secondary cutting edges contribute to the generation of AE in drilling of steel (C45). In order to separate the impact of different tool features on the generated AE, the authors pre-machined the workpiece in such a way to limit the contact of different tool features at different times, as shown in Figure 11. In this way, during drilling of the first section of the workpiece, only the main cutting edges were

engaged in cutting. During drilling of the second section, the entirety of the tool tip (i.e. chisel edge and main cutting edges) was engaged. Finally, in the third section the whole tool was in contact with the workpiece, including the secondary cutting edges. According to the results, the chisel edge and the main cutting edges contribute to a similar extent to the generation of AE, while the engagement of the secondary cutting edges only yields a minor increase. Although the experimental work was carried out on medium carbon steel, it is reasonable to speculate that similar results are likely to be observed when drilling metals commonly found in aerospace assemblies (mainly aluminium and titanium). Carrying out a similar experimental assessment on CFRP would be beneficial, as its substantially different material properties could affect the generation of AE during machining.



**Figure 11: Workpiece design to allow for separation of tool features engagement (Klocke et al., 2019).**

### *Vibration*

During machining, the engagement between tool and workpiece contributes to the vibrations generated (Teti et al., 2010). For this reason, extensive research, most recently by Patra et al. (2017), Balaji et al. (2018) and Liu et al. (2018), has been carried out using vibration signals as an indicator for the condition of various cutting processes. For the purpose of process monitoring, it is important to isolate the vibrations arising from the cutting process from those generated by other sources, such as the vibration of other machine components or other machinery transmitted through foundations or unbalance of rotating parts of the machine (Teti et al., 2010).

A broad variety of techniques has been used for sensing vibration. Currently, the most common one is piezoelectric transduction (Byrne et al., 1995; Teti et al., 2010), which uses a seismic mass attached to a piezoelectric transducer. This transducer emits a charge in proportion to the force applied as a result of the acceleration of the seismic mass. Klocke (2011) defines three

different accelerometer types based on whether the charge transfer is generated by normal forces, shear forces or flexural forces. Multiple accelerometers can be stacked together in different orientations in order to record over multiple degrees of freedom, and Klocke believes that tri-axial measuring accelerometers are best suited for process monitoring of cutting operations. With regards to positioning, the magnitude of the signal recorded from an accelerometer is strongly influenced by the distance from the cutting point, as is the case with AE sensors. For this reason, Klocke recommends placing the sensors as close as realistically possible to the machining point. Specifically, placing the sensor on the tool holder rather than the workpiece yields more consistent results, as the distance between the accelerometer and the cutting point is kept constant (Shuaib, 2018). Depending on the application, this may not always be possible, as shown by the various process monitoring studies (Binsaied et al., 2009; Liu et al., 2018 and Patra et al., 2017 amongst others) in which the employed accelerometers had to be fitted on the workpiece or the vice, setups which are not feasible for most industrial applications.

### *Temperature*

The cutting temperature is an important characteristic of most machining processes, as it allows for the evaluation of various cutting conditions, such as thermal stress or wear rate (Rawat and Attia, 2009). Ramirez et al. (2014) and Sorrentino et al. (2016, 2017) derived information about borehole surface quality and induced thermal damage when drilling fibre reinforced polymers using temperature monitoring. Ramirez et al. (2014) and Sorrentino et al. (2016) embedded K-type thermocouples within the workpiece, which requires machining of cavities to fit the sensors, thereby compromising the structural integrity of the component. In contrast, Sorrentino et al. (2017) attached the thermocouples to the tool. Albeit giving very accurate results, the latter setup required the tool to remain stationary and the workpiece to rotate in order to avoid the thermocouple wires getting entangled with the tool. In an industrial environment this would often not be practical due to the workpiece's size. However, the rapid development of wireless technologies may allow temperature monitoring to become increasingly applied for process monitoring purposes, as suggested by the results obtained by Le Coz et al. (2012), who employed a wireless transmitter to transfer the recorded signals from the thermocouples to the data conditioning system.

Beno and Huling (2012) and Sato et al. (2013) used fibre optic pyrometers to measure temperatures. This technique required the pyrometer's optical fibre to be positioned at a

constant distance from the heat source, i.e. the cutting point (Benou and Hulling, 2012), which makes such a setup rather difficult and challenging to implement in a production environment. Angelone et al. (2018) used a thermographic camera to monitor the cutting temperatures when drilling CFRP/CFRP stacks. Similarly, Cuesta et al. (2016) utilised infrared thermography to carry out temperature measurements in drilling of Inconel 718. The main challenge they encountered was the broad range of emissivity values, which were found to be strongly influenced by both cutting and cooling conditions. In addition, the infrared thermography equipment is particularly expensive when compared to most of the other monitoring techniques reviewed here. It is also worth mentioning that it is incompatible with cutting fluids, which are used in many of today's manufacturing processes, a disadvantage it shares with most of the aforementioned techniques, apart from thermocouples.

#### *Other sensor types*

In addition to those sensors mentioned in previous sections, various other sensing techniques have been used for process monitoring. Eneyew and Ramulu (2014b) used an air-coupled audio microphone positioned on the workpiece-mounting fixture to monitor tool wear during drilling of composite materials. The authors noticed that the magnitude of the acoustic signal decreased with an increase in tool wear. It is worth noting that as sound waves travel from the source (i.e. the cutting point) to the sensor (i.e. microphone) a portion of their energy is converted into heat, because of various phenomena, such as heat conduction, shear viscosity and molecular relaxation (Crocker, 2007). Thus, the recorded signal amplitude decreases with an increase in the distance between sensor and cutting point. Eneyew and Ramulu (2014b) do not specify whether one or more holes were drilled on each of the CFRP coupons, i.e. whether this distance was kept constant or not. If more than one hole was drilled, it is possible that the experienced decrease in signal amplitude could, to some extent, be attributed to an increase in the distance between sensor and machining point. Similarly to AE sensors and accelerometers, placing the sensor on the tool holder, thereby fixing this distance, could result in more consistent measurements.

To monitor the re-contouring process of aircraft engine components, Denkena and Flöter (2012) used electromagnetic force measurements to develop a closed-loop control system capable of adjusting process parameters in order to ensure that the actual (i.e. measured) thrust force and torque match the pre-defined ones. Their experiments were carried out on a milling machine whose Z-axis, carrying the spindle, is guided by the principle of magnetic levitation.

By measuring the air gaps between the spindle's electromagnetic rails, a proportional-integral state-space controller calculated corrective forces to be actuated at each magnet. The main drawback of the proposed system is that variations in thrust force and torque would lead to deviations in the original tool path. As suggested by the authors, this can be compensated by developing an adaptive NC program capable of adjusting the path each time a change in thrust force and torque is applied by the controller. Although the initial results obtained by Denkena and Flöter appear to be promising, the use of such a technology is restricted to machine tools containing a magnetically levitated spindle.

Optical measurements have also been used for process monitoring. Martins de Carvalho (no date) developed a procedure for the standardisation of tool images for neural network processing of image data aimed at tool wear characterisation. In their study, after each minute of cutting, the machining was interrupted and two monochromatic images were taken with a video camera: one focusing on the rake face and one focusing on the flank face to capture the extent of crater wear and flank wear, respectively. The pictures were then digitalized by recording a numerical value per pixel, i.e. forming 2D matrixes, and processed in Matlab to carry out matrix transformation and picture standardisation. The author claims that standardised tool wear images can be used as inputs in an intelligent monitoring system aiming for automatic tool wear recognition on an online inter-process basis. Similarly, Caggiano et al. (2017) used digital image analysis to evaluate the most representative parameters describing the quality of holes drilled into CFRP. However, according to Teti et al. (2010), object illumination notably impacts the reliability of vision systems used for process monitoring, which suggests that there is a risk that these techniques become ineffective when the amount of light the monitored object receives is subject to changes, which is often the case in an industrial (i.e. factory) environment.

### *Sensor fusion*

Sensor fusion is defined as “an integrated sensing strategy designed to improve the performance and reliability of manufacturing process monitoring by utilizing various sensor outputs” (Emel and Kannatey-Asibu, 1989). Matsushima and Sata (1980) were amongst the first to use sensor fusion to monitor tool wear. In their study, features extracted from different signals (thrust force, torque and machine power) were combined to detect tool breakage. Similar studies were later carried out by Emel and Kannatey-Asibu (1989) and Dornfeld and DeVries (1990), who combined cutting force and AE signals in their monitoring systems. More

recently, by combining information received from a dynamometer, Hall sensor, accelerometer, AE sensor and audio microphone, Ghosh et al. (2007) developed an online monitoring system capable of estimating the average flank wear of the main cutting edge in face milling. Arul et. (2007) analysed thrust force, torque and AE to predict borehole quality in drilling of polymeric composites, while Segreto et al. (2013) developed a sensor fusion system capable of extracting information from AE signals as well as three-dimensional vibration and force readings to monitor tool wear during turning of nickel alloys.

Möhring et al. (2018) aimed at developing an intelligent process control system for milling of CFRP, which highlights the interest of the research community in the realisation of adaptive machining through the monitoring of process signals. Their system monitored thrust force, torque, acceleration, AE, airborne sound and spindle power during milling of CFRP, with the acceleration and AE measured by a 3-axis accelerometer and high-frequency-impulse-measurement sensor, respectively. These were fixed on a dynamometer, which instead measured the thrust force and torque. A condenser microphone was used for measuring the airborne sound, while current clamps were employed to monitor the spindle power. The process signals recorded when machining with both a new and worn tool, see Figure 12, show that AE exhibited the strongest correlation to tool wear amongst all the assessed signals, whereas the thrust force was the least affected process signal. Notably, a reduction in AE was noticed with an increase in wear, particularly at higher frequencies. The authors also observed a strong correlation between tool wear and delamination depth during the initial tool life stage, which they suggest could be a result of the change in wear mechanisms after the tool run-in period.

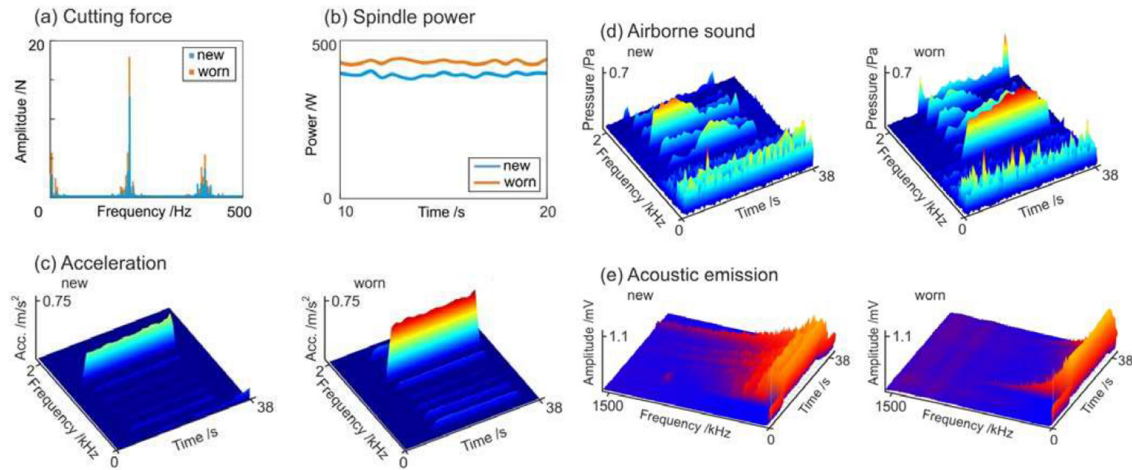


Figure 12: Comparison of process signals for new and worn tool (Möhring et al., 2018).

### 2.2.2 Signal processing and feature extraction

To develop a functioning monitoring system, a suitable measurement range and resolution should be selected. Using an inappropriate measurement range can lead to signal saturation and consequent loss of information (Lauro et al., 2014). The measurement resolution is determined by the sampling rate, which is a crucial parameter of process monitoring systems. If the sampling rate is too low, aliasing may occur, resulting in sets of measured samples appearing to have different frequency contents from the real signal (Quinn, 2016). Using an excessively high sampling rate on the other hand would result in a substantial increase of the computing resources necessary to acquire and process the signal, thereby increasing the time required by the system to analyse the data. To define an appropriate sampling rate, various researchers (e.g. Binsaeid et al., 2009; Caggiano et al., 2017) have used the Nyquist-Shannon theorem, which asserts that the sampling rate should be at least twice the highest frequency component of the signal of interest (Nyquist, 1928; Shannon, 1949), whereas National Instruments recommends sampling at a frequency of at least 10 times the highest frequency component of interest (National Instruments, 2016). Regardless, the sampling rate is generally adjusted empirically in order to achieve the required trade-off between accuracy and computing requirements.

After a signal is recorded by an appropriate sensor, signal processing is required to extract meaningful information. The different stages of signal processing are shown in Figure 13. Firstly, the raw signal is pre-processed (e.g. filtered, amplified, converted in digital form etc.) in order to suppress noise and adjust for continuous biases. Secondly, significant features are extracted from the conditioned signal. This can either be performed in time domain, frequency domain, or time-frequency domain. From the extracted SFs, only those that relate to the process event to be monitored (e.g. tool engagement, material transition, tool wear etc.) should be selected and fed to the relevant decision-making method (Teti et al., 2010).

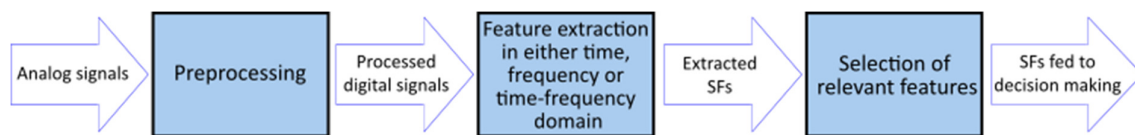


Figure 13: Signal processing stages (based on Teti et al., 2010).

With regards to pre-processing, according to Klocke (2011) the energy component of a signal generated from a sensor is often relatively low when compared to environmental noise. For this reason, the signal is often pre-amplified in order to improve the signal-to-noise ratio.

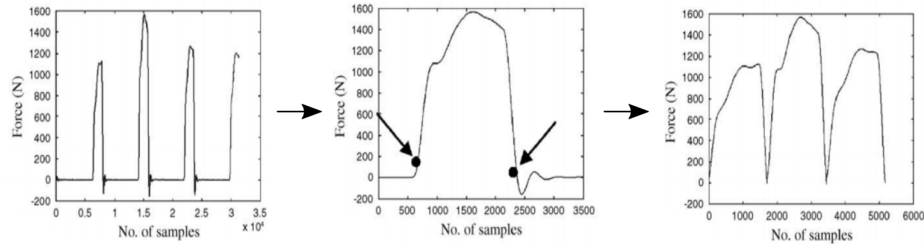
Subsequently, the signal is usually filtered to exclude any data having frequency components lying outside the range of interest. In the filtering stage, it is important to remove those components of the signal that are not related to the monitored process parameters. Filtered-out components could arise from environmental disturbances, such as vibrations of nearby machines and electromagnetic fields, or they could be data recorded from the process that is not relevant to the specific application. Optionally, the signal can be demodulated in root-mean-square (RMS) values, using the equation below:

$$s_{RMS} = \sqrt{\frac{1}{T} \int_0^T s^2(t) dt} \quad (1) \text{ (Holman, 2011)}$$

Where  $s$  is the recorded signal and  $T$  is the time constant of the RMS converter. This should be carefully defined, also considering the subsequent extraction method of the significant features (Teti et al., 2010). Data in RMS form can be processed at much lower frequencies than the raw signal, which results in a drastic decrease in the computing resources required for data processing. For this reason, RMS demodulation is particularly common when processing signals recorded at high sampling rates, such as AE (Liang and Dornfeld, 1989; Patra, 2011; Pv et al., 2015) or vibration (Patra et al., 2017). Depending on the application, further amplifying or filtering may be required before the analogue signal is digitalised by an analogue-to-digital converter. For example, to improve the signal processing accuracy, Teti et al. (2010) recommend amplifying the signal just before digitalisation such that the signal voltage range corresponds to the maximum input range of the analogue-to-digital converter.

Once the data is transformed into digital form, digital filtering can be performed to further improve a signal's correlation to the process variable to be measured. For example, Abellan-Nebot and Romero Subirón (2010) suggest filtering cutting force signals after digitalisation to assess them only at the tooth-engagement frequency, which according to Haber et al. (2004) is the best index for tool wear monitoring. Optionally, the signal can be segmented, which means that it is analysed only during certain periods of time, as for example when the tool is removing material at a steady state, whereas periods of unsteady cutting or cutting in fresh air are discarded. An example of signal segmentation performed for every tooth-engagement period is shown in Figure 14.





**Figure 14: Signal segmentation (based on Ghosh et al., 2007).**

After pre-processing, SFs are extracted from the signal(s) using either time domain, frequency domain or time-frequency domain analysis. According to Ambhore et al. (2015) “time domain analysis refers to a display of response parameter as a function of time”. While the time domain analysis assesses how a signal changes with time, the frequency domain analysis, also known as spectral analysis, shows how a signal is distributed over a range of frequencies (Ambhore et al., 2015). Some of the most commonly extracted features from time domain signals are presented in Table 1. It is also common to calculate various ratios of the presented signal features (Ghosh et al., 2007). Carrying out process monitoring using only one SF can lead to unreliable results, because of which the selection of a sufficient number of SFs is crucial. Furthermore, it should be ensured that the established relationships between process incidence and the selected SFs do not deteriorate or weaken with tool wear (Teti et al., 2010).

One of the main advantages of feature extraction in the time domain is that it does not require frequency domain transformation, which is particularly time-consuming from a computing point of view (Klocke, 2011). Yet, a common drawback of SFs extracted in the time domain is the fact that they do not provide information on periodicities (Li, 2006). More advanced approaches of time domain analysis apply time series modelling to the recorded waveform data. The most commonly used ones in process monitoring are: auto regressive, moving average and auto regressive moving average. Even though models of up to the 100<sup>th</sup> order have been tested (Suprock et al., 2007), frequently only the first or first and second order coefficients are used as features (Altintas and Aslan, 2017; Griffin et al., 2016; Scheffer and Heyns, 2001). This is because higher-order models require increasingly greater computing resources, thereby becoming inadequate for online monitoring purposes, where the system’s response time is crucial. Various other parameters and methods for time domain analysis have been reported on in the literature, such as principal component analysis (Karimi et al., 2012; Shi and Gindy, 2007), singular spectrum analysis (Salgado and Alonso, 2006) and permutation entropy (Li et al., 2008).

**Table 1: Commonly employed time domain features.**

Feature	Mathematical expression	Used by
Magnitude ( $ x $ )	$ x  = \begin{cases} x & \text{if } x \geq 0 \\ -x & \text{if } x < 0 \end{cases}$	(Aliustaoglu et al., 2009; Dong et al., 2006; Ghosh et al., 2007; Gierlak et al., 2017; Heinemann et al., 2007; Heinemann and Hinduja, 2012; Pezzullo, n.d.; Portillo et al., 2012)
Gradient ( $\dot{x}$ )	$\dot{x} \approx \frac{x_0 - x_{-1}}{h}$	(Bakker et al., 2015b; Lee and Lee, 1999; Neugebauer et al., 2012; Shuaib, 2018; Wertheim et al., 2012)
Range	$\text{Range} = \max_i x_i - \min_i x_i$	(Binsaeid et al., 2009; Ghosh et al., 2007)
Root-mean-square (RMS)	$\text{RMS} = \sqrt{\frac{1}{N} \sum_{i=1}^N (x_i)^2}$	(Aliustaoglu et al., 2009; Binsaeid et al., 2009; Ghosh et al., 2007; Gierlak et al., 2017; Heinemann et al., 2007; Heinemann and Hinduja, 2012; Patra, 2011; Pv et al., 2015; Renganathan et al., 2015; Salgado and Alonso, 2006)
Crest Factor (CF)	$\text{CF} = \frac{\text{Range}}{\text{RMS}}$	(Binsaeid et al., 2009; Scheffer and Heyns, 2001; Sun et al., 2004)
Arithmetic mean ( $\bar{x}$ )	$\bar{x} = \frac{1}{N} \sum_{i=1}^N x_i$	(Aliustaoglu et al., 2009; Bhattacharyya et al., 2007; Binsaeid et al., 2009; Caggiano et al., 2017; Dong et al., 2006; Ghosh et al., 2007; Gierlak et al., 2017; Heinemann and Hinduja, 2012; Kim and Ahn, 2002; Salgado and Alonso, 2006; Scheffer and Heyns, 2004, 2001; Sun et al., 2004; Zhu et al., 2009)
Variance ( $\sigma^2$ )	$\sigma^2 = \frac{1}{N-1} \sum_{i=1}^N (x_i - \bar{x})^2$	(Aliustaoglu et al., 2009; Binsaeid et al., 2009; Dong et al., 2006; Gierlak et al., 2017; Heinemann and Hinduja, 2012; Kim and Ahn, 2002; Salgado and Alonso, 2006; Scheffer and Heyns, 2004, 2001; Zhu et al., 2009)
Skewness (Sk)	$\text{Sk} = \frac{1}{N} \frac{\sum_{i=1}^N (x_i - \bar{x})^3}{\sigma^3}$	(Binsaeid et al., 2009; Dong et al., 2006; Gierlak et al., 2017; Salgado and Alonso, 2006; Scheffer and Heyns, 2001; Shuaib, 2018; Zhu et al., 2009)
Kurtosis (Ku)	$\text{Ku} = \frac{1}{N} \frac{\sum_{i=1}^N (x_i - \bar{x})^4}{\sigma^4}$	(Binsaeid et al., 2009; Gierlak et al., 2017; Scheffer and Heyns, 2001; Shuaib, 2018; Zhu et al., 2009)

When the time domain signal is processed through the application of the Fourier transform, the data is transformed into the frequency domain and can be displayed as a function of frequency. The most common algorithm for frequency domain transformation is the Fast Fourier Transform (FFT). When compared to time domain analysis, frequency domain analysis has the

capability of identifying and isolating certain frequency components (Ambhore et al., 2015). In process monitoring, this is particularly useful when analysing complex signals made up of various components, as it helps to separate the frequencies that are most representative of the process from those that do not add meaningful information and, hence, can be filtered out. Frequency domain analysis is commonly applied when assessing vibration signals (Balaji et al., 2018; Gierlak et al., 2017; Liu et al., 2018; Patra, 2011), AE (Binsaeid et al., 2009; Haber et al., 2004; Karimi et al., 2015; Patra, 2011) and sound signals (Robben et al., 2010).

With regards to feature extraction, the use of the Fourier coefficients is avoided due to spectral leakage (Teti et al., 2010). Instead, other parameters are commonly considered, such as the amplitude of main spectral components (Balaji et al., 2018; Gierlak et al., 2017; Robben et al., 2010), signal power and energy in frequency band (Binsaeid et al., 2009; Sun et al., 2004; Tangjitsitcharoen, 2009), and statistic parameters of the power spectrum (Binsaeid et al., 2009; Gierlak et al., 2017; Sun et al., 2004). The main limitation of frequency domain analysis is that it averages the frequency components of the signal over its entire duration, with constant resolution. Although this is not of particular concern when assessing stationary signals, frequency analysis fails to adequately depict the characteristics of transient components in nonstationary signals (Bhuiyan and Choudhury, 2014). For example, Arul et al. (2007) performed frequency domain analysis on the recorded AE during drilling of glass fibre reinforced polymers. The authors found the dominant peaks of the AE frequency spectrum to range from 30 kHz to 150 kHz during machining of the workpiece. After drilling of the thirtieth hole however, sudden rises in signal amplitude were noticed at 70 kHz, suggesting that the tool had started to wear out considerably. If a similar analysis were to be carried out on a multi-material stack, which is the workpiece of interest in this PhD project, it would not be possible to distinguish which frequency peaks are characteristic of the cutting of each of the materials, as the signal frequency components would be averaged throughout the entire drilling cycle.

To better characterise the spectral behaviour of nonstationary signals, time-frequency domain analysis is used. According to Teti et al. (2010), amongst the various methods that can be applied to perform time-frequency domain analysis, Short-Time Fourier Transform (STFT), Wavelet Transform (WT) and Hilbert-Huang Transform are particularly common. A short-time Fourier transform performs separate fast Fourier transforms on the signal for consecutive time intervals, thus allowing one to analyse the frequency spectrum of the signal as a function of time. Liu et al. (2018) performed short-time Fourier transform on the recorded vibration signal to study candlestick drilling of glass fibre reinforced laminates. In their offline time-frequency

domain analysis, they observed that the vibration signal was found to be highly related to the drilling process, and that the inner tip angle played a major role on the delamination damage at borehole exit.

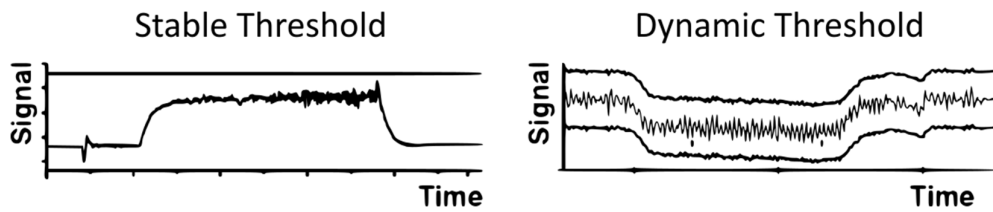
The main limitation of short-time Fourier transforms is that the width of the time interval establishes both the temporal and spectral resolution. For this reason, when a narrow time interval is required to detect rapid changes in the signal (high time resolution), it will be impossible to detect frequency components below a certain limit (low spectral resolution). For the same reason, if a large time interval is required to detect low frequency components (high spectral resolution), sudden variations in the signals may not be recognised (low time resolution). The wavelet transform overcomes this limitation by adapting the time interval width depending on the frequency component to be analysed (Mallat, 1989), using larger intervals for lower frequencies and narrower intervals for higher frequencies. Furthermore, using wavelet transforms allows one to reconstruct the transformed signal in the time domain entirely by performing inverse wavelet transformation (Klocke, 2011). This is not possible when carrying out transformations based on the Fourier transform, in which the temporal information of the signal is lost. Numerous variations of the wavelet transform, such as the discrete wavelet transform (Bhattacharyya et al., 2007; Sun et al., 2005) and the wavelet packet transform (Karimi et al., 2015; Patra, 2011) have been used for process monitoring purposes.

The Hilbert-Huang transform, established by Huang et al. (1998), is another method for carrying out time-frequency analysis, dedicated to nonstationary and nonlinear signals. Unlike the short-time Fourier transform and the wavelet transform, which can be considered theoretical tools, the Hilbert-Huang transform follows a more empirical approach, where an algorithm is applied to a data set. The results are subsequently plotted in time-frequency distributions called Hilbert spectra (Teti et al., 2010). Numerous researchers (Bakker et al., 2015a; Bassiuny and Li, 2007; Kalvoda and Hwang, 2010; Kuo et al., 2017) have successfully used Hilbert-Huang transforms for monitoring manufacturing processes.

### 2.2.3 Decision-making

The selection of an appropriate decision-making strategy is of crucial importance to ensure the reactivity and reliability of a process monitoring system. According to Klocke (2011) the simplest form of decision-making technique is the use of stable thresholds. When using this technique, signals are recorded during undisturbed machining in a preliminary analysis, in order to define a reference profile, based on which thresholds are then set to the extracted SFs.

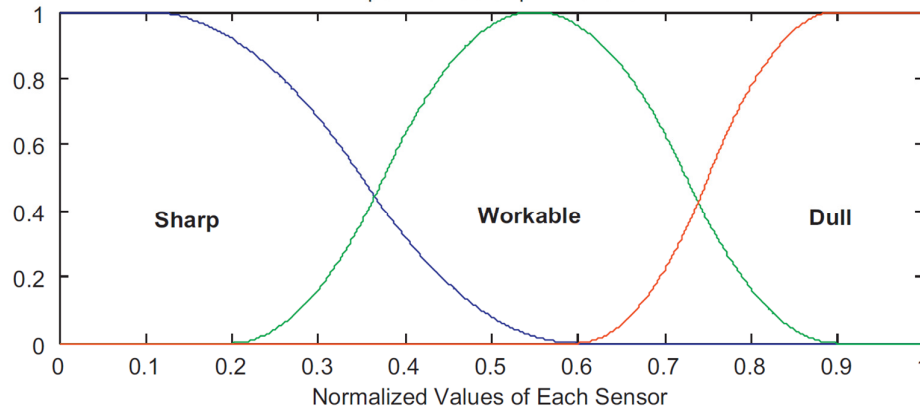
When any of the SFs exceed their corresponding thresholds, the system can trigger pre-defined actions. Monitoring strategies employing stable thresholds have been used, amongst others, by Hsu et al. (2001), Heinemann and Hinduja (2012) Fang et al. (2015) and Renganathan et al. (2015). A more sophisticated monitoring approach relies on dynamic thresholds, where a moving average is computed on a recorded reference profile. This moving average is then correlated to a certain percentage addition and reduction, which act as dynamic thresholds for the triggering of process incidences (Klocke, 2011). Examples of stable and dynamic thresholds are shown in Figure 15.



**Figure 15: Examples of stable and dynamic thresholds (based on Klocke, 2011).**

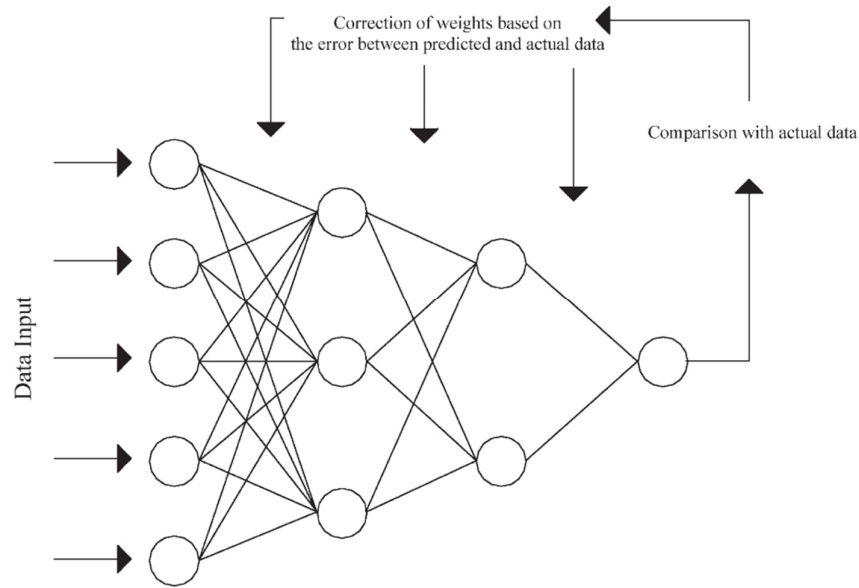
Although studies on using alternative ‘intelligent’ decision making techniques have been reported on in the literature for quite some time (Teti and Kumara, 1997), the development of such techniques is accelerating rapidly, with artificial intelligence-based algorithms being increasingly employed for process monitoring (Caggiano et al., 2018a, 2018c). Specifically, fuzzy logic and artificial neural networks (NNs or ANNs) were found to be popular decision-making techniques reported on in the literature. Fuzzy logic is based on the fuzzy set theory (Zadeh, 1965). In a fuzzy set, elements are contained with a partial degree of membership and without precisely described boundaries. Fuzzy set elements can be any real number between two set values (usually 0 and 1). Fuzzy sets aim to formalise making rational decisions in an environment of partiality of truth and possibility (Zadeh, 2008). For this reason, they are fundamentally opposed to the Boolean logic, in which the truth values of variables may only be the integer values 0 or 1. The input data are first ‘fuzzified’, i.e. membership functions are applied to quantify their degree of membership to a certain variable (e.g. material hardness). An example of the membership functions utilised in a tool condition monitoring system is shown in Figure 16. A number of ‘if-then’ rules is subsequently applied to the input data (e.g. IF (material hardness is high) THEN (cutting speed is low)). The results of these rules are combined to obtain a final ‘fuzzy’ result, which can be ‘defuzzified’, using a variety of algorithms, to obtain a final ‘crisp’ output (Hashmi et al., 2000). Fuzzy logic systems have been applied as decision-making methods for various process monitoring applications, as for

example by Kanish et al. (2014) to predict the improvement of surface roughness in magnetic-field-assisted abrasive finishing and by Cuka and Kim (2017) for monitoring tool condition in end milling.



**Figure 16: Fuzzy logic membership functions for tool condition monitoring system (Aliustaoglu et al., 2009).**

An artificial neural network is a computational architecture which aims to replicate the functioning of a biological neural network. According to Dornfeld and DeVries (1990), the three characteristics that artificial NNs share with biological NNs are: (i) they are made up of a large number of simple processing elements, called neurons, which work in parallel; (ii) each neuron is connected to various other neurons, and (iii) the overall functionality of the NN is a result of the strengths of the connections between neurons. These can be adjusted during a learning phase. The use of efficient training methods is of crucial importance to use NN effectively (Sun et al., 2006). A popular learning algorithm is back propagation, in which a training set of input and expected output patterns is fed to the NN, as shown in Figure 17. The strength of the connections (weights) between neurons is then manually adjusted based on the error, i.e. the difference between the NN output and the expected one. The process is then repeated in an iterative fashion by feeding not-before presented sets of inputs and adjusting the weights until the error is minimised (Dornfeld and DeVries, 1990; Rumelhart et al., 1986). Unsupervised training methods, where the NN is only fed sets of inputs and learns to group data based on recurrent features, are also available (Teti et al., 2010).



**Figure 17: Back propagation learning mechanism in neural networks (Benardos and Vosniakos, 2003).**

Neural networks have been extensively used in process monitoring. Jemielniak et al. (1998) used NNs with back propagation to assess tool wear based on thrust force, torque and AE signals recorded during turning. They found that training these networks can quickly lead to overtraining and the deterioration of their response. To avoid this, the authors suggest introducing random distortions in the network weights, or to distort the weights by the same amount, alternating between additions and subtractions. Pani and Mohanta (2015) investigated the performance of three NN models (back propagation, radial basis function, generalised regression) in estimating the product size in cement grinding, and the back propagation NN was found to generate the most accurate results for output prediction of unknown data. More recently, Mikołajczyk et al. (2018) used flank wear images as an input to NNs to automatically measure tool wear and predict the remaining tool life in turning. Although the proposed system yielded higher errors than direct measurements, their work proves the feasibility of automatic tool wear monitoring by combining image recognition software with NNs. As noted by Teti et al. (2010), audible signals appear to be amongst the most relevant input for NNs, given that the NN would replace the operator's ability to correlate sound information to a particular process condition. Interestingly, however, Rubio and Teti (2009) appear to be the only researchers having conducted work in this area. Even though the results obtained in experimental studies are very promising, it is important to recognise that NNs require expensive training in order to become effective decision-making techniques (Ripley, 1996). This can often be a significant limitation that prevents NN from being adopted in industrial applications on a large scale. In

addition, it should be considered that the sets fed into the NN during the training stage are often representative of lab conditions. On the shop floor, there are various other factors that can influence the actual output of a certain system, yielding results that may contrast those given in the training sets, thereby resulting in ‘overfitting’ (Goodfellow et al., 2016). In scenarios where this is the case, the NN may struggle to find the right correlation and, thus, fail in its monitoring purpose.

Fuzzy logic and NN theory can be combined to create neuro-fuzzy decision-making methods. In these, logic rules with adequate membership functions are created using a fuzzy interference system, the parameters of which are tuned by NNs after a suitable training process (Jović et al., 2017). Saw et al. (2018) used a neuro-fuzzy interference system to predict tool wear and optimal cutting parameters when drilling mild steel. The system, which comprised of a five-layer NN trained by ‘if-then’ fuzzy rules, uses the drill diameter, feed rate, spindle speed as well as the average thrust and torque, measured with a dynamometer, to provide an estimate of the tool flank wear. According to the authors, thrust and torque data are the most effective inputs for tool wear prediction, but spindle speed, feed rate and drill diameter also appeared to be suitable inputs.

## 2.3 Process monitoring applications

### 2.3.1 Tool Condition Monitoring (TCM)

Tool Condition Monitoring (TCM) is by far the most investigated process monitoring application in drilling. Heinemann and Hinduja (2012) developed a TCM system for small diameter twist drills in deep-hole drilling (diameter 1.5 – 3.5 mm, 10 x D) of carbon steel (AISI 1045). In their study, mean and variance in time domain were extracted as SFs from the recorded AE (in RMS form) and spindle power signals. To enhance the change in SFs and improve the TCM system’s reliability, signal segmentation was performed. This resulted in SFs to be extracted from the signals only in certain phases of the drilling cycle, for example towards the end of the drilling cycle, as it was observed that the impact of tool wear on the selected features increases with borehole depth. The SFs were then compared to reference values, recorded during drilling of holes 25-30, as the first 25 drilling cycles were not taken as reference since brand new tools exhibited a running-in period. An alarm indicating imminent tool failure was triggered if five SFs exceeded their prescribed thresholds twice within the last 10 drilling cycles. This helped avoiding alarms being triggered due to singular phenomena causing sudden variations in the SFs which were not correlated to tool wear, e.g. chip clogging.



This paper suggests that the use of a single signal in combination with one SF could lead to pre-mature warnings, as a result of random signal fluctuations typical for drilling. It is however questionable whether this was a result of the rather large borehole depth ( $10 \times D$ ), which is considerably greater than the majority of the boreholes drilled in the aerospace sector.

Aliustaoglu et al. (2009) used sensor fusion and fuzzy logic to predict tool wear in drilling. In their study, thrust force, torque, vibration and airborne sound were measured using a dynamometer, accelerometer and microphone, respectively. Statistical parameters (mean, maximum, RMS and standard deviation) for each of these signals were then fed into a two-stage fuzzy interference system. In the first stage, each signal was processed separately by a dedicated fuzzy model. The crisp outputs were then used as inputs for another (i.e. second stage) fuzzy model, whose single crisp output was then compared to threshold values in order to determine whether the tool was sharp, workable or dull. The results obtained by the authors are in agreement with Heinemann and Hinduja (2012) and further demonstrate the benefits of using multiple sensors during process monitoring, as different signals often have varying sensitivities to the phenomena that are to be monitored. For example, the thrust force and torque were found to be particularly sensitive to tool wear, whilst airborne sound was found to be the best indicator for detecting tool breakage.

Patra (2011) developed a tool wear monitoring system based on AE signals acquired during drilling of mild steel. The signals were first band-pass filtered to limit noise from low frequency vibrations (500 Hz - 50 kHz). The upper bound of the filter was set in order to limit data storage and memory retrieval, thereby reducing the required computing resources. After being filtered, the signal was analysed in both time and time-frequency domain, using two back propagation NNs to predict tool wear. In addition to the process parameters (tool diameter, spindle speed and feed rate), the NN operating in the time domain also used AE RMS values as input, whilst the NN operating in the time-frequency domain used two wavelet packet features. According to the experimental results, tool wear monitoring using wavelet packet features led to more accurate tool wear predictions when compared to those obtained by using time domain features. It is pertinent to note that, due to the offline nature of the analysis, the authors were not restricted by the amount of time required to process the recorded data. Therefore the fact that wavelet packet transforms requires significant computing resources, particularly when performed on high frequency AE signals, was of no concern in their study. The processing time may however constitute a significant limitation for the implementation of an online monitoring strategy.

Corne et al. (2017) conducted research in order to ascertain whether the spindle power recorded by a power meter fitted to the spindle motor can be used as a substitute for the thrust force and torque recorded using a dynamometer when predicting tool wear in drilling of a Nickel-based super alloy (Inconel 625). For this, spindle power, thrust force and torque were fed through two separate but identical NNs after being amplified. Tool wear was predicted by correlating the power data, thrust force and torque to the drilling parameters (cutting speeds and feed rate), and was then validated against the actual wear measured with an optical microscope. The NN which used the dynamometer data as inputs produced slightly more accurate results, which the authors attribute to the fact that the power meter was affected by power losses due to spindle inertia and friction, as well as chip jamming. Using the power meter allowed carrying out online TCM within an error range of 0.8–18%. Overall, the authors' findings indicate that the measurement of power is a practical alternative to measuring the thrust force and torque directly, as power and current transducers can easily be implemented in industrial applications without affecting productivity and machine fragility.

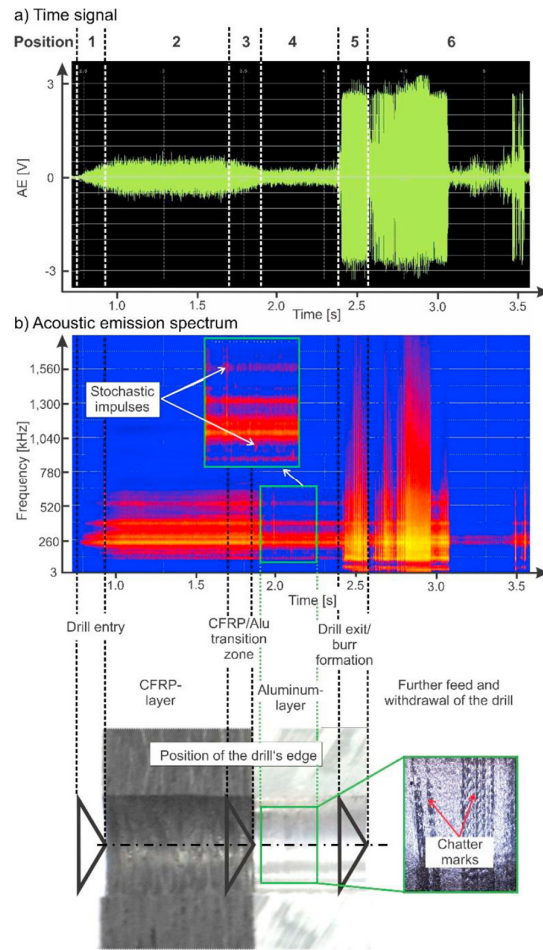
### 2.3.2 Process monitoring in drilling of aerospace stacks

Focusing on process monitoring in drilling of aerospace stacks, Caggiano et al. (2017) monitored both the thrust force and cutting torque to predict tool wear during drilling of CFRP/CFRP stacks. In their work, segmentation was performed on the recorded signals to only extract information when the tool is actually removing material. The authors believe that the high scatter present in the recorded signals is a result of the alternation of several cutting mechanisms due to the varying fibre cutting angle, an observation also made by Bonnet et al. (2015). After segmentation, Caggiano et al. carried out a frequency domain analysis on the data using fast Fourier transforms. Several peaks were detected at frequencies in the range of 100 Hz – 400 Hz for both the thrust and torque signals. Again, they believe this to be due to the different cutting mechanisms taking place during drilling of CFRP. The authors also noticed that the amplitude of many of the observed peaks increased gradually with tool wear, suggesting a potential correlation. The peak amplitudes, which were statistically found to exhibit the strongest correlations with tool wear, were then used as SFs to be fed into a NN, which predicted tool wear through pattern recognition algorithms. Specifically, two sets of inputs were assessed: the first one contained SFs extracted only from the thrust force signal, while the second comprised features extracted from both the thrust and torque signals. The latter was found to achieve better results due to its inclusion of features extracted from more than one signal, thereby resulting in a more complete representation of the cutting process.

These results support the claim made by Aliustaoglu et al. (2009) that extracting features from different signals is beneficial to the reliability of the monitoring system.

More recently, Caggiano et al. (2019) monitored the thrust force and torque during drilling of Aluminium/CFRP stacks, analysing the recorded signals in both the time and frequency domain. The authors reported an increase in both the thrust force and torque with increasing wear, but they also pointed out that the latter was found to be more strongly correlated to the tool wear condition. Although this study strongly supports the suitability of both time and frequency domain analysis to aid the fundamental understanding of drilling applications, the analysis of frequency domain features could require excessive computing resources to be used in online monitoring systems capable of detecting a process incidence and initiating a corresponding reaction in quasi real time. This is possibly why, when developing a tool condition monitoring system capable of forecasting tool flank wear online in a different research work (Caggiano et al., 2018b), the authors selected only time domain features as an input to the decision-making system.

Möhring et al. (2018) used AE to investigate drilling of CFRP/Aluminium stacks. According to the authors' findings, the different cutting mechanisms taking place in the two workpiece layers causes the AE generated during drilling of aluminium to be generally lower when compared to the AE generated when machining of CFRP, as shown in Figure 18. Furthermore, while machining of CFRP was dominated by relatively homogenous AE, drilling of aluminium was characterised by stochastic impulses, which the authors attribute to friction between the drill and borehole wall, as well as chip breakage and jamming. Drill exit from the aluminium layer and tool retraction were characterised by substantial increases to the AE across the whole frequency spectrum, which the authors believe is a result of burr formation-related phenomena and jamming of chips that are still within the drill's flutes. The research work also included an assessment of tool wear, which was not found to yield significant variations in the generated AE.



**Figure 18: AE signal in drilling of CFRP/Al stacks;**  
**(a) time domain (b) time-frequency domain (H.-C. Möhring et al., 2018).**

Kimmelmann et al. (2019) investigated exit burr formation when drilling CFRP/Aluminium stacks using AE. The AE signature was assessed by linking it to images captured by a high speed camera, in order to correlate different stages of the burr formation process to variations in the AE signal. The tests were carried out with tools exhibiting two different point angles ( $104^\circ$  and  $180^\circ$ ), which according to Dornfeld (1994) cause different burr formation mechanisms. After performing a time-frequency analysis via the application of short-time Fourier Transforms, the authors identified variations in the dominant frequencies of the recorded AE during the burr formation process. Once the last layer was penetrated, effectively changing the workpiece geometry, the considerable change in workpiece dynamic properties resulted in substantially lower frequencies of the recorded AE. This reduction was found to be more easily identifiable for the tool exhibiting the larger point angle due to the sudden breakage of the burr cap, as opposed to the more gradual peeling process characteristic of the tool with the smaller point angle. For this reason, the proposed method to estimate the generated burr

height based on the time during which the AE frequencies characteristic of the burr formation mechanisms are present was found to yield acceptable results only for the tool exhibiting a larger point angle. This study highlights the effectiveness of AE as a process signal to allow for a fundamental understanding of the stack drilling process, as well as its potential use for process monitoring applications. It is pertinent to note that in their study, the authors selected tool point angles that represent the extremes of the range commonly used in drilling operations. It is possible that tools exhibiting more traditional point angles (e.g. 120-150°) result in a combination of different burr formation mechanisms and, consequently, lead to a more complex AE signature.

Another investigation on the effect of tool wear on AE in drilling was conducted by Mascaro et al. (2005), using CFRP/Titanium stacks as the workpiece material. During drilling of the CFRP layer, it was observed that an increase in tool wear resulted in a reduction in AE across the entire frequency spectrum. The authors attribute this to the increase in drilling time as a result of the rounding of the cutting edge corners (i.e. tool wear), which appears to have been made possible by the use of an electric drilling device for the experiments, for which unfortunately the authors failed to provide any detail. The reported reduction in feed velocity is unlikely to occur when using traditional computer numerical control (CNC) machining centres or state-of-the-art automatic drilling units, as these are capable of maintaining a constant feed rate.

Angelone et al. (2019) used a thermographic camera to monitor the tool and composite temperature during drilling of Aluminium/CFRP stacks, in order to optimise the machining parameters. Although temperature monitoring allowed for a fundamental understanding of the possible temperature-related defects in the composite, it was only limited to the underside of the composite layer. Thus, thermographic cameras appear to be unsuitable for online detection of process incidences throughout the drilling cycle as the cutting temperature information is restricted to either the initial or final stage of the drilling cycle, i.e. tool entry or exit.

### 2.3.3 Tool position monitoring

Tool position monitoring was found to be a popular topic on process monitoring of stacked structures, which can be attributed to the fact that the ability to detect tool engagement, material transition and tool disengagement is a fundamental requirement to achieve adaptive drilling when machining stacked assemblies. Portillo et al. (2012) developed a monitoring system using spindle power as an input to detect material transition and predict tool wear when drilling stacks

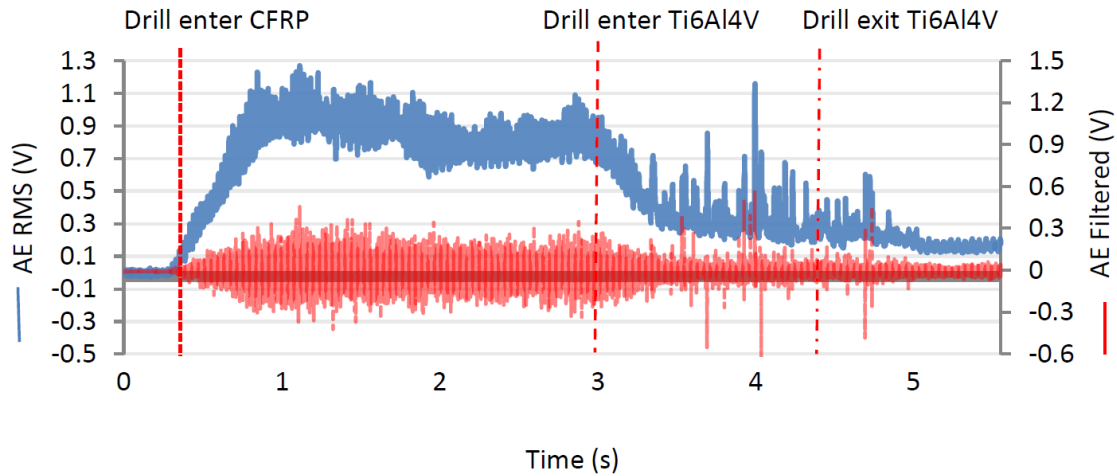
comprising aluminium, cast iron and steel. To identify material transition, the specific cutting force ( $K_c$ ) of the machined material is calculated using the following equation:

$$K_c = A \times \frac{P_c}{f D^2 n} \quad (2) \text{ (Portillo et al., 2012)}$$

where  $P_C$  is the measured spindle power (kW),  $f$  is the feed rate (mm/rev),  $D$  is the drill diameter (mm),  $n$  is the rotational speed (rpm) and  $A$  is a constant used to output  $K_C$  in ISO units. Depending on the computed specific cutting force, the workpiece material being machined can be deduced. Additionally, to determine tool wear, the average power consumption per drilling cycle was measured and compared to the average power required during the first drilling cycle, i.e. with a new tool. The authors observed that as the cutting edges wore out an increasing amount of power was required to cut the material. Using this knowledge, the authors devised a system that triggered an alarm once the average power required for a drilling cycle exceeded a certain threshold, to flag imminent tool failure. The research conducted by Portillo et al. suggests that relying on single SF can lead to success, but it is pertinent to note that the material layers chosen by them exhibit very different properties, so much so that the differences in specific cutting energy are significant. The use of stacks comprising materials that are more similar in terms of their mechanical properties might render the proposed approach less useful. Another limitation of the above monitoring technique is that if the power required for a particular drilling cycle increases for a reason other than tool wear (e.g. chip jamming), the system could mistakenly display an imminent tool failure alarm, or erroneously detect a material transition. To avoid this, as suggested by Heinemann and Hinduja (2012), false alarms can be limited by increasing the number of SFs used as input to a process monitoring system.

Renganathan et al. (2015) used AE recorded both in RMS and filtered (50 kHz – 1MHz) form to monitor tool position during drilling of CFRP/Titanium stacks, see Figure 19. While both signals are fairly stable during drilling through the upper layer (CFRP), several transient peaks were recorded during drilling of the lower layer (Titanium), which according to the authors was a result of collisions between the titanium chips and the borehole wall, chip breakage and chipping of the tool's cutting edges. Even after the tool had broken through the bottom surface, the signal remained fairly noisy, which the authors believe was due to chips travelling upwards and rubbing against the drill flutes and borehole wall. To detect incidences in the drilling cycle, an algorithm was developed to calculate the AE crest factor and compare it against stable thresholds. When the magnitude of the crest factor was found to exceed a threshold, the

respective process incidence was detected. The authors noticed a delay from the actual point of tool engagement and material transition to when the system detected it (less than 0.1 seconds for tool engagement and around 0.4 seconds for material transition). Specifically, in the material transition phase, the crest factor was noticed to rise suddenly only once the cutting edges were fully engaged in the lower titanium layer. This contributed to increasing the delay between breakthrough of the drill tip and material transition detection. The authors failed to detect tool disengagement, which they believe was a result of the particularly noisy AE signal during tool exit. Although the authors claim to have successfully designed a monitoring system to detect tool engagement and material transition, the fact that both chip jamming and tool wear majorly affect AE (Heinemann, 2004; König et al., 1992) questions this system's ability to function correctly over the entire tool life.



**Figure 19: AE RMS and AE band pass filtered, together with the actual time of process incidences, for one drilling cycle (Renganathan et al., 2015).**

Neugebauer et al. (2012) and Wertheim et al. (2012) also used AE signals for monitoring drill position when drilling stacks comprising an aluminium and CFRP layer, in order to identify tool engagement, material transition and tool disengagement. In their experiments, a twist drill and a step drill were employed, and both stacking sequences (i.e. CFRP/Aluminium and Aluminium/CFRP) were investigated. Prior to being fed to the relevant decision-making algorithms, the AE signal was converted into RMS form and low-pass filtered. To detect tool engagement and disengagement, an algorithm based on detecting large gradients of the AE signal, which suddenly increases when workpiece cutting begins and decreases rapidly when the tool exits the workpiece, was employed. To detect material transition, the gradient and average of the AE signal recorded since tool engagement was computed together with the

gradient and average of the last 30 AE measurements, and these were compared against three predefined stable thresholds. The system detected a material transition once the conditions for a local minimum were met. In contrast to the stacking sequence, which was not found to significantly influence the system's accuracy and reliability, the use of the stepped drill resulted in an increase in reliability, which according to the authors is due to the larger time window available to recognise each of the incidences before the full tool diameter was engaged. Overall, the authors state that the system was able to detect incidences with a delay time of a few hundred milliseconds. However, drill wear was found to negatively affect the system's accuracy, so much so that after 40 boreholes, its reliability drastically decreased, resulting in several non-identified incidences. Although it is clear that further investigation is required to study the effect of tool wear on the extracted SFs, the results obtained by the authors demonstrate the feasibility of using time domain analysis to monitor drill position. Furthermore, the observations made on the influence of tool geometry on the recorded signals disclose an area which was not found to be studied extensively in the literature and is thus believed to be worthy of further investigation.

Fang et al. (2015) indirectly measured the thrust force to detect material transition during orbital drilling of CFRP/Titanium. In their work, the authors developed a so-called 'cutting force observer', which monitors the feed-drive motor current and estimates the thrust force by calculating the losses within the system. The measurements of the proposed system were found to differ by 13% at most when compared to dynamometer readings during drilling of CFRP/Titanium stacks. To detect process incidences, the measured cutting force is compared to a predicted cutting force. This is calculated using a time-force function  $F = A \cdot t + B$ , where the parameters  $A$  and  $B$  are calculated by linear regression of the force values of the previous drilling cycles. When the difference between the indirectly measured and the predicted cutting force exceeds a set threshold, the incidence detection is triggered. In terms of time delay between incidence occurrence and its detection, the results obtained are comparable to those recorded by both Neugebauer et al. (2012) and Wertheim et al. (2012). The proposed system appears to achieve drill position monitoring of CFRP/Titanium stacks using solely indirect monitoring of the thrust force, which would be ideal from an industrial point of view as it would avoid employing expensive and fragile sensors. However, it is not clear whether a similar method to that proposed by the authors, intended for orbital drilling applications, could be employed for process monitoring during conventional drilling. Furthermore, the tools employed in the study had a diameter of 6 mm, but the authors failed to provide any information



about the spindle's maximum power output. However, there was a strong degree of similarity between the measured cutting force (using a dynamometer) and the calculated force (based on the spindle motor current), so much so that both exhibited a similar sensitivity to dynamic changes in the process, which suggests that the spindle assembly including motor exhibited rather low inertia (Jantunen, 2002). The good correlation of agreement between the measured and predicted cutting force reported by Fang et al. (2015) provides evidence that indirect cutting force measurements are suitable for process monitoring when using small diameter tools. This is further supported by the work carried out by Kakinuma and Kamigochi (2012), who similarly to Fang et al. (2015) used a cutting force observer which indirectly measured the cutting force based on spindle motor current to determine tool engagement in micro drilling of borosilicate glass. The proposed system identified the aforementioned incidence when the difference between the measured cutting force and its moving average exceeded a set threshold. As observed by the authors, the major benefit of comparing the instantaneous signal to a moving average is that it minimises the impact of noise.

Guerin and Costa (2015) developed a handheld electrical tool with a built-in process monitoring system for carrying out process monitoring during drilling of Aluminium/Stainless steel stacks, which they patented in 2013 (Guerin, 2013). The system monitors the drilling process by measuring the thrust force and torque using a sensor mounted on the spindle axis, and adjusts the cutting parameters depending on information recorded. The authors claim that the apparatus is capable of detecting tool engagement and disengagement, as well as material transition. They also claim that it is simpler to identify the material transition when the tool is transitioning from a soft material to a harder one. This, the authors believe, is due to the machining of hard materials being characterised by the generation of higher thrust force and torque, which in turn results in a higher signal-to-noise ratio. Although this paper is the only one reported on in the literature where the authors claim to have achieved the design of a process monitoring system for adaptive drilling, they failed to provide details not only about how both the thrust force and torque were measured, i.e. directly or indirectly, but also about the decision-making methodology employed. Consequently, the lack of information makes it difficult to assess the proposed technology and to significantly further the knowledge on process monitoring of drilling operations.

Eneyew and Ramulu, (2014a) made use of a range of signals (thrust force, vibration, AE and airborne sound) to estimate the height of the interlayer gap in drilling of CFRP/CFRP stacks. The interlayer gap size was determined by measuring the time between the chisel edge breaking

through the upper layer and it then making contact with the lower layer, and multiplying this time by the feed velocity. The occurrence of tool breakthrough and re-entry was defined manually based on the magnitude of the assessed process signals, which were low-pass filtered in the post processing phase. The required manual detection could jeopardise the feasibility of their approach in an industrial environment, where monitoring systems are required to operate online without slowing down the process. The lack of description of aspects related to signal processing could also suggest that the authors did not attempt to create an algorithm to automate signal processing and feature recognition, but treat their work as a fundamental study focusing on making observations between process incidences and changes in signals recorded by various sensors, as well as allowing for an estimation of the interlayer gap width, which as discussed earlier is a parameter which majorly influences the stack drilling process.

#### 2.3.4 Monitoring of workpiece damage

Although extensive work has been carried out on detection of material failure using AE (Behrens et al., 2016; Gutkin et al., 2011; Strantza et al., 2017), relatively little research has been conducted on online monitoring of workpiece damage in manufacturing processes. One of the few studies in this area was conducted by Karimi et al. (2012), who assessed the effect of delamination on both thrust force and AE during drilling of composite materials. According to their results, both push-out and peel-up delamination bring about an increase in the AE amplitude. Moreover, in the case of push-out delamination, the thrust force was also found to decrease, but in a stepwise fashion, with each step corresponding to the opening of an additional crack. More recently, Karimi et al. (2015) studied the occurrence of matrix cracking, fibre pull-out and delamination in composite drilling. These phenomena were all found to be major sources of AE, which the authors used as the input for a monitoring system designed to identify and distinguish them. Through time-frequency analysis carried out by fast Fourier transforms and wavelet packet transforms, specific frequency ranges were identified for friction (0-62.5 kHz), matrix cracking (62.5–125 kHz), delamination (187.5-250 kHz) and fibre breakage (312.5-375 kHz). Although the data analysis was carried out offline, it is reasonable to assume that an online system could be designed that uses a similar methodology, i.e. recognising workpiece damage by assessing the spectral component of the AE signal during certain stages of the drilling cycle. The fact that the occurrence of workpiece damage does not require instantaneous detection, unlike tool position monitoring where events have to be recognised immediately, would make this approach practical for assessing if workpiece damage has occurred within a drilling cycle.

### 2.3.5 Other relevant applications

Relevant findings were also reported on applications that are not directly related to drilling of aerospace stacked structures. Eschelbacher et al. (2019) developed a process monitoring strategy based on recording AE to recognise different workpiece materials during milling of wood and wood-based materials. The strategy was based on defining dominant frequency bands for the cutting of different materials, and by comparing them to the recorded AE, after conversion in the time-frequency domain via short-time Fourier transform. Different thicknesses of the same material were however found to result in different dominant frequency bands. To address this, the authors proposed a two-stage strategy in which the workpiece material is first identified by monitoring of the frequencies' normalised amplitude, and at a later stage its thickness is estimated based on the frequencies' absolute amplitude. In their off-line tests, the authors claim that workpiece detection occurred within 0.4 s from the start of machining. However, it is unclear whether the same pre-processing and decision-making algorithms could be used online within a similar time frame, the main concern being the requirement for high speed sampling (800 kHz) and data processing. Furthermore, the impact of tool wear on the generated AE was not assessed. This could influence the recorded signal, though not to the same extent as for the cutting of CFRP and metals, and hinder the reliability of the process monitoring strategy.

Lukyanov et al. (2017) developed a monitoring system with a torque threshold for deep-hole drilling, to facilitate chip disposal and avoid premature tool breakage. It is not clear whether the torque was directly or indirectly measured. During the drilling cycle, when the torque exceeded the defined threshold, which was based on the torsional strength of the tool, the machine tool halted machining and retracted the drill to allow for chip removal before restarting the downwards feed motion. The authors observed that although the use of higher feeds resulted in a faster linear speed, it also increased the number of times the torque threshold was exceeded and, consequently, the tool had to be retracted. Thus, according to the authors, a trade-off in the selected feed velocity is required to minimise the drilling cycle time. Implementing a similar monitoring strategy on an adaptive drilling system could potentially yield significant improvements in terms of tool life, especially when machining hard materials, such as titanium.

Min et al. (2011) developed a monitoring system capable of detecting tool-workpiece contact to measure tool length and determine the Z-position of the workpiece in micro end-milling using tools between 100  $\mu\text{m}$  and 500  $\mu\text{m}$  in diameter. According to the authors, the AE-based

system was capable of detecting tool-workpiece contact using the data acquired from the AE sensor within 60 ms. The system was tested using a continuous approach, where the tool was fed towards the workpiece with a constant velocity of 1 mm/min, and an incremental approach, in which the tool progressed in increments of 1  $\mu\text{m}$ , after which tool movement was stopped for 200 ms to allow for sufficient signal processing time. Although the former approach greatly reduced the time required to establish the workpiece datum, it yielded more extensive workpiece surface damage. This was the result of the time required to process the data and, thereupon, make the decision about whether contact had been established or not, during which the tool continued moving towards (or into) the workpiece. In the case of the latter approach, the dwell time of 200 ms was sufficient to analyse the recorded AE signal and make the decision as to whether carry on with another 1 micron step or, because contact had been identified, abandon any further movement. The authors also observed an increase in contact detection accuracy when carrying out experiments on workpieces with higher elastic modulus, which they believe is due to the stronger AE signals being produced when deforming hard materials. The negative aspect of workpiece damage is less of a concern when trying to establish tool engagement in drilling, as the damaged material would be directly underneath the tool and, thus, would be machined away straight after contact detection. For this reason, the use of dwell times to allow any monitoring system to analyse the data before carrying on with a tool movement would be of significantly less benefit, as long as the impact does not cause any damage to the tool or the workpiece beyond the hole perimeter.

In the field of adaptive control, Oyelola et al. (2020) developed an adaptive control system for the machining of Ti6Al4V when postprocessing components manufactured by directed energy deposition. In their work, the forces recorded by a 3-axis dynamometer were fed to a microcontroller which used proportional integral derivative (PID) control to adapt the feed rate and spindle speed of a CNC machining centre, to minimise subsurface deformation of the workpiece material and minimise machining chatter. Similar studies were carried out for other manufacturing processes, such as welding (Kershaw et al., 2021) and turning (Fallah and Moetakef-Imani, 2019).

In the area of biomedical applications, Hsu et al. (2001) developed a bone drilling system capable of discriminating between layers of different tissue, by monitoring the electric current consumed by the drilling spindle, i.e. indirectly measuring the cutting torque. In the proposed monitoring system, stable thresholds are specified, so that when a sudden drop in the signal is recorded, i.e. when the tool enters a layer of softer tissue, power supply to the drill is cut off,

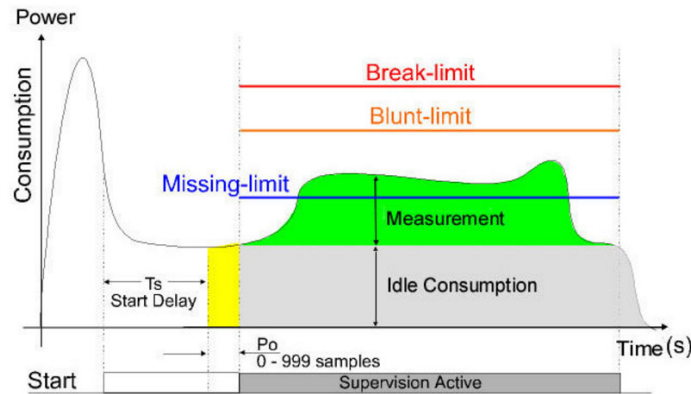
thereby limiting the damage to nearby areas which are not meant to be removed. More recently, Schwarz et al. (2015) designed a monitoring system that uses a resistance-sensitive sensor integrated into the drill bit used for implant osteotomy, with the aim of preventing the drill from cutting into softer tissue. The sensor slightly protruded beyond the tip of the drill and, thus, allowed the system to detect whether the drill was about to penetrate into softer tissue, in which case the power to the drilling unit was cut-off. Although the authors' idea appears to be highly effective with regards to drilling soft material such as bone tissue, integrating a sensor into the tip of the tool would be detrimental to the tool's capability to remove aerospace materials, which are significantly harder. This is because the area where the sensor is located will most likely not exhibit any cutting teeth and, therefore, will not be able to remove the material.

## 2.4 Systems available on the market

Apart from the process monitoring systems reported on in the previous sections, which have been primarily designed and used in an academic context, certain companies have been providing process monitoring systems for industrial applications. Unfortunately, most of the manufacturers tend to only highlight the capabilities and advantages of their products, while being very careful in disclosing information about the devices' actual functioning and limitations. Thus, relatively little information could be gathered on the details of the process monitoring techniques used in the products reviewed.

Techna-tool developed a TCM unit, 'TC-USB' (Techna-Tool, 2018), capable of measuring true power consumption (i.e. total power consumption minus idle consumption) of a machine spindle or axis drive. Based on the power consumption recordings, the company claims that the system is able to predict whether the tool is either new, worn-out or broken, and to stop operation if required. As shown in Figure 20, the monitoring system appears to be based on stable thresholds which, when exceeded, trigger either a 'blunt' or 'broken tool' alarm. The figure also suggests that the supervision window begins after a finite amount of time has passed. This start delay could help avoid the triggering of false alarms due to increases in power consumption as a result of spindle switch-on. The unit is also equipped with an accelerometer, to verify whether the experienced vibrations by the spindle fall within a pre-defined range. If the recorded vibration falls outside this pre-defined range, the system outputs a fault that immediately stops the machine. Based on the true power consumption measured on the spindle,

the system allegedly is also able to trigger a similar reaction if the job setup is not carried out correctly (e.g. due to a missing tool or an already machined workpiece).



**Figure 20: TC-USB unit and power consumption monitoring example (Techna-Tool, 2018).**

According to its manufacturer, the process monitoring system ‘Genior Modular’ developed by ARTIS (Artis, 2019) is capable of capturing and processing digital signals recorded directly from a machine’s control unit, carrying information about the power consumption of both spindle and feed drives. Allegedly, the system can be integrated into various machines and expanded to accommodate additional sensors or control modules, thanks to its modular nature. In addition to displaying the measured signals online, its monitoring algorithm can automatically stop the machine if power consumption thresholds set for the recorded signals are exceeded. Similarly, Nordmann Tool Monitoring (Nordmann, 2020) proposes different process monitoring units and sensors for tool monitoring applications. Based on the monitored signals and required system reactivity, the monitoring unit can use stable and dynamic thresholds to quantify tool wear, detect tool failure and control workpiece measurements.

The latest generation of electric portable drilling units for automated drilling applications is capable of some basic adaptive drilling capabilities (Fives, 2020; Lübberring, 2020; Seti-tec Desoutter Industrial Tools, 2020). According to the manufacturers’ specifications, the drilling units are capable of adjusting the cutting parameters when drilling different layers of a multi-material stack by measuring the current flowing in the motor(s) driver and comparing it against pre-specified thresholds, which have to be set by the operator prior to usage.

Overall, as shown by the reviewed products, it is extremely difficult to gain information on the functioning and effectiveness of the process monitoring systems currently used in industry. In particular, very little details could be gathered on which features are extracted from the signal, or how they are processed and analysed. From the available information, it appears however

that all the reviewed products utilise simple time domain analysis to carry out process monitoring. Given that it is essential that the monitoring system responds to variations in the process within a timeframe that allows for counteractions to be taken, simple time domain signal processing and decision-making methods are preferred over computing-intensive frequency domain transformations to ensure satisfactory reactivity of the system.

## 2.5 Conclusions

The literature review revealed that machining of materials commonly used in aerospace stacked structures, i.e. aluminium, titanium and CFRP, is characterised by different cutting mechanisms. For this reason, the recommended cutting parameters vary greatly. Drilling multi-material stacks with the same cutting parameters throughout the drilling cycle is thus not desirable. Instead, utilising specific cutting parameters for each of the different material layers a stack comprises would lead to substantial gains in terms of both borehole quality and tool life. The literature review has also revealed several challenges related to drilling of multi-material stacks which would benefit from further investigation.

The literature agrees that for some sensors, particularly accelerometers, microphones and AE sensors, the best location for placing them is on the tool holder, as it results in a constant distance between sensor and cutting point. Additionally, the literature suggests that some measurement approaches, albeit producing very accurate results that can greatly aid fundamental studies on manufacturing processes, are not believed to be suitable for industrial applications due to cost or practical constraints. These include, for example, directly measuring thrust force and torque using dynamometers and image-based techniques.

Process monitoring techniques were found to be aided by frequency and time-frequency domain analysis. However, the analysis in either of these domains are currently believed to require excessive computing resources for it to be viable in online monitoring systems capable of detecting process incidences and initiating corresponding reactions in quasi real time. This was further evidenced by the substantial gap between academic studies, which often involve sophisticated time-frequency analysis tools, and commercially available process monitoring systems, the majority of which appear to rely on relatively simple time domain analysis combined with decision-making algorithms based on thresholds. A reduction of this gap in response to technological developments in the area of computing, thereby enabling frequency and time-frequency domain analysis in online process monitoring using relatively affordable

equipment, is possible. However, literature supporting speculation to this regards has not been found.

Finally, the literature review revealed several gaps in the existing knowledge which strengthen the motivation for this research work:

1. Research aimed at investigating interlayer burr formation when drilling stacked materials exhibits two major shortcomings. Firstly, the actual width of the interlayer gap throughout the drilling cycle was not directly determined, thereby making it difficult to correlate a particular gap width to a certain burr height. Because of the setups used in previous research, which in many cases involved large plates as workpieces, the established relationships between gap width and burr size are specific to the particular setups rather than generic and universally applicable. Secondly, the stacks were drilled with the two layers in direct contact, and no publication was found where an interlayer medium was applied prior to drilling, such as the sealants commonly used in wing box assemblies that are needed to prevent fuel leakage. However, in order to achieve one-way assembly, the separation of the two layers between drilling the boreholes and inserting the fasteners must be avoided, which means that the sealant has to be applied at the stack interface prior to clamping and drilling. The presence of this sealant film is likely to affect the width of the interlayer gap, consequently resulting in the possibility that it influences burr formation. Research is therefore required to allow for an assessment of the impact of interlayer gap width on burr formation in a one-way assembly scenario.
2. When drilling CFRP/metal stacks, the literature recognises the interface between the composite and metal layer as the region most vulnerable to severe damage. However, some key aspects related to the cutting at and the resulting quality of the interface between stack layers still need to be addressed. Due to the difficulty in inspecting the complex tool-work interaction, little research has been carried out on the physics governing interface drilling. Tool point angle and interlayer gap width were identified as two factors directly affecting interface drilling, as these determine the distance over which the drill's cutting edges are simultaneously engaged in both the materials. The impact of either on stack interface quality has however not been investigated.
3. If adaptive drilling is carried out on stacked assemblies, another gap in the knowledge arises from the lack of information regarding the point at which the cutting parameters should be switched over during material transition. In all the reviewed studies on drill position



monitoring in stack drilling, with the exception of Renganathan et al. (2015), the authors failed to clearly define the drill position relative to the interface where the parameters are changed over, i.e. whether it is the chisel edge breaking through the upper layer, the cutting edges being fully engaged in the lower layer, or somewhere in-between. As this is believed to play a crucial role, research needs to be conducted to establish a relationship between parameter switch-over position and borehole quality.

4. In the case of publications related to process monitoring, many authors failed to appropriately justify the selection of the SFs used in the proposed solutions. Additionally, only a few studies seem to have assessed the effect of tool wear on the selected SFs, which, based on the findings of those who did, is essential for ensuring a high reliability of the adopted process monitoring technique throughout a tool's life. Thus, fundamental research aimed at correlating features of recorded signals to borehole and tool condition, as well as the assessment of the validity of these correlations throughout the life of a cutting tool is required to develop a reliable adaptive drilling system.
5. The majority of the reviewed studies on incidence detection during stack drilling were conducted on large CNC machining centres, whereas only one paper was found to report on this aspect using one of the portable handheld drilling unit typically operated in the aerospace industry. Therefore, a gap in the knowledge arises from the question of whether the understanding gained from those studies using machining centres can be reliably transferred to drilling using portable equipment. The research to be carried out during this PhD will consequently provide an insight about how transferrable the already existing knowledge (gathered from large CNC machines) is to other (smaller and portable) machining equipment.
6. Although some of the automated drilling units available on the market are equipped with process monitoring systems which their manufacturers claim provide some basic adaptive drilling capabilities, their effectiveness and reliability in a robust scientific context is unknown. Research will thus be conducted to investigate and evaluate the process monitoring strategies employed by different manufacturers. This information will be useful not only to assess the capabilities of the products currently on the market, but also to aid the development of more advanced process monitoring strategies.

## Chapter 3: Experimental setup

### 3.1 Workpiece material and clamping jig

Three different workpiece materials were used to form the stacks investigated in this research: Aluminium 7010, Titanium Ti6Al4V and CFRP. As evidenced by the literature review, these materials are commonly used in the aerospace industry to form stacked structures. The properties of the three materials are listed in Table 2.

**Table 2: Al 7010, Ti-6Al-4V and CFRP specifications.**

Al 7010	
Condition	T651 tempered
Chemical Composition (%wt)	Al 87.9-90.6 Zn 5.7-6.7 Mg 2.1-2.6 Cu 1.5-2.0 Zr 0.1-0.16
Elastic Modulus	70 GPa
Tensile strength	570 MPa
Thermal conductivity	150 W/(mK)
Ti6Al4V	
Condition	Annealed
Chemical Composition (%wt)	Ti 87.6-91 Al 5.5-6.75 V 3.5-4.5
Elastic Modulus	110 GPa
Tensile strength	950 MPa
Thermal conductivity	7.0 W/(mK)
CFRP	
Manufacturing method	Autoclave cured
Matrix material	Epoxy
Fibre volume	60%
Stacking sequence	[45°, 135°, 0°, 0°, 45°, 135°, 0°, 0°, 90°, 0°] <sub>4s</sub>
Nominal ply thickness	0.254 mm
Number of plies	40 [enclosed within two M21/1080 glass cured plies]

The material was supplied in 50 mm x 50 mm coupons. Although the use of large plates would have been more representative of aerospace assembly operations, it would have resulted in a significant loss of control over the interlayer gap width, not only at different borehole locations, which would vary substantially along the length of the component, but also throughout each individual drilling cycle. The decision to conduct the experiments using small coupons was thus based on the intention to ensure that a pre-set gap width not only can be achieved accurately prior to drilling, but that it can also be maintained throughout the drilling cycle and

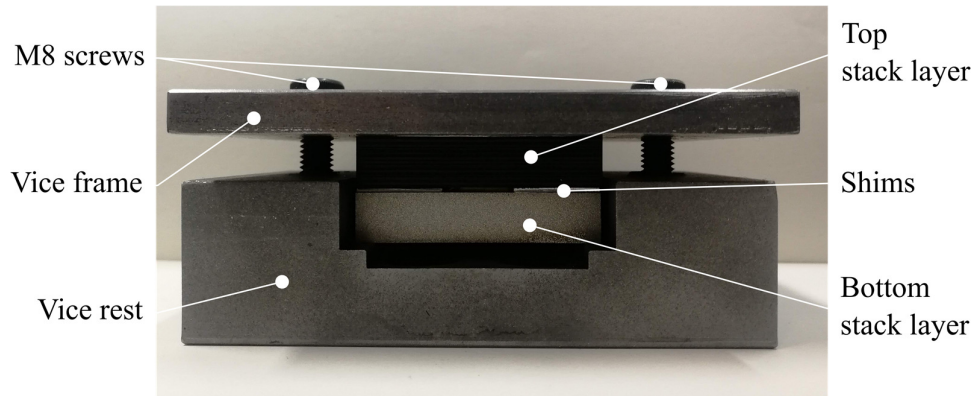
for all boreholes drilled. Calculations revealed that the maximum deflection of the stack during a drilling cycle was in the order of 2-3  $\mu\text{m}$ , based on a thrust force of 650 N, determined experimentally. Despite the setup being an artificial scenario, the fundamental information gathered with regards to the relation between interlayer gap width and burr size can be applied to the drilling of larger components, where the interlayer gap is subject to change during a drilling cycle, the more the further the hole is located away from the clamping point, as observed by Melkote et al. (2010).

The stack combinations used for the various experimental assessments are listed in Table 3. The majority of the experiments were carried out on CFRP/Aluminium stacks, which given their widespread use in aerospace assembly applications was selected as the principal combination to be investigated. Other stack combinations were also used in some of the experiments, as they were found to be better suited to the investigation of the parameters of interest. The literature review revealed that burr formation is associated with the drilling of metals and does not normally occur when cutting CFRP, thus Aluminium/Aluminium stacks were selected as the workpiece material for the assessment of the impact of interlayer gap width on interlayer burr formation (Chapter 4). The challenges associated with the cutting of CFRP/Titanium stacks, particularly during interface drilling, made this stack combination suitable for the investigation of tool point angle and interlayer gap width on interface quality (Chapter 5).

For most experiments, both the top and bottom stack layers had a thickness of 10 mm. In Chapters 5 and 6, which focus on the impact of process parameters on interface borehole quality, thinner bottom layers were used. It was assumed that this would minimise the amount of abrasion of the upper composite layer as a result of the upward-travelling metallic chips generated during cutting of the lower layer, which would have made the impact of the parameters of interest (i.e. interlayer gap width and parameter changeover position) on interface borehole quality less visible.

The drilling jig used for this research work is shown in Figure 21. A custom-made vice comprising a lower steel base ('vice rest') and an aluminium frame containing a square cut-out ('vice frame') was used to clamp the coupons by tightening two M8 screws. The vice rest allowed the bottom layer of the stack to rest on a 5 mm wide shoulder on either side, leaving a 40 mm wide strip below the centre of the stack to permit breakthrough of the drill. For the research investigating the impact of interlayer gap width (Chapter 4 and 5), shims (i.e. thin

metal strips serving as spacers) were placed in between the two layers to achieve the required gap.



**Figure 21: Stack clamping jig.**

### 3.2 Tools and cutting parameters

Several tungsten carbide tools were employed throughout the research, based on the stack composition, drilling equipment used and availability. The specifications of these are listed in Table 3. The majority of the experiments were carried out using tools with a diameter of either 6 mm or 6.35 mm (1/4 inch), which is the most common size used in wing-box aerospace assembly (Bagshaw, 2018). When assessing the impact of certain process parameters (i.e. stack clamping force, parameter changeover position) on interface quality, tools with a larger diameter (14 -15 mm) were used, in order to produce boreholes which could be inspected with the metrology equipment available. Although some of the tool geometries exhibited a countersink section, only the cylindrical portion of the tools was used, i.e. no countersunk holes were drilled.

With the exception of some of the experiments outlined in Chapter 7, where tool wear tests were carried out in dry condition to increase the wear rate, all the cutting tests were carried out with a water-based coolant (5% concentration), which was either Accu-Lube LB-4000 (Viscosity at 40°C: 9 mm<sup>2</sup>/s, Density at 20°C: 0.90g/cm<sup>3</sup>) or Blaser Blasocut BC 25 MD (Viscosity at 40°C: 49 mm<sup>2</sup>/s, Density at 20°C: 0.95g/cm<sup>3</sup>), depending on availability. The cutting parameters, i.e. cutting speed and feed rate, were selected based on industrial practice, and are included in Table 3.

**Table 3: Workpiece and tooling details for the experimental work.**

Stack combination	Tool Manufacturer	Tool Coating	Tool Geometry	Cutting speed (m/min)	Feed rate (mm/rev)	Chapter No.
Al/Al (10+10 mm)	Sandvik	Uncoated	Ø12.7 mm, 140° point, 40° helix, enlarged chip flutes, four-facet with notches	55	0.039	4
CFRP/Ti (10+10/5 mm)	Walter	Uncoated	Ø6 mm, 118° point, 31.5° helix, enlarged chip flutes, four-facet with notches	40	0.1	5
	Walter	TiAlCrN	Ø6 mm, 140° point, 30° helix, standard chip flutes, six-facet	40	0.1	
	Walter	TiAlN	Ø6 mm, 150° point, 30° helix, enlarged chip flutes, four-facet with notches	40	0.1	
	Walter	TiAlN	Ø6 mm, 180° point, 30° helix, enlarged chip flutes, four-facet with notches	40	0.1	
CFRP/Al (10+6 mm)	Walter	TiAlCrN	Ø15 mm, 140° point, 30° helix, standard chip flutes, six-facet	57/95	0.038/0.16	6
CFRP/Al (10+10 mm)	Walter	Uncoated	Ø6 mm, 118° point, 25° helix, enlarged chip flutes, four-facet with notches	40	0.1	7
	Ham	Diamond	Ø6.35 mm, 155° point, 20° helix, enlarged chip flutes, four-facet with notches, with pilot	40	0.05	
CFRP/Al (10+10 mm)	Unimerco	Diamond	Ø6.35 mm, 130° point, 30° helix, enlarged chip flutes, four-facet with notches, with pilot	120	0.05	8
CFRP/Al (10+10 mm)	Walter	Uncoated	Ø6 mm, 118° point, 25° helix, enlarged chip flutes, four-facet with notches	40	0.1	9
	Ham	Diamond	Ø6.35 mm, 155° point, 20° helix, enlarged chip flutes, four-facet with notches, with pilot	20	0.05	

### 3.3 Machine tools

Three different machine tools were used in the research: a CNC machining centre and two Airbus-loaned portable electric drilling units. The machining centre was used for the fundamental research investigating the impact of process parameters on interface borehole quality. The research was later moved onto the drilling units as they allowed for a more accurate representation of the industrial application. The machining centre was also used in those experiments which required the drilling of a substantial number of boreholes ( $> 100$ ), as the setup for the portable drilling unit only allowed drilling of a few boreholes per hour. An assessment on the degree of transferability of results between the machining centre and the automated portable drilling units is presented in Chapter 7.

The machining centre (Takisawa MAC-V3, equipped with a Semer Anlagen Technik minimum quantity lubrication system) is shown in Figure 22. To mimic the coolant supply of the portable drilling units, the air supply was reduced to its limit (1 bar) during the experiments, to allow large drops of coolant to be sprayed directly onto the tool, realising a flow rate of approximately 2 l/h. It is worth noting that, in contrast to the portable drilling units, the machining centre does not provide through-tool coolant supply, thereby making it necessary to supply the fluid externally. Given the small depth-to-diameter ratio of the drilled boreholes ( $< 3.5 \times D$ ) this was not considered to be problematic. To replicate the suction system equipped in many portable drilling units, an industrial vacuum cleaner (Vacmaster Power 38 HEPA/VK1638SWC, 1.6 kW, 240 Air Watts) was incorporated into the experimental apparatus. Assuming the suction system was operating at its nominal flow rate (60 l/sec), using a nozzle with a 30 mm diameter results in a theoretical air flow speed of approximately 80 m/sec. The location of the coolant and suction nozzle are shown in Figure 23.


	<p><b>Power</b></p> <p>Spindle drive motor: 5.6 kW  X-Y feed motor: 0.85 kW  Z feed motor: 1.2 kW</p> <p><b>Machine capacity</b></p> <p>Table size: 600 x 400 mm  Table x-y travel: 510 x 400 mm  Spindle z travel: 300 mm</p> <p><b>Other</b></p> <p>Spindle speed: 30 – 6000 rpm  Rapid traverse velocity: 4000 mm/min  Controller: MDSI Open CNC</p>
---	---

Figure 22: Takisawa MAC-V3.

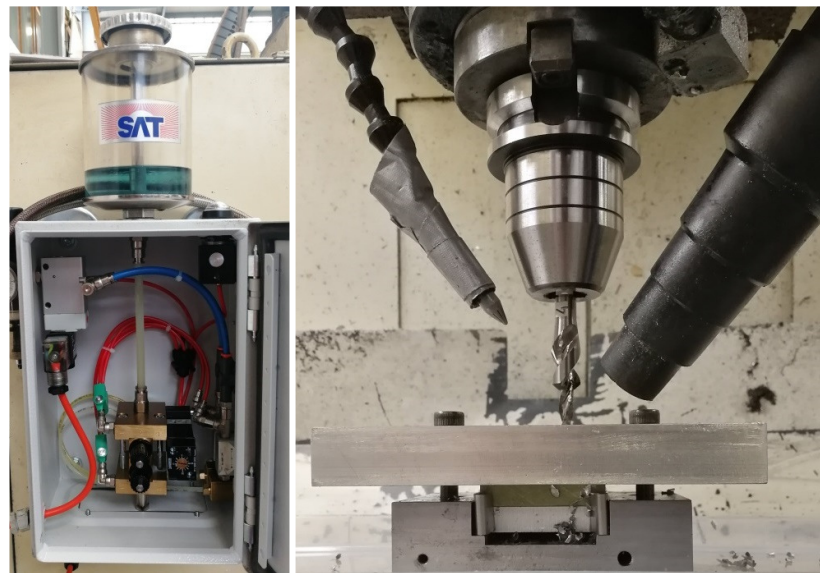
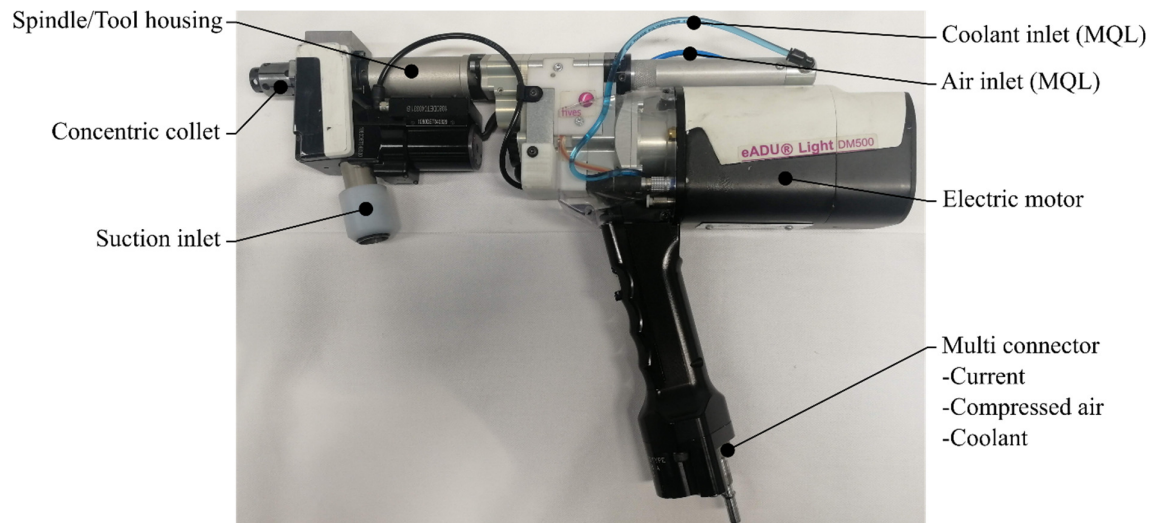


Figure 23: Machining centre auxiliary equipment; [left] coolant-supply unit control box, [right] coolant-supply and suction nozzles.

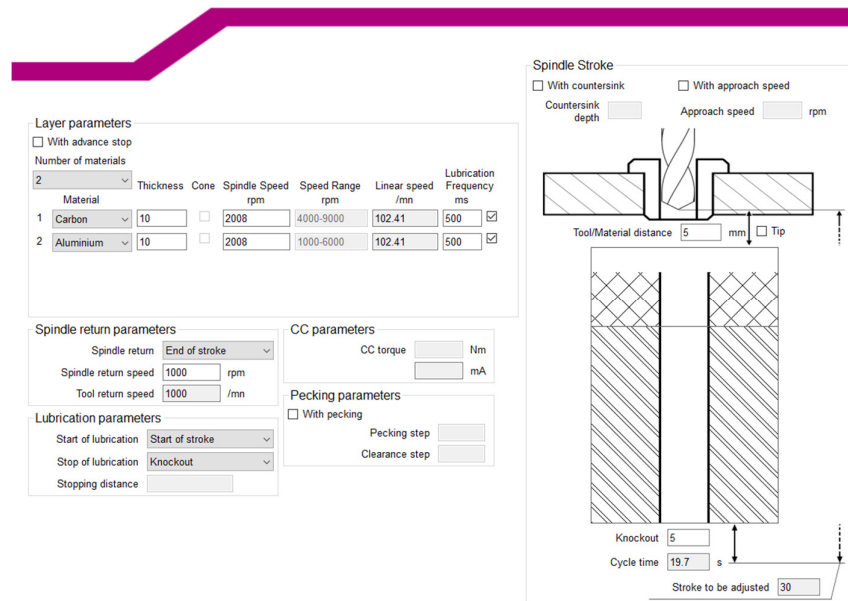
The two portable electric automated drilling units used in the research were a Seti-tec éVo Light EDU® and a Fives Light-eADU®. The Fives Light-eADU is shown in Figure 24. The main spindle is driven by an electric motor, which also provides the feed motion via a fixed-ratio gear box. This means that a change of the spindle driver settings (i.e. spindle speed) will also change the feed velocity (in mm/s). The spindle speed can be easily changed via the drive

unit of the Light-eADU, which effectively controls the speed of the electric motor. The feed rate (in mm/rev) in contrast is constant, as it is determined by the gear ratio of the gearbox, and can only be changed by manually replacing individual gears. The end-of-stroke and retract positions are set by manually adjusting the position of a rear and front stop, respectively. In order to facilitate chip breakage and evacuation (Seeholzer et al., 2019) and reduce thrust force and torque (Hussein et al., 2019) the unit is equipped with a vibration-assisted drilling module (MITIS). Chip suction is provided by connecting the ad hoc inlet, shown in Figure 24, to an industrial vacuum-cleaner. To allow for fixing on the workpiece clamping fixture, an expanding concentric collet is located on the nosepiece of the drilling unit. The Light-eADU is connected via a reinforced cable to a control box which powers the unit and supplies it with coolant and compressed air, used for both through-spindle coolant supply and operation of the concentric collet. The control box accommodates the driver of the motor, control board, coolant pump and pneumatic management system, and communicates via USB to a PC used to set the cutting speed and lubrication strategy via the ‘eADU communications’ software. One of the software’s interfaces is shown in Figure 25. Further specifications on the drilling unit are provided in Table 4.



**Figure 24: Fives Light-eADU electric drilling unit.**



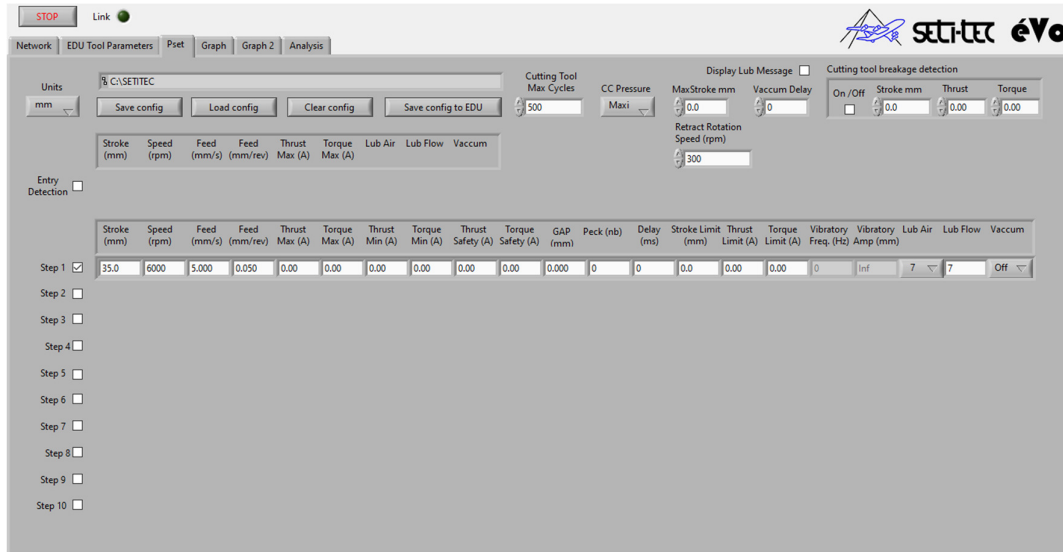


**Figure 25: Fives eADU communication software.**

The second drilling unit used was a Seti-tec éVo Light EDU, shown in Figure 26. Its specifications are listed in Table 4. The main difference between this unit and the Fives Light-eADU is that it is equipped with two three-phase electric motors. The rotation of the main spindle is determined by the primary motor, which from here on for ease of clarification is referred to as the ‘spindle motor’, whilst the feed velocity and direction derive from the combination of the spindle motor and the secondary motor, from here on referred to as the ‘feed motor’. As a result of its two-motor design, both the spindle speed and feed velocity can easily be changed individually via the drilling unit’s motor controllers. An example of the Seti-tec software’s interface is shown in Figure 27.



**Figure 26: Seti-tec éVo Light EDU electric drilling unit (Airbus, 2019).**



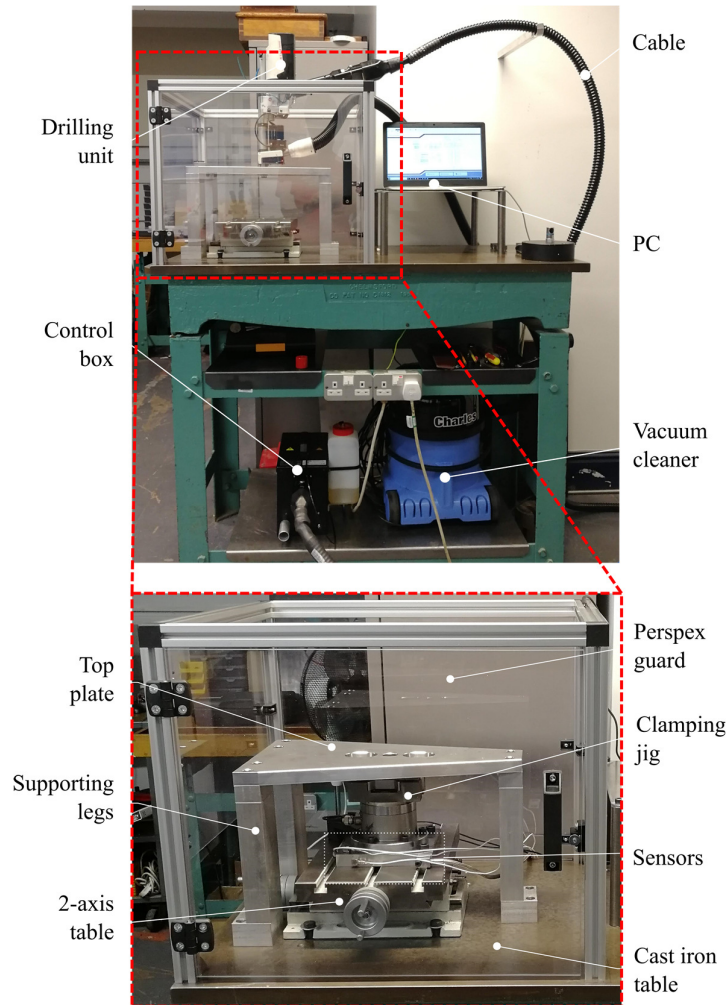
**Figure 27: EVO V2.0.14 software interface.**

**Table 4: Seti-tec éVo Light EDU and Fives Light-eADU specifications.**

	Seti-tec éVo Light EDU	Fives Light-eADU
Power		
Nominal power spindle motor	3 kW	900 W
Voltage max	48 V	350 V
Current max	70 A	14 A
Motor/spindle speed ratio	0.79:1	2:1
Machine capacity		
Spindle speed range	500 – 8000 rpm	375 – 4500 rpm
Torque	2.2 Nm up to 6500 rpm	1 – 4 Nm
Vibration-assisted drilling	0.15mm @ 5 osc/rev (Mitis)	0.1mm @ 2.5 osc/rev (Mitis)
Other		
Feed mechanism	Dedicated feed motor	Mechanical gear connection
Coolant supply	Through spindle	Through spindle
Feed velocity/rate	0.5 – 13 mm/s	0.03, 0.05, 0.08, 0.10, 0.16 mm/rev
Motor controller	Embedded in control unit	Embedded in control unit
Software	EVO V2.0.14	eADU Communication

To carry out drilling tests with the portable drilling units, a rig was designed and manufactured, see Figure 28, which comprised a supporting frame to allow for the clamping of the drilling unit and a two-axis machine table. The entire jig was mounted on a steel table and encased by an aluminium/Perspex enclosure. The top plate of the supporting frame contained a borehole to accommodate the drilling unit's concentric collet as well as two pockets to provide access

to the tightening screws of the stack-holding clamping vice. An industrial vacuum cleaner (Numatic Charles CVC370) was incorporated into the experimental rig to provide chip suction. When drilling with the tools of diameter 6 mm and 6.35 mm, it was decided to drill 5 boreholes in each of the 50 x 50 mm coupons, to meet a balance between coupon utilization and avoiding overlapping.

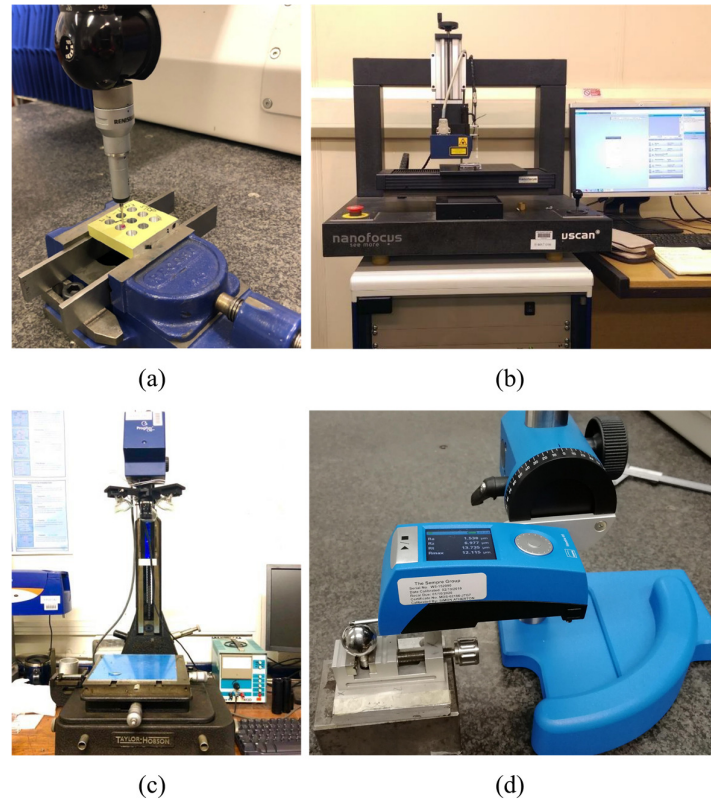


**Figure 28: Bespoke experimental rig for testing with portable drilling units.**

### 3.4 Borehole quality inspection

To assess the quality of the boreholes produced, four quality indicators were identified: borehole diameter, surface roughness, burr height and damage ring. The borehole diameter was measured with a coordinate measuring machine (LK G90C, Renishaw TP20 touch trigger probe). For each diameter measurement, five points along the borehole circumference were recorded. To verify whether the borehole exhibited variations in diameter along the axial direction, multiple borehole diameter measurements were taken at different z-heights. The

surface roughness of the borehole wall was measured with a surface roughness tester (Hommel Waveline W5, Probe T1E,  $2\mu\text{m}/90^\circ$ ). For each borehole, three surface roughness measurements were taken. Burr height was measured using a contactless profilometer (Nanofocus  $\mu\text{scan}$ ), which performed two line scans across the centre of the borehole, at  $0^\circ$  and  $90^\circ$ , thereby measuring the burr height in four locations, i.e.  $0^\circ$ ,  $90^\circ$ ,  $180^\circ$  and  $270^\circ$ . To quantify the surface damage on the CFRP surface, images were taken with an optical microscope (Jenoptik Progress C10 Plus), and the damage factor was determined as the ratio between the maximum extent of any visible damage (e.g. delamination, fibre pull-out and matrix thermal degradation) and the nominal borehole diameter. The equipment used to assess the quality of the produced boreholes is shown in Figure 29. Unless otherwise specified, the standard error was used as the statistical measure displayed in the graphs in which the results are presented, and each measurement was repeated three times.

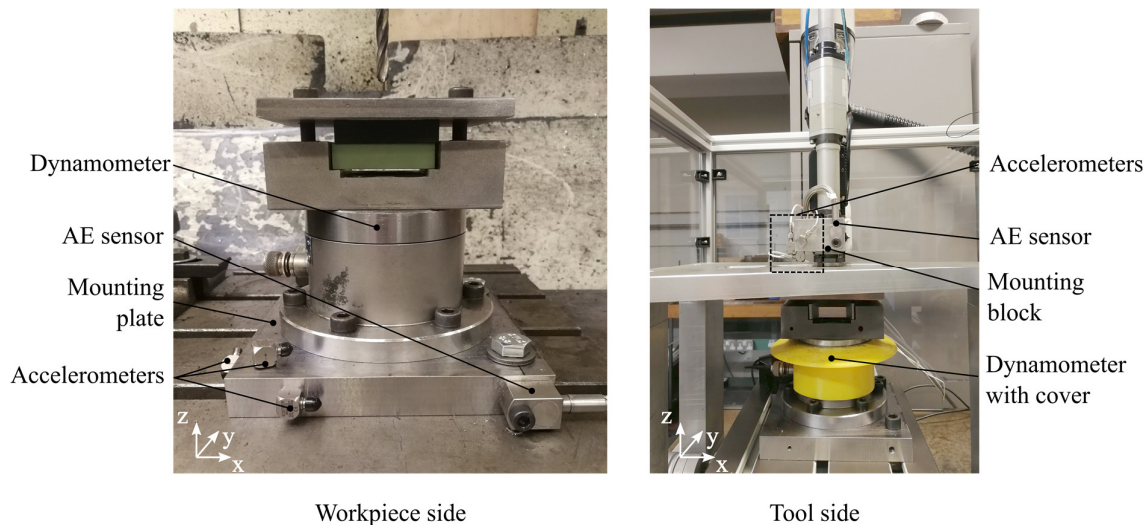


**Figure 29: Equipment used for borehole quality measurements; (a) coordinate measuring machine, (b) contactless profilometer, (c) optical microscope, (d) surface roughness tester.**

### 3.5 Equipment used for process signals acquisition

A variety of sensors were used to record different process signals during the drilling tests. To measure the thrust and torque, a 2-component piezo-electric dynamometer (Kistler 9271A) was

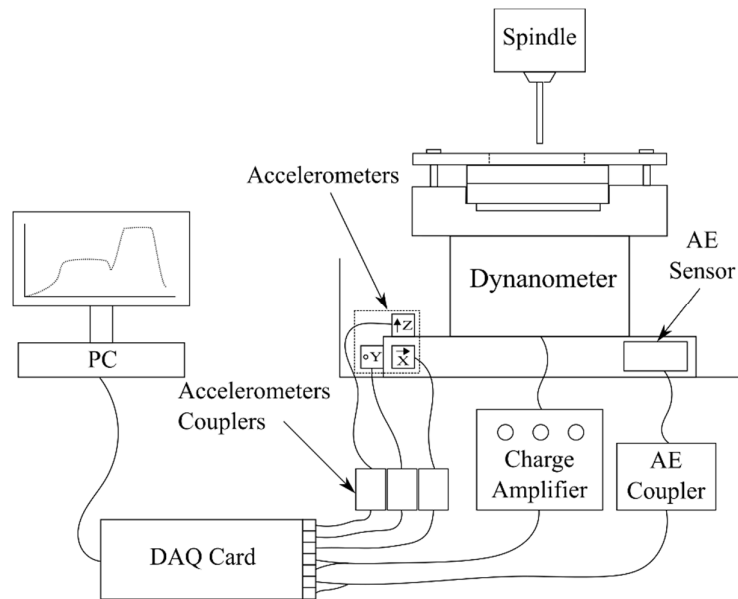
used. The dynamometer was fixed underneath the clamping rig and rested on a steel plate. To measure AE and vibration acceleration, an AE sensor (Kistler 8152B121) as well as three accelerometers (Kistler 8640A10) oriented in different directions were used. When carrying out the experiments, the accelerometers and AE sensor were placed at two different locations, see Figure 30. For the experiments discussed in Chapter 7, the accelerometers and AE sensor were placed on the workpiece side, on a steel plate fixed in between the dynamometer and the moving table. As evidenced in the literature review, placing the sensors on the workpiece side can potentially result in substantial variations in signal magnitude, as a result of the varying distance between the cutting point and sensors (Klocke, 2011; Shuaib, 2018). However, placing the sensors on the tool side was not possible on the machining centre as the rotating tool holder is not a suitable location to fix wired sensors, and the distance between the tool point and the spindle head was considered to be too large. For the experiments discussed in Chapter 8, in which the Seti-tec éVo Light EDU was used, the sensors were bolted to a small steel mounting block which was attached to the unit's housing. In order to improve the signal transfer between mounting surface and sensor (Theobald et al., 2008), silicon grease was applied between the AE sensor's mounting surface and measuring tip.



**Figure 30: Sensor mounting locations.**

Figure 31 shows a schematic of the data acquisition chain. The dynamometer was connected to a charge amplifier (Kistler 5006), whereas the accelerometers and the AE sensor were connected to dedicated couplers (Kistler 5108A and Kistler 5125B respectively). While the accelerometer couplers were simply used to power the sensors and amplify their outputs, the AE coupler also calculated the Root-Mean-Square (RMS) of the output signal through an in-

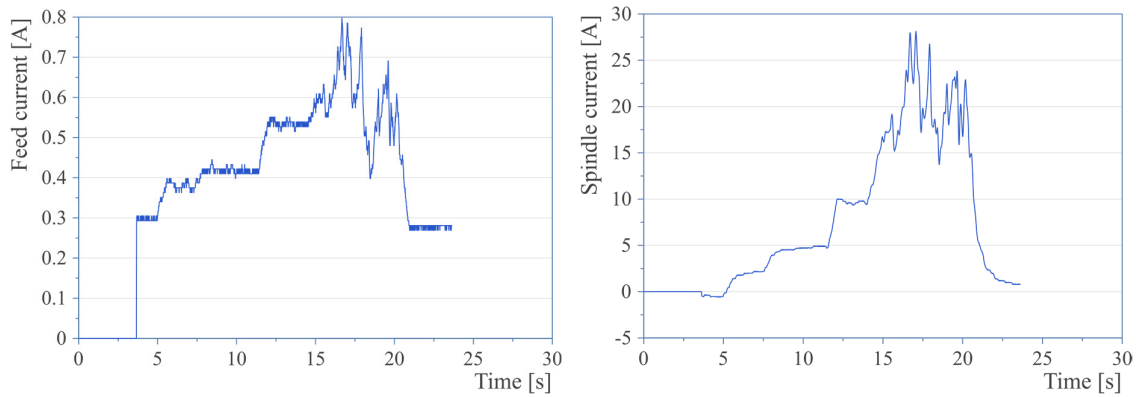
built converter (1.2 ms time constant). The outputs of the charge amplifier and couplers were recorded by a data acquisition card (NI 6356) connected to a computer. The software used for data recording and analysis were Labview and DIAdem, respectively, by National Instruments.



**Figure 31: Data acquisition chain.**

The Seti-tec éVo Light EDU control unit is equipped with a measuring system using current transducers capable of recording the current flowing through the spindle and feed motor controllers. During each drilling cycle, the signals are processed and displayed with an update rate of 100 Hz. An example of the output data from the unit's software is shown in Figure 32. Due to the lack of information available regarding the type and parameters of the various signal processing stages performed on the raw signal, it was decided to modify the data acquisition system in such a way that the output from the current transducers can be directly extracted, prior to any signal processing. This provided three benefits: Firstly, it enabled recording the current signals with substantially higher sampling rates. This allowed for an assessment on the impact of sampling rate on the accuracy and reliability of a process monitoring system. Secondly, it enabled the acquisition and analysis of data prior to tool-workpiece engagement and during tool retraction, something that is not possible with the built-in software as the data is automatically segmented to only include that portion of the drilling cycle during which the cutting edges are engaged with the workpiece. Thirdly, recording all signals via a single data-acquisition system allowed for more straightforward comparisons and correlations between signals recorded by different sensors, thereby reducing timing errors that would have negatively affected the synchronisation between signals.



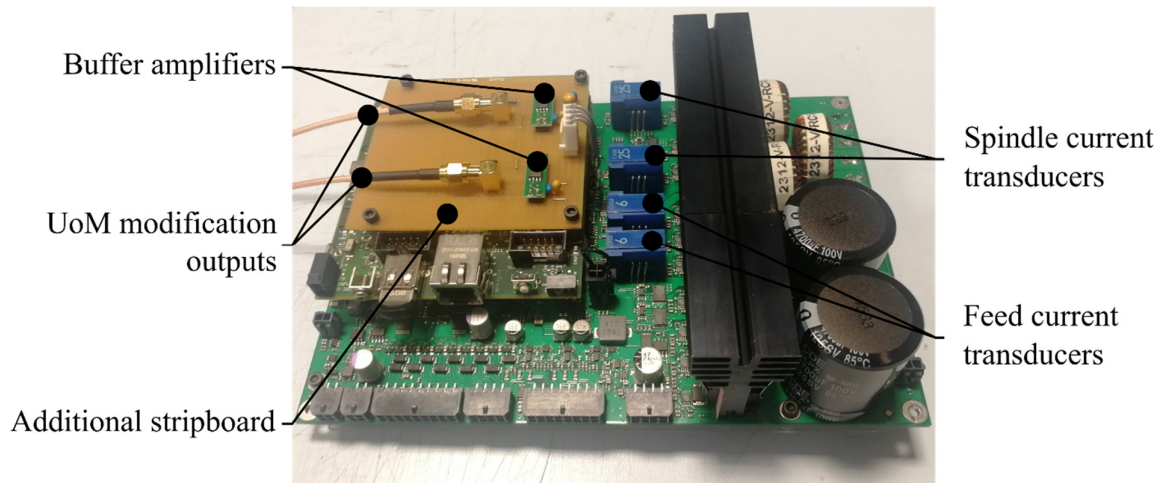


**Figure 32: Feed and spindle current processed signal from Seti-tec software.**

Figure 33 shows the EDU control board after disassembly of the control unit. Inspection of the control board revealed a total of four current transducers, two measuring the current flowing through the spindle motor controller (CASR 25-NP) and two measuring the current flowing through the feed motor controller (CASR 6-NP). Two current transducers are used with each three-phase motor in what is known as the 'two wattmeter' or 'Blondel' configuration, which enables the measurement of total electrical power, regardless of variations in voltage, current and loading. The voltages applied by the controller to two of the motor phase windings are measured with reference to the third phase, and the currents flowing through those windings are measured by the current transducers. Thus, the controller can compute the electrical power applied to the load in order for it to be capable of flexible control schemes such as constant power, speed or torque, given the relationship between those quantities. The mechanical power available at the tool is effectively the electrical power with all the varied losses subtracted, thus it is fair to say that the linear relationship between motor torque and current can be used to good advantage, and each quantity can be derived from the other using the motor's torque constant ( $K_t$ ). For the purpose of indirectly measuring the thrust force and torque, the recording of only one of the motor current's phases was considered sufficient. Thus, the output of one of the current transducers for both the spindle and feed motor was fed to the external data acquisition system.

The voltage signature outputs of the current transducers exhibit exceptionally low impedance; an external data acquisition system with its long cabling would therefore present an additional load to the current transducers which would cause measurement errors, both in the manufacturer's original data acquisition system and the external one. To overcome this issue, a 'buffer' or 'envelope follower' was constructed for each current transducer, using a general purpose operational amplifier (op-amp) exhibiting a high input impedance and a relatively high

current-driving output capability. The output voltage of the buffer accurately follows that of its input (the 'envelope') whilst presenting negligible load to the current transducer and being capable of supplying signals to the external data acquisition system without interference. The outputs of these amplifiers are then fed out of the control unit via two additional connectors, shown in Figure 34. All the additional hardware required for the modification is shown in Figure 33.



**Figure 33: Modification to éVo Light EDU control board.**



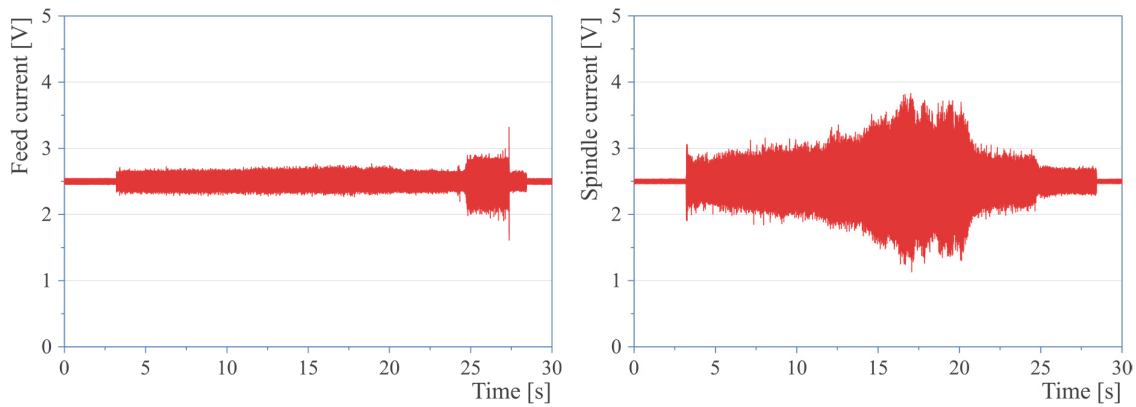
**Figure 34: Additional connectors implemented on the control unit to output spindle and feed current signals.**



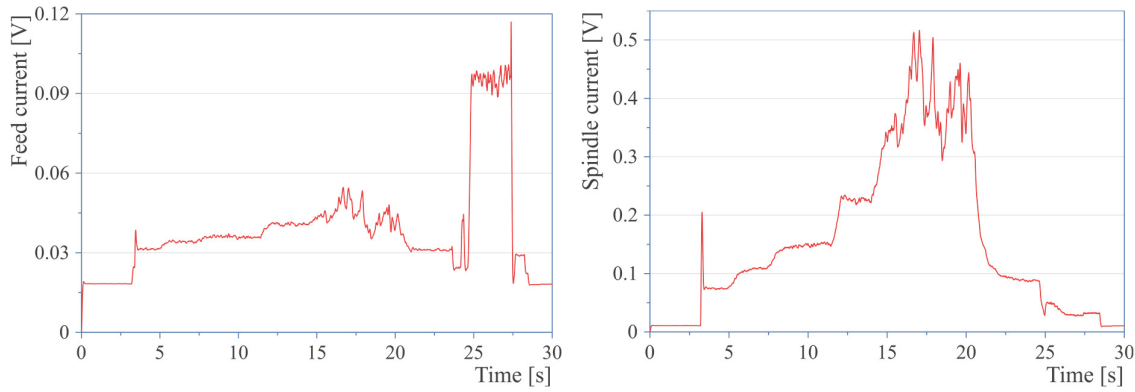
### 3.6 Validation of the bespoke modification on the portable drilling unit

To validate whether the modification carried out on the Seti-tec éVo Light EDU actually does allow for direct measurement of the feed and spindle current flowing through the motor controllers, five boreholes were drilled into a CFRP/Al 7010 stack (thickness 10+10 mm) with the drilling unit, whilst also measuring the thrust force and torque directly using a dynamometer.

The raw current signals were sampled at a rate of 100 kHz for both the feed and spindle motor controllers, via the modified measuring system, are shown in Figure 35. Since these were measured via the modified measuring system presented in section 3.5, these will be referred to as ‘University of Manchester (UoM) signals’ from here onwards. Both the signals were found to oscillate about 2.5 V with an output voltage ranging between 0.345 V and 4.625 V, as specified in the current transducers’ datasheet (LEM, 2015). To allow for comparison with the Seti-tec processed output (i.e. manufacturer’s output), some signal processing operations were performed on the UoM feed and spindle current signals. Firstly, the signals were offset to 0 V. Secondly, a root-mean-square conversion with an interval width of 30 points was performed on the signals, which were subsequently passed through a 5 Hz Butterworth digital low-pass filter. Finally, to allow for a direct comparison, both the UoM feed and spindle current signals were under-sampled to simulate a sampling rate of 100 Hz, which is equal to the display update frequency of the Seti-tec signals. The resulting UoM processed signals are shown in Figure 36.



**Figure 35: UoM raw feed and spindle current signals.**

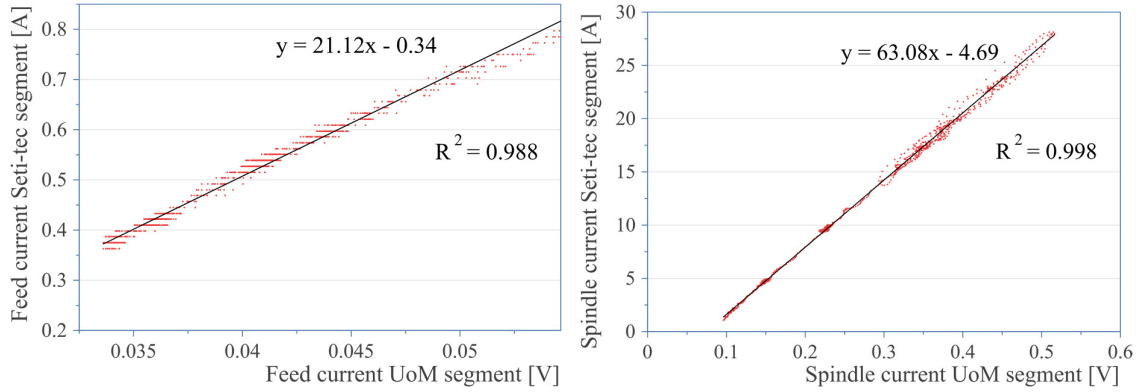


**Figure 36: UoM processed feed and spindle current signals.**

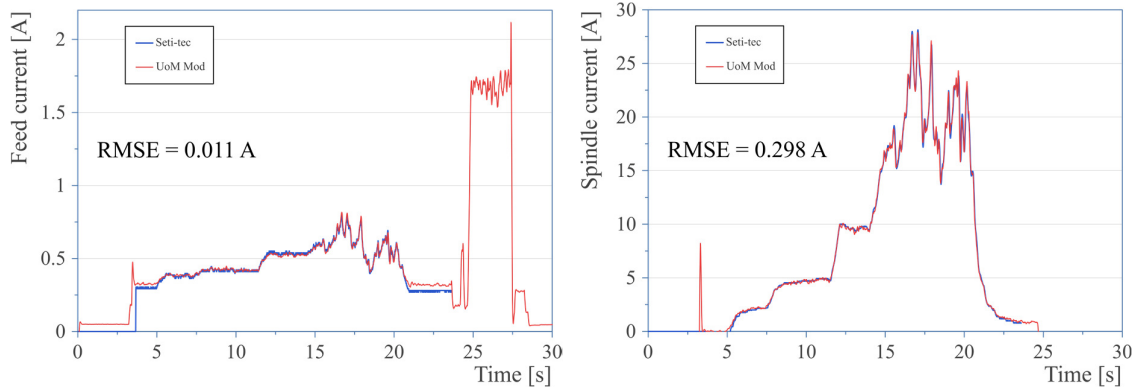
To convert the units of the spindle and current signals from volts to amperes, the Seti-tec output was used as a reference. The processed UoM feed and spindle current (in volts) were plotted against the Seti-tec outputs (in amperes), as shown in Figure 37. It can be observed that both the UoM spindle and feed current signals appear to be correlated linearly to their respective Seti-tec signal. The calculated scaling function for the feed current signal resulted in a lower coefficient of determination ( $R^2$ ) than that calculated for the spindle current signal, which can be explained by the combination of two factors. Firstly, according to the manufacturer's datasheet, the overall accuracy of the current transducer for the feed controller is  $\pm 0.1$  A. Within a drilling cycle, the average measured feed current was approximately 0.5 A, thereby suggesting a considerable source of measurement error for both the Seti-tec and UoM readings. In contrast, the overall accuracy of the current transducer for the spindle controller was  $\pm 0.25$  A, which is substantially smaller than the average measured spindle current (approx. 12 A). Secondly, as shown in Figure 32, the relatively low resolution of the Seti-tec analogue-to-digital conversion resulted in a large quantization error in the feed current signal, which was substantially lower than the spindle current. This would have further reduced the accuracy of the Seti-tec feed current data. The presence of an offset in the case of both the spindle and current scaling functions, see Figure 37, is the result of the Seti-tec system compensating for the current required to keep the electric motor running without a load. The purpose of this is to allow an estimation of the current flowing through the feed and spindle controllers which is necessary for material removal, effectively permitting an indirect estimation of the thrust force and torque.

The derived scaling functions were applied to both the UoM spindle and feed current signals, and the scaled curves are shown in Figure 38. This shows that the scaled UoM curves follow

closely the Seti-tec ones, with a root-mean-square error (RMSE) equivalent to 1.4% and 1.1% of the maximum recorded current for the feed and spindle current signals, respectively.



**Figure 37: UoM feed and spindle currents plotted against Seti-tec outputs.**

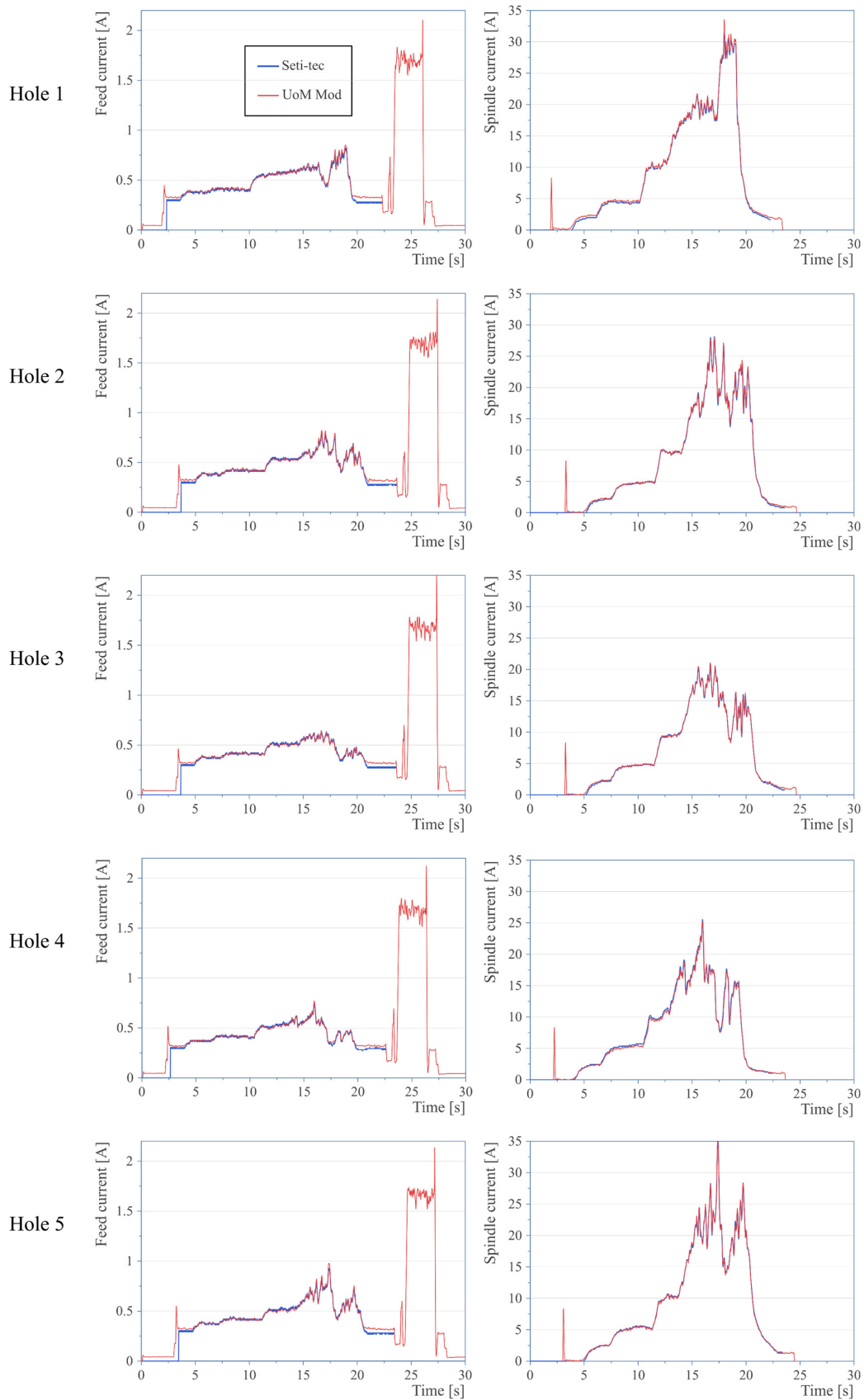


**Figure 38: Scaled UoM feed and spindle currents compared to Seti-tec signals.**

The same procedure was repeated for the remaining four boreholes and the determined coefficients for the various computed linear relations are listed in Table 5. To avoid having to carry out an ad hoc correlation for each individual borehole, a set of standardised linear coefficients were determined by averaging each gradient (m) and y-intercept (q) for all the drilled boreholes. The resulting linear functions were found to be  $y = 21.4x - 0.4$  and  $y = 63.0x - 4.6$  for the feed and spindle current, respectively. These ‘averaged’ linear functions were then used to scale the recorded signals for each of the boreholes drilled. The resulting RMSE between the UoM scaled curves and the reference Seti-tec ones for both the ad hoc and average approach are listed in Table 5, while Figure 39 illustrates the scaled signals using the average approach. As shown by both the numerical and graphical results, the difference observed is relatively small, thus linearly scaling the signals using the standardised average coefficients is believed to be suitable.

**Table 5: Linear coefficients for each borehole and RMSE for both ad hoc and average linear scaling (Seti-tec/UoM).**

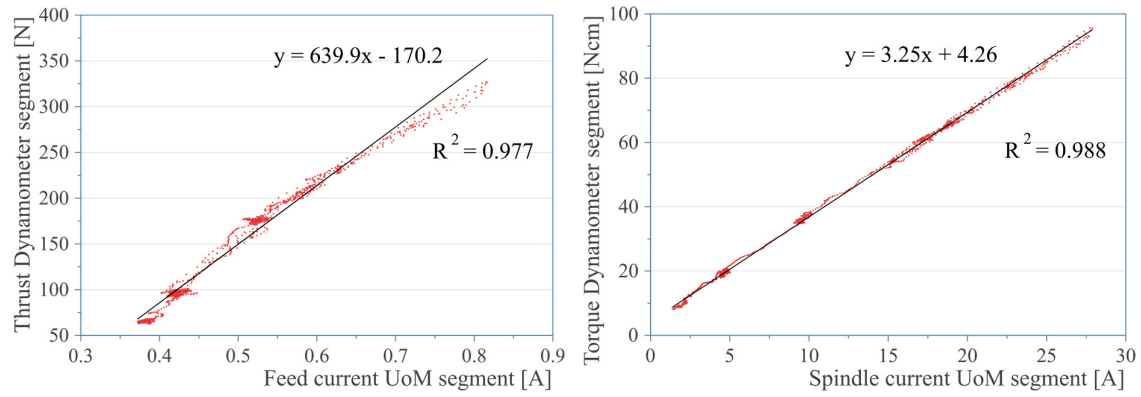
Linear relation coefficients										
	Hole 1		Hole 2		Hole 3		Hole 4		Hole 5	
	m	q	m	q	m	q	m	q	m	q
Feed Current	21.1	-0.3	21.1	-0.3	22.3	-0.4	22.2	-0.4	20.3	-0.3
Spindle current	62.7	-4.8	63.1	-4.7	63.3	-4.7	63.1	-4.4	62.9	-4.5
Root-mean-square error (Amps)										
	Hole 1		Hole 2		Hole 3		Hole 4		Hole 5	
Scaling	Ad hoc	Average	Ad hoc	Average	Ad hoc	Average	Ad hoc	Average	Ad hoc	Average
Feed Current	0.012	0.013	0.011	0.012	0.009	0.010	0.010	0.011	0.011	0.013
Spindle current	0.233	0.340	0.298	0.305	0.175	0.179	0.320	0.415	0.271	0.277



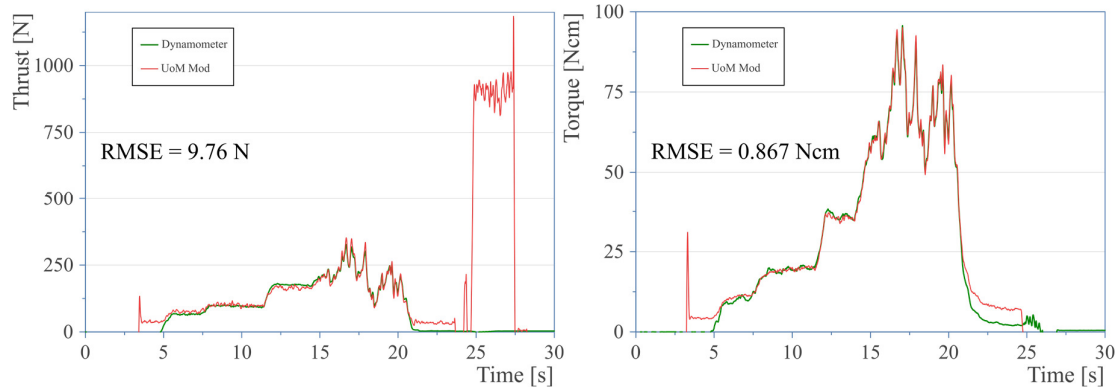
**Figure 39: Feed and spindle currents with average linear scaling.**

After having achieved an adequate scaling for the UoM feed and spindle current signals, a similar assessment was carried out to evaluate the degree of correlation between the motor currents and the thrust force and torque measured by the dynamometer, thereby allowing for an evaluation of the feasibility of indirectly measuring the thrust force and torque by monitoring the currents flowing through the motors' controllers. For this, a similar procedure to the one presented earlier was carried out. Firstly, the thrust and torque signals measured by the dynamometer were processed to exhibit a dynamic behaviour which is comparable to that of the scaled feed and spindle current signals. This enabled an assessment of the correlation between signals recorded by different sensors. Figure 40 shows the correlation between the processed UoM feed and spindle currents and the thrust and torque measured by the dynamometer. It appears that both the UoM spindle and, to a lesser extent, the feed current are correlated linearly to the torque and thrust, which suggests that an indirect estimation of the thrust force and torque based on the current flowing through the motor controller is possible. The computed scaling functions were then applied to both the UoM spindle and feed current signals. Figure 41 shows that the indirectly measured UoM thrust force and torque follow closely the dynamometer's ones, with an RMSE equivalent to 2.7% and 0.9% of the maximum recorded current for the thrust and torque signals, respectively.

Similarly to the correlation between the UoM and Seti-tec motor currents, the linear conversions from motor currents to thrust force and torque was performed by both directly determining the linear coefficients for each borehole and performing a standardised scaling. The applied linear relationships based on the average of the linear coefficients were  $y = 634.6x - 165.3$  and  $y = 3.38x - 3.32$  for the thrust and torque, respectively. The resulting RMSE between the UoM indirectly measured thrust force and torque and the reference dynamometer forces for both the ad hoc and average approach are listed in Table 6. Figure 42 depicts the UoM indirectly measured thrust force and torque obtained using the standardised approach compared to the dynamometer signals. The resulting errors are larger than the equivalent ones for the correlation between UoM and Seti-tec motor currents (Table 5), which can be explained by the fact that in this case the two assessed signals were actually being measured by two fundamentally different sensors (i.e. current transducer vs. piezo-electric dynamometer). Nonetheless, from the results it appears that applying a linear conversion based on the determined standardised linear coefficients is a suitable approach to indirectly measuring the thrust force and torque with reasonable accuracy.



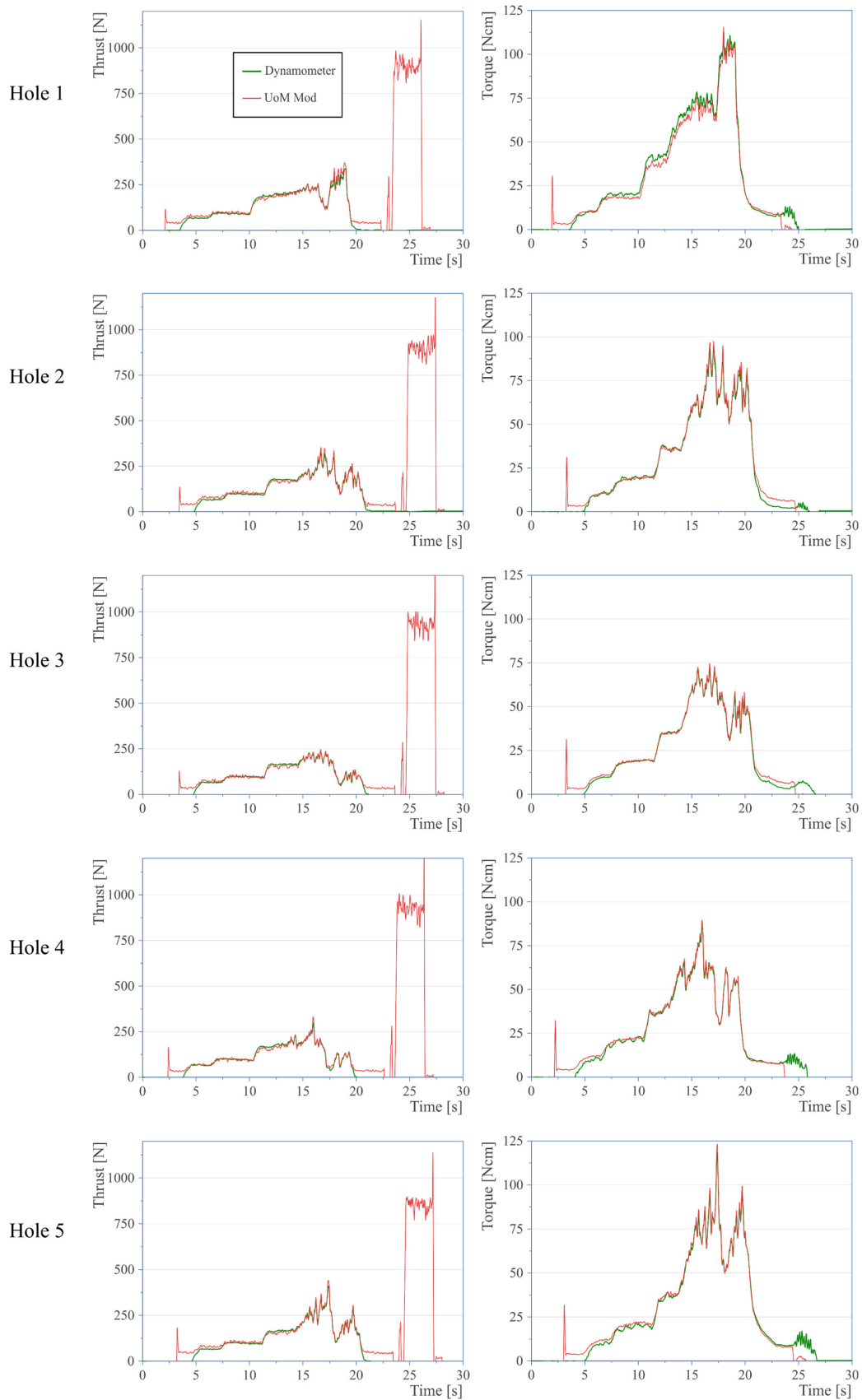
**Figure 40: UoM feed and spindle current plotted against dynamometer thrust force and torque.**



**Figure 41: UoM indirectly measured thrust force and torque compared to dynamometer reference thrust force and torque.**

**Table 6: Linear coefficients for each borehole and RMSE for both ad hoc and average linear scaling (Dynamometer/UoM).**

Linear relation coefficients										
	Hole 1		Hole 2		Hole 3		Hole 4		Hole 5	
	m	q	m	q	m	q	m	q	m	q
Thrust (N)	601.0	-148.7	639.9	-170.2	662.6	-177.1	642.5	-167.1	626.9	-163.3
Torque (Ncm)	3.5	5.4	3.3	4.3	3.4	2.9	3.4	2.4	3.4	1.7
Root-mean-square error										
	Hole 1		Hole 2		Hole 3		Hole 4		Hole 5	
Scaling	Ad hoc	Average	Ad hoc	Average	Ad hoc	Average	Ad hoc	Average	Ad hoc	Average
Thrust (N)	10.7	11.3	9.8	10.0	7.1	7.6	8.5	8.7	9.4	9.6
Torque (Ncm)	1.5	3.4	0.9	1.3	0.7	0.9	1.1	1.3	1.0	1.6



**Figure 42: Thrust and torque current with averaged linear scaling.**

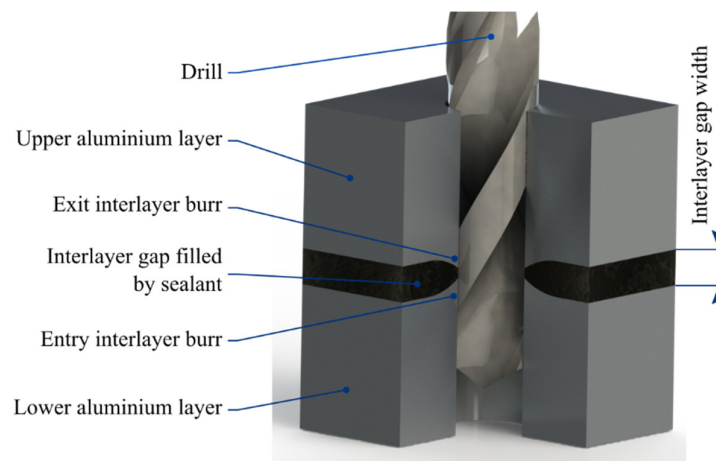


## Chapter 4: Influence of interlayer gap width on interlayer burr formation

The literature review revealed that, although various studies have investigated the interlayer burr formation process, it is still unclear how this is influenced by the interlayer gap width. This aspect is of particular importance for one-way assembly, which demands that the generated interlayer burr fits within the specified tolerance, as no interface deburring operations can be carried out after drilling. Moreover, a fundamental understanding of how the interlayer gap width is affected by the stack clamping force and how it affects borehole quality is essential for determining appropriate parameters for the aerospace stack drilling process, without which other aspects of this research project might not be fully understood. Thus, this chapters aims at establishing a relationship between interlayer gap width and burr height when drilling Aluminium/Aluminium stacks in the presence of sealant at the interface. To achieve this, initially, the correlation between interlayer gap width and clamping load applied is determined and, subsequently, the effect of the interlayer gap on interlayer burr formation is investigated.

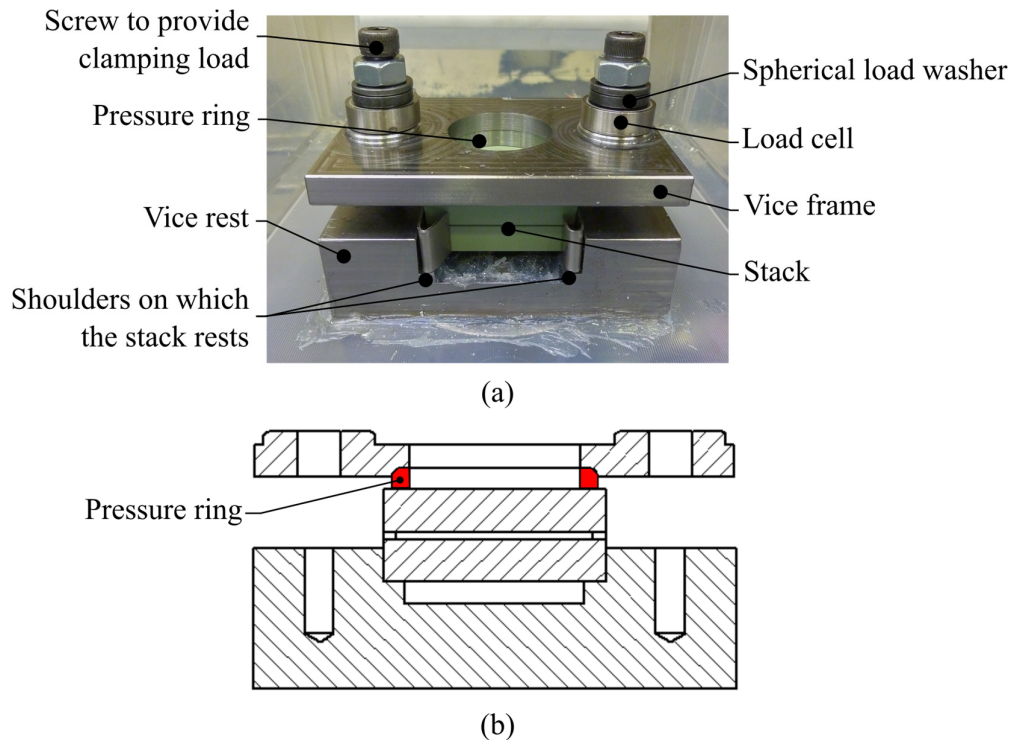
### 4.1 Correlation between interlayer gap width and clamping load

The experiments were carried out on stacks comprising two layers of aluminium 7010-T651, each with a thickness of 10 mm. Figure 43 illustrates the composition of the stack, the definition of the interlayer gap width as well as the location of the exit and entry interlayer burrs.



**Figure 43: Stack composition.**

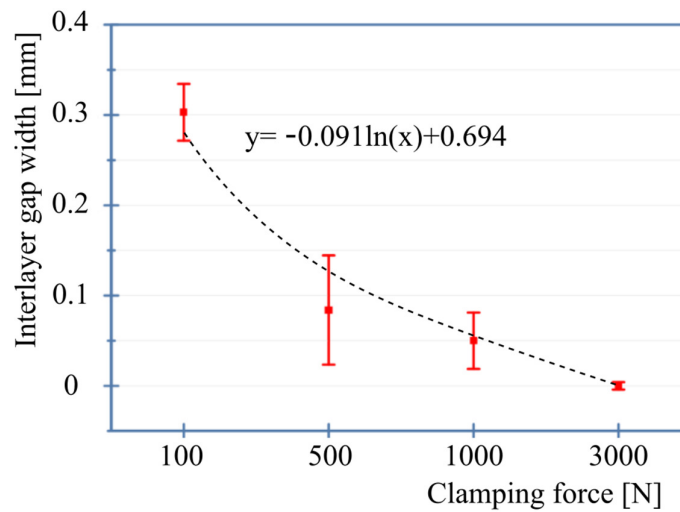
The coupons were clamped using the custom-made vice described in Chapter 3. As this set of experiments was conducted on a standard three-axis vertical machining centre (Takisawa MAC-V3), the upper plate of the vice was modified by adding a recess to accommodate a pressure ring, which was included to mimic the so-called nose piece used in aerospace portable drilling units. Two load cells (Omega LCWD-2K) using a strain indicator (VPG Strain indicator P3) were incorporated into the vice to determine the axial clamping load applied to the stack through the pressure ring when tightening the M8 screws, see Figure 44.



**Figure 44: Vice with load cells and pressure ring used to clamp the stack with pre-set clamping forces; (a) labelled image, (b) cross section view with pressure ring location.**

In order to establish the relationship between clamping load and resultant interlayer gap width, a coordinate measuring machine (LK G90C) was used to determine the actual thickness of the stack, i.e. coupons plus polymeric sealant (PR1782-C12). After having clamped the stack in the vice with a layer of sealant at the interface, the distance between the stack's top and bottom surfaces was determined. Clamping loads ranging from 100 N to 3,000 N were applied, and three different measurements were taken per clamping load, each time removing and reapplying the sealant layer. The thickness of the interlayer gap width was then determined as the difference between the measured total stack thickness (i.e. including sealant layer) and the combined thickness of the two aluminium coupons (i.e. without sealant), which had been determined prior to this test.

The measurements reveal that an increase in clamping load brings about a noticeable reduction in the interlayer gap width, as shown in Figure 45. This can be attributed to sealant movement within the interlayer as well as to some of the sealant being progressively squeezed out of the stack with increasing clamping force. In the case of the smallest clamping load, i.e. 100 N, the gap width was around 0.3 mm, which was reduced to 0.1 mm once the clamping load had been increased to 500 N. When applying the maximum load of 3,000 N, the gap width was reduced to approximately zero, indicating that almost all of the sealant had been squeezed out from the gap. The relationship between clamping load and gap width can be represented by the equation shown in the figure, in which x represents the clamping force width and y the interlayer gap width.



**Figure 45: Interlayer gap width of stack with sealant in relation to clamping force.**

## 4.2 Interlayer burr formation investigation

The drilling experiments were carried out using shims (i.e. thin metal strips serving as spacers) of thicknesses similar to the interlayer gap widths measured when applying clamping loads ranging from 100 N to 3,000 N. These shims served three purposes. Firstly, they made sure that the interlayer gap width could be set to pre-defined values representative of the range of clamping forces investigated (0 mm, 0.1 mm, 0.2 mm, 0.3 mm, 0.4 mm). Secondly, they ensured that no sealant was squeezed out from the interface during the drilling cycle in response to the thrust force, which would have resulted in a change of the interlayer gap width. Thirdly, the presence of shims prevented changes of the interlayer gap width as a result of variations in the amount of sealant applied.

Prior to clamping, a sufficiently large quantity of sealant was applied to the bottom plate of the stack to cover 80-90% of the plate's area, and two narrow metal shims were placed in between the two layers along two opposite edges of the stack. The stack was then placed inside the vice and the two screws connecting the vice's rest and frame were tightened to provide the total clamping load. One borehole was then drilled at the centre of each coupon. The drilling tools used were two-fluted twist drills manufactured by ProCorp/Sandvik with a diameter of 12.7 mm (specifications listed on Table 3, page 73). The procedure was repeated using shims of different thicknesses to represent different interlayer gap widths. Two coupons were drilled for each pre-set interlayer gap.

After separation, the plates were washed in dichloromethane for around 60 seconds, which was sufficient to dissolve the sealant without having to apply any force to the part, thereby potentially damaging the burr. It was decided to measure the height of the exit interlayer burr, i.e. the burr on the bottom surface of the top layer, which is considered the main contributor to the overall interlayer burr formation in stack drilling (Zhu et al., 2018).

A visual assessment of the scan profiles obtained from the contactless profilometer revealed that a burr of traditional shape, i.e. a ridge of material adjacent to the borehole wall and protruding out from the surrounding material, was only present in a very few of the samples, most commonly those which were drilled without pre-set interlayer gap. For the majority of the samples, a much less uniform accumulation of material of varying height and width around the borehole was observed. In some cases there was actually no accumulation of material whatsoever but a rounded off borehole edge, suggesting that the removal of some material must have taken place. This removal was particularly noticed in the case of boreholes that were drilled with larger interlayer gaps, as the borehole edge profiles in Figure 46 show.

This made it very difficult to quantify any burr height, because as defined by ISO 13715 (International Standards Organisation, 2017) and Ko and Dornfeld (1991) a burr is a protruding feature, and in many cases the only protruding features identified were bulges of material in the vicinity of the borehole, but not directly located at the edge. The graph shown in Figure 47 therefore refers to a 'maximum surface level' rather than a burr height, in order to quantify the maximum height of any material accumulation around the borehole, but not necessarily directly adjacent to it, and protruding out from the original workpiece surface. From the graph it can clearly be seen how actual burrs were mainly measured around boreholes that were drilled without pre-set interlayer gap. In contrast, for the other experiments the recorded maximum

surface levels are quite constant and could well be a measure of the surface roughness of the shot-peened coupons as opposed to that of a burr formed on the borehole edge.

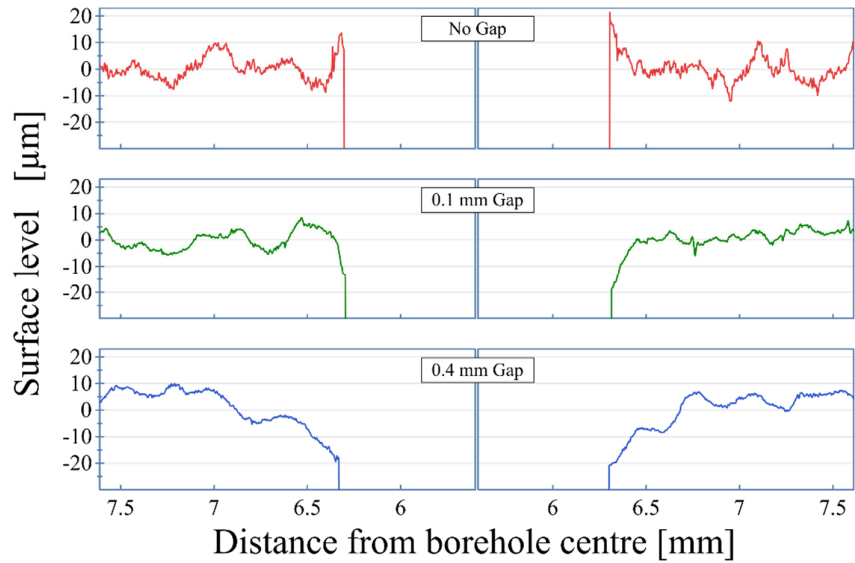


Figure 46: Typical borehole edge profiles when drilling stacks with different interlayer gap widths.

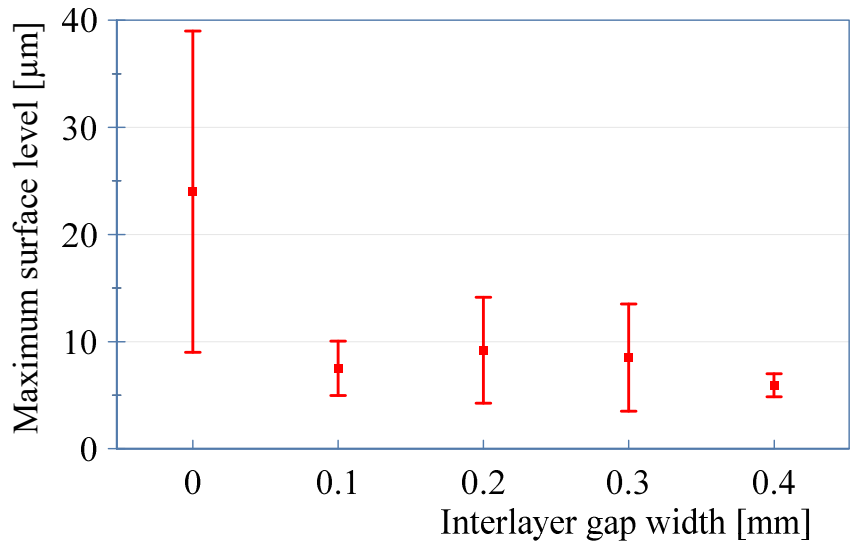
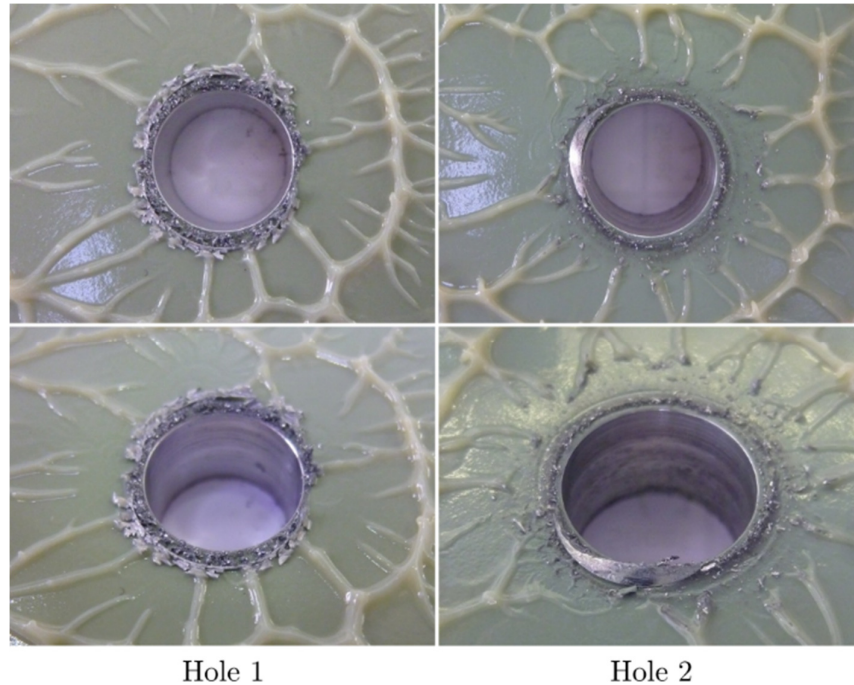


Figure 47: Average maximum surface level with different pre-set interlayer gap widths.

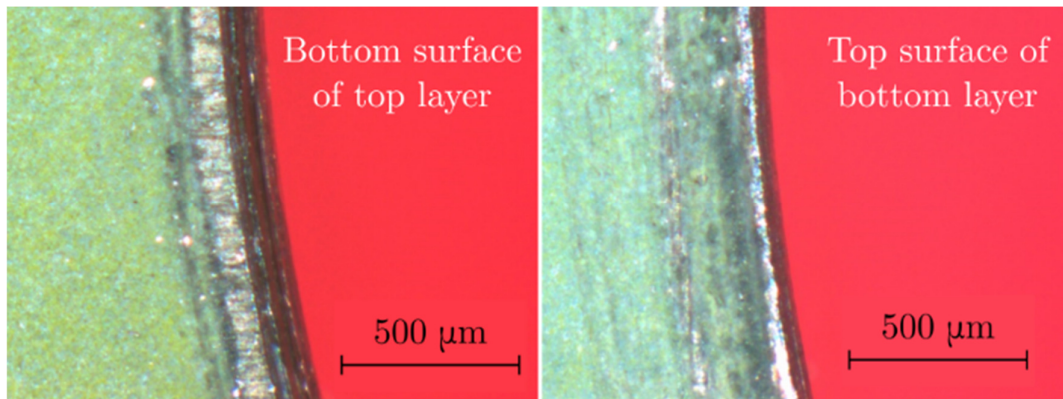
The separation of the plates after drilling often revealed significant swarf ingress in the interlayer gap, as can be seen in Figure 48, which shows the coupon's bottom surface of the top layer around two boreholes drilled with an interlayer gap width of 0.3 mm. A large amount of chips of varying size, ranging from tiny microscopic particles to large chip segments, accumulated around the borehole on both the top and bottom plate. The largest portion of the

swarf was typically located near the borehole edge, but in many cases smaller chip particles were found up to several millimetres away from the hole. Although it is reasonable to assume that some spreading of the swarf took place during the separation of the two plates – these were pulled apart in opposite directions – the extent of this cannot be quantified.



**Figure 48: Accumulation of swarf around the borehole on the bottom surface of the top layer (interlayer gap width 0.3 mm).**

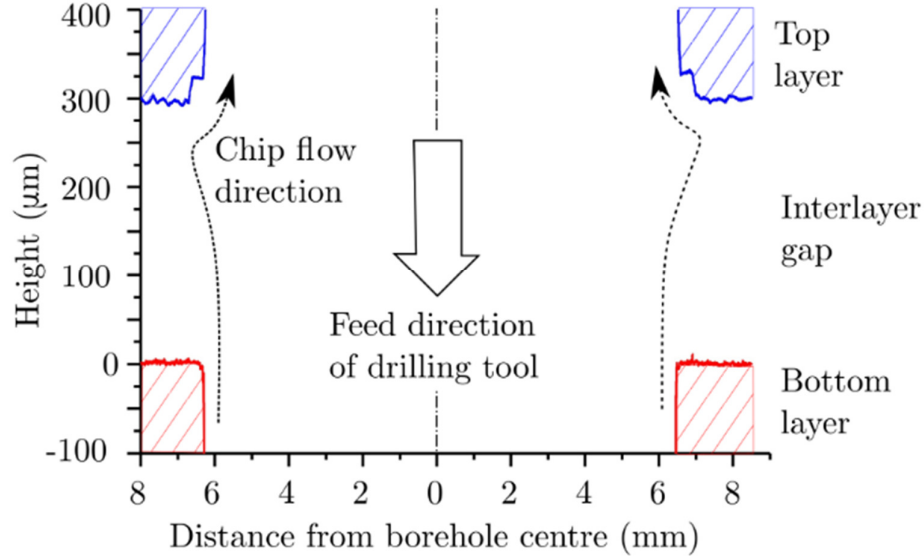
Based on a visual assessment of the boreholes using an optical microscope, an example of which is shown in Figure 49, it appears that some abrasive action must have taken place around the material adjacent to the hole edges. From the images it can be seen how the area adjacent to the borehole is covered with small scratch marks, which are believed to be the result of chips having penetrated into the interlayer gap and then being dragged around the hole by the rotation of the drill. In addition, substantial workpiece material abrasion at the borehole edge has occurred on the bottom surface of the upper layer, to the extent that the edge of the hole has the appearance of a chamfer or fillet. This implies the presence of considerable pressure between chips and workpiece material, and it is possible that the elevated process temperatures will have promoted this abrasive action as a result of thermal softening of the aluminium. It is thus believed that chip ingress and subsequent chip movement in the stack interface is the reason for the almost complete absence of any traditional burr in the case of pre-set interlayer gaps.



**Figure 49: Surface damage of the material adjacent to the borehole for both interlayer surfaces.**

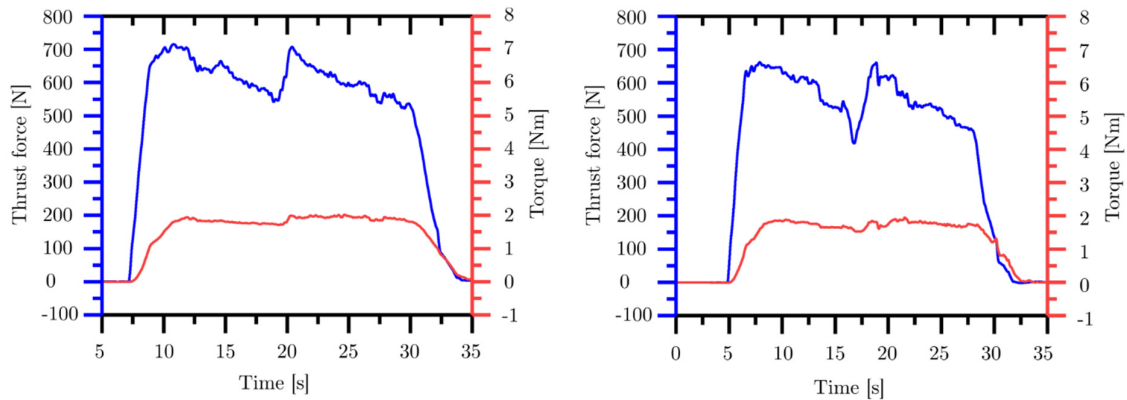
To gain a better understanding of the cause for this material abrasion around the borehole edges, the extent of interlayer damage at both the upper and lower interlayer surfaces was assessed in more detail. Figure 50 shows the profile scans of one of the holes drilled. The two blue curves represent the edge profile of the exit of the borehole on the bottom surface of the top layer, whereas the red curves represent the edge profile at the hole entrance on the top surface of the bottom layer. It can clearly be seen that the two profiles show significant differences, inasmuch that the borehole edge on the bottom surface of the top plate has been completely rounded off. The radii along the edges of these holes were measured to be approximately 50-70  $\mu\text{m}$ . The step in the blue profile, adjacent to the borehole edge, coincides with the clearly visible dark ring around the hole shown in Figure 49. The borehole's edge in the bottom plate, despite some rounding, exhibits a noticeably smaller radius, of approximately 10-15  $\mu\text{m}$ . Similar differences were observed for all holes inspected, and these are believed to be a result of the direction of chip flow (indicated by the two dashed lines). With the tool moving into the stack, the chips flow in opposite direction to the feed, i.e. in this case upwards. As a consequence, they will flow over the borehole's edge in the bottom plate, thereby causing some abrasion and edge rounding. They will then flow further upwards, where some of them appear to get caught by the borehole edge on the underside of the top plate. Some will even manage to penetrate into the interlayer gap, where they are then being spun around by the rotating tool and, as a result, scrape over the interlayer surfaces, leaving behind scratch marks and, eventually, grinding away the burr that might have formed during tool exit from the top layer.





**Figure 50: Profiles of the interlayer surfaces in close proximity to the borehole (interlayer gap width 0.3 mm).**

The thrust force and torque were consulted to find further evidence of this hypothesis. Typical examples of these are shown in Figure 51. The point where the drill reaches the stack interface, i.e. where it exits the top layer and is about to enter the bottom plate, can be clearly identified by the abrupt drop and then sudden rise in the thrust force, particularly in the case of a stack with a 0.3 mm interlayer gap. An increase in the torque signal dynamics when the tool is engaged in the bottom layer was also observed, in particular when drilling a stack with a 0.3 mm interlayer gap. This is believed to be in response to the chip ingress in the interlayer gap and the scraping of the chips over the interlayer surfaces, as a result of the rotating motion of the tool. In contrast, a change in the torque amplitude could not be observed. Neither were there any changes with regards to the thrust force.



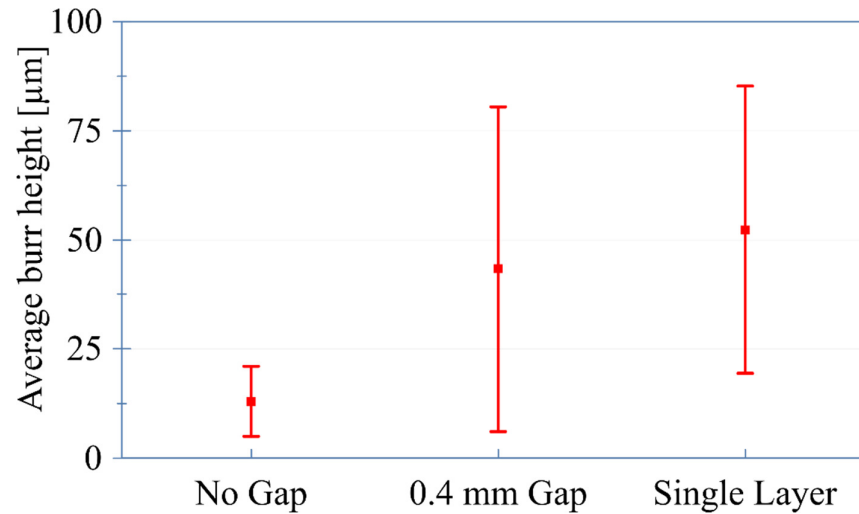
**Figure 51: Thrust and torque recorded when drilling a stack with different pre-set interlayer gap widths; no interlayer gap (left) and with 0.3 mm interlayer gap width (right).**



As a result of the drilling tool geometry and the cutting conditions utilised, both of which were in-line with current industrial practice, it was noticed that the chips generated were relatively thin, which would have made it easier for them to enter the interlayer gap. The thin chips also resulted in extensive chip nesting, which would have constrained the chip flow along the drill flutes, thereby increasing the chance of chips becoming entrapped in the interlayer gap and, consequently, abrading the newly formed burr.

To further validate the assumption made in the previous section, a second set of experiments was conducted, in which the drilling cycle was stopped once the tool's cutting edges got fully engaged with the second stack layer. The aim was to replicate the interval during which the exit interlayer burr is fully formed, i.e. drilling of top layer plus initial engagement with the bottom layer, whilst preventing any potential removal of the freshly formed burr by drilling through the bottom layer thereafter. This set of experiments was carried out using a stack without pre-set interlayer gap (i.e. gap width 0 mm) and one with a 0.4 mm gap width. In addition to this, a further experiment was conducted using a single layer, to allow for the comparison between a constrained (i.e. stack interlayer) and unconstrained (i.e. single layer) condition.

In contrast to the burrs observed when drilling through an entire stack, the burrs produced when stopping the drill's progression shortly after entering the bottom layer exhibited a more traditional profile. Moreover, not continuing drilling through the bottom plate also revealed that the presence of a pre-set interlayer gap results in a substantial increase in interlayer burr height, see Figure 52. Drilling a single layer, thereby creating the largest possible "interlayer" gap width, resulted in the largest exit burr. These observations confirm that during the previous experiments interlayer burrs were indeed formed and that these grew in height with the interlayer gap width, which is in agreement with previous research (Jie, 2013; Melkote et al., 2010), but that these burrs were then eroded away by the upwards-travelling chips during the subsequent drilling of the bottom layer.



**Figure 52: Burr height measurements for drilling of top stack layer plus initial engagement with bottom stack layer at different interface conditions.**

### 4.3 Summary

The research presented in this chapter provides an understanding of the influence of interlayer gap width on interlayer burr formation when drilling Aluminium/Aluminium stacks with sealant being present at the interface. Pre-load clamping of stacks causes the sealant to be squeezed out from the stack interface. Increasing the clamping load results in an increase in the amount of sealant being squeezed out and, thus, in a reduction of the interlayer gap width. For the small-sized coupons used, a clamping force of 3,000 N was sufficient to reduce the interlayer gap width to zero, indicating that almost all sealant had been displaced.

In drilling, the size of the burr strongly depends on the space available for the burr to protrude into. Introducing a pre-set interlayer gap to a stack results in a substantial increase in interlayer burr height as opposed to drilling a stack with no interlayer gap. Similarly, drilling single layers results in larger exit burrs when compared to the interlayer burrs formed in stacks drilled with a pre-set interlayer gap. The presence of an interlayer gap can however be detrimental to the burr size, as a result of two phenomena: the sliding action of the upwards-travelling chips over the borehole edges, in combination with some of the chips entering the gap and being spun around by the rotating tool. This abrasion is considerable at the borehole edge of the upper layer (i.e. exit interlayer burr), but less pronounced at the edge of the bottom layer (i.e. entry interlayer burr). This is attributed to the fact that the former represents a greater obstacle to the chip flow and, hence, experiences a more intimate workpiece-chip contact. The abrasive action of the chips intensifies with an increase in the interlayer gap width, as this provides more space

available for the chips to enter the interface and, thus, erode the burr. Hence, larger interlayer gap widths can not only result in the complete removal of the interlayer burr, but can also lead to a substantial rounding of the borehole edge, which could jeopardise the quality of the workpiece as it affects the geometry of the borehole.

## Chapter 5: Influence of tool point angle and interlayer gap width on interface quality

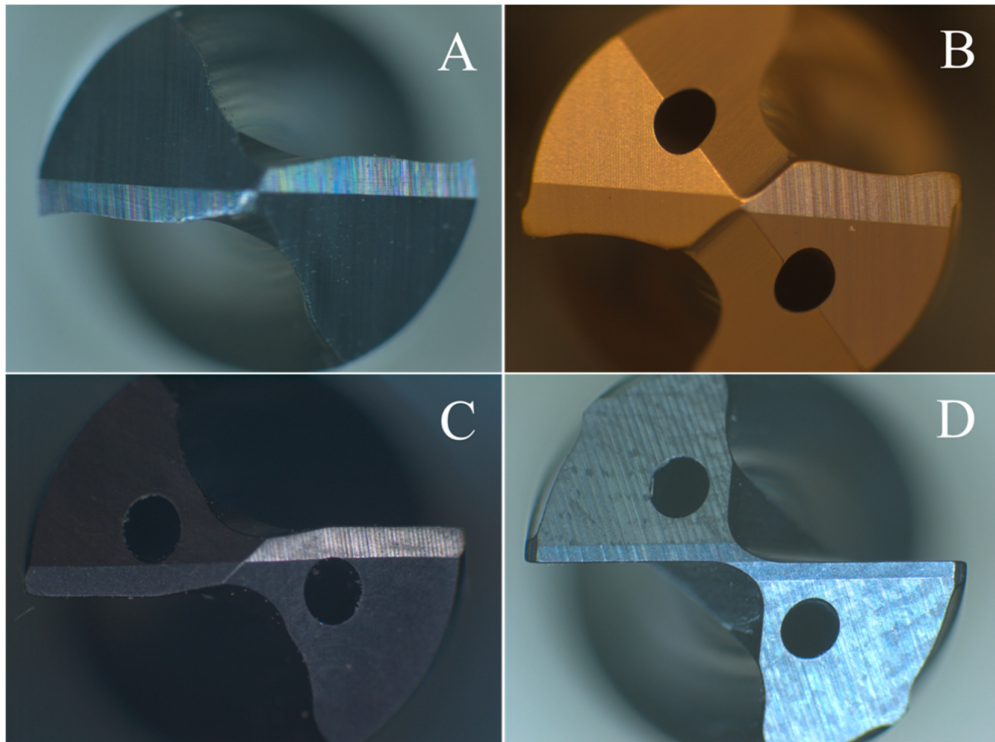
As evidenced by the literature review and the research presented in the previous chapter, drilling of a stack's interface region, i.e. when the tool's cutting edges are simultaneously engaged with different stack layers, is considered to be a highly complex operation. Two factors that directly affect interface drilling are the tool's point angle and the interlayer gap width, as these determine the distance of travel along the tool's axis over which the drill's cutting edges are simultaneously engaged in both the materials. To investigate the impact of these two parameters on borehole quality, with a focus at the interface region, several experiments were conducted, the results of which are presented in this chapter.

### 5.1 Influence of tool point angle on CFRP interface quality

The experiments were carried out on CFRP/Titanium stacks, with the CFRP layer on top. The thicknesses of the CFRP throughout all experiments was 10.4 mm; the thickness of the titanium layer was 10 mm for the first set of experiments, where the focus was on the impact of tool point angle on interlayer borehole quality, and 5 mm for the second set, which focused on the impact of interlayer gap size on interlayer damage. The motivation for reducing the thickness originated from the research presented in the previous chapter, where it was observed that the presence of very large interlayer gaps (in excess of 0.1 mm) resulted in substantial damage at the interface. Bearing in mind that the previous research was carried out on Aluminium/Aluminium stacks, it was assumed that the drilling of CFRP/Titanium stacks would have led to significantly more damage, as a result of the softer nature of the top layer, in this case CFRP, and the considerably harder and more abrasive nature of the chips produced when drilling into the bottom layer, in this case titanium. In order to limit the abrasion of the CFRP by the titanium chips and thus prevent excessive damage to occur on the top layer, it was decided to significantly reduce (by 50%) the amount of titanium chips flowing through the existing borehole by halving the thickness of the titanium layer to 5 mm.

In the first set of experiments, two-fluted tungsten carbide twist drills with four different geometries were used. Figure 53 shows images of their tip geometries, and Table 7 lists the tools specifications. These tool geometries were selected in order to cover the widest possible range of point angles whilst maintaining other important geometric features, such as for

example their helix angle and point geometry, as closely as possible. The observations made by Shyha et al. (2011) gave reason to believe that the different coating conditions were not going to affect the resulting borehole quality. For each tool geometry, three drills were used. Throughout the tests, tool usage was limited to only a very small number of boreholes (9) to ensure that tool wear did not reach a level where it would noticeably affect cutting performance. Nonetheless, the extent of tool wear was regularly checked using an optical microscope (Jenoptik C10 Plus). For reasons of comparability it was decided to run all drilling tests with one set of cutting parameters.



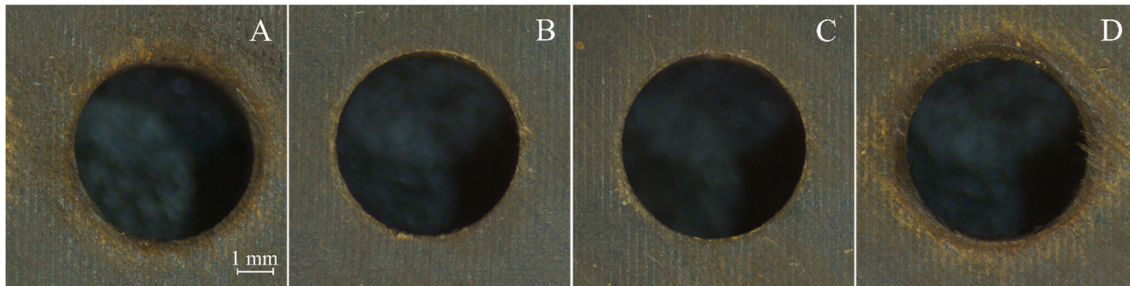
**Figure 53: Tip geometries of the tools used in the drilling tests.**

**Table 7: Workpiece and tooling details.**

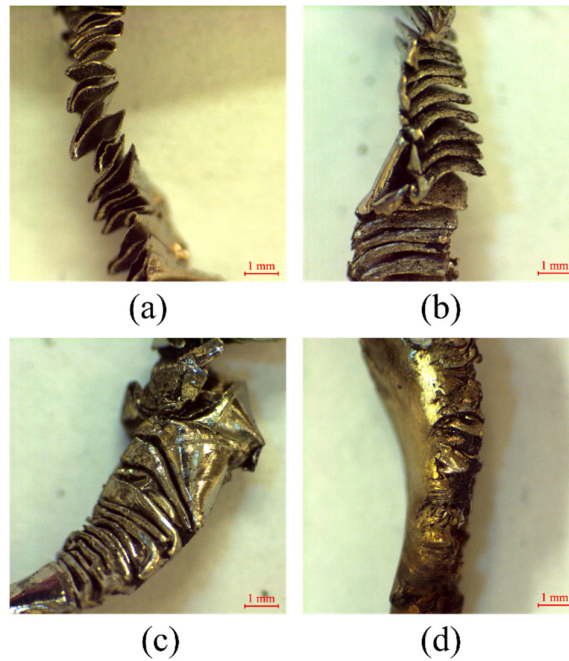
Stack combination	Tool Manufacturer	Tool Coating	Tool Geometry	Cutting speed (m/min)	Feed rate (mm/rev)
CFRP/Ti (10+10/5 mm)	Walter	Uncoated	Ø6 mm, 118° point, 31. 5° helix, enlarged chip flutes, four-facet with notches	40	0.1
	Walter	TiAlCrN	Ø6 mm, 140° point, 30° helix, standard chip flutes, six-facet	40	0.1
	Walter	TiAlN	Ø6 mm, 150° point, 30° helix, enlarged chip flutes, four-facet with notches	40	0.1
	Walter	TiAlN	Ø6 mm, 180° point, 30° helix, enlarged chip flutes, four-facet with notches	40	0.1

Figure 54 shows a typical example of the interlayer (i.e. exit) surface of the CFRP layer, for the four different tool geometries under investigation. The first observation to be made is that the width of the damage zone around the borehole is fairly uniform, regardless of the tool geometry. This is in contrast to drilling single layer unidirectional CFRP, where the damage zone typically exhibits an elliptical shape, with the main extension in the direction of the fibres, as observed by Fu et al. (2018). Moreover, the appearance of the damage is noticeably different to that resulting from drilling single layer CFRP, so much so that the colour of the damage zone indicates thermal degradation rather than purely mechanical damage, e.g. delamination or fibre pull-out. This is due to the fact that the majority of the damage observed in this experiment is not caused by the cutting of the CFRP, but is a result of three phenomena related to the subsequent drilling of the titanium layer underneath the CFRP. Firstly, as observed by both Xu and El Mansori (2016) and Brinksmeier and Janssen (2002), the upwards-travelling titanium chips not only cause extensive erosion due to their shape and sharp serrated edges, see Figure 55, but they also contribute to thermal damage, as part of the heat stored within the chips is released to the CFRP layer surrounding the tool. Secondly, the cutting heat generated when the drill begins to engage in the titanium layer, illustrated as stage 1 in Figure 56, does not disperse into the titanium due to its poor thermal conductivity, but instead accumulates at the stack interface. A portion of this heat then migrates into the CFRP layer, thereby causing thermal softening and degradation of the matrix. The relatively higher thermal conductivity of the tool material (80 W/mK for cemented tungsten carbide, as opposed to 7 W/mK for titanium) makes it likely that the cutting tool provides an additional passageway for some of the cutting heat to

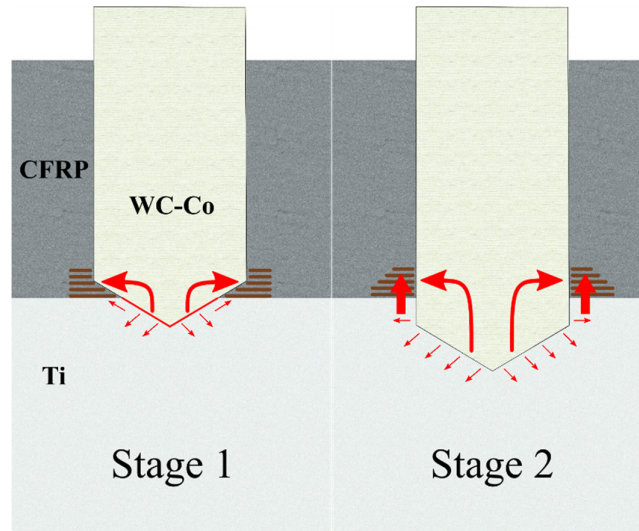
migrate into the CFRP. Once the drill tip is fully engaged in the titanium layer, illustrated as stage 2 in Figure 56, a significant portion of the cutting heat is still transferred into the underside of the CFRP layer, both via the tool and directly at the periphery of the borehole. Lastly, as a result of the high temperatures generated when drilling the titanium, the tool experiences thermal expansion, which causes its margins to progressively rub over the already drilled CFRP borehole surface, thus promoting both abrasive and thermal damage.



**Figure 54: CFRP interface damage of the holes drilled using tools with different geometries.**



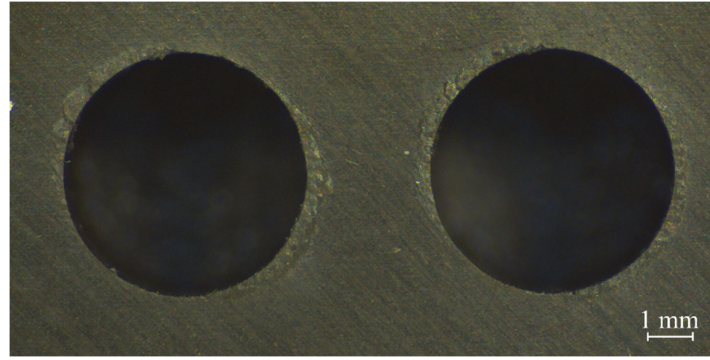
**Figure 55: Titanium chips formed by different tool geometries; (a) tool B; (b) tool C; (c) tool A; (d) tool D.**



**Figure 56: Accumulation of cutting heat at CFRP interface and heat migration from the titanium layer into the CFRP layer.**

To provide further evidence for the aforementioned explanations, some boreholes were drilled into a CFRP/CFRP stack, where the tool was retracted once its cutting edges had fully broken through the upper layer. This scenario was designed in order to replicate that part of the CFRP/Titanium stack drilling process where the drill is only engaged with the top CFRP layer, thereby eliminating any detrimental effect that might arise from the drill's engagement with the bottom titanium layer whilst at the same time providing support to the top CFRP layer. The bottom surfaces of the boreholes drilled with this setup, two of which are shown in Figure 57, exhibit damage whose width is not uniform but instead extends in the direction of the fibres (at 45° in this case). Moreover, the damage area does not show any of the scratches or burn marks observed before when drilling CFRP/Titanium stacks. These two observations provide evidence that the thermal damage observed in Figure 54 is indeed to be attributed to that part of the drilling cycle that occurred after the tool had completed drilling the top composite layer and had started to penetrate into the lower titanium layer.





**Figure 57: Interface damage on the top layer of CFRP/CFRP stack.**

A second observation that can be made in connection with Figure 54 is that the boreholes drilled with tools A ( $118^\circ$  point angle) and D ( $180^\circ$  point angle) exhibit significantly larger composite interface surface damage than those drilled with tools C ( $150^\circ$  point angle) and, to a slightly larger extent, tools B ( $140^\circ$  point angle). The corresponding damage factors were found to be 1.29, 1.14, 1.16 and 1.50 for tool geometries A, B, C and D, respectively.

Heisel and Pfeifroth (2012) observed that an increase in point angle leads to an increase in exit damage when drilling CFRP, which they attribute to the greater chip thickness and the higher forces at the periphery of the tools. With regards to this research, looking at the results obtained from tools B, C and D, the difference in the extent of damage on the CFRP layer at the stack interface is in agreement with Heisel and Pfeifroth, inasmuch that an increase in tool point angle increases the extent of damage. However, tools A do not follow this trend, as the damage recorded is significantly larger than that observed for tools B and C. This suggests that another phenomenon must be affecting the outcome. Since the research conducted by Heisel and Pfeifroth was only concerned with drilling single layer CFRP, the results obtained from this research indicate that the introduction of a titanium layer underneath the CFRP has a profound impact on the interlayer borehole quality. This can be related to the fact that the drilling of titanium is characterised by the generation of considerable heat energy that as a result of the material's poor thermal conductivity remains in the vicinity of the borehole. Part of this heat, as alluded to before, migrates into the CFRP layer, where it causes substantial thermal damage. The tool point angle directly affects the amount of cutting heat generated, inasmuch that a decrease in tool point angle results in an increase in the length of the drill's cutting edges and, consequently, an increase in the drilling torque and cutting temperature. Further to this, the tool point angle also affects the chip shape, which again is attributable to the change in cutting edge length. An increase in the tool point angle will reduce chip width but increase chip thickness,

whereas a decrease will lead to a thinner but wider chip. The images taken of the chips, as well as the torque signals recorded, clearly demonstrate that both extremes, i.e. very wide but thin as well as narrow and thick chips, are difficult to evacuate from the borehole through the drill's chip flutes. The shapes of the chips collected when using tools B and C, see Figure 55 (a) and (b), exhibit either a much tighter fold-up or are severely crushed and/or compressed, which suggests that these chips were exposed to substantial compressive forces during the evacuation process through the drill's flutes. This is supported by the recorded torque curves, see Figure 58. In the case of tools A and D, a strong rise in amplitude combined with a rise in fluctuation towards the latter part of the drilling through the titanium layer indicate significant chip jamming. The torque curves for tools B and C instead show a smooth and stable torque amplitude, suggesting that the flow of chips was hardly obstructed. As a consequence of the obstructed chip flow in the cases of tools A and D, which meant that the chips resided within the drill's chip flutes for a considerably longer period of time, a relatively larger part of the heat stored within the chips – compared to the scenario characterised by a smooth chip flow – was released to their surroundings, i.e. the tool and the neighbouring borehole material, the upper part of which was CFRP. Moreover, the movement of densely compacted chips within the drill flutes would have resulted in strong friction between chip, tool and borehole, which would have caused additional heat to be generated, thereby further increasing the thermal damage on the CFRP layer.

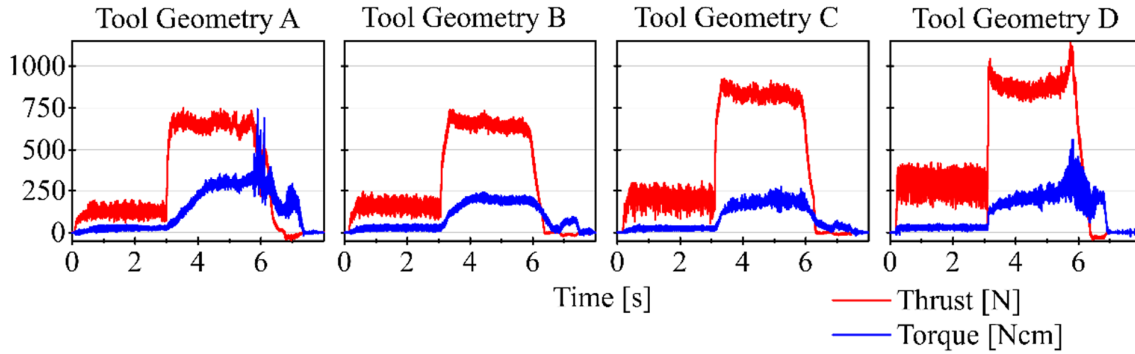
For all the assessed tools, the thrust force and torque produced when drilling CFRP were found to be significantly lower than those recorded when drilling titanium, which can be attributed to the softness of the former and, therefore, the lower cutting energy required for material removal. The results also show that tools exhibiting smaller point angles generated a larger torque, which is the result of the increase in cutting edge length with decreasing point angle. It was also observed that the change in thrust force and torque during transition from CFRP to titanium becomes more abrupt as the drill point angle increases. This is due to the fact that larger point angles result in shorter interface drilling times, i.e. the time during which the tool's cutting edges are simultaneously engaged in the cutting of both the upper and lower layer (see Figure 56, stage 1), and during which the forces generated are a combination of the cutting of the two different materials. This was also found to be the reason why the rate of change of the thrust force and torque as a result of tool-workpiece engagement and disengagement is larger with an increase in drill point angle. When using tools D and – to a lesser extent – tools B and C the thrust force exhibits its highest amplitude during the initial engagement with the titanium

layer, after which it gradually decreases. This can be explained by the untwisting of the tool during initial engagement with the workpiece through the chisel edge, which results in a slight elongation and, thus, a sudden increase in thrust force (Hoff, 1986). This is then followed by a slight relaxation as a result of the system comprising tool, workpiece and machine tool reaching equilibrium, bringing with it a shortening of the drilling tool and, consequently, a drop in thrust force (Spur, 1961). Another factor that would have contributed to the reduction in thrust force is the increase in cutting temperature with an increase in drilling depth, leading to thermal softening of the titanium, as suggested by Zeilmann and Weingaertner (2006).

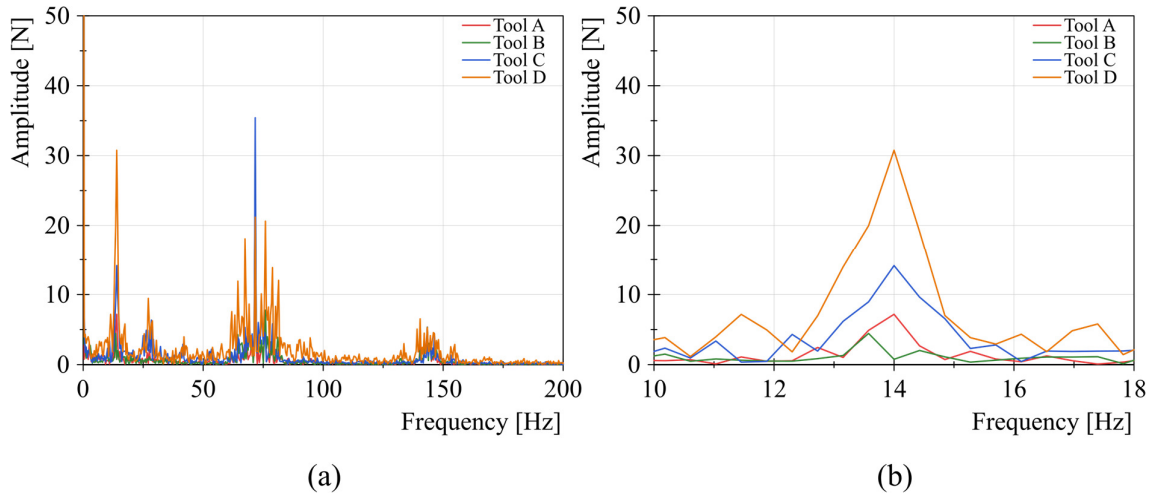
Cutting of the CFRP was characterised by strong fluctuations in the thrust force, which is attributable to the stacked nature of the material. Considering the interfaces between adjacent plies as soft spots, the engagement of the tool tip with these soft spots results in an instantaneous decrease in the thrust force, as the tool tip moves from one unidirectional ply to the next. The results obtained from this research suggest that there is a relationship between the tool point angle and the extent of which the thrust force fluctuates whilst the drill is penetrating through the CFRP material, such that the amplitude of these fluctuations was higher for tools with larger point angles. This can be explained by the fact that the point angle dictates the number of ply interfaces (i.e. soft spots) that the tool tip is engaged with at any one time. In the case of tools D ( $180^\circ$  point angle) the tip is engaged with only one single ply interface, whereas the tip of tool A ( $118^\circ$  point angle, resulting in a tip height of approximately 1.8 mm) is simultaneously engaged with up to 7 plies.

In order to substantiate this claim, the thrust force signals recorded during a period of the drilling cycle where the tool tip was fully engaged in the material were analysed in the frequency domain, by conducting a fast Fourier transform. The results are shown in Figure 59 (a), looking at a frequency range of 0 to 200 Hz, and Figure 59 (b), which zooms in to a range around the dominant peak at 14 Hz, which is the ply engagement frequency. This corresponds to a period of 0.07 s, that is equal to the time taken for the drill to move through one CFRP ply (thickness 0.254 mm) with a feed velocity of 215 mm/min, as was used for these tests. The curves in Figure 59 (b) clearly show that the tools with the largest point angle (i.e. tools D,  $180^\circ$ ) caused the strongest fluctuation of the thrust force, followed by tools C ( $150^\circ$ ), and then tools B ( $140^\circ$ ) and A ( $118^\circ$ ). However, it is pertinent to note that tools B actually showed slightly smaller fluctuations at the frequency of interest (i.e. 14 Hz) despite possessing a larger point angle compared to tools A. The reason for this is yet not fully understood, but could be attributable to the difference in point geometry (4-facet with notches in the case of

tools A, 6-facet in the case of tools B). Nonetheless, considering the time domain, the amplitude of the thrust force fluctuations follows the above-mentioned trend, as it increases with an increase in point angle.



**Figure 58: Thrust force and torque generated by the assessed tool geometries.**



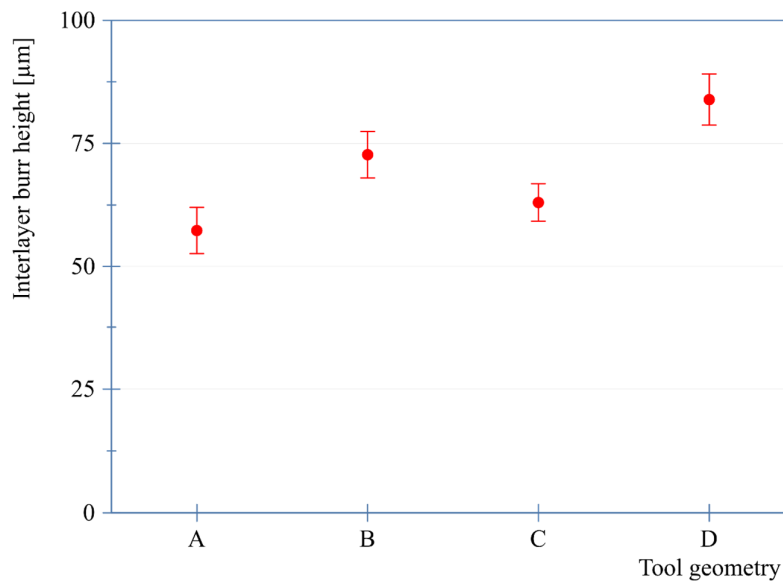
**Figure 59: Thrust force signal frequency domain analysis; (a) 0-200 Hz spectrum, (b) 10-18 Hz spectrum.**

## 5.2 Influence of tool point angle on titanium interface quality

Measuring the height of the entry interlayer burr on the top surface of the titanium layer revealed average values ranging from 57  $\mu\text{m}$  to 84  $\mu\text{m}$ , see Figure 60. It was observed that, overall, an increase in tool point angle brings about an increase in entry interlayer burrs. A possible explanation for this is that during material engagement the sudden rise in thrust force is more pronounced for tools with larger point angles, as for a given increment in the axial direction a larger radial portion of the tool tip is fed into the material. In other words, the tool tip plunges into the material more suddenly, whereas for a tool with a smaller point angle this engagement happens more progressively. The larger the thrust force during tool entry, the more

plastic deformation will take place in the material directly underneath the tool tip, thereby resulting in the formation of larger burrs.

Some degree of tool skidding is also likely to take place during material transition, when the chisel edge breaks through the CFRP and pushes against the upper surface of the titanium layer. In the case of a drill with a small point angle ( $118^\circ$ ), the damage resulting from tool skidding is rectified as the cutting edges get progressively engaged with the workpiece and thereby remove initial damage that may have been formed (including burrs). As the point angle increases, the capability of the tool tip to remove previous damage diminishes, because the distance the tool travels in axial direction between initial engagement and when the cutting edges are fully engaged decreases, to the point where in the case of tools D ( $180^\circ$ ) the entire tool tip gets engaged at once. The consequence of this is that any damage that was caused during initial tool engagement could not be removed by subsequent portions of the tool's tip, which explains why the tools with a point angle of  $180^\circ$  produced significantly larger burrs compared to the other tools investigated.

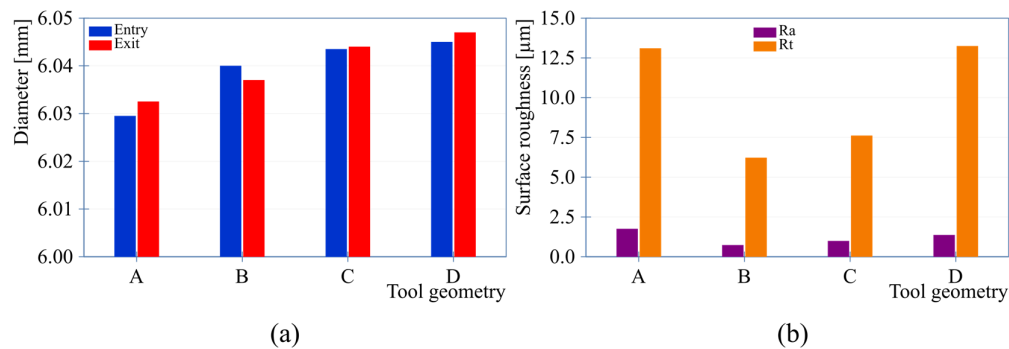


**Figure 60: Average entry interlayer burr on the top surface of the bottom titanium layer.**

The measurements of the entry and exit borehole diameters, see Figure 61 (a), appear to be related to the tool point angle, so much so that an increase in tool point angle results in an increase in borehole diameter. This can be explained by the findings made by Spur (1961), who observed that the not perfectly symmetrical geometry of drilling tools results in the formation of a small radial force, which leads to the bending and, consequently, tumbling of the drilling tool. This in turn causes an increase in the diameter of the boreholes produced. As alluded to

before, an increase in tool point angle results in a larger thrust force, which will further contribute to the radial force caused by the asymmetry of the tool, thereby leading to more pronounced tumbling of the tool, resulting in larger borehole diameters. Except for tools B, where the entry diameter was slightly smaller than the exit diameter, all other tools created boreholes that exhibited a smaller entry than exit diameter. This can be explained by the fact that despite tungsten carbide having a similar coefficient of thermal expansion as titanium, its thermal conductivity is almost ten times higher. As a consequence, the tool heats up and expands more rapidly than the surrounding titanium whilst it progresses through the material and, thus, produces boreholes of increasingly larger diameter. The relatively longer chisel edge in the case of tools B will have caused more pronounced skidding during tool entry as compared to the other tool geometries, which explains the larger entry than exit diameter, an observation that is in agreement with Heinemann (2012).

The lowest surface roughness, quantified by the arithmetic mean roughness  $R_a$  and total height of roughness profile  $R_t$ , of the boreholes drilled into the titanium layer was produced with tools B and, to a slightly lesser extent, tools C, see Figure 61 (b). In contrast, tools A and D resulted in substantially higher surfaces roughness values. These results correlate with the dynamics of the recorded cutting torque, shown in Figure 58, inasmuch as larger oscillations in the torque signal coincide with an increased surface roughness. The correlation between oscillations in the torque signal and surface roughness can be explained by the occurrence of substantial chip clogging, as observed in the case of tools A and D, which causes the drilling process to become increasingly unstable, resulting in poorer surface finish. Tools B instead exhibited the most stable cutting process, brought about by the steadiest chip evacuation, as shown by the small dynamic component in both the thrust force and torque, and thus produced the boreholes with the lowest surface roughness.

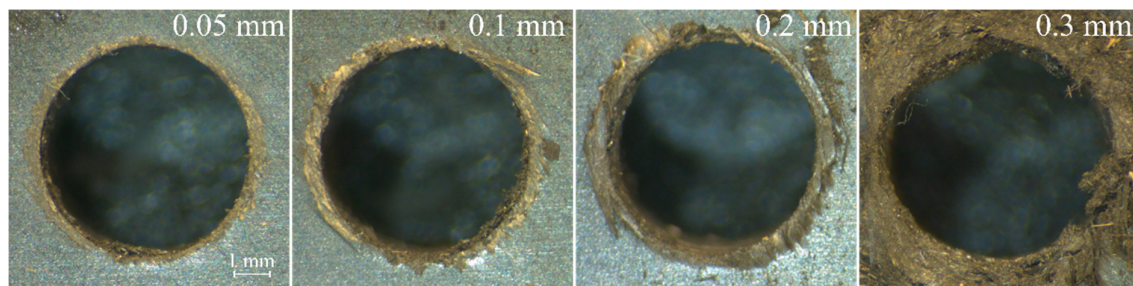


**Figure 61: Borehole quality measurements of titanium layer for different tool geometries; (a) borehole diameter, (b) surface roughness.**

### 5.3 Influence of interlayer gap size on interface quality

In the second set of experiments, four different interlayer gap widths were created, by using shims of thicknesses 0.05 mm, 0.1 mm, 0.2 mm and 0.3 mm. Tools of type B ( $140^\circ$  point angle) were used for these tests, as they were found to result in the most stable cutting process during the first set of experiments.

Photographic images of the interface CFRP surface around the borehole after drilling with different pre-set interlayer gap widths are shown in Figure 62. These show a ring of damage, similar to a corona, along the borehole's edge, characterised by erosion of the CFRP. With an increase in interlayer gap width, this damage ring increases in width, from approximately 0.5 mm in the case of the smallest interlayer gap (0.05 mm) to around 3 mm when drilling a stack with an interlayer gap width of 0.3 mm. This erosive damage on the CFRP layer is the result of some of the upwards-travelling hot titanium chips penetrating the interlayer gap and then being spun around by the rotating tool. Increasing the interlayer gap width eases the ingress of titanium chips into the stack interface, allowing a growing amount of chips to accumulate between the two layers, thus leading to more pronounced damage as they scrape over the surface. The aforementioned damage due to abrasion is further exacerbated by the CFRP's low degradation temperature, which with approximately  $160^\circ$ - $200^\circ$  (Fu et al., 2018; Merino-Pérez et al., 2016) is significantly lower than the cutting temperatures typically found when drilling titanium. These, depending on the cutting parameters, vary between  $400^\circ$  and  $800^\circ$  (Lazoglu et al., 2017; Patne et al., 2017; Zeilmann and Weingaertner, 2006). With the cutting temperature this high it is reasonable to assume that the temperature of the titanium chips as they travel through the drill flutes is still significantly higher than the CFRP's degradation temperature, thereby further contributing to the observed extensive damage.

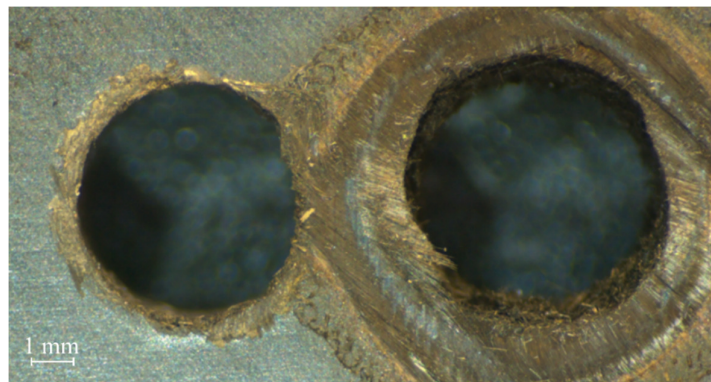


**Figure 62: CFRP interface damage for different interlayer gaps.**

It is pertinent to note that chip flow in drilling is considered as a stochastic process (Mathew and Vijayaraghavan, 2016), meaning that the flowing of chips in the tool flutes, and with it the



overall process stability, can change considerably between drilling cycles despite the process-defining parameters remaining unchanged. For this research, as a consequence, it means that the variation in interface quality observed between samples drilled with identical experimental parameters at times was quite significant. For example, Figure 63 shows two boreholes drilled into a stack with a 0.1 mm pre-set interlayer gap width. While the borehole on the left represents what is considered to be a typical interlayer surface for this tool operating with the set parameters – based on the other boreholes produced – the borehole on the right exhibits significantly greater surface damage. This is the result of chip jamming inside the tool's flutes, which caused not only a greater amount of chips being pushed into the stack interface and causing abrasion, but also a larger amount of heat having migrated into the surrounding CFRP layer, further promoting heat-related damage. Variations in borehole quality between tests carried out with the same experimental conditions were observed more frequently in the case of larger interlayer gaps, which is understandable as larger interlayer gaps make it easier for chips to penetrate into the interface. These chips then further disrupted the chip flow, causing a chain reaction, leading to additional chip clogging and yet more chips being pushed into the interface, ultimately resulting in further workpiece damage.

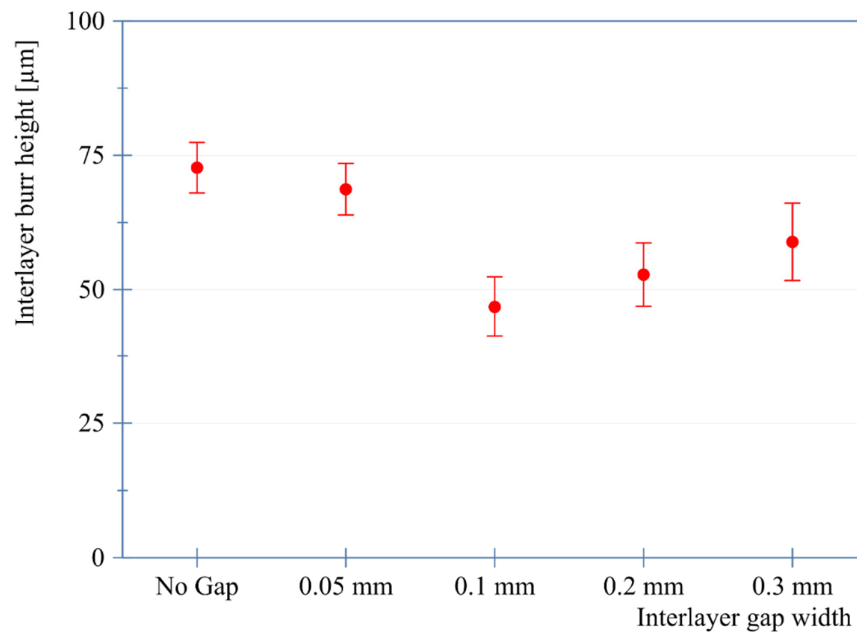


**Figure 63: Variation in CFRP interlayer surface damage within two boreholes drilled with the same parameters.**

Although some noticeable differences in average entry interlayer burr height were recorded on the titanium layer in relation to the pre-set interlayer gap width, as shown in Figure 64, a clear trend between interlayer gap width and burr height cannot be identified. Drilling a stack without or with only a very small interlayer gap (0.05 mm) resulted in the largest burrs, whereas the introduction of a gap of at least 0.1 mm caused the burr height to be considerably reduced. When drilling Aluminium/Aluminium stacks (Chapter 4), chip ingress in the stack interface was found to result in abrasion of the borehole edges, leading not only to the complete removal



of the exit interlayer burr, but also to some reduction of the entry interlayer burr height. The use of titanium as the bottom layer in these experiments might explain why the extensive erosion observed in Chapter 4 did not take place here, as a result of its significantly higher strength and hardness as compared to aluminium. In other words, the entry burrs formed were strong enough to withstand excessive erosion and, thus, did not get completely abraded by the upwards-travelling chips. Further research however is required to allow for a more in-depth assessment of the correlation between interlayer gap width and interlayer burr formation when drilling stacks comprising titanium layers.



**Figure 64: Entry interlayer burr height in titanium for different pre-set interlayer gaps.**

## 5.4 Summary

This chapter presented an investigation on the influence of tool point angle and interlayer gap width on interlayer borehole quality when drilling CFRP/Titanium stacks. The observed damage on the CFRP interlayer surface was found to be caused by the drilling of the titanium layer below and can be attributed to the upwards-travelling titanium chips as well as heat accumulation in the tool and the stack interface. Tools exhibiting a fairly stable titanium cutting process and chip evacuation were found to produce significantly better boreholes than tools that were found to exhibit – on average – a less smooth chip flow and, as a consequence, poorer process stability. In the titanium interlayer surface, an increase in tool point angle results in larger entry burrs. This is due to the positive correlation between tool point angle and thrust

force, as well as the increased capability of tools with low point angles to remove damage generated by surface skidding during initial tool entry.

The introduction of a pre-set interlayer gap promotes the ingress of upwards-travelling titanium chips into the stack interface, thereby leading to extensive abrasive and thermal damage of the CFRP interlayer surface. The wider the interlayer gap, the easier it becomes for titanium chips to penetrate the interface and, consequently, the greater the composite interlayer damage. Although the introduction of a pre-set interlayer gap appears to result in a slight reduction in the entry interlayer burr in the titanium layer, which could be caused by the abrasion of upwards travelling titanium chips, a clear relationship between interlayer gap width and interlayer burr formation in the titanium surface could not be established.

## Chapter 6: Influence of parameter changeover position on interface quality

The realisation of adaptive drilling on multi-material stacks requires cutting parameters to be switched over when the tool transits between two layers of different materials. When employing traditional drilling tools, the fact that these exhibit some shape of conical point geometry results in the position at which the cutting parameters are changed to be at any point during the interface drilling phase, i.e. when the cutting edges are engaged with two different layers simultaneously. As evidenced by the literature review, there is a lack of understanding on how this position affects the borehole quality. Thus, this chapter reports on the experimental work carried out to determine the impact of parameter changeover position on interface borehole quality, with a focus on CFRP/Aluminium stacks.

### 6.1 Parameter changeover positions

For the research presented in this chapter, the cutting parameters and cooling strategy were changed over when the drill transitioned from CFRP to aluminium, using the parameters listed in Table 8. Whilst the CFRP was drilled dry, the aluminium was drilled with coolant. The cutting fluid supply was switched on 1 mm before the tool's chisel edge broke through the CFRP layer, to ensure that some of the externally-supplied coolant was able to reach the drill tip by the time it engaged with the bottom layer. The cutting speed and feed rate in contrast were changed at three positions relative to the interface, see Figure 65. Position 1 refers to the cutting speed and feed rate being changed over when the tool's chisel edge made contact with the aluminium layer. This results in the final part of the CFRP layer being drilled with the aluminium-specific cutting parameters. Positions 2 and 3 refer to the changeover of cutting parameters taking place when half of the tool tip (position 2) or the entire tool tip (position 3) was engaged in the lower layer, meaning that half of the interface region or none of it, respectively, was drilled with the aluminium-specific parameters. To ensure that once the changeover depth was reached, the entire remainder of the borehole was machined with the aluminium-specific parameters, a dwell time of 100 ms in the feed motion was introduced. Furthermore, to prevent tool wear affecting the results, a new tool was used for each different changeover position, and the tool condition was checked with a digital optical microscope after every two holes drilled. For each changeover position, a total of eight boreholes were drilled.

To evaluate the condition of the borehole at the stack interface, three quality parameters were assessed: diameter, damage factor and burr height.

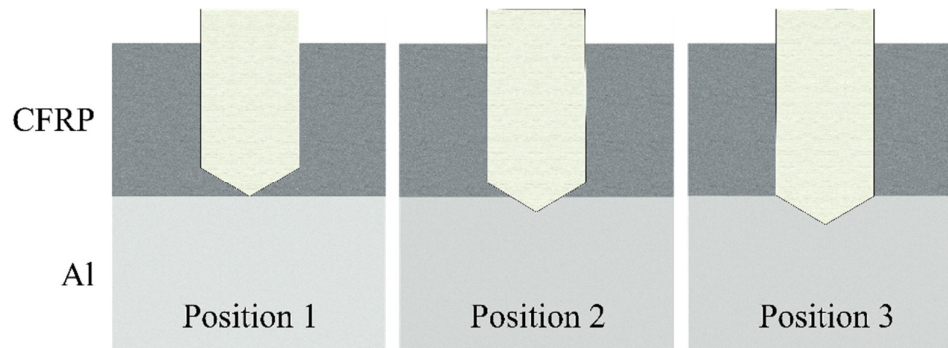


Figure 65: Changeover positions investigated.

Table 8: Workpiece and tooling details.

Stack combination	Tool Manufacturer	Tool Coating	Tool Geometry	Cutting speed (m/min)	Feed rate (mm/rev)
CFRP/Al (10+6 mm)	Walter	TiAlCrN	Ø15 mm, 140° point, 30° helix, standard chip flutes, six-facet	57/95	0.038/0.16

## 6.2 Borehole diameter

The measurements of the average borehole diameters at entrance and exit of each of the stack layers are provided in Figure 66. The first observation made is that all boreholes drilled were noticeably larger than the nominal tool diameter (15 mm). A second observation is that the interface diameters of the aluminium boreholes were found to be consistently slightly larger than the interface diameters in the CFRP layer, regardless of the changeover position. It is likely that two phenomena contributed to this. Firstly, the difference in elastic modulus between aluminium and CFRP, which leads to different amounts of elastic recovery (Ashrafi et al., 2014; Brinksmeier and Janssen, 2002; Shyha et al., 2011). Secondly, the possibility of tool skidding occurring when the tool engages with the lower layer, i.e. wandering of the tool tip on the workpiece surface when it first establishes contact. This would result in a slightly larger entrance diameter in the aluminium and, to a lesser extent, exit diameter in the CFRP. Further evidence for the occurrence of tool skidding during interface drilling is given by the fact that the borehole diameters at CFRP entry and aluminium exit (i.e. away from the interface), where

tool skidding is highly unlikely to occur, were found to be significantly smaller than their corresponding interface diameters.

With regards to the effect of changeover position on borehole diameter, Figure 66 shows a decrease in interface diameter, particularly in the CFRP layer, the later the parameters were changed with respect to the interface. This is believed to be a result of the position of the chisel edge when both the cutting speed and feed rate were increased. When changeover occurred in position 1, the parameters were changed over as the chisel edge made contact with the lower aluminium layer, suggesting that tool skidding might have occurred with a relatively high feed rate. Tool skidding is related to the thrust force, which to a great extent is created by the chisel edge (Klocke, 2011). In the case of changeover positions 2 and 3, the parameters were instead changed over after the chisel edge was already engaged with the aluminium layer. This resulted in the chisel edge and half of the drill tip (in the case of position 2) or the full height of the drill tip (position 3) to experience material transition at a significantly lower feed rate and, thus, lower thrust force. Lower feed rates therefore appear to result in a less pronounced tool run-out when transitioning between stacks comprising CFRP and aluminium, which in turn yields interface diameters closer to the nominal tool diameter.

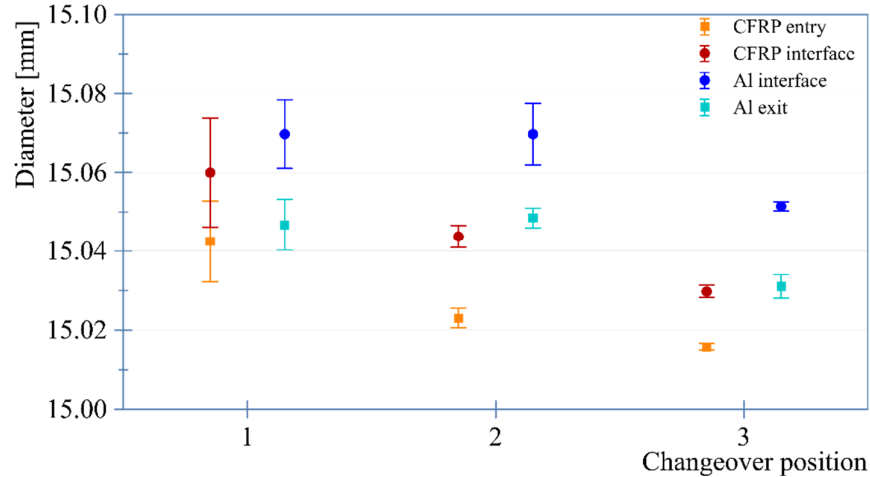
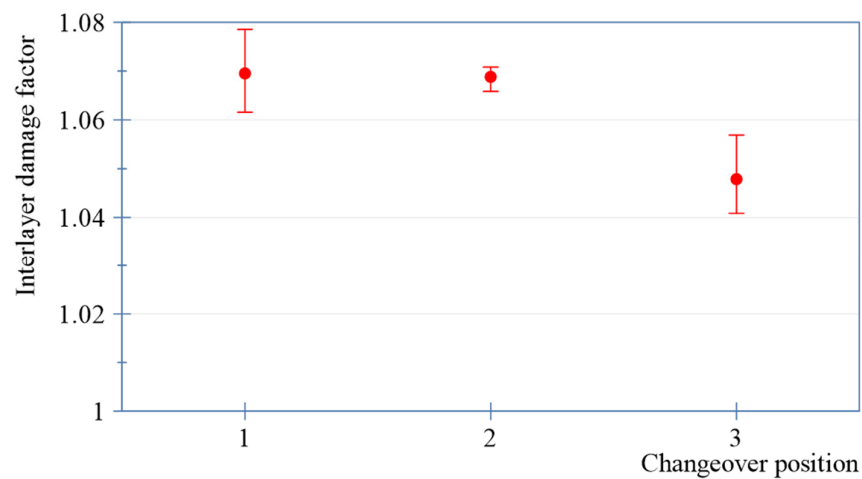


Figure 66: CFRP and aluminium borehole diameters in relation to parameter changeover position.

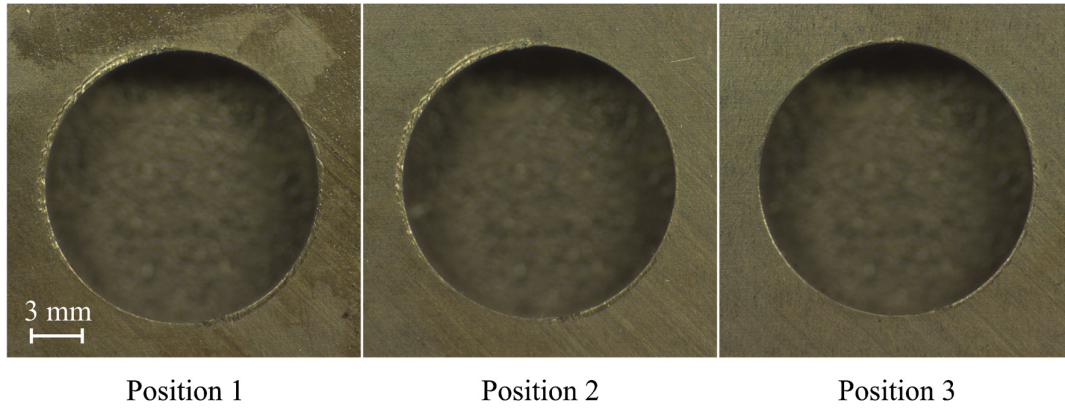
### 6.3 Interlayer damage factor

The average interlayer damage factors at the CFRP interface surface for different changeover positions are shown in Figure 67, whilst Figure 68 depicts the typical interface damages on the CFRP layer surface. Overall, the resulting interface damage is small for all changeover positions investigated, suggesting the adequacy of the combination of tool and cutting

parameters, and the small scatter in the results implies that the drilling cycles were stable. Whilst the measured damage factor is similar when performing the parameter changeover at positions 1 and 2, it is lower at changeover position 3. This can be attributed to the fact that when the parameters are changed over at position 3, the cutting speed and feed rate are increased once the drill has cleared the CFRP layer. Consequently, the tool breaks through the composite layer with a substantially lower feed rate and, thus, reduced thrust force, which is directly correlated to the delamination at borehole exit (Feito et al., 2018; Qiu et al., 2014; Xu et al., 2014). The similarity of results obtained from changing the parameters over at positions 1 and 2 suggests that the outer cutting edge corners are the tool feature that mostly influences the resulting CFRP layer damage. It is possible that the chisel edge, as a major contributor to the thrust force (Klocke, 2011), initially causes some damage in the form of delamination, but that this damage is then removed by the cutting edges prior to full breakthrough of the composite layer.



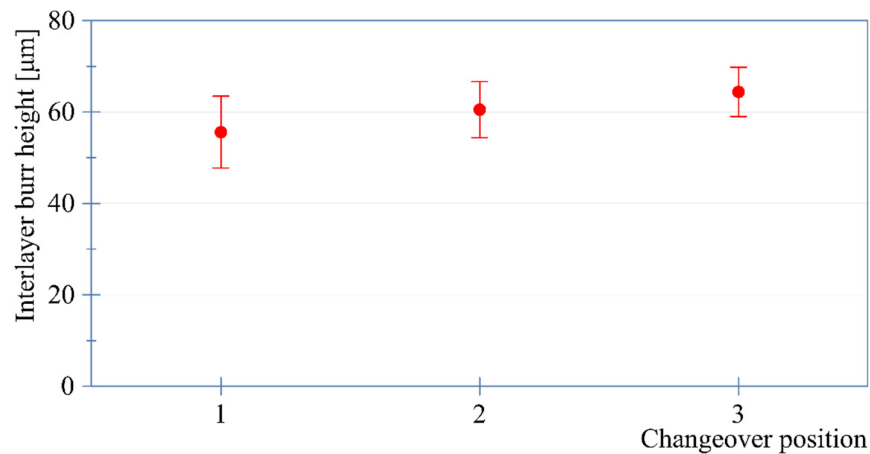
**Figure 67: Interlayer damage factor at CFRP interface in relation to cutting parameter changeover position.**



**Figure 68: CFRP interface surface for different changeover positions.**

#### 6.4 Interlayer burr formation

Figure 69 shows the interlayer burr heights at the entry of the lower aluminium layer for different changeover positions. The generated interlayer burr height appears to be strongly correlated to the changeover position, inasmuch as the deeper inside the material the cutting speed and feed rate are increased, the larger the burr. This can be explained by the low feed rate employed when drilling the CFRP layer, which results in a significantly longer cutting edge path and engagement time when compared to drilling the aluminium layer. As a consequence, when the interface is machined with a low feed rate (i.e. changeover positions 3 and, to a lesser extent, 2), higher temperatures occur at the cutting point due to the significantly greater amount of friction energy generated. The increase in temperature in turn leads to an increase in the plastic flow of the aluminium during the burr formation process, as a result of the thermal softening of the workpiece material.



**Figure 69: Interlayer burr height at entry of aluminium layer.**

## 6.5 Summary

The research presented in this chapter serves the purpose of providing an understanding of the impact of parameter changeover positions on interface borehole quality. When drilling CFRP/Aluminium stacks, adapting the cutting parameters and cooling strategy based on the workpiece material being machined at any point of time was found to result in a stable cutting process and to generate boreholes that exhibit only small interface damage, as by doing so each layer is machined with its optimal parameters. This provides further evidence to the effectiveness of adaptive drilling.

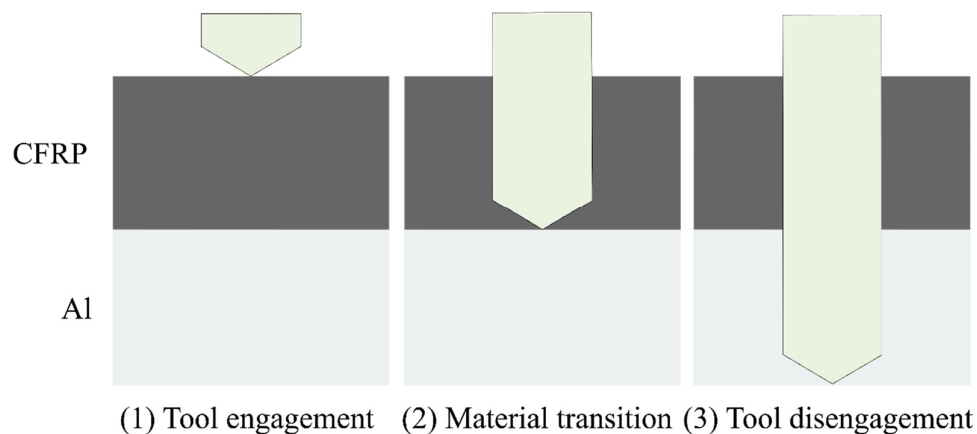
When transitioning from CFRP to aluminium, tool skidding resulted in a slightly larger entrance diameter in the aluminium and, to a lesser extent, exit diameter in the CFRP. The later, relative to the interface, the cutting speed and feed rate are increased, the smaller the interface diameter, particularly in the CFRP layer. The surface damage of the CFRP at the interface is smallest if the cutting speed and feed rate are increased once the entire drill tip has broken through the CFRP layer, as in this case any delamination caused by an increase in feed rate whilst machining at the interface is avoided. Interlayer burr height is strongly correlated to the changeover position, so much so that the later the cutting speed and feed rate are increased, the larger the burr. Machining at the interface using a low feed rate characteristic for drilling CFRP results in more heat energy being generated and, thus, higher temperatures, which consequently promotes workpiece material flow during the burr formation process.



## Chapter 7: Process signals characterisation

The literature review revealed a shortage of fundamental research aimed at correlating signal features to the occurrence of process incidences relevant to adaptive drilling, as well as assessing the validity of these correlations throughout the life of a cutting tool. It is also unclear whether the understanding gained from previous studies on process monitoring of drilling of stacked assemblies, which was conducted on large CNC machining centres, can be reliably transferred to aerospace drilling operations, in which small portable automated drilling units are used to generate the majority of boreholes. Thus, this chapter aims to establish relationships between stack drilling process incidences and process signals using different machining equipment, and to assess the validity of these relationships at different stages of tool wear.

The relevant process incidences to enable adaptive drilling when cutting a two-layer multi-material stack are illustrated in Figure 70: (1) tool engagement, which is when the tool first makes contact with the first layer of the stack; (2) material transition, which is when the tool moves from the first to the second layer of the stack, and (3) tool disengagement, which is when the tool breaks through the second layer of the stack. To gain an understanding on the suitability of a range of signals with regards to the identification of these process incidences, a number of initial experiments were conducted on a large CNC machining centre. These were followed by experiments aimed at establishing the degree of transferability of signals between machining centres and portable drilling units, as the latter are typically used in many aerospace assembly operations.



**Figure 70: Investigated process incidences.**

## 7.1 Process signals characterisation at different tool life stages

The experiments were carried out on CFRP/Aluminium stacks, and three twist drills of the same geometry were employed for this research, see Table 9. Sixteen boreholes arranged in a 4x4 matrix were drilled into each of the stacks. When drilling these holes, thrust force, torque, AE and vibration acceleration were recorded. To extend the tool life under investigation without increasing the number of boreholes drilled into the coupons, a CFRP dummy plate was used to wear out the drilling tools. This meant that after a borehole was drilled into the stack fixed in the clamping jig, 10 holes, each 15 mm deep, were drilled in the CFRP dummy plate. Thus, holes 1, 12, 23, etc. were drilled into the stack, whereas holes 2-11, 12-22, etc. were drilled into the dummy plate. A total of 111 holes were drilled with each of the tools, which on average resulted in a tool flank wear length  $v_B$  of approximately 0.3 mm, see Figure 71 and Figure 72. One of the three tools employed was later used to drill more holes to further investigate the effect of tool wear on the AE signal.

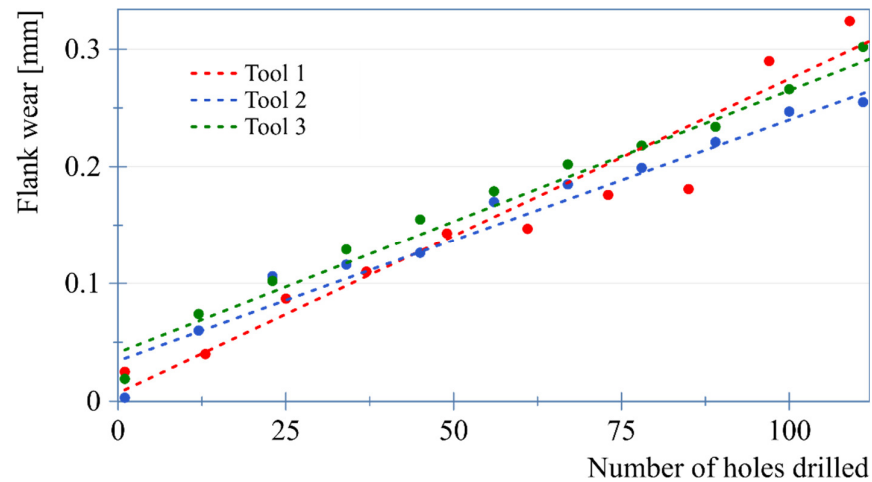


Figure 71: Comparison of wear for different tools.

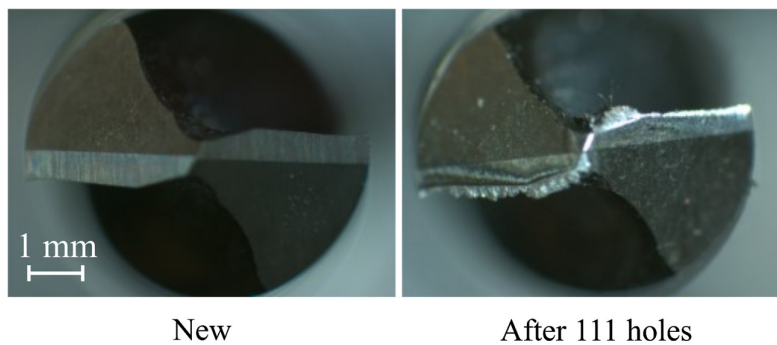


Figure 72: Tool tip aging after 111 holes.

**Table 9: Workpiece and tooling details**

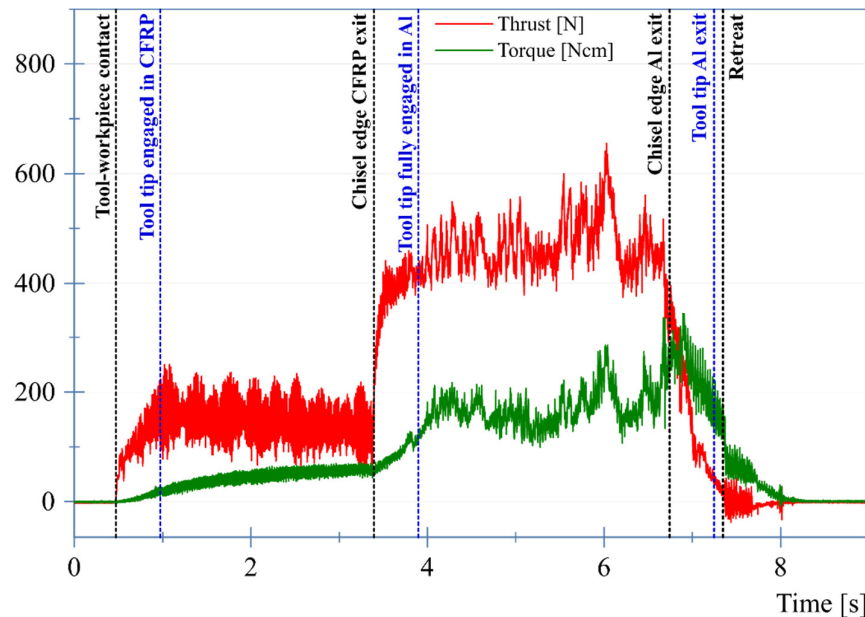
Stack combination	Tool Manufacturer	Tool Coating	Tool Geometry	Cutting speed (m/min)	Feed rate (mm/rev)
CFRP/Al (10+10 mm)	Walter	Uncoated	Ø6 mm, 118° point, 25° helix, enlarged chip flutes, four-facet with notches	40	0.1
	Ham	Diamond	Ø6.35 mm, 155° point, 20° helix, enlarged chip flutes, four-facet with notches, with pilot	40	0.05

### 7.1.1 Thrust force and torque

A typical example of the recorded thrust force and torque is shown in Figure 73. The thrust force was found to rapidly increase as a reaction to tool engagement. As the cutting edges begin to engage with the workpiece, the torque experiences a more gradual increase, which stabilises once the tool tip is fully engaged in the workpiece material. While drilling the CFRP layer, both the thrust force and, to a lesser extent, the torque were found to oscillate with a relatively low frequency. This is attributed to the stacked nature of the workpiece, as observed in Chapter 5. Furthermore, when drilling the CFRP layer, both the thrust force and torque were found to be significantly lower than when machining aluminium, due to the softness of the CFRP matrix, making the identification of material transition unambiguous.

During drilling of the aluminium layer, the thrust force experiences a gradual increase with depth. This could be a result of the increasing volume of chips within the drill flutes, as well as the increase in friction due to a larger portion of the tool's margins being in contact with the borehole wall, in turn leading to a greater resistance in the feed direction. This gradual increase was not as pronounced in the torque, which instead initially remains fairly constant. It is pertinent to note that, throughout the tests, strong fluctuations in both thrust force and torque were recorded towards the end of the drilling cycle. These are believed to be a result of chip jamming, which becomes increasingly likely the deeper the tool penetrates into the workpiece. When the chisel edge breaks through the lower layer, the thrust force and torque rapidly drop to zero. Tool retraction is characterised by a noticeable increase in the dynamic component of both the thrust force and the torque. This is a result of the rubbing between the chips adhered to tool and the borehole edge, as well as between the upwards-travelling tool and the CFRP fibres protruding out into the borehole as a result of incomplete shearing and partial fibre pull-out, as observed by Sobri (2017). Overall, the thrust force was consistently found to be more

responsive to the process incidences than the torque, which can be attributed to the chisel edge, which is the part of the tool to first engage (or disengage) with each stack layer, generating around 70% of the thrust force (Klocke, 2011).

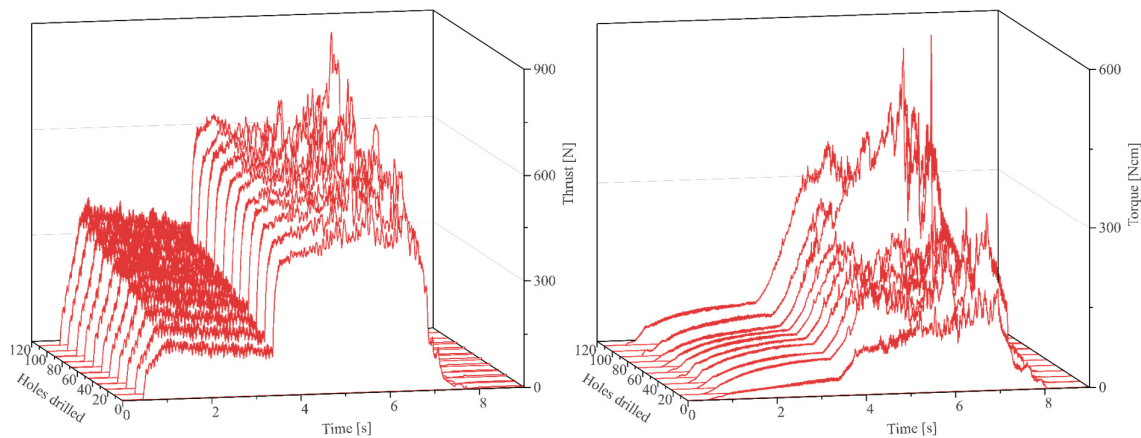


**Figure 73: Recorded thrust force and torque during a drilling cycle.**

The evolution of the thrust force and torque throughout the tool life is shown in Figure 74. Both thrust force and torque increased substantially with growing tool wear for all the three drills employed. During drilling of the CFRP layer, the continuously increasing rounding of the cutting edges as a result of abrasion wear led to a linear increase in the thrust force and torque. Apart from the previously mentioned oscillations, resulting from the stacked nature of the composite, when drilling CFRP both thrust force and torque did not experience any sudden variation within individual drilling cycles, even at the stage where the tool exhibited significant wear. This is believed to be due to the machining of the CFRP resulting in very tiny, almost powder-like chips, which are easily removed and thus do not disrupt the chip flow inside the drill flutes, thereby resulting in a stable cutting process. In contrast, cutting of the aluminium layer was characterised by an increase in both the frequency of occurrence and the magnitude of sudden oscillations due to chip clogging with tool wear. This can be attributed to the larger chip size, longer distance to be travelled by the chips to escape the flutes and workpiece material adhesion to the drilling tools, which is typical for dry drilling of aluminium, especially at relatively low cutting speeds (Klocke, 2011). The observed workpiece adhesion gives rise to built-up edge formation, which further affects the chip size and chip flow. The growth in tool

wear would have promoted workpiece material adhesion due to the associated rise in cutting temperatures, thereby promoting the aforementioned phenomena.

Interestingly, from Figure 74 it can be observed that the proportional increase in thrust force with tool wear when drilling CFRP (300%) is significantly higher than that observed when drilling aluminium (50%). With regards to the torque signals, an increase of around 150% can be observed when the drill is engaged in the CFRP layer. However, when engaged in the aluminium layer, determining an overall increase in the torque magnitude is less straightforward due to the frequently occurring chip clogging, which causes the torque signal to become highly dynamic. Nonetheless, considering the first second of engagement between the tool and the aluminium layer, i.e. the period during which chip clogging is unlikely to occur, an increase in torque of at least 300% was observed.

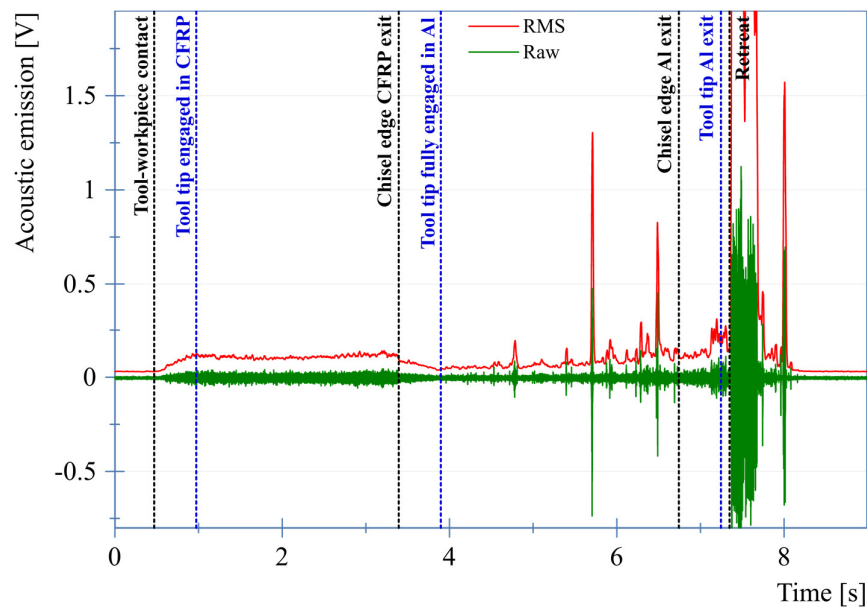


**Figure 74: Progression of thrust force and torque with tool wear.**

### 7.1.2 Acoustic emission

An example of the raw and RMS-converted AE signal is shown in Figure 75. Tool engagement results in a substantial increase in AE, which stabilises once the cutting edges are fully engaged in the CFRP. Similarly to the thrust force and torque, the AE signal during drilling of the composite layer is characterised by high stability. During material transition from CFRP to aluminium, a substantial drop in the AE signal magnitude was observed, which remained at this lower level – except for a few bursts – for a period of around 2 to 3 seconds. The higher AE magnitude observed when drilling CFRP can be explained by the higher stiffness of the composite, which during material removal results in the generation of more elastic energy for the same amount of impact when compared to aluminium (Min et al., 2011, 2008), ultimately generating a stronger AE signal. Furthermore, according to Klocke (2011), the strong AE

magnitude characteristic of drilling CFRP is also a result of crack initiation and propagation during the brittle fracture of the carbon fibres. Drilling of aluminium, in contrast, is characterised by plastic deformation and less crack initiation and propagation, thus leading to lower AE. However, with an increase in the drilling depth, chip clogging becomes more likely, and its occurrence often leads to sudden spikes in AE. Interestingly, these spikes were found to correlate to rises in the thrust force, torque and acceleration, which suggests that all the signals assessed are strongly affected by chip clogging. Tool disengagement was often characterised by an increase in AE. It is possible that this is due to plastic deformation of the material underneath the tool tip and crack propagation, both associated with burr formation, as a similar increase was not observed when exiting the CFRP layer, which as a result of its nature is not characterised by burr formation during tool exit in the traditional sense (Xu et al., 2018).



**Figure 75: Recorded AE during a drilling cycle.**

With regards to the drilling of the top CFRP layer, an increase in tool wear appeared to result in a gradual decrease of the AE, as shown in Figure 76. When analysing the average RMS signal over the number of holes drilled, see Figure 77, a low frequency oscillation can be observed, which is believed to be the result of the setup and how the experiments were conducted. Holes were drilled in a 4x4 matrix into the stack (i.e. four rows, each one comprised four holes), and the AE was often found to gradually decrease from the first to the last hole of each row (e.g. from hole 1 to hole 4). When drilling the first hole of the next row (e.g. hole 5), the AE signal was found to be higher than when drilling the last borehole of the previous row (e.g. hole 4), but often still lower than when drilling the first hole of the previous row (e.g. hole 1).

1). This can be explained by the varying distance between the sensor location and the drilling site, as observed by Shuaib (2018). Furthermore, as the workpiece acts as a medium for the AE waves, the presence of one (or more) borehole(s) can also affect the workpiece's dynamic properties, and consequently change the way AE propagates.

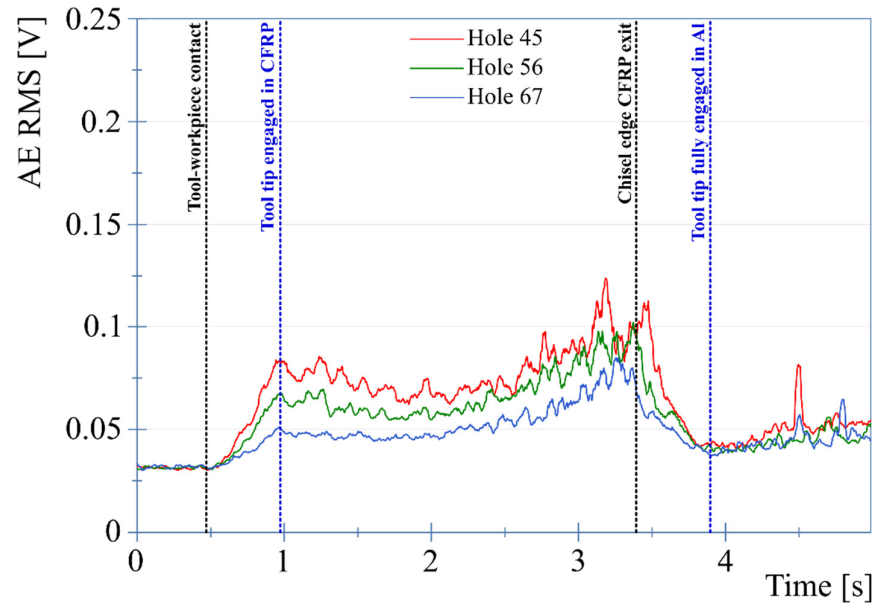


Figure 76: AE RMS signal during drilling of the CFRP layer with increasing tool wear.

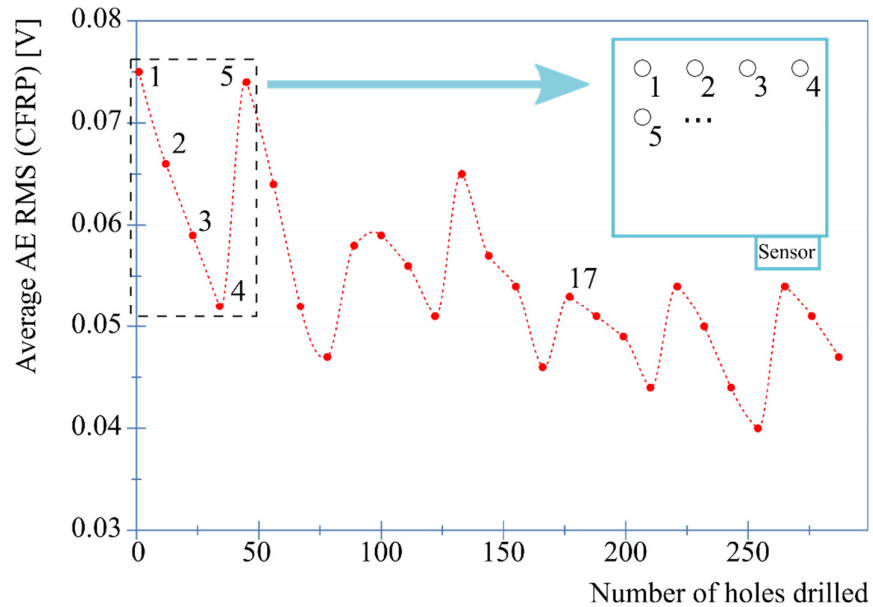


Figure 77: Progression of the average AE RMS signal during drilling of the CFRP layer with an increase of the number of holes drilled (extended drilling tests).

### 7.1.3 Acceleration

An example of the recorded vibration accelerations is shown in Figure 78. Although some variations in the signal magnitude in all the three directions were observed, with the x-direction being the most sensitive to the drilling process, the accelerations in all three directions appear to be highly correlated. Drilling of CFRP was found to generate stronger acceleration than drilling of aluminium in stable conditions (i.e. without chip jamming). Similarly to AE, material transition was characterised by a drop of the acceleration magnitude. During the first 2 seconds after the transition period, the acceleration signal remains at a lower level than that characteristic of CFRP drilling. Akin to the other recorded process signals, peaks were observed during the final stages of the drilling of the aluminium layer, and the frequency of the occurrence of these was found to increase with the number of boreholes drilled. These peaks could be attributed to a deteriorating chip flow, which is promoted by tool wear (Heinemann and Hinduja, 2012). Tool disengagement and retraction cause a sudden increase in the acceleration, which in the case of the former could potentially be due to burr formation, often leading to the saturation of the three acceleration signals.

With regards to the drilling of the CFRP layer, tool wear appears to have resulted in a slight reduction in the acceleration signal, as can be seen in Figure 79. Similarly to the AE signal, a correlation was found between borehole position and acceleration magnitude, due to the varying distance between the sensor and the signal source. Like in the case of the AE sensor, it is not possible to define a clear relationship between tool wear and acceleration during drilling of the aluminium layer, due to the strong vibration caused by frequent chip jamming. Overall, since the acceleration signal exhibits a strong correlation to the AE signal, it appears that the monitoring of both signals in the time domain would produce redundant data that does not add substantial benefit to a process monitoring system for adaptive drilling of the assessed stack combination.



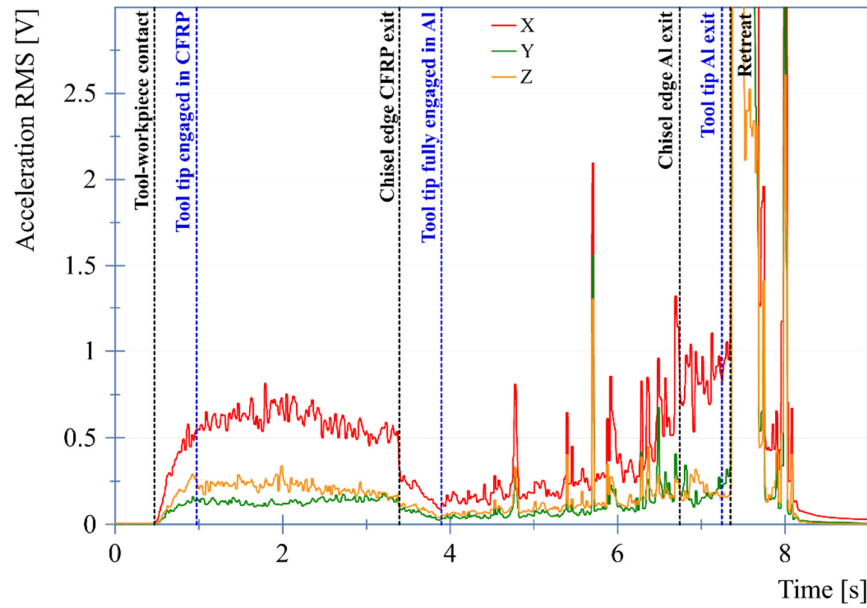


Figure 78: Recorded acceleration during a drilling cycle.

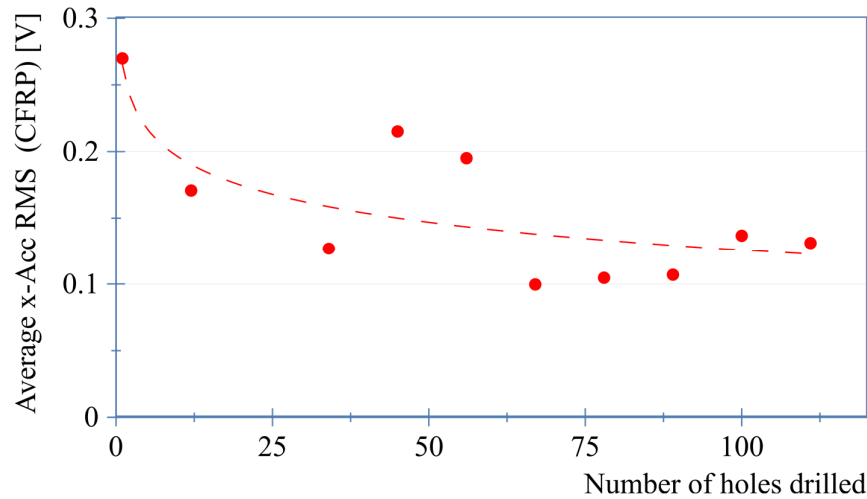


Figure 79: Progression of the average acceleration RMS signal during drilling of the CFRP layer with an increase of the number of holes drilled.

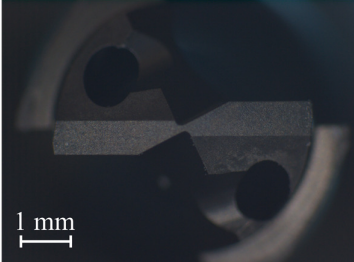

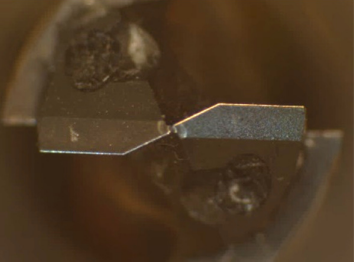

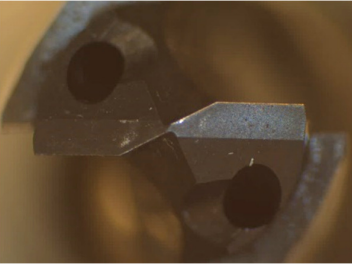
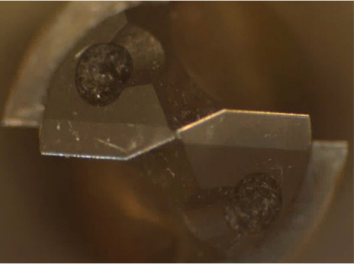


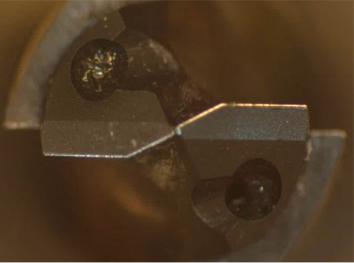
## 7.2 Investigating the effect of different machine tools on process signals

To assess the suitability of sensors and process signals for the equipment the adaptive drilling system is intended for, as well as to allow for establishing a degree of transferability of signals between a large CNC machining centre and a small portable drilling unit, a second set of experiments was carried out.

For this, three Ham drills with pilot section (see Table 3, page 73) were used. For each tool, 15 holes were drilled with the Fives eADU before drilling another 15 holes with the machining

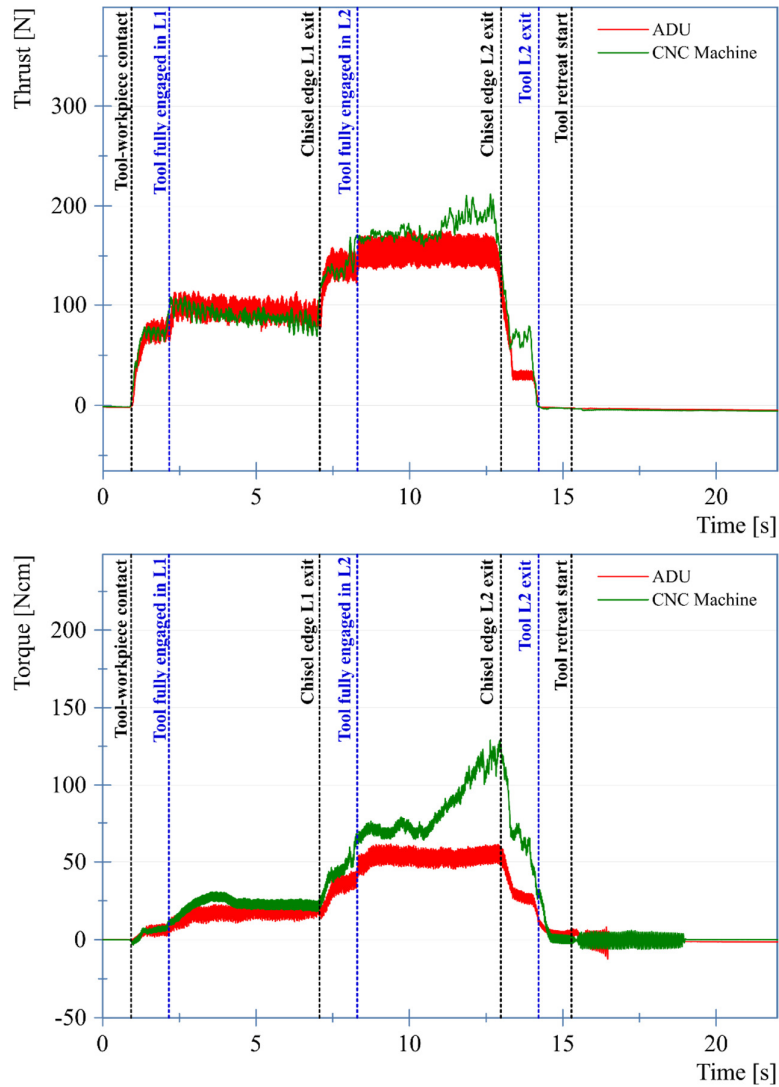
centre (Takisawa MAC-V3). Five boreholes were drilled in each coupon, which means in total six coupons per tool were used. The experimental parameters used in the drilling tests are provided in Table 3 (page 73). To replicate the suction and coolant supply of the portable drilling unit, the machining centre was equipped with an MQL unit and external suction, as shown in Figure 23 (page 75). The location of the dynamometer, AE sensor and accelerometers was the same for the two different machine tools, i.e. on the clamping jig. To allow for a direct comparison between process signals recorded when drilling with two different pieces of machining equipment, the experiments were designed in a way to avoid significant wear. According to the images in Table 10, none of the drills experienced noticeable wear after having drilled 30 holes, allowing for a direct comparison between process signals recorded when drilling with the two different pieces of machining equipment. The behaviour of the thrust force and torque recorded during the experiments further supports this, as no noticeable increase was recorded with an increase in the number of drilled holes.

**Table 10: Tool wear assessment.**

	New	After ADU drilling	After CNC machine drilling
Drill 1			
Drill 2			
Drill 3			

Two examples of the smoothened thrust force and torque are shown in Figure 80, one from the machining centre and the other from the drilling unit. Because the drilling unit was equipped with a vibration-assisted drilling module, the additional axial oscillations meant signal smoothening was necessary for the thrust force and torque signals, as these exhibited a strong dynamic component. The thrust force and torque during drilling of the CFRP layer were found to be fairly similar between the two different machines, although the machining centre exhibits a slight reduction in both the thrust force and cutting torque with an increase in drilling depth. This can be explained by the fact that, with an increase in drilling depth, the external coolant supply of the machining centre becomes less efficient as it becomes increasingly difficult for the cutting fluid to reach the drill tip, unlike in the case of the through spindle coolant supply of the drilling unit. This leads to an increase in the cutting temperatures and, consequently, the softening of the CFRP matrix, thereby reducing the thrust force and torque required to machine the material.

During drilling of the lower aluminium layer, the thrust force and torque exhibited a more substantial difference. The thrust force and, to an even greater extent, the torque experience a substantial increase halfway through the drilling of the lower layer when using the machining centre, whereas they remain stable throughout the drilling cycle when using the portable drilling unit. This can be attributed to chip clogging, which is more likely to happen on the machining centre than on the portable drilling unit for three reasons. Firstly, the portable drilling unit benefits from vibration-assisted drilling, which has been found to aid chip breakage and evacuation (Li et al., 2019; Seeholzer et al., 2019). Secondly, the portable drilling unit's through-spindle coolant supply facilitates chip evacuation (Klocke, 2011). Thirdly, although the same vacuum cleaner provided chip suction for both machine tools, applying suction through the nosepiece of the portable drilling unit is believed to be more efficient due to the sealed suction path.

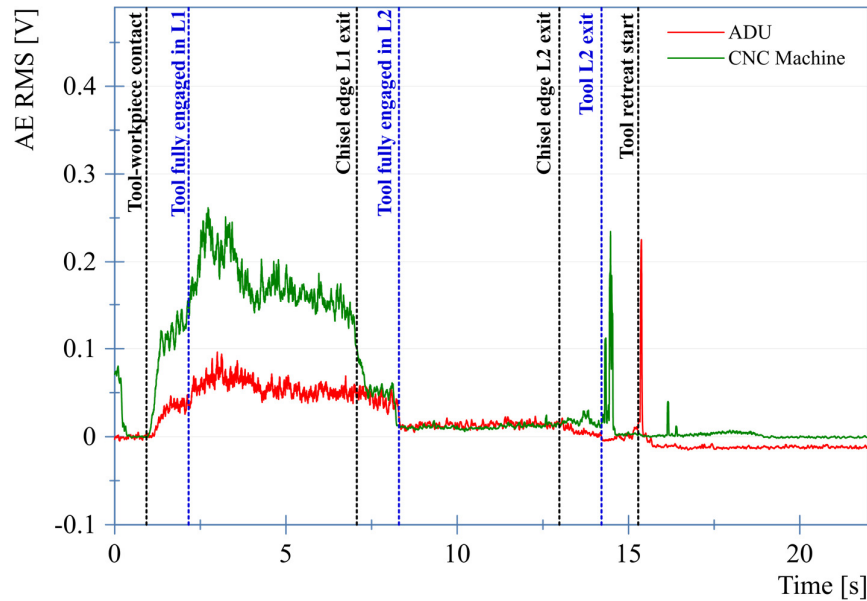


**Figure 80: Recorded thrust force and torque using portable drilling unit and machining centre.**

To isolate the AE generated by the cutting process from other AE sources, the signal recorded with the spindle and feed drive running and the tool rotating in air was measured for the two machine tools. This was found to be, on average, 0.027 V and 0.45 V for the machining centre and the portable drilling unit, respectively. These values were then subtracted from the recorded AE signal during each drilling cycle. The compensated AE RMS signal is shown in Figure 81. When drilling the CFRP, the AE generated when using the machining centre was found to be significantly larger than that recorded when using the drilling unit, whereas during drilling of the aluminium layer the AE signals were similar. This can be explained, to some degree, by the difference in eccentricity in the tool rotation ('tool tumbling') due to the different tool clamping mechanisms, which was found to be 20  $\mu\text{m}$  for the portable drilling unit and 30  $\mu\text{m}$  for the machining centre, both measured at the start of the drill flutes. This difference can be

explained by the less constrained tool clamping provided by the drill chuck used in the machining centre as opposed to that provided by the portable drilling unit, where the tool is threaded into a tool holder fixed onto the end of the spindle. However, as this difference is believed to be too small to fully explain the observed difference in AE when cutting the CFRP layer, it is reasonable to argue that the portable drilling system in its entirety, i.e. sealed suction, through spindle coolant supply and vibration-assisted module, will have collectively affected the tool-workpiece interaction and, thus, the generation of AE.

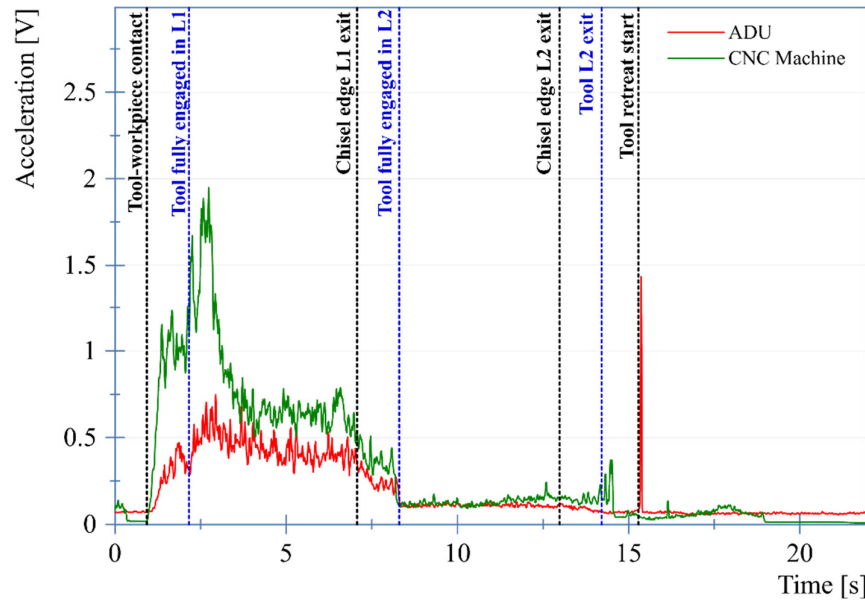
Towards the end of the drilling cycle, a rapid but brief increase in the AE signal was noticed just after tool disengagement when using the machining centre, while a spike in the signal was observed straight after the beginning of tool retraction when using the portable drilling unit. A possible explanation for the former is the larger extent of burr formation as a result of the hindered chip evacuation and continuous cutting, whereas the latter is believed to be a result of the machine's mechanical triggering of tool retraction i.e. a limit switch having been triggered. When using the machining centre, tool retraction is instead initiated by monitoring the z-stage position, thereby preventing contact between moving parts.



**Figure 81: Recorded AE RMS using portable drilling unit and machining centre.**

As detailed in the previous section, the accelerations in the three recorded directions are highly correlated. Thus, for clarity only the acceleration RMS signal in the z-direction is shown in Figure 82. Similarly to the AE signal, the acceleration recorded during drilling of the upper CFRP layer was significantly higher when using the machining centre than when using the

portable drilling unit. The acceleration signal exhibited a similar magnitude during drilling of aluminium for both machine tools, and tool retraction was characterised by the same occurrences reported on when analysing the AE signal. The strong correlation between the acceleration and AE observed in these experiments further strengthens the argument that monitoring only one of these signals appears to be sufficient for a process monitoring system for drilling of aerospace stacks.



**Figure 82: Recorded z-acceleration RMS using portable drilling unit and machining centre.**

### 7.3 Summary

The research presented in this chapter established relationships between process incidences and process signals recorded from a variety of sensors and determined the degree of transferability of signals between a large CNC machining centre and a small portable drilling unit.

Significant differences in thrust force, torque, AE and acceleration were observed when the tool transitions from CFRP to aluminium, thereby making these signals suitable for material transition detection. The thrust force was found to be the most responsive signal to tool engagement, material transition and tool disengagement, which makes this signal particularly suitable for a highly responsive adaptive drilling system. Acceleration signals were found to exhibit similar behaviours in the three directions assessed. Because the acceleration generated from the drilling process appears to be strongly correlated to the AE, the monitoring of only one of these signals appears to be sufficient for detecting the occurrence of the investigated process incidences. For both AE and acceleration, varying the distance between the sensor and

the machining site results in variations in the recorded signals. Sensors to be included in process monitoring systems for adaptive drilling should therefore be located in places where they can maintain a constant distance to the machining point.

All recorded process signals were found to exhibit some differences when switching from a CNC machining centre to a portable drilling unit, which are believed to be the result of the latter's ability to improve chip evacuation by vibration-assisted drilling, sealed suction and through spindle coolant supply. For that reason, to ensure that the data recorded in the following chapters is representative of the industrial application, the research was carried out using a portable drilling unit.

## Chapter 8: Investigation on the feed and spindle current signals

According to the findings of the previous chapter, the directly recorded thrust force and torque were found to be highly valuable process parameters, as they exhibited strong correlations to the occurrence of all three process incidences of interest. However, they are considered impractical to implement in commercial process monitoring systems due to the sensors' fragility and high cost. To address this, the research presented in this chapter includes an investigation on the effectiveness of indirectly measuring the thrust force and torque generated by aerospace ADUs based on the current flowing inside the feed and spindle motor driver, using a modified portable drilling unit's control box, the details of which can be found in section 3.6. For this part of the research, the machining setup, i.e. machine tool, tool and cutting parameters, were selected to represent industrial practice, which initially required an investigation as to how these industrial parameters affect the other recorded process signals, i.e. thrust force, torque, AE and acceleration.

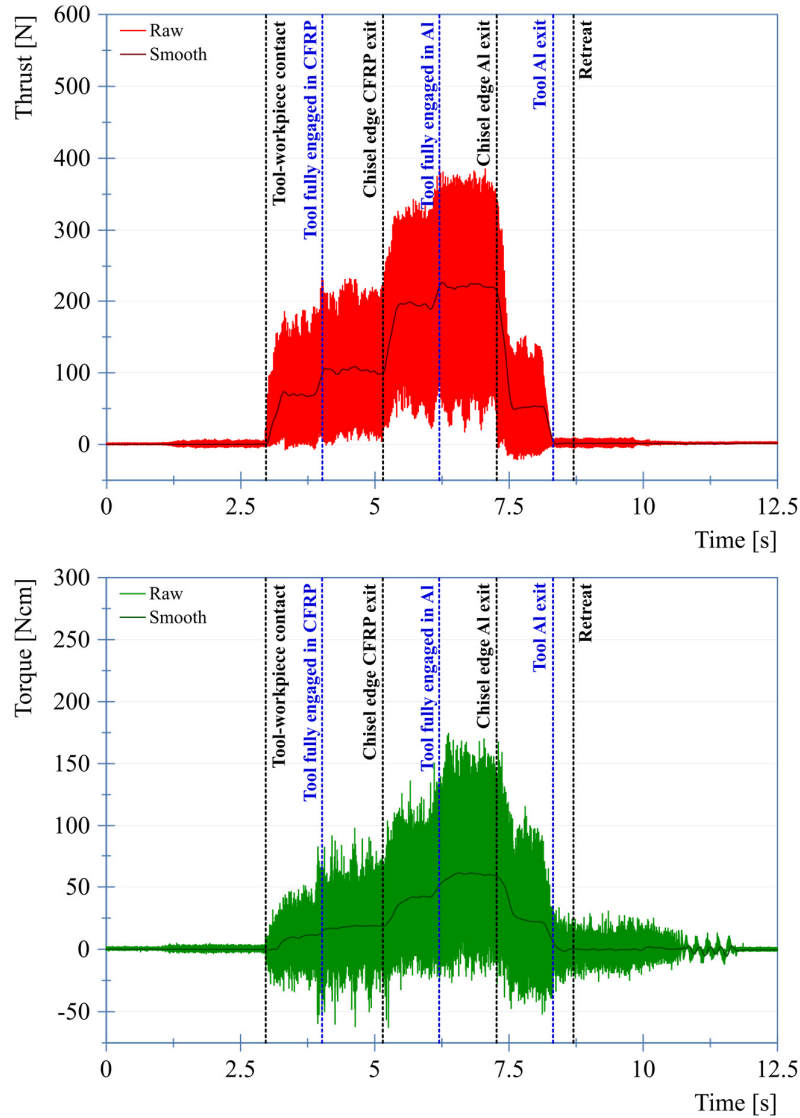
### 8.1 Impact of the utilisation of industrial parameters on process signals

The experiments were carried out with a Seti-tec éVo Light EDU, with the cutting parameters listed in Table 3 (page 73) and the accelerometers and AE sensors placed on the tool side, as shown in Figure 30 (page 81). For the three drills employed, five boreholes were drilled in each coupon with the portable drilling unit, and after every coupon was drilled 95 boreholes were machined on a CFRP dummy plate to introduce wear to the drilling tool. A total of 1005 boreholes per tool were drilled.

Typical examples of the thrust force and torque recorded using this setup are shown in Figure 83. These show that the presence of the low-frequency vibration-assisted drilling module in combination with the relatively high feed velocity (300 mm/min) resulted in strong dynamic oscillations in both the thrust force and torque. In the case of the torque, some negative values were recorded during cutting of both the CFRP and aluminium layer, thereby suggesting the presence of a force acting against the clockwise rotational motion of the drill as a result of the tool's axial oscillation. Nonetheless, as shown in the figure, smoothening the signals with a window of 50 milliseconds (5000 datapoints) revealed a very stable drilling cycle, with clear transitions following the engagement of the two sections of the stepped tool in the different workpiece layers. This suggests that, if a process monitoring system based on time domain



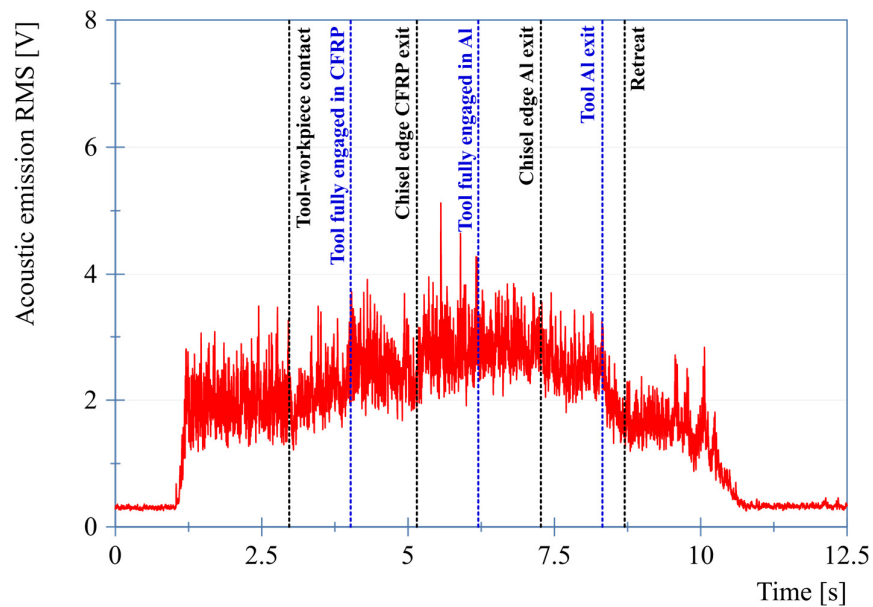
features extracted from the directly recorded thrust force and torque is to be implemented on a drilling unit equipped with a vibration-assisted drilling module, low-pass filtering could be beneficial to minimise the strong dynamic component and ease the identification of certain parameters, such as the slope of the signals.



**Figure 83: Raw and smoothened thrust and torque signal.**

The RMS AE signal recorded for a typical drilling cycle is shown in Figure 84. When compared to the experiments presented in Chapter 7, which were carried out with the sensor on the workpiece side, for this set of experiments the sensor was placed on the portable drilling unit. When the machine was switched on (at 1.2 s on the graph), the recorded AE increased substantially, even though the tool was rotating in air and was not engaged in cutting of the workpiece. After tool-workpiece contact, the engagement between the tool and the composite

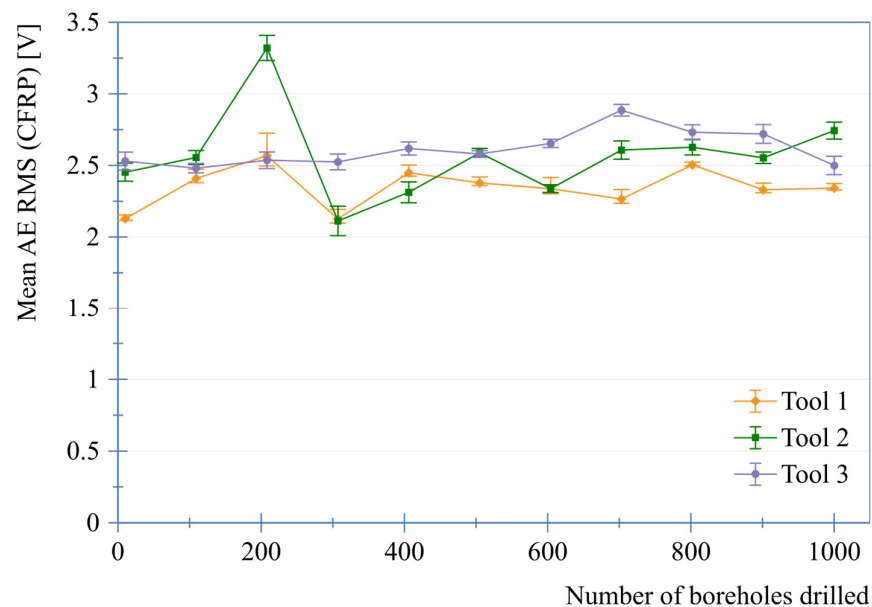
layer resulted in a slight increase in AE, albeit to a significantly lower extent if compared to that recorded when the sensor was placed on the workpiece side, shown in Figure 81. A less pronounced variation in AE was also observed for the other process incidences. This is believed to be caused by the shorter path between the machine's gearbox and the sensor, which results in the meshing of the gears within the ADU to be the more dominant source of AE as compared to the tool's cutting action. Nonetheless, throughout the experiments the occurrence of the various incidences resulting from the progression of the tool through the stack was always followed by a slight but noticeable change in the AE RMS magnitude. Specifically, the AE gradually increases as the tool progresses into the stack, before starting to progressively decrease when the tip of the first diameter breaks through the lower aluminium layer, thus initiating tool exit from the stack.



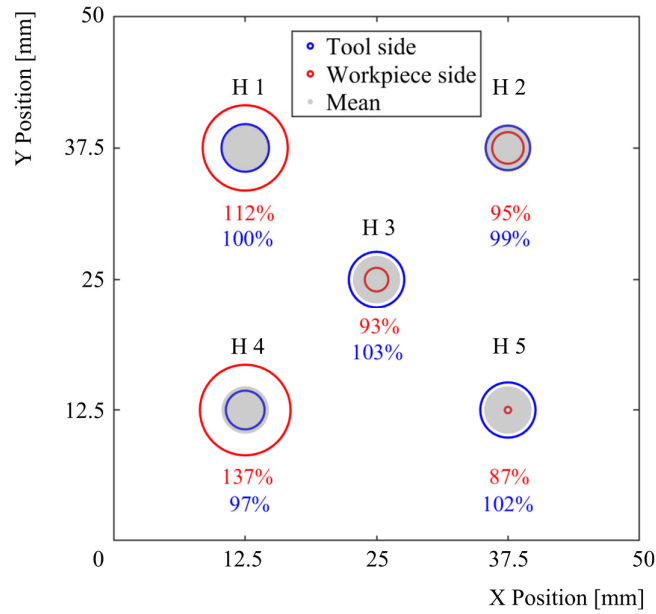
**Figure 84: Acoustic emission RMS signal.**

Figure 85 shows the mean AE signal calculated during cutting of the CFRP layer over tool life, for each of the three tools used. Tool wear does not seem to majorly affect the generated AE, which suggests that if AE is to be used as a process signal for a condition monitoring system, the decision-making algorithm would not require adjustments based on the tool condition. These results outline a different picture to the one drawn from the experiments previously carried out in this research, where it appeared that increasing wear resulted in a decrease in AE, albeit with substantial oscillations (see Figure 77, page 131). This can be explained by the different sensor location, the impact of which on the signal was investigated further.

Figure 86 shows a comparison of the percentage variation from the mean value calculated over the five boreholes drilled in each coupon of the AE signal generated during cutting of the CFRP layer. The red circles represent the tests where the sensor was placed on the workpiece side, whilst the blue circles represent the tests where the sensor was placed on the tool side. Placing the sensor on the tool side resulted in substantially more consistent measurements compared to when the sensor is placed on the workpiece side, which can be explained by the fixed sensor-to-signal-source distance. These reduced variations in the recorded signal allow for an improved accuracy and reliability of the process monitoring system. Moreover, placing the sensor on the tool side would reduce the chance of the signal experiencing variations due to the occurrence of events which are not directly linked to the drilling cycle, for example the simultaneous drilling of different boreholes in other locations of the stack. For this reason, to ensure the effectiveness of the process monitoring system, it is recommended that the sensors are placed on the tool side, if possible.



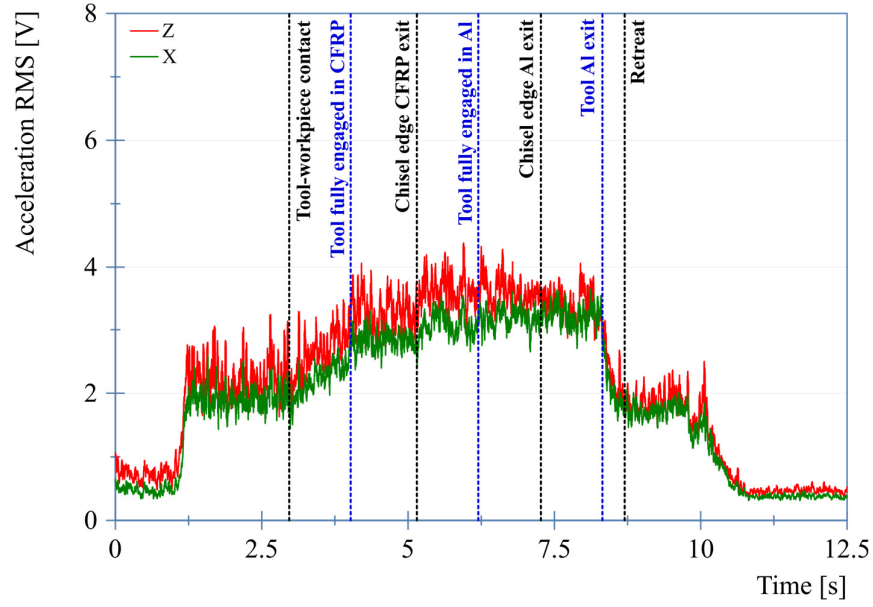
**Figure 85: Progression of average AE during cutting of the CFRP layer with tool wear.**



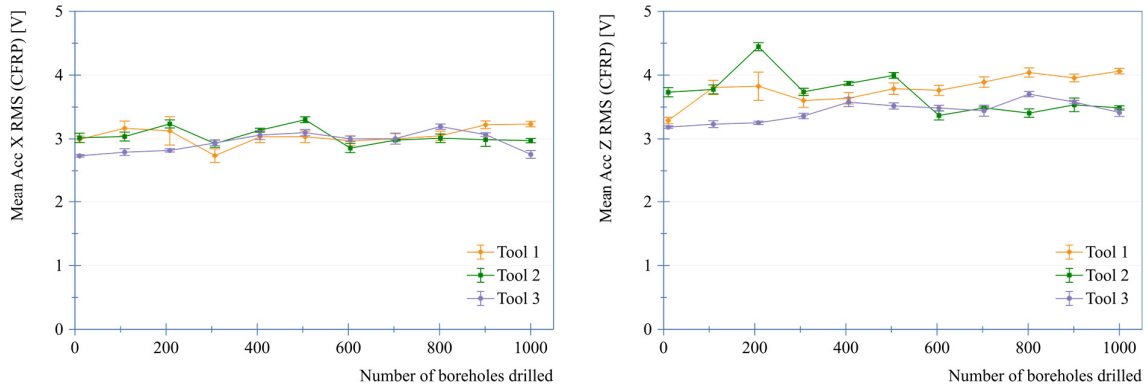
**Figure 86: Comparison of the percentage variation from the mean value of the AE RMS signal between the drilling tests carried out with the sensor placed on the tool and on the workpiece.**

Figure 87 shows the accelerations after RMS conversion in the X and Z direction for a typical drilling cycle, whilst Figure 88 shows the signal average over tool life. The acceleration in the Y direction was not measured in this set of experiments due to the limited number of inputs of the data acquisition card, to allow for the measurement of the ADU's feed and spindle current. Overall, the acceleration signals were found to be strongly correlated to the AE ones, which is in agreement with the results of the previous experiments.

As shown in Figure 88, a peak in both the AE and acceleration in Z direction was observed when drilling the third coupon using the second tool. This suggests a direction sensitivity of the AE sensor, which was oriented in the same direction as the Z-axis accelerometer. Similarly to the AE signal, the acceleration was not found to be majorly affected by the number of boreholes drilled. A possible explanation for this is that the vibrations generated by the spinning of the electric motors and the gearbox within the ADU are strong enough to cover signal variations resulting from a change in cutting mechanisms in response to tool wear. Nonetheless, each of the process incidences of interest resulted in a noticeable change in the acceleration magnitude, throughout the tool lives. Given the observed strong correlations between the AE and acceleration signal, accelerometers are considered to be more suitable sensors for a process monitoring system to detect tool engagement, material transition and tool disengagement, due to their lower cost and the lower sampling rate required.



**Figure 87: X and Z acceleration RMS signals.**

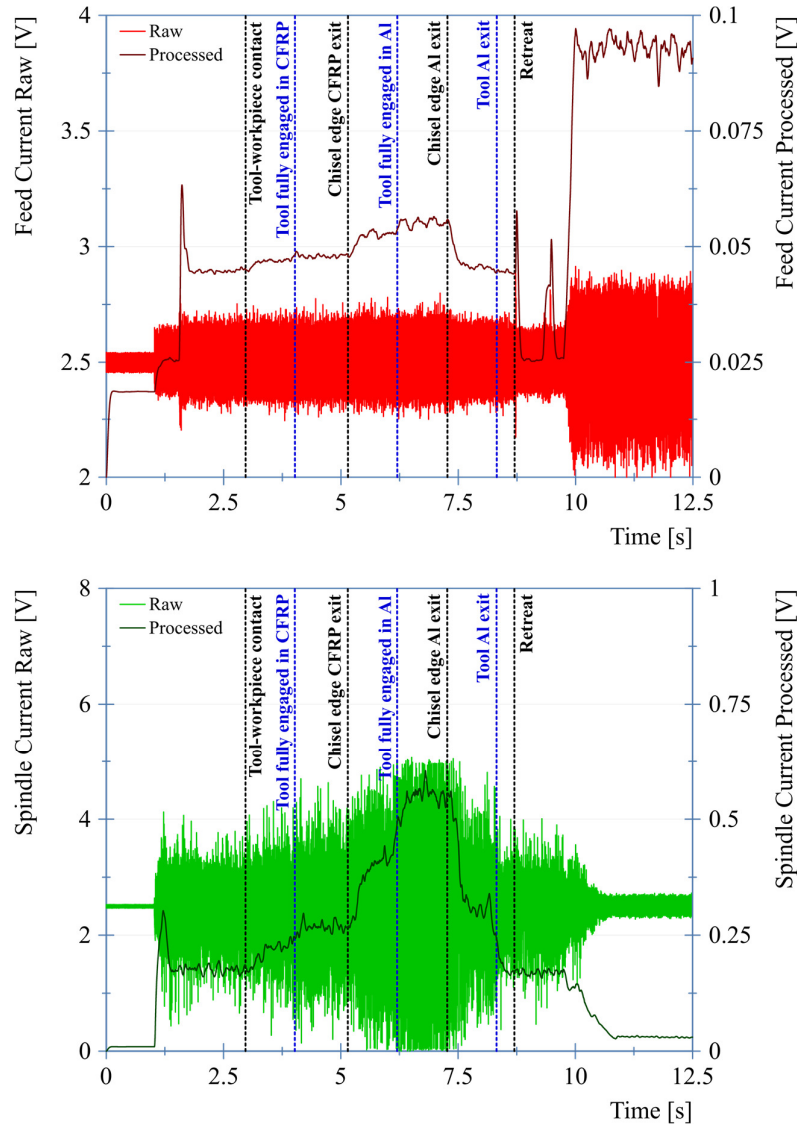


**Figure 88: Progression of average acceleration in X and Z directions during cutting of the CFRP layer with tool wear.**

## 8.2 Assessment of feed and spindle current signals

The feed and spindle current raw and processed signals recorded from the modified measuring system outlined in sections 3.5 and 3.6 are shown in Figure 89. Both the feed and the spindle raw signals oscillated around 2.5 V with an output voltage ranging between 0 V and 5 V. The raw signals were processed by: (i) performing an offset correction so that they oscillated about 0 V, (ii) calculating the root-mean-square with an interval width of 30 points, and (iii) passing the result through a 5 Hz Butterworth digital low-pass filter. The feed current signal was found to be substantially lower than the spindle current signal, which can be explained by the significantly smaller motor used for the feed drive. As shown in Figure 89 the occurrence of each of the process incidences of interest results in a substantial change in the magnitude of the

processed signals, for both the stepped tool's pilot section diameter and nominal diameter. According to Figure 89 the spindle raw signal becomes saturated when both tool diameters are engaged in the aluminium layer (i.e. between 6.25 s and 7.5 s). However, the processed signal does not flatten out at a specific value, because the raw signal comprises high frequency components which result in oscillations and are accumulated in the RMS conversion. This behaviour was confirmed for the boreholes which were drilled with the tools exhibiting the most wear (i.e. after 1000 holes), where the thrust force and torque, and consequently the feed and spindle current, were highest.



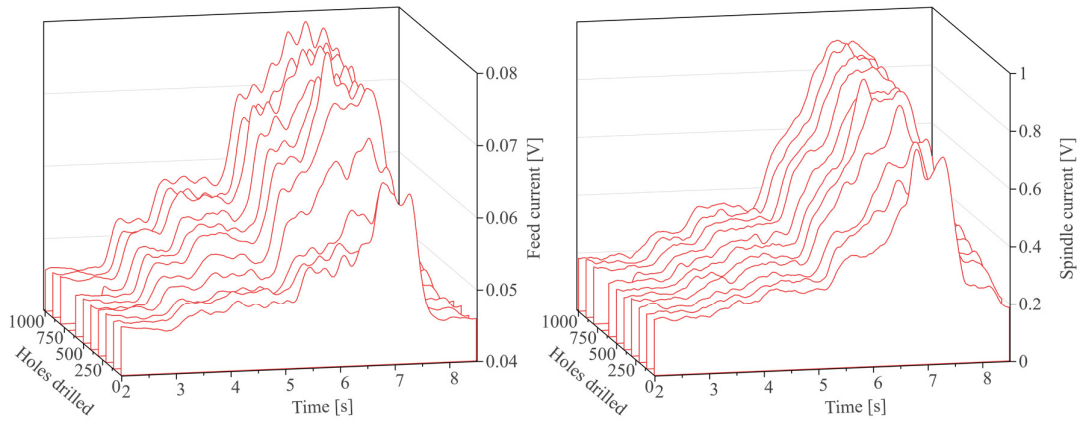
**Figure 89: Feed and spindle current signal, raw and processed.**

The evolution of feed and spindle current signals throughout tool life is shown in Figure 90. Similarly to the observations made on the directly recorded thrust force and torque in section

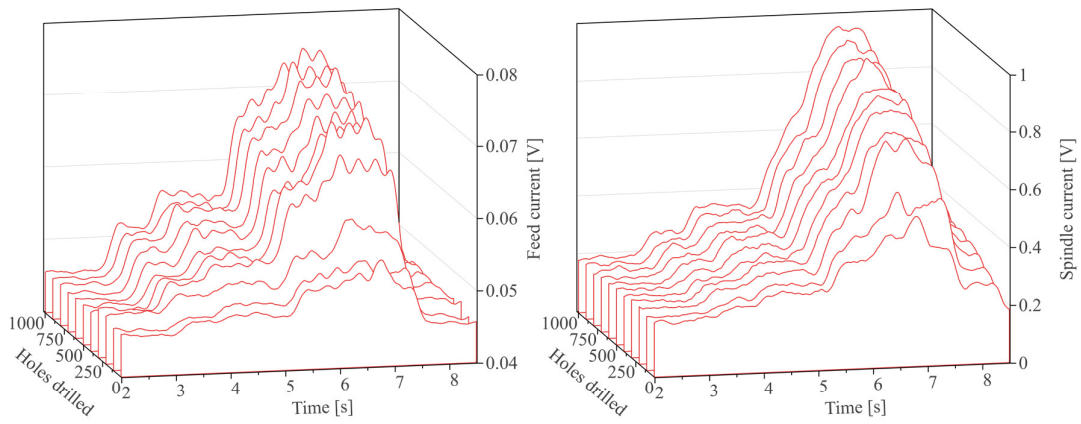
7.1.1, the magnitude of both feed and spindle current signals increased substantially as the tools wore out. Throughout the tests, the feed current, but not the spindle current, exhibited a low frequency oscillation, which can be attributed to the use of the vibration-assisted drilling module. During the first few drilling cycles, the cutting of the aluminium layer was characterised by sudden spikes in both the feed and spindle current, especially towards the end of the drilling cycle. It is believed that this was caused by an unstable chip evacuation during the running-in period of the tools, which is fairly common for coated twist drills and is brought about by the initial surface roughness of the chip flutes as a result of the coating process (Heinemann and Hinduja, 2012).

The drilling of both the CFRP and aluminium layer is characterised by a gradual increase in the feed and spindle current with an increase in the number of boreholes drilled, most likely a result of the progressive rounding of the cutting edges. The relative increase in the feed and spindle current recorded during cutting of the CFRP layer throughout the tool life was 16% and 23%, respectively, which is lower than what was observed for the drilling of the aluminium (increases of 28% and 52%, respectively). Overall, the proportional increase of the feed and spindle current was found to be substantially lower than that observed in the directly recorded thrust force and torque analysed in section 7.1.1. This is because, whilst the directly recorded thrust force and torque are solely due to the cutting action, inasmuch as they are equal to zero prior to and after the drilling cycle, the feed and spindle signal also include components which are not directly linked to material removal, such as the actuation of motors that make the tool rotate and move in axial direction whilst the tool is not engaged in any cutting.

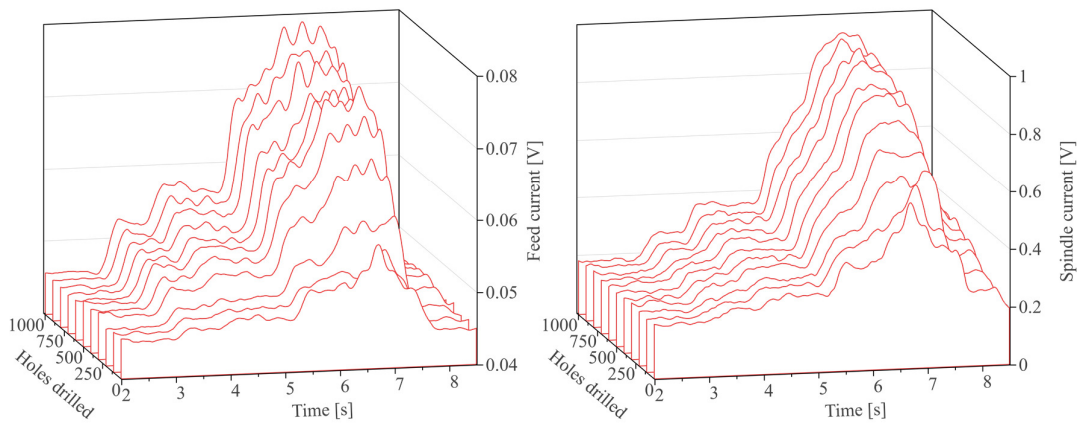
Despite some oscillations during cutting of the aluminium layer, the overall behaviour was found to be very similar for all the three drills employed in this research. Hence, to avoid unnecessary repetition in the time-frequency domain analysis and part of the significant features assessment presented in the following pages, only the results for a single tool are shown.



Tool 1



Tool 2



Tool 3

**Figure 90: Progression of feed and spindle current with tool wear.**



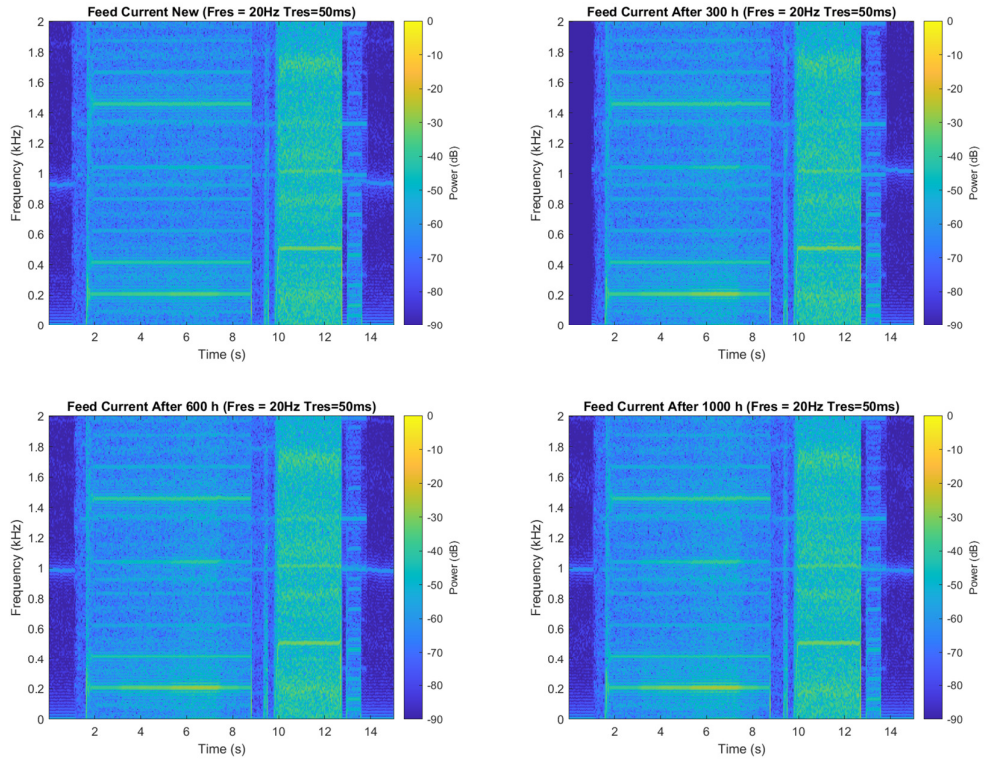
The time-frequency power spectra, obtained by computing the short-time Fourier transform (50 ms time resolution equivalent to 5000 datapoints; rectangular window; 20% overlap) for the feed and spindle current signals at four different tool wear stages are shown in Figure 91. As a result of the reduced pre-trigger size (200,000 datapoints instead of the 300,000 used for the other experiments), 100,000 zeros were prepended to the signal recorded after 300 holes to synchronise it with the other drilling cycles, which explains the very flat spectrum recorded for the first second in the feed and spindle current signals observed.

The dominant frequency for the feed current signal when cutting the stack was 200 Hz, which increased to 500 Hz (+150%) during tool retraction. These frequencies appear to be directly related to the feed velocity, which was 5 mm/s during cutting and 12.5 mm/s (+150%) during tool retraction. Similarly, the dominant frequencies for the spindle current signal were 600 Hz during cutting and 30 Hz (-95%) during tool retraction, which corresponds to the change in spindle speed from 6000 rpm during drilling to 300 rpm (-95%) during tool withdrawal.

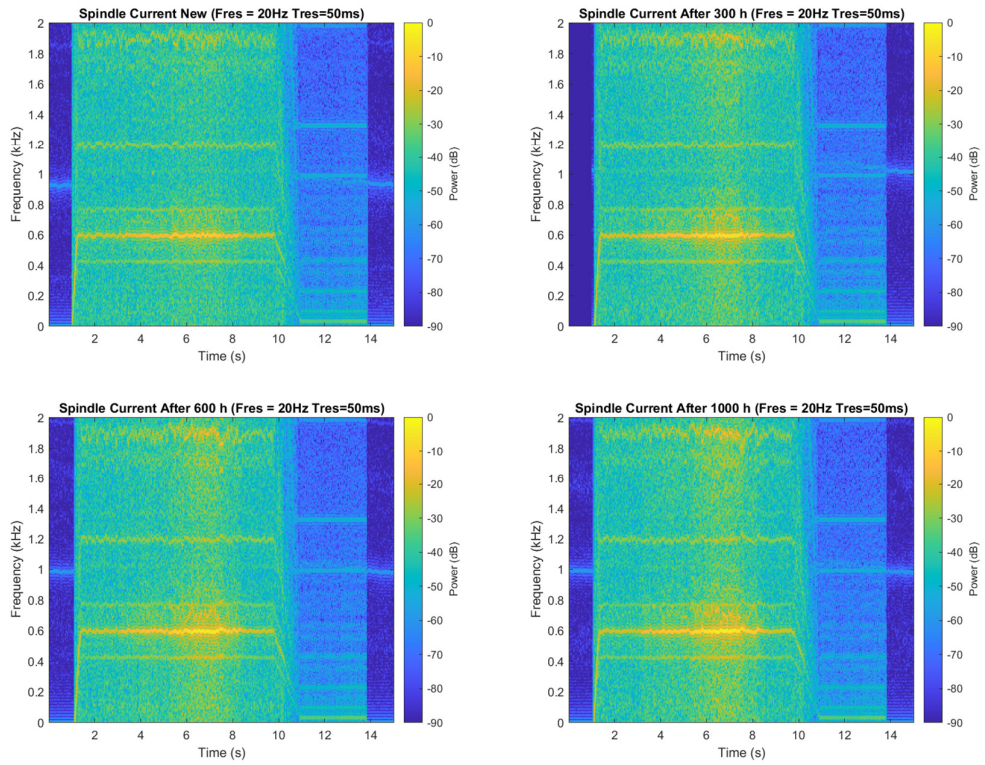
The fact that the relative variation in the feed and spindle velocity is exactly the same as the variation of the dominant frequency of the respective motor current signal suggests that the dominant frequency is related to the rotation of the electric motors or some other component within the gearbox. To further assess this, the rotational frequency of each of the gears during cutting of the stack was calculated. The rotational frequency of the feed gear, for example, was calculated based on the rotation of the spindle (6000 rpm, equivalent to 100 Hz), the pitch of the leadscrew (1.5 mm) and the feed rate (0.05 mm/rev), which resulted in:

$$\begin{aligned}\omega_{feed\ gear} &= \frac{\omega_{spindle} \times (pitch - feed\ rate)}{pitch} = \frac{100 \times (1.5 - 0.05)}{1.5} \\ &= 96.7\ Hz\end{aligned}\quad (3)$$

This is because the feed gear has to spin in the opposite direction to the spindle gear, to slow down the axial advancement of the tool, which would otherwise be solely driven by the leadscrew's pitch, and hence achieve the specified feed rate.



(a)

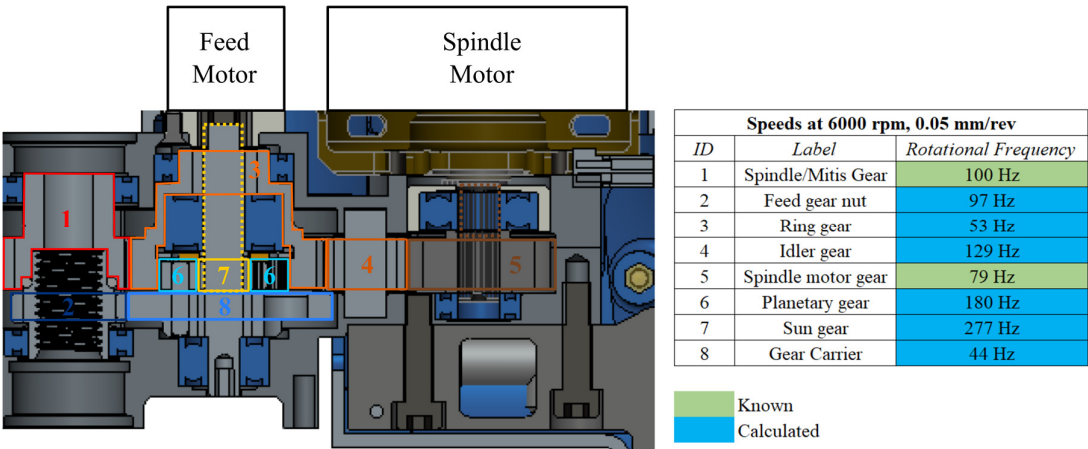


(b)

Figure 91: Spectrogram for current signals; (a) feed current, (b) spindle current.

The calculated speeds of all the gears within the gearbox are presented in Figure 92. It is important to point out that the calculation of some gear ratios and rotational speeds was possible on an approximate basis only, as this had to be done based on drawings of the gearbox obtained from documents and images taken during an on-site setting up of the device; a full list of parts was not available, neither was a full disassembly of the unit possible. Nonetheless, the rotational velocities and tooth engagement frequencies of most of the gears are in the range of the dominant frequencies of the power spectra. In particular, the rotation of the planet gears appears to cause a dominant frequency, which is reasonable as they are considered as a major source of vibration. According to the drawings, as well as observations made during the on-site setting up, the planet gears were simply supported by dowel pins pressed into the carrier, with the connection between gears and pin being a rather loose clearance fit.

Throughout the drilling tests, no noticeable variations in the dominant frequencies of the feed and spindle current signals were observed between cutting of the CFRP and aluminium layers. Thus, monitoring predetermined frequency ranges does not appear to be an effective approach to determine the occurrence of the process incidences of interest, for which the use of time domain signal features appear to be more suitable. With regards to the effect of tool wear on the power spectra, the observed increase in the current signal for both the feed and spindle current was found to be evenly distributed across all frequencies. This can be explained by the gradual rounding of the cutting edges and resulting increase in thrust force and torque and, consequently, motor load.



**Figure 92: Gearbox schematic with the rotating speed of the different components during cutting of the workpiece.**

### 8.3 Significant feature assessment

To identify significant features that are strongly correlated to the process incidences of interest and study how these are affected by tool wear, a detailed assessment was carried out on the range and the gradient of the current signals. These two features were selected as, based on a visual assessment of the process signals, they appeared to exhibit variations in response to the occurrence of the process incidences of interest.

Figure 93 shows the range of the feed and spindle raw signals, which was calculated as the difference between the signals' maximum and minimum magnitudes within a time window of 0.15 s. The range of both the feed and spindle current increases for the first time when the machine is switched on and the tool rotates and advances in air, peaking at 1.5 s during the acceleration to the specified velocities. The feed current signal only exhibits a small variation in its range after tool engagement and throughout the drilling of the CFRP, making the detection of tool-workpiece contact difficult. The transition of the tool into the aluminium layer results in a more noticeable, yet still rather small, change in the signal. The final section of the drilling cycle, where the tool penetrates through the aluminium layer and is most susceptible to chip clogging, is characterised by sudden increases in the signal range. These peaks become more common with tools exhibiting more extensive wear, as the likelihood of chip clogging increases. The feed current range then decreases gradually as the tool breaks through the aluminium layer and then dwells once it reaches the final z position, before rising again during tool retraction, which took place at the maximum allowable feed velocity (12.5 mm/s).

Similarly to the feed, the range of the spindle current also rose rapidly during machine switch-on. From initial tool engagement onwards, the range increased gradually, as the tool progressed into the workpiece material. In the case of the spindle current signal, substantial changes in the extracted feature were observed as a result of the three process incidences of interest. During cutting of the aluminium layer using tools which had drilled more than 300 boreholes, the range levelled off at 5 volts due to the saturation of the raw current signal, as shown in Figure 89. Tool exit is characterised by a decrease in the signal range, which becomes more pronounced when the outer cutting edges of the stepped tool break through the aluminium layer, as these are the main contributors to the drilling torque. The range then plateaus when the tool dwells after reaching the final Z position, as the spindle still rotates at the rotational speed set for cutting (6000 rpm), and only later drops once the spindle slows down to 300 rpm once tool retraction is initiated.

To ascertain whether the width of the time window has any noticeable impact on the changes in the feature ‘signal range’, the window size over which the feature was computed was changed to 0.05 s and 0.25 s. The results, shown in Figure 94, reveal that reducing the time window leads to a higher resolution of the signals’ range in the time domain. On the one hand this would increase the responsiveness of a system based on range monitoring, but on the other hand would result in high frequency oscillations which could lead to erroneous detection and a lower system accuracy. Increasing the time window has the opposite effect, as it decreases the resolution but increases the smoothness of the signal.

Overall, although some information can be extracted from the range of both current signals, this feature seems to lack both significance and reliability for the detection of tool engagement, material transition and tool disengagement during drilling of multi-material aerospace stacks.

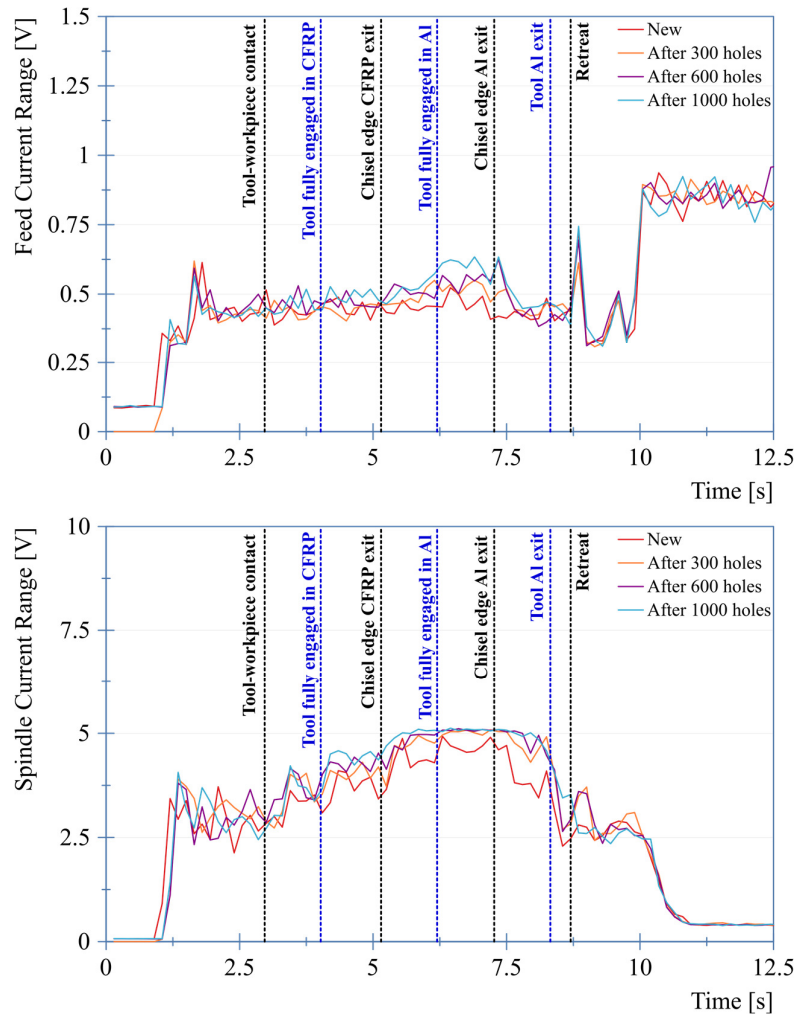
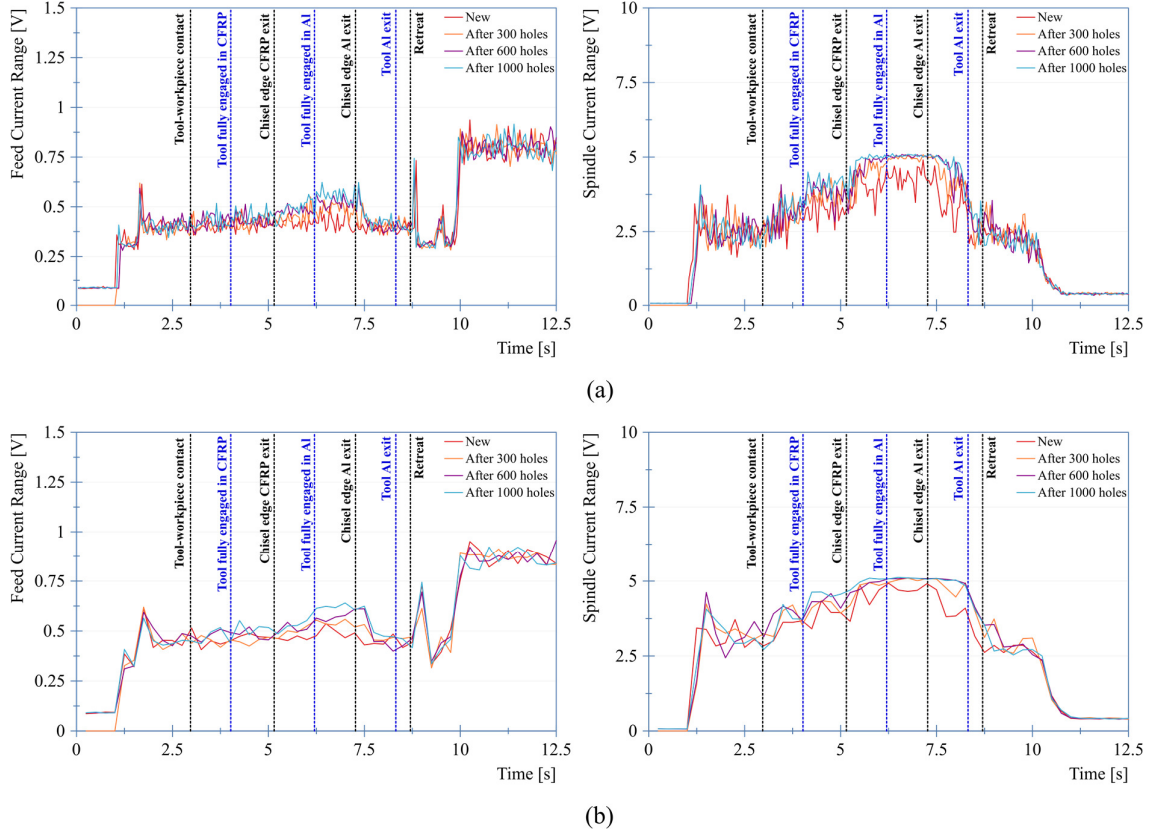


Figure 93: Feed and spindle current range (time window: 0.15 s).





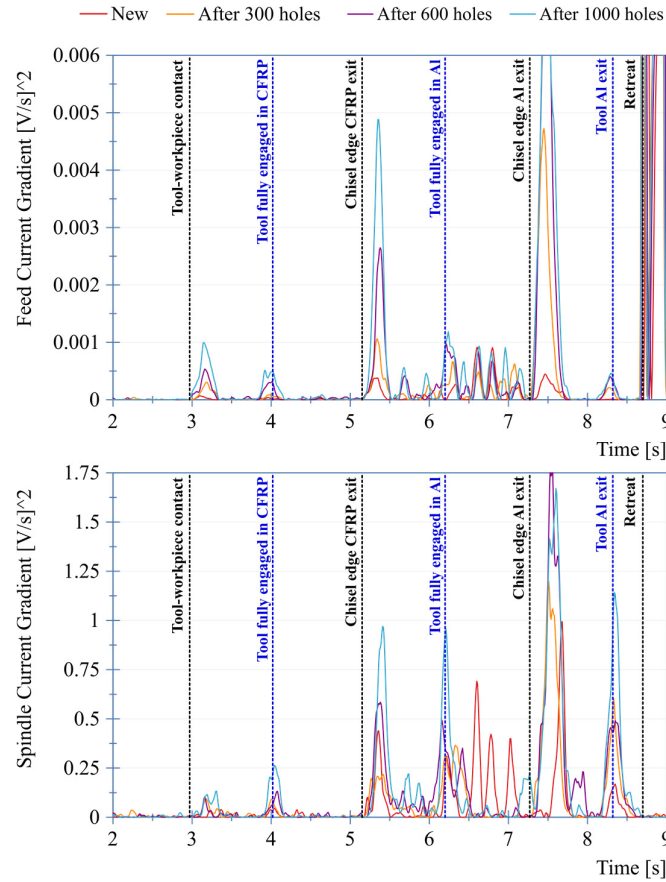
**Figure 94: Feed and spindle current range using different time windows; (a) 0.05 s, (b) 0.25 s.**

The second significant feature investigated was the signal gradient, which was calculated using the forward difference quotient, which was then squared to increase the signal-to-noise ratio. The forward difference quotient was calculated by the data processing software (NI Diadem) and is defined as:

$$y'_n = \frac{y_{n+1} - y_n}{x_{n+1} - x_n} \quad x'_n = \frac{y_{n+1} - x_n}{2} \quad (4) \text{ (Diadem, 2021)}$$

Figure 95 shows the calculated gradient for the feed and spindle current, at four different tool wear stages. The figure clearly shows that all process incidences of interest resulted in a noticeable increase in the squared signal gradient, as a result of the substantial changes in signal magnitude between the different stages of the drilling cycle. The increase in the squared signal gradient becomes even more substantial with growing tool wear, as this requires an increase in the current provided to perform material removal for both the CFRP and aluminium layer. Consequently, as a result of the larger differences in signal magnitude between the different stages of the drilling cycle, the gradient during these transitions becomes larger.

A time delay was observed between the occurrence of the process incidences of interest and the corresponding peak in the signals' gradient. This delay was substantially lower for the feed signal compared to the spindle signal. This is because the feed current is related to the thrust force, whose main contributor is the chisel edge, which is the first part of the tool to establish contact with and separate from the workpiece material during initial engagement and final break through, respectively. In contrast, the main contributor to the spindle current are the cutting edges, which originate from the chisel edge and lean backwards as a result of the tool's point angle. Consequently, the change in load on the spindle motor drive as a result of tool engagement, transition or breakthrough will occur slightly later and less abruptly. The noisy behaviour in the spindle current gradient observed during cutting of the aluminium layer can be explained by the stochastic occurrence of chip clogging. The oscillations were particularly strong during the running-up period of a brand new tool, where the rough coated surface of the chip flutes appears to have deteriorated the chip flow, thereby resulting in sudden increases in the motor load. However, the gradient measured during cutting of the aluminium layer stabilises after the running-in period. Although squaring the gradient substantially eases the distinction between signal changes resulting from the occurrence of the incidences of interest and other variations, it makes it impossible to identify the direction in which these changes happened, i.e. an increase (positive) or decrease (negative) in the motor current. To retain this ability, the squared signal needs to be multiplied with the original gradient's sign.



**Figure 95: Feed and spindle current gradient (new, after 300, 600 and 1000 holes).**

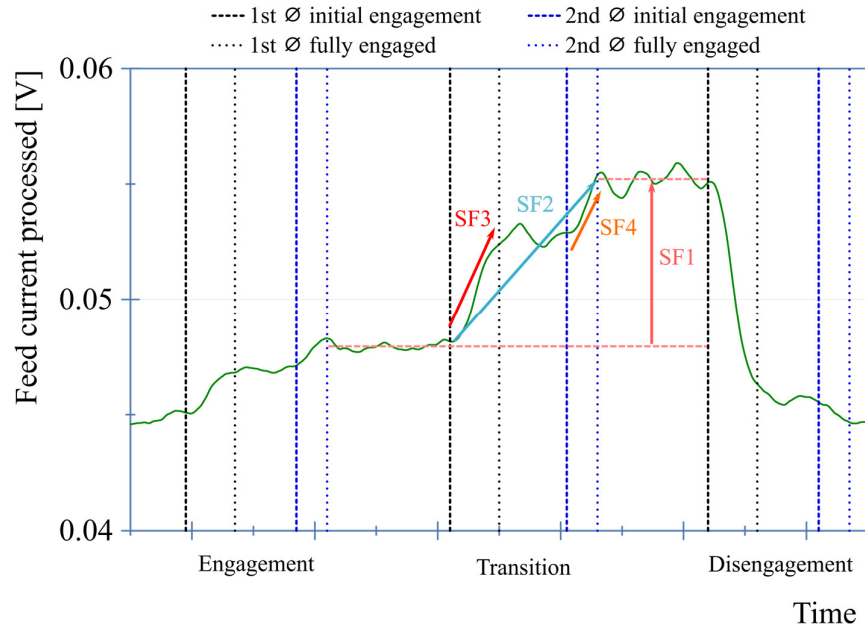
In general, strong relationships were observed between motor current gradient and tool engagement, material transition and tool disengagement. To further analyse these relationships, a quantitative assessment on the most effective way to extract information related to the signal gradient at different stages of tool wear was carried out. For this, four different significant features were extracted from the feed and spindle current signals, which are:

- SF1: Difference between the average signal magnitude during single-material cutting after full engagement of the second tool diameter and the average magnitude prior to the initial engagement of the first tool diameter.
- SF2: Gradient of the signal between initial engagement of the first tool diameter and full engagement of the second tool diameter.
- SF3: Gradient of the signal between initial engagement and full engagement of the first tool diameter.



- SF4: Gradient of the signal between initial engagement and full engagement of the second tool diameter.

Figure 96 graphically illustrates what these represent for tool transition. The extracted features at different stages of tool wear for tool engagement, tool transition and tool disengagement are shown in Figure 97 to Figure 99.



**Figure 96: Gradient features extracted from the motor current signals.**

With regards to tool engagement considering the feed current, all features were found to increase with tool wear. The smallest variations were exhibited by SF1 and SF2, as they were computed over a much larger time window (i.e. greater number of datapoints) than SF3 and SF4. Although SF2 appears to be the feature least affected by the increase in tool wear, throughout the tests it exhibited an extremely small magnitude, which would make tool engagement hard to detect and prone to false detection. In contrast, SF3 and SF4 were characterised by substantially larger amplitudes. In addition, SF4 exhibited substantial variations during the final tool life stage, as the periphery of the cutting edges, the area most prone to abrasion wear, experienced substantial rounding. When cutting with a new tool, SF3 exhibited the largest magnitude amongst all significant features, as it was only calculated during engagement of the first diameter, which as the main contributor to the thrust force requires a major part of the feed current generated. Consequently, a relatively large threshold could be used for detecting engagement when using SF3 extracted from the feed current, which

would ensure the incidence is detected rapidly after occurrence whilst at the same time avoiding false detection resulting from oscillations in the motor current due to other factors.

Despite the substantially larger magnitudes as a result of the larger spindle motor, the spindle current SFs and feed current SFs exhibit quite similar trends overall. Tool wear did not appear to noticeably affect SF2, whilst SF4 exhibited even greater oscillations at earlier tool life stages than those observed for the feed current. This is possibly because the occurrence of chip clogging has a greater effect on the cutting torque than the thrust force, resulting in substantial spikes in the spindle motor load. In contrast, a slightly smaller magnitude was exhibited by SF3, which was found to be less affected by oscillations.

The extracted significant features at different stages of tool wear for material transition are shown in Figure 98. An initial decrease was observed in SF1 and SF3 before the subsequent rise associated to tool wear, as a result of the effect of the tool running-in period on the thrust force and torque. Larger magnitudes were observed for SF3 when compared to tool engagement, particularly when drilling the first 200 boreholes. Similarly to what was observed for tool engagement, SF2 was only slightly above zero for the first 10 boreholes (i.e. 2 coupons), which would make the detection of the process incidences of interest very prone to false detection. SF4 instead varied significantly throughout the tool life for all the tools used, sometimes even exhibiting negative values. This can be explained by the second tool step only minorly affecting the thrust force and consequently the feed current, which at this stage of the drilling cycle is instead subject to strong variations as a result of the presence of chips within the chip flutes.

The extracted significant features at different stages of tool wear for tool disengagement are shown in Figure 99. All of the investigated SFs exhibited a negative amplitude, as the load in both the feed and spindle drive decreases when the tool breaks through the lower layer and exits the stack. The SFs experienced greater oscillations compared to tool engagement and material transition, as the increasing deterioration of the chip flow and resulting increase in friction between compacted chips inside the flutes and the borehole wall during this part of the drilling cycle significantly affects the feed and spindle motor loads. The features extracted during drilling of the first five boreholes, in particular SF3 and SF4, were found to vary noticeably, which is believed to be caused by the rather unstable chip flow during the tool's running-in period. The stronger oscillations of SF3 and SF4 compared to SF1 and SF2 can be attributed to the smaller number of datapoints used to compute the former two.

Similarly to what was observed for the other two process incidences, SF1 and SF2 were found to be subject to less oscillations and exhibit lower magnitudes than SF3 and SF4. For the purpose of detecting tool disengagement, these oscillations over the tool's life are not believed to be problematic as long as the magnitude of the SF stays well below zero, as this would allow setting a threshold with a negative reference value. The features extracted from the feed current signals were found to be once again more stable than those extracted from the spindle current as a result of the weaker impact of the chip flow on the thrust force than on the torque.

Overall, despite the substantial oscillations observed during tool disengagement, SF3 appears to be the most suitable feature to be extracted from the feed and spindle motor current, as it consistently presented non-zero values for all the process incidences under investigation. Furthermore, extracting features from data recorded during engagement of the first diameter would substantially increase the responsiveness of the incidence detection. SF4 could however still be used as a means of confirming whether the detected incidence actually took place, in which case the respective transition of the second tool diameter would also produce a noticeable signal variation.

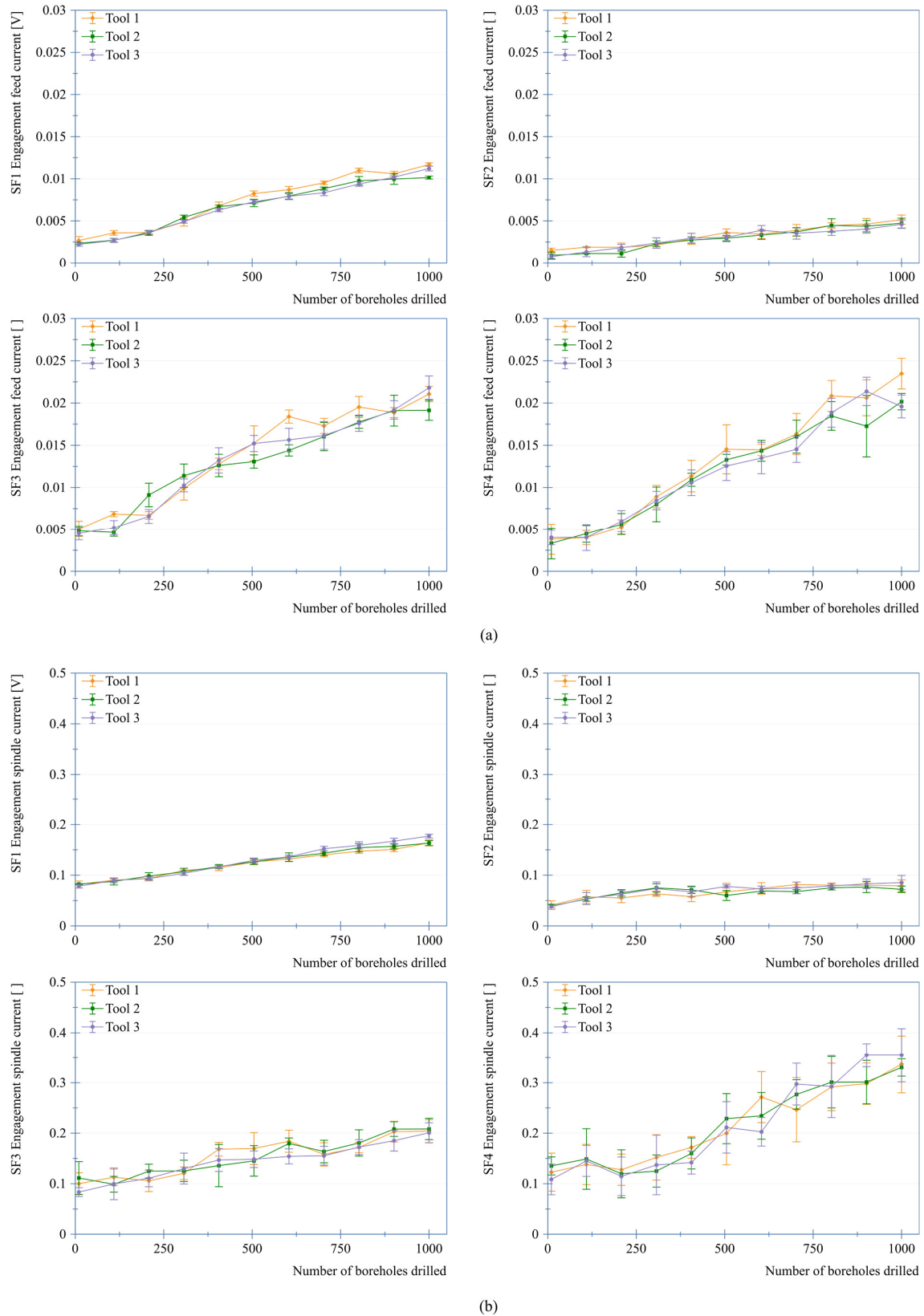
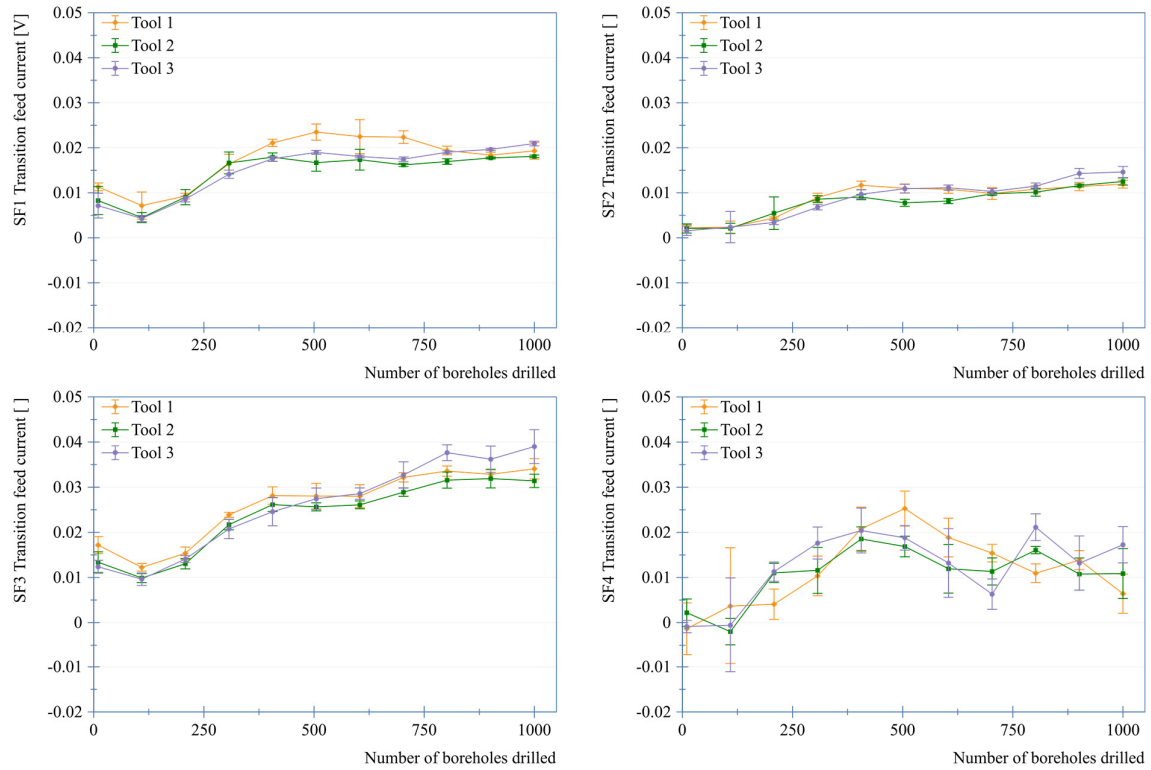
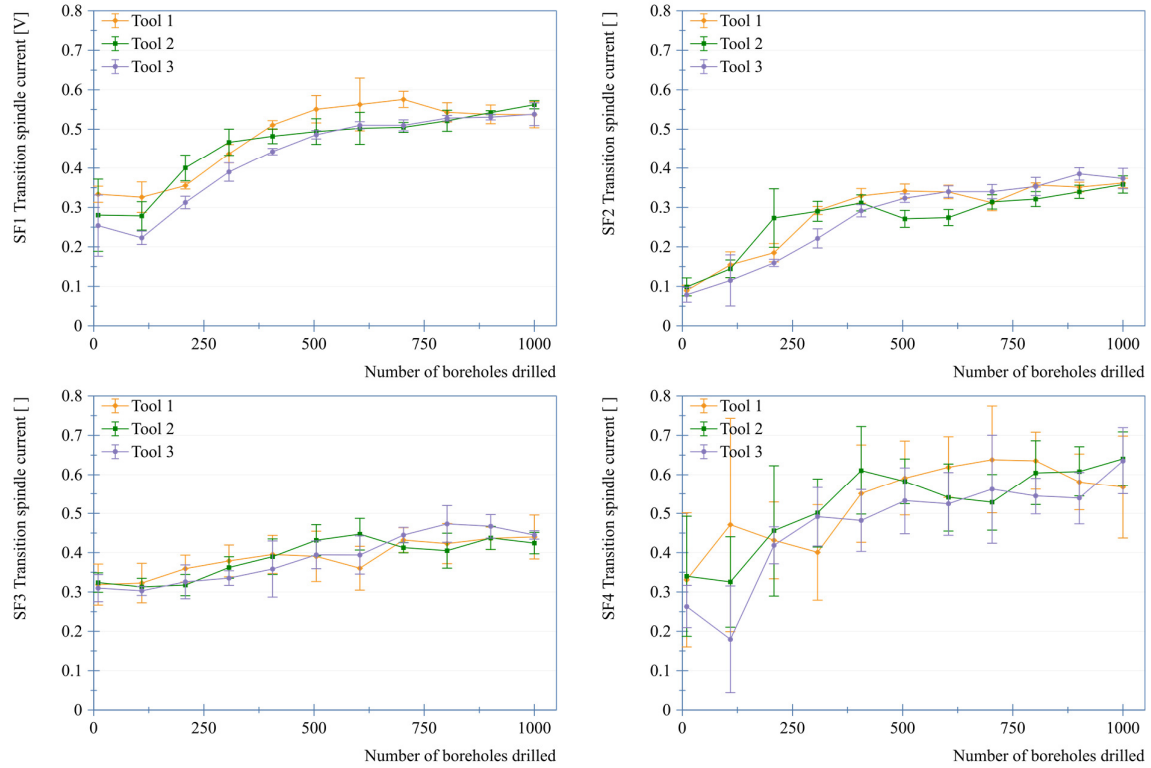


Figure 97: Tool engagement SF 1-4; (a) feed current; (b) spindle current.

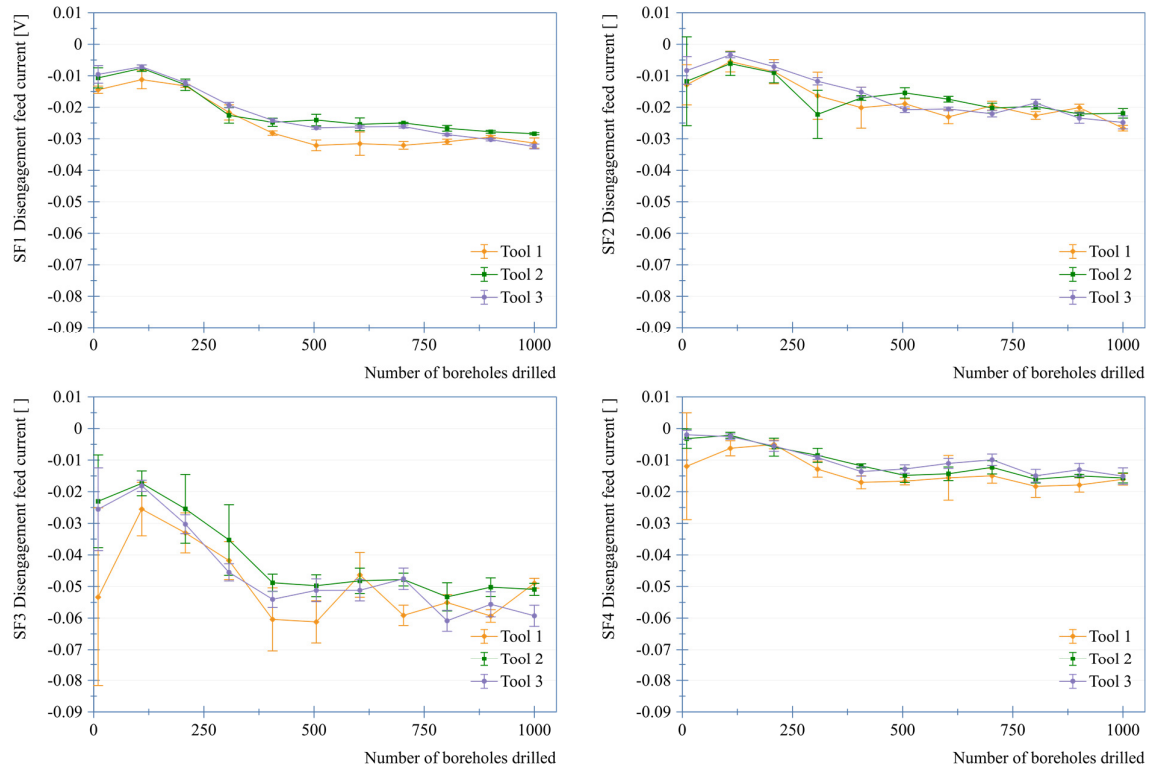


(a)

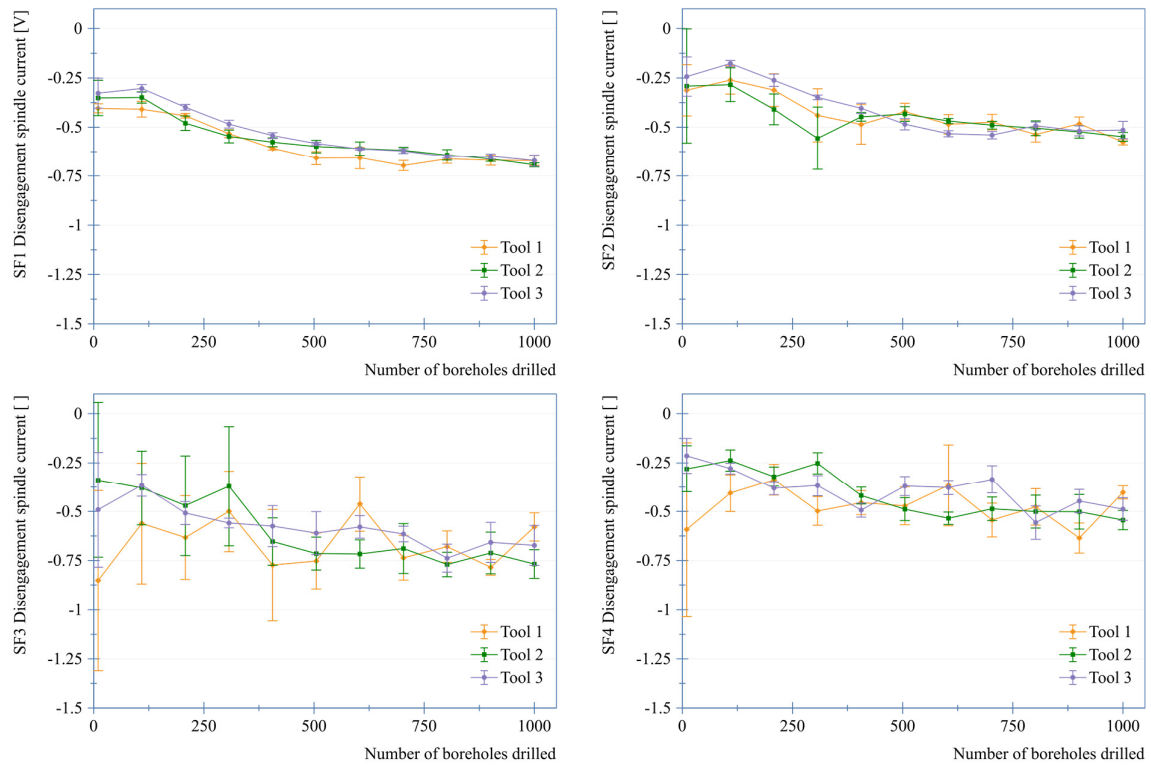


(b)

**Figure 98: Material transition SF 1-4; (a) feed current; (b) spindle current.**



(a)



(b)

**Figure 99: Tool disengagement SF 1-4; (a) feed current; (b) spindle current.**

## 8.4 Summary

This chapter presented the results of a detailed investigation on the suitability of measuring indirectly recorded thrust force and torque as process signals to detect tool engagement, material transition and tool disengagement, by means of monitoring the current flowing inside the motor controller of an automated drilling unit.

Both the feed and spindle current showed a high correlation to the directly recorded thrust force and torque. A time-frequency domain analysis revealed no noticeable variations in the signals' dominant frequencies when the tool transitions from the CFRP to the aluminium layer, thereby suggesting that a time-domain analysis represents a more suitable approach for the achievement of adaptive drilling. Out of the four significant features extracted from the feed and spindle current signal, the gradient of the signal between initial engagement and full engagement of the first tool diameter (SF3) is believed to be the most suitable, as it consistently represented non-zero values for all the investigated process incidences. Furthermore, performing feature extraction from data recorded during engagement of the first diameter would substantially increase the responsiveness of the incidence detection.

## Chapter 9: Decision-making strategy design and assessment

The research presented in Chapters 7 and 8 allowed for the identification of signal features and patterns that are related to the three process incidences of interest (i.e. tool engagement, material transition and tool disengagement), as well as providing an understanding of how these features are affected by tool wear. This chapter presents the design and development of a decision-making strategy to detect these process incidences. The strategy's performance was assessed by comparing it to those used by commercially available drilling units that, according to their manufacturers, are capable of adaptive drilling. This assessment was carried out offline by feeding pre-recorded data to an analyser script, using process signals recorded under two different experimental conditions. This chapter also includes an investigation on the relationship between sampling rate and signal information richness, as well an assessment on how a reduction in sampling rate affects the efficacy of the decision-making strategies.

### 9.1 Decision-making strategies design

Three different decision-making strategies were assessed. The first two are representative of algorithms used in commercially available units, whilst the third one was developed by the author based on the findings presented in the previous chapters. All the decision-making strategies aimed at detecting the occurrence of the three process incidences of interest: tool engagement (i.e. when the tool first makes contact with the upper layer of the stack), material transition (i.e. when the tool moves from the upper to the lower layer of the stack) and tool disengagement (i.e. when the tool breaks through the lower layer of the stack). The occurrence of each incidence was taken relative to the chisel edge, i.e. the lowermost portion of the tool.

Decision-making strategy A consists of a single threshold  $T_0$  per process incidence, which is kept constant throughout the tool's life. When the magnitude of the recorded signal exceeds the threshold for tool engagement or material transition, the algorithm triggers the system to mark that particular point as where the incidence was detected. Likewise, in the case of tool disengagement, the incidence is detected when the signal falls below the specified threshold. To reduce the amount of user input, the thresholds for tool disengagement and tool engagement were set to the same value, as in both cases the tool transitions from cutting the workpiece to rotating in air, or vice versa.



In the case of decision-making strategy B, two thresholds for each incidence are defined:  $T_0$  for a new drilling tool and  $T_w = wT_0$  for a worn tool that has undergone  $h_w$  drilling cycles. To take into account the changes in the signal as a result of tool wear, the thresholds for each incidence are linearly scaled, as a function of the number of already drilled boreholes,  $h$ , according to:

$$T(h) = T_0 + (T_w - T_0) \times (h / h_w) \quad (5)$$

The system registers a process incidence when the monitored process signal crosses the respective threshold. Similarly to strategy A, the same threshold was used for tool engagement and disengagement.

In view of the knowledge obtained in the previous stages of the research and presented in Chapter 7 and 8, it appears questionable as to how well these two strategies (A and B) are capable of maintaining a satisfactory accuracy and reliability throughout tool life. The research conducted during the course of this project has shown that signal features are subject to significant changes as a result of the unavoidable deterioration of the tool, which could result in delayed process incidence detection and/or false alarms. The identification of this shortcoming has therefore led to the design and development of a third decision-making strategy, C. Unlike strategies A and B, strategy C relies on monitoring the signal gradient, which throughout the tool life exhibits strong correlations to the process incidences of interest. Such a gradient-based approach has already been successfully employed in other manufacturing applications (e.g. Bakker et al., 2015b; Shuaib, 2018). In this decision-making strategy, the process signal's gradient is computed using a 3-point backward finite difference stencil. To enhance the signal-to-noise ratio and intensify the variations caused by the occurrence of the process incidences of interest, the gradient was squared. To retain the ability to discriminate between positive (e.g. during tool engagement and material transition) and negative (e.g. during tool disengagement) signal variations, the squared signal was then multiplied by the gradient's sign.

The strategy relies on a parameter,  $T_0$ , which is kept unmodified throughout the tool's life, based on which two thresholds are defined to detect the three process incidences of interest. The first threshold is equal to  $T_0$  and is used for detection of tool engagement and material transition. The second threshold, used for tool disengagement, is equal to  $-kT_0$ , with  $k$  being a pre-defined value that is constant for a combination of tool and material. As shown in Figure 95 (page 156), chip clogging is increasingly likely towards the end of the drilling cycle and can result in rapid changes in process signals, which would cause a spike in the computed gradient.

Thus,  $k$  is normally set greater than 1 to prevent erroneous detection of tool disengagement, as a result of substantial rises in the signal gradient due to chip clogging. In addition, after each incidence is detected, the system needs to wait for a certain amount of time to allow for the gradient to drop below the threshold again, as otherwise the detection of the next incidence would be immediately triggered. It was therefore decided to allow for the tool tip to complete the transition into the next layer before restarting monitoring the signal, by computing a delay based on the height of the tip and the feed velocity. A limitation of this approach is that the layers need to be of a certain minimum thickness, below which the system cannot be given enough time to recover.

## 9.2 Assessment of decision-making algorithms

Two sets of previously recorded data during drilling of CFRP/Aluminium stacks were used for the assessment. The data recorded with two of the three twist drills used for the analysis presented in Chapter 7 was used for the first set. The experiments were carried out on a CNC machining centre. For each drill, 11 boreholes were drilled into the stack whilst recording the thrust force and torque. To acquire cutting force data representing different tool wear stages, a CFRP dummy plate was used for wearing out the drilling tools by carrying out 10 drilling cycles, each 15 mm deep, in-between each borehole drilled on the CFRP/Aluminium stack. Thus, boreholes 1, 12, 23, etc. were drilled into the stack, whereas boreholes 2-11, 13-22, etc. were drilled into the dummy plate. A total of 111 boreholes were drilled with each tool which, on average, resulted in a tool flank wear length  $v_B$  of approximately 0.3 mm. The second set of data was recorded whilst using a portable electric drilling unit (Fives Light-eADU). A tool with a stepped geometry for aerospace stack drilling (see Table 3 on page 73) was employed. Two sets of six boreholes were drilled into the stack. In between those, 100 boreholes were drilled on a CFRP dummy plate to wear out the cutting tool.

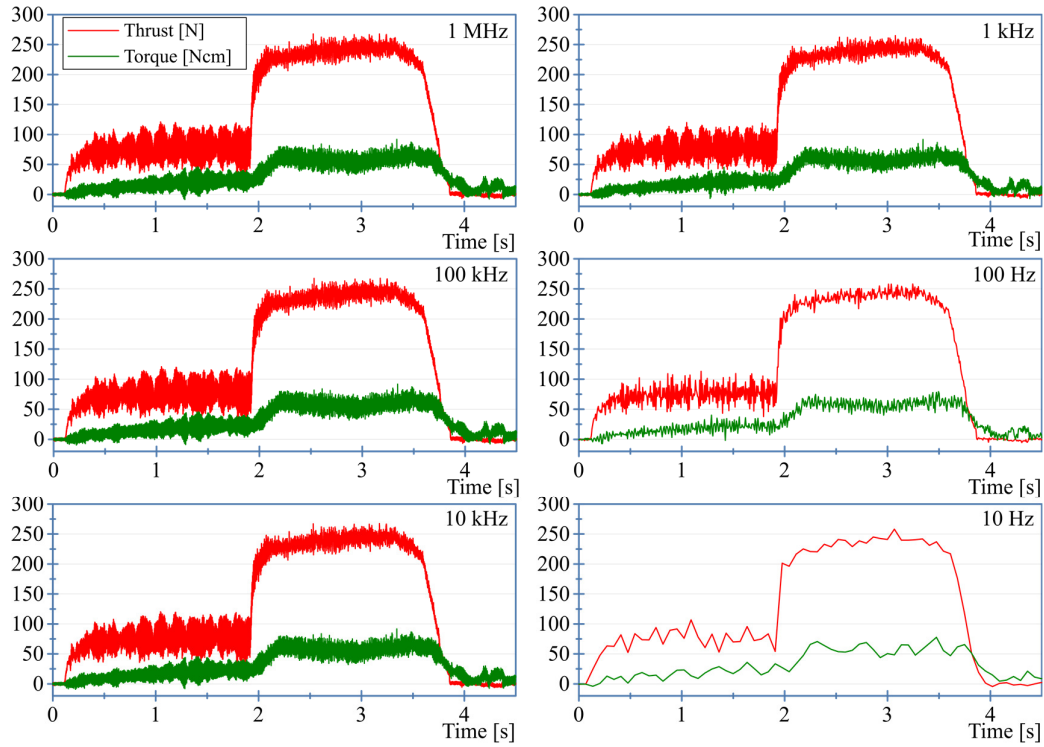
For the first set of experiments, the thrust force recorded by the dynamometer was used as the input signal to the decision-making strategies. For the second set of experiments, a voltage proportional to the current flowing through the motor controller was used as the input.

The ability of a process monitoring system for real-time analysis depends on two factors: the amount of data presented to the system and the computing resources available to process the data. The amount of data fed to the system is affected by the rate at which the process signals are sampled. Computing resources are particularly restricted in portable drilling units, due to

economic considerations and the limited space available to safely store fragile hardware (Bagshaw, 2018). It thus felt appropriate to carry out an analysis to identify a suitable sampling rate for the decision-making strategy assessment which guarantees that enough information is acquired to accurately depict the drilling cycle in the time domain whilst minimising the required computing resources.

Figure 100 shows the typical thrust force and torque recorded during a drilling cycle on a CFRP/Aluminium stack. The signals were recorded with a sample rate of 1 MHz, which is the maximum sampling rate of the data acquisition card used (NI 6356), and then repeatedly under-sampled by a factor of 10 to simulate lower sampling rates. The graphs clearly show that no noticeable differences in thrust force and torque were observed when the sampling rate was decreased from 1 MHz to 100 kHz and then 10 kHz. Reducing the sampling rate even further to 1 kHz would have resulted in the majority of information still being accurately depicted, with the exception of some dynamic components of the thrust force and torque. In contrast, sampling at a rate of 100 Hz or 10 Hz, which is in the region of the sampling rates used by the majority of the online monitoring systems available on the market (Bagshaw, 2020), would result in a gradual loss of information in both the thrust force and torque signal. Based on this observation, the assessment of the decision-making strategies initially used signals sampled at a rate of 1 kHz, and then lower sampling frequencies to further assess the responsiveness and accuracy of the strategies, as presented in section 9.4.

Prior to being fed to the different decision-making strategies, both the thrust force and the motor current were lowpass-filtered using a backwards-sided Gaussian filter with a sample length of 500 datapoints (0.5 s at a sample rate of 1 kHz). As suggested by Figure 83 on page 141, smoothening the signal reduces the likelihood of false triggering as a result of signal noise.



**Figure 100: Impact of sampling rate on cutting force signals.**

To set the parameters of the assessed decision-making strategies for the first set of experiments, carried out using the machining centre, the data recorded during cutting of the first and last borehole were analysed. Based on the characteristic values of the signal magnitude and gradient during the different stages of these two drilling cycles, the parameters listed in Table 11 were defined. For the second set of data, recorded when using the portable electric drilling unit, the parameters were initially scaled proportionally to the change in feed velocity between the CNC and drilling unit tests. Whilst decision-making strategy C succeeded in detecting the relevant process incidences, proportional scaling of the algorithms' parameters resulted in erroneous detections for decision-making strategies A and B. Thus, the parameters for these two strategies were set by manually analysing the first and last boreholes of the second set of experiments, similarly to the machining centre tests.

To assess the reliability and responsiveness of the decision-making strategies, an offline analyser script was developed in C++. For each of the drilled boreholes, the data stream from the recorded process signals was fed to the script, which for each of the three decision-making strategies output the time at which the process incidences were detected. This was achieved by comparing, in sequence, each of the processed signal datapoints to the thresholds of each strategy, which were calculated based on the parameters listed in Table 11. Due to the use of

different feed rates during the experiments, the time at which the process incidences were detected was then converted into a tool position in the z-direction, which was compared to the actual z-position of the respective incidence. For example, for a stack comprising two 10 mm thick layers, tool engagement would have occurred at a z-position of 0, whereas material transition and tool disengagement would have occurred at z-positions of -10 mm and -20 mm, respectively. The difference between the actual position where the incidence took place and the position where the tool was when the system identified the incidence, expressed in mm, will be referred from here on as the ‘delay’.

**Table 11: List of selected parameters for the decision-making algorithms.**

	Strategy A		Strategy B		Strategy C	
	CNC	EDU	CNC	EDU	CNC	EDU
$T_0$ , (Dis)Engagement	50 N	30 V	30 N	20 V	20 k (N/s) <sup>2</sup>	1081 (V/s) <sup>2</sup>
$T_0$ , Material transition	320 N	250 V	200 N	200 V	20 k (N/s) <sup>2</sup>	1081 (V/s) <sup>2</sup>
$w$ , Worn-out scaling	-	-	2	1.5	-	-
$h_w$ , number of holes worn-out tool	-	-	110	111	-	-
$k$ , Disengagement scaling	-	-	-	-	5	5

The resulting delay for each of the assessed decision-making strategies for the first set of tests are shown in Figure 101. Strategies A and B detected tool engagement and material transition on average 1 mm after the chisel edge made contact and broke through the first layer, respectively. In contrast, strategy C detected tool engagement and material transition with a delay of about 0.2 mm. With regards to tool disengagement, strategies A and B detected the process incidence around 3 mm after the chisel edge broke through the aluminium layer, whilst strategy C resulted in a delay of less than 1 mm. Therefore, for all three process incidences, strategy C resulted in a substantially more accurate process incidence detection than strategies A and B.

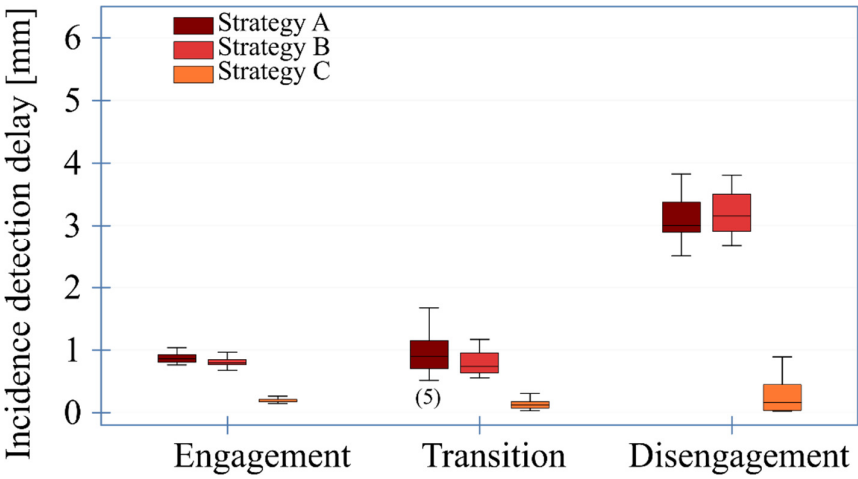
The higher responsiveness of strategy C compared to strategies A and B is explained by the different features being monitored by the decision-making algorithms. Figure 102 shows a typical example of the recorded thrust force’s raw and smoothened magnitude and gradient during a drilling cycle, together with the thresholds for each of the assessed strategies, for both a new and worn tool. As shown in Figure 102 (a), the amount of time required by the smoothened thrust force magnitude to reach each of the specified thresholds for Strategy A and, to a lesser extent, strategy B is substantially larger than that required by the gradient. For example, for the detection of the ‘material transition’ incidence, labelled as (2), the resulting

delays were 1.45 mm, 0.63 mm and 0.04 mm for Strategies A, B and C, respectively. This difference arises because of the signal magnitude being more sensitive to signal variations due to chip flow and tool wear, thereby forcing the selection of a more conservative threshold to avoid false detection and substantial filtering of the signal magnitude. Such filtering introduces a small delay as the high frequency content is filtered out of the signal, affecting the first and second order derivatives.

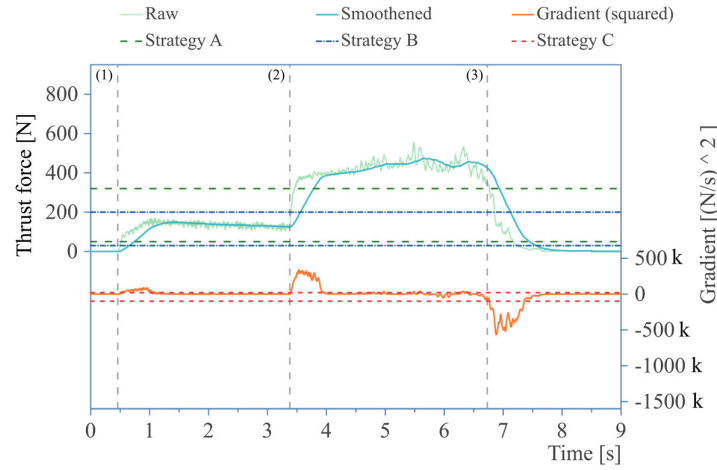
Out of the 22 boreholes investigated, strategy A failed to detect material transition on five occasions, all of them when the tools exhibited extensive wear. As shown in Figure 102 (b), drilling with a worn tool resulted in significantly higher thrust force and torque as compared to a new tool. This increase is high enough for the smoothened thrust force applied while drilling the CFRP layer to already trigger the incidence ‘material transition’. The linear scaling applied in strategy B solves the problem, as the thresholds are gradually raised with an increase in the number of boreholes drilled, thereby taking into account the effect of growing tool wear on the thrust force and torque recorded. This approach also resulted in more responsive triggering than in the case of strategy A, where the use of a single, constant threshold forced a compromise between the optimal threshold for a new tool and a worn out tool. Nonetheless, it should be noted that to successfully employ strategy B, some input related to the tool wear state, like the number of drilled boreholes in this case, is required. This could pose a problem in case the tool is used to drill different stacks, in terms of both material composition and layer thicknesses, as this would cause it to undergo wear mechanisms at varying rates.

Whilst the average delay in recognising tool engagement and material transition for strategies A and B was less than 1.5 mm, tool disengagement was recognised with a delay of approximately 3.4 mm. The reason for this noticeable increase is that in order to employ a unified threshold for both engagement and disengagement, the threshold needs to be substantially lower than the thrust force generated when cutting aluminium. To improve the system’s responsiveness a specific disengagement threshold could be added, but this would require another parameter to be defined by the operator. It is worth pointing out that, most likely, any change in operating condition at this stage, e.g. switching off coolant supply, variation in feed velocity or initiation of tool retraction, would not need to be initiated at a precise position along the borehole axis in order to prevent damage to the tool or workpiece, or both. This makes the detection of disengagement less crucial than the detection of engagement and transition. Moreover, in the case where a stepped tool is used, with the chisel

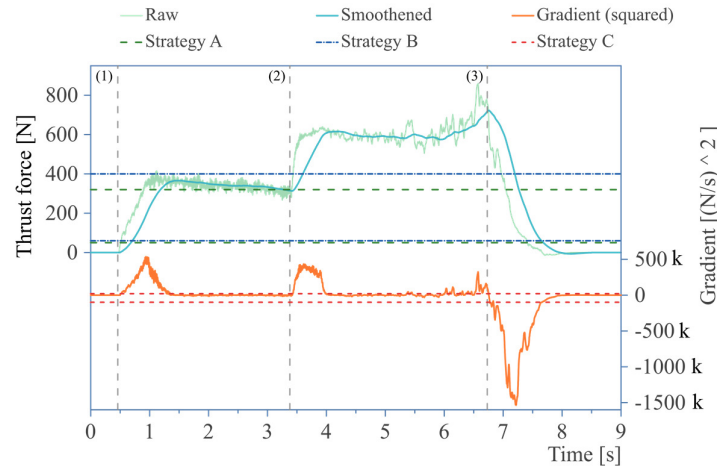
edge being the reference point, some time would be required to allow for the full tool tip to break through the stack anyway.



**Figure 101: Variation between incidence detection and occurrence (machining centre). Missed incidences are denoted in brackets.**



(a) New tool



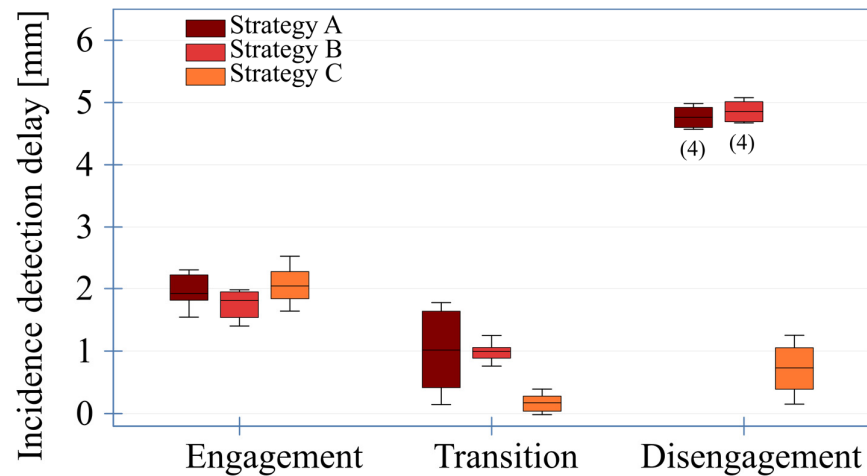
(b) Worn tool

**Figure 102: Thrust magnitude and gradient with decision-making thresholds: (a) new (0 boreholes) and (b) worn tool (after 110 boreholes).**

The resulting delays for each of the assessed decision-making strategies for the second set of tests are shown in Figure 103. Overall, the results are similar to those observed in the tests carried out on the machining centre, supporting the before-made claim that both the thrust force and motor current are suitable parameters to detect the process incidences of interest. Albeit exhibiting a higher responsiveness when detecting material transition and tool disengagement, strategy C exhibits a similar reaction time to strategies A and B for tool engagement. It is believed that this is due to the softness of the CFRP layer. During transition and disengagement such a behaviour was not observed, which can be attributed to the greater hardness of aluminium, generating higher thrust force and torque and, thus, requiring a greater current flow.



Out of the twelve boreholes drilled in the second set of tests, strategies A and B failed to detect tool disengagement four times, again when the tools exhibited extensive wear. This is because when drilling with a worn tool, the motor current did not always rapidly drop to zero after breakthrough of the tool tip due to the deteriorated chip flow, which resulted in more densely packed chips inside the drill's flutes, in turn generating more friction between tool and workpiece and requiring a greater motor current to keep the tool rotating. This was not a problem for decision-making strategy C though, as the rate at which the motor current decreased was strong enough to rapidly exceed the predefined threshold.



**Figure 103: Variation between incidence detection and occurrence (electric drilling unit). Missed incidences are denoted in brackets.**

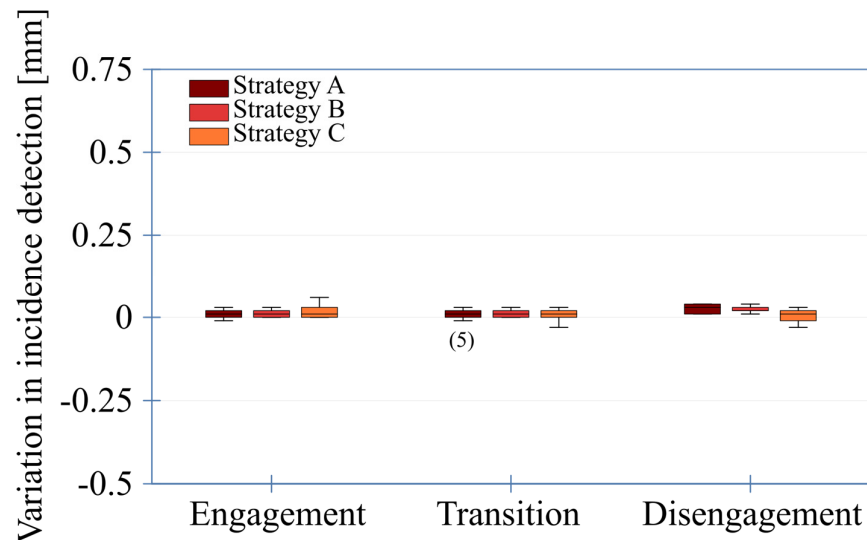
### 9.3 Impact of lower sampling rates on the responsiveness of the decision-making strategies

The process signals used for the assessment presented in the previous sections of this chapter were sampled at 1 kHz. However, substantially lower rates are employed in the process monitoring systems available on the market (Bagshaw, 2020). Thus, to investigate whether recording the process signals with lower sampling rates would have impacted the responsiveness and reliability of the assessed decision-making strategies, the process signals recorded in the first set of experiments were under-sampled prior to being fed to the analyser script, to simulate a sampling rate of 100 Hz and 10 Hz.

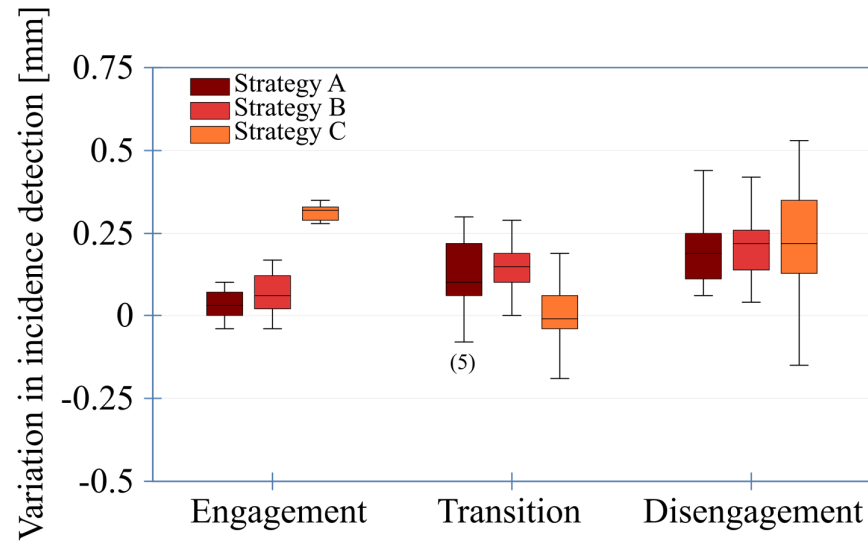
Figure 104 and Figure 105 show the difference in z-axis travel between the point where a process incidence was detected when using a sampling rate of 1 kHz and where it was detected when using a sampling rate of 100 Hz and 10 Hz, respectively. For all three process incidences,

using a sampling rate of 100 Hz resulted in a delay in detection of approximately 20  $\mu\text{m}$ , which is around 1% of the tool point length (1.8 mm), see Figure 104. This small difference in the results obtained is believed to be a result of the low-pass filtering carried out on the process signals, which minimises the impact of high frequency oscillations whilst ensuring high correlation with the process incidences of interest. As a result of the low-pass filter employed, it is expected that using sampling frequencies greater than 1 kHz would not significantly improve the responsiveness of the decision-making strategies. Based on the assumption that detecting any of the incidences assessed with such additional delay will not cause major differences to the drilling process and the resulting borehole quality, using a sampling rate of 100 Hz appears appropriate for the assessed monitoring strategies.

In contrast, a sampling rate of 10 Hz was found to result in a substantially longer delay for all the process incidences of interest, up to 0.5 mm, which is equivalent to 28% of the tool point length, see Figure 105. An increase in the detection delay of such magnitude during material transition can significantly impact the quality of the stack interface, as evidenced by the findings presented in Chapter 6, and it is reasonable to assume that tool engagement and disengagement can also be affected. This suggests that recording the process signals with a sampling rate of 10 Hz affects the responsiveness of all the assessed decision-making strategies to such an extent that it is detrimental to the borehole quality.



**Figure 104: Variation in incidence detection (machining centre tests, signals under-sampled at 100 Hz). Missed incidences are denoted in brackets.**



**Figure 105: Variation in incidence detection (machining centre tests, signals-under sampled at 10 Hz). Missed incidences are denoted in brackets.**

## 9.4 Summary

The research presented in this chapter allowed for an evaluation of a bespoke decision-making strategy which was developed based on the knowledge gained from the experimental assessments presented in the previous chapters. The decision-making strategy proposed was found to successfully detect the occurrences of tool engagement, material transition and tool disengagement when drilling CFRP/Al stacks on both a CNC machining centre and a portable drilling unit, with a significantly higher responsiveness and reliability than two of the systems currently available on the market.

Both the thrust force and the current flowing through the motor controller of portable drilling units were found to be suitable inputs to a process monitoring system used for detection of tool engagement, material transition and tool disengagement. Recording the process signals with sampling rates of 100 Hz and 1 kHz was found to be suitable for the assessed decision-making strategies, whilst using a sampling rate of 10 Hz significantly decreased the systems' responsiveness. For new tools, decision-making strategies based on comparing the process signal magnitude with constant thresholds can successfully detect the process incidences of interest. However, as tool wear increases, the system's responsiveness and reliability decreases. Ultimately, if the relative increase in the monitored parameters as a result of tool wear is high enough, strategies based on constant thresholds become unreliable. Linearly adjusting the magnitude of the thresholds based on the tool wear state substantially increases the reliability and responsiveness of the decision-making strategy. Such an approach however requires some

measurement of tool wear, which is challenging when the same tool is used for drilling a variety of different stacks and is subject to different wear mechanisms at varying rates. Compared to these magnitude-based approaches, the use of a decision-making strategy based on gradient monitoring yields substantial improvements in terms of both reliability and responsiveness. After appropriate signal conditioning, it is possible to set gradient thresholds which not only allow for a substantially more responsive detection of the three process incidences of interest, but also achieve high accuracy when the tool is subject to increasing wear.

## Chapter 10: Conclusions and suggestions for future work

The literature review revealed a number of gaps in the knowledge related to the drilling of aerospace stacks, in particular with regards to the impact of interlayer gap width and tool geometry on interlayer burr formation and borehole quality, the effect of metal chip evacuation over composite boreholes, the impact of parameter changeover position in an adaptive drilling scenario, the selection of signals, SFs and sensor location for process monitoring, the effect of different machine tools on process signals and the assessment of the reliability and effectiveness of adaptive drilling strategies. This research has made a significant contribution to the generation of knowledge in all of these aspects, and this chapter will draw conclusions based on the research findings. Suggestions for future research work on the subject are also presented.

### 10.1 Conclusions

- Introducing a pre-set interlayer gap to a stack comprising aluminium layers results in a substantial increase in interlayer burr formation, as opposed to drilling a stack with no interlayer gap. However, the presence of an interlayer gap can ultimately be detrimental to the final burr size, as a result of two phenomena: (i) the sliding action of the upwards-travelling chips over the borehole edges and (ii) some of the chips entering the gap and being spun around by the rotating tool. The abrasive action of the chips intensifies with an increase in the interlayer gap width, as this provides more space available for the chips to enter the interface and, thus, erode the burr. Hence, larger interlayer gap widths can result in the complete removal of the interlayer burr and even cause noticeable rounding of the borehole edge.
- When drilling CFRP/Titanium stacks, the upwards-travelling titanium chips together with the heat accumulating in the tool and at the stack interface were found to be the cause of the damage on the CFRP interlayer surface. Therefore, tools that allow the chips to be evacuated effectively produce significantly better boreholes than those where the chip flow is problematic.
- On the titanium interlayer surface, an increase in tool point angle results in larger entry burrs, as a result of the positive correlation between tool point angle and thrust force, as well as the increased capability of tools with low point angles to remove damage

generated by surface skidding during initial tool entry. The introduction of a pre-set interlayer gap promotes the ingress of upwards-travelling titanium chips into the stack interface, thereby leading to extensive abrasive and thermal damage of the CFRP interlayer surface.

- Using specific parameters for each layer rather than a common set results in a stable cutting process and generates boreholes that exhibit only small interface damage, which provides further evidence for the effectiveness of adaptive drilling. When adapting cutting parameters and cooling strategy based on the material being machined in CFRP/Aluminium stacks, the surface damage of the CFRP at the interface is smallest if the cutting speed and feed rate are increased once the entire drill tip has broken through the composite layer. In such case any delamination caused by an increase in feed rate whilst machining at the interface is avoided. However, machining at the interface with low feed rates characteristic for drilling CFRP results in more heat energy being generated and, thus, higher temperatures, which consequently promotes burr formation in the metal layer.
- Thrust force, torque, AE and acceleration were found to be suitable process signals for the detection of tool engagement, material transition and tool disengagement, with the thrust force being the most responsive to the occurrence of all three process incidences. Thus, its monitoring is recommended to realise a highly responsive adaptive drilling system. Acceleration signals were found to exhibit similar behaviours independent of direction and are similar in characteristics to the AE. Thus, the monitoring of only one of these signals appears to be sufficient for a process monitoring system capable of facilitating adaptive drilling.
- For both AE and acceleration, varying the distance between the sensor and the machining point results in substantial variations in the recorded signals. Sensors to be included in process monitoring systems for adaptive drilling should thus be located on the tool side, so that they maintain a constant distance to the machining point.
- The type of machine used for the drilling work has a noticeable impact on the data being generated and the stability of the actual drilling process, which makes the transfer of process-specific knowledge between different machines difficult. Substantial differences in thrust force and torque, AE and acceleration were observed when drilling

with a CNC machining centre and a portable automated drilling unit. These differences were particularly pronounced towards the end of the drilling cycle, where the portable drilling unit's superior provision of chip evacuation led to a more stable drilling process and, consequently, more stable process signals.

- Indirectly monitoring the thrust force and torque by means of measuring the current flowing through the motor controller of electric aerospace drilling units results in an accurate representation of the drilling cycle, as the feed and spindle current signals exhibit a good correlation to the directly recorded thrust force and torque throughout tool life.
- The gradient of both the feed and spindle current is strongly affected by the occurrence of tool engagement, material transition and tool disengagement. When using stepped tools, extracting the gradient during transition of the first diameter is the most suitable way to reliably and responsively detect the occurrence of the process incidences of interest.
- The proposed decision-making strategy based on gradient monitoring can successfully detect the occurrence of tool engagement, material transition and tool disengagement when drilling CFRP/Aluminium stacks on both a CNC machining centre and a portable drilling unit. The proposed strategy maintains its reliability and responsiveness without the need of readjustments regardless of the extent of tool wear, which significantly affects the process signals. Systems based on signal magnitude monitoring, in contrast, are characterised by a significantly slower responsiveness. Decision-making strategies based on stable magnitude thresholds become unreliable when exposed to signals generated by tools with growing wear, which can be remedied by linearly adjusting the magnitude thresholds based on the tool wear state.

## 10.2 Suggestions for further research

The research work presented in this thesis opens up various new opportunities for future research activities aimed at further improving both the fundamental understanding and technological development of the drilling of aerospace stacked structures.

Interlayer gap width was found to substantially affect the drilling process of both Aluminium/Aluminium and CFRP/Titanium stacks. Although this research focused on the

most common stack compositions and layer thickness of wing-box assemblies, various other stacked structures are used in the aerospace industry. Further research should focus on establishing whether the knowledge obtained can be transferred to different material combinations and layer thicknesses. For example, tests could be carried out on Titanium/Titanium stacks, as this would allow for an assessment of the impact of interlayer gap width on both entry and exit interlayer burr for this workpiece material.

When drilling stacked structures comprising a CFRP layer on top and a metal layer underneath, the research revealed that the resulting borehole quality of the composite layer is majorly influenced by the cutting of the metal layer. This made it difficult to determine the impact of the process parameters under investigation on the cutting of the composite layer. For this reason, further drilling tests could be carried out on stacked structures comprising only CFRP layers, or on multi-material structures where the composite layer is drilled last. This would avoid hot metal chips travelling through the already drilled CFRP borehole and consequently worsen the resulting borehole quality. This research could be further expanded by conducting experiments to assess whether the manufacturing process used to produce the CFRP (e.g. vacuum bag moulding, autoclave curing) has an impact on the resulting borehole quality, both during the drilling of the composite itself and also during the cutting of any subsequent material layers.

This research assessed the effect of three parameter changeover positions on borehole quality. Other changeover positions and drilling strategies could be tested to further improve the cutting at the stack interface. For example, the parameters could be changed prior to the drill breaking through the upper layer or after the tool tip has fully engaged in the bottom layer, to ensure the entirety of the interface drilling phase is performed with constant cutting parameters. Other drilling strategies that could be investigated are to change the cutting parameters gradually, to avoid sudden variations in the thrust force and torque, and to employ a set of bespoke ‘interface’ parameters to be used when the tool’s cutting edges are simultaneously engaged in two different materials.

In the experiments carried out to assess the influence of tool point angle and parameter changeover position on interlayer borehole quality, some degree of tool skidding is believed to have taken place during material transition. Although tool skidding, also known as tool wandering, is a well-known phenomenon when drilling single layer workpieces (Amini et al., 2017; Heinemann, 2012), its occurrence when drilling multi-material stacks was not reported



on in the literature. Therefore, research could be conducted to further investigate the impact of tool skidding on borehole quality.

Due to the strong influence of chip jamming on both the AE and acceleration signals, often leading to their saturation, a detailed assessment of the impact of tool wear on these process signals was not possible for the cutting of the aluminium layer when drilling without a vibration-assisted drilling module. To overcome this, a reduction in the thickness of the workpiece or a selection of cutting parameters aimed at reducing the extent of chip clogging is suggested.

During this research, substantially higher AE and acceleration were detected when drilling CFRP with a small portable drilling unit as compared to a large CNC machining centre. This was attributed to the significant differences in machining equipment. Further research could be carried out to identify what part of the machine is contributing to the observed change in the process signals. To achieve this, experimental tests could be performed in which the vibration-assisted drilling module, internal coolant supply and chip suction of the portable drilling unit are individually switched off, as this would allow to isolate their impact on the recorded process signals.

Even though this research focused on the assessment of different process signals and features to detect the occurrence of process incidences during drilling of multi-material aerospace stacks, the information gained could potentially also be used for the development of an adaptive control system, which regulates the cutting parameters to minimise borehole damage and tool wear. This could be achieved by designing a process monitoring system that makes use of the knowledge of relationships between process signals, tool wear and borehole quality. Based on the signal features extracted, such a system could be capable of not only adapting the cutting parameters to minimise the occurrence of workpiece defects, but also making an accurate estimate of the tool condition and the quality of the borehole produced.

When using portable drilling units, the time-frequency analysis of the motor current signals revealed dominant frequencies that appear to be related to the machining hardware rather than the cutting process. Although such an approach does not appear to be suitable for the detection of the process incidences investigated in this research, it could prove very useful for maintenance monitoring of the machining equipment. Research could be carried out to investigate whether frequency and time-frequency domain analyses could be used to estimate the amount and type of machine wear, thereby allowing for the design and development of a

predictive maintenance system. For example, by monitoring the frequency content of the motor current signals, it could be possible to identify which component within the gearbox is exhibiting wear and needs replacing.

The effectiveness and versatility of the proposed decision-making strategy based on gradient monitoring could be tested further by carrying out more offline tests using process signals recorded during experiments performed with different tools and cutting parameters, as well as on other stacked workpieces. Following on from these, the experimental apparatus could be modified to enable the portable drilling unit to change the cutting parameters after the process monitoring system detects a certain incidence. This would allow carrying out experiments online, which would be essential if such a process monitoring strategy was to be implemented in an industrial environment. Running drilling tests in a real production environment, where the signals would be affected by various disturbances typical of production processes, would allow for the assessment of the adaptive drilling system's robustness. Furthermore, the performance of the proposed decision-making strategy, which is based on the monitoring of a single signal, could be tested against other strategies that instead rely on multi-sensor data fusion and employ deep learning algorithms, as the data gathered during this project could be used for further research on these fields.

## List of references

- Abdelhafeez, A.M., Soo, S.L., Aspinwall, D.K., Dowson, A., Arnold, D., 2015. Burr formation and hole quality when drilling titanium and aluminium alloys. *Procedia CIRP* 37, 230–235.
- Abellan-Nebot, J.V., Romero Subirón, F., 2010. A review of machining monitoring systems based on artificial intelligence process models. *International Journal of Advanced Manufacturing Technology* 47, 237–257.
- Abrão, A.M., Faria, P.E., Rubio, J.C.C., Reis, P., Davim, J.P., 2007. Drilling of fiber reinforced plastics: A review. *Journal of Materials Processing Technology* 186, 1–7.
- Airbus, 2019. Key Characteristics L-EDU LÜbbering – Seti-Tec LEDU.
- Al-Sulaiman, F.A., Baseer, M.A., Sheikh, A.K., 2005. Use of electrical power for online monitoring of tool condition. *Journal of Materials Processing Technology* 166, 364–371.
- Aliustaoglu, C., Ertunc, H.M., Ocak, H., 2009. Tool wear condition monitoring using a sensor fusion model based on fuzzy inference system. *Mechanical Systems and Signal Processing* 23, 539–546.
- Alonso, U., Calamaz, M., Girot, F., Iriondo, E., 2019. Influence of flute number and stepped bit geometry when drilling CFRP/Ti6Al4V stacks. *Journal of Manufacturing Processes* 39, 356–370.
- Altintas, Y., Aslan, D., 2017. Integration of virtual and on-line machining process control and monitoring. *CIRP Annals - Manufacturing Technology* 66, 349–352.
- Ambhore, N., Kamble, D., Chinchankar, S., Wayal, V., 2015. Tool condition monitoring system: A review, in: *Materials Today: Proceedings*. Elsevier, pp. 3419–3428.
- Amini, S., Soleimani, M., Paktinat, H., Lotfi, M., 2017. Effect of longitudinal–torsional vibration in ultrasonic-assisted drilling. *Materials and Manufacturing Processes* 32, 616–622.
- Angelone, R., Caggiano, A., Improta, I., Nele, L., Teti, R., 2019. Characterization of hole quality and temperature in drilling of Al/CFRP stacks under different process condition. *Procedia CIRP* 79, 319–324.
- Angelone, R., Caggiano, A., Improta, I., Nele, L., Teti, R., 2018. Temperature Measurements for the Tool Wear and Hole Quality Assessment during Drilling of CFRP/CFRP Stacks. *Procedia CIRP* 67, 416–421.
- Artis, 2019. Genior Modular Tool and Process Monitoring. Available at:

<https://www.marposs.com/eng/product/tool-and-process-monitoring-system-2> [accessed 5.15.21].

- Arul, S., Vijayaraghavan, L., Malhotra, S.K., 2007. Online monitoring of acoustic emission for quality control in drilling of polymeric composites. *Journal of Materials Processing Technology* 185, 184–190.
- Ashrafi, S.A., Miller, P.W., Wandro, K.M., Kim, D., 2016. Characterization and effects of fiber pull-outs in hole quality of carbon fiber reinforced plastics composite. *Materials* 9, 1–12.
- Ashrafi, S.A., Sharif, S., Farid, A.A., Yahya, M.Y., 2014. Performance evaluation of carbide tools in drilling CFRP-Al stacks. *Journal of Composite Materials* 48, 2071–2084.
- ASM International, 1990. Properties and Selection: Nonferrous Alloys and Special-Purpose Materials, in: ASM Handbook.
- Bagshaw, L., 2020. Personal communication [conversation, 28 February].
- Bagshaw, L., 2018. Personal communication [conversation, 4 April].
- Bagshaw, L., 2017. Personal communication [conversation, 10 October].
- Bakker, O.J., Gibson, C., Wilson, P., Lohse, N., Popov, A.A., 2015a. Linear friction weld process monitoring of fixture cassette deformations using empirical mode decomposition. *Mechanical Systems and Signal Processing* 62, 395–414.
- Bakker, O.J., Ratchev, S.M., Popov, A.A., 2015b. Towards a condition-monitoring framework for quality assurance in intelligent multistage manufacturing environment. *IFAC-PapersOnLine* 28, 2089–2094.
- Balaji, M., Venkata Rao, K., Mohan Rao, N., Murthy, B.S.N., 2018. Optimization of drilling parameters for drilling of Ti-6Al-4V based on surface roughness, flank wear and drill vibration. *Measurement: Journal of the International Measurement Confederation* 114, 332–339.
- Barré, S., Benzeggagh, M., L., 1994. On the use of Acoustic Emission to investigate damage mechanisms Glass-Fibre-Reinforced Polypropylene. *Composites Science and Technology* 52, 369–376.
- Bassiuny, A.M., Li, X., 2007. Flute breakage detection during end milling using Hilbert-Huang transform and smoothed nonlinear energy operator. *International Journal of Machine Tools and Manufacture* 47, 1011–1020.
- Behrens, B.A., Bouguecha, A., Buse, C., Wölki, K., Santangelo, A., 2016. Potentials of in situ

- monitoring of aluminum alloy forging by acoustic emission. *Archives of Civil and Mechanical Engineering* 16, 724–733.
- Benardos, P.G., Vosniakos, G.C., 2003. Predicting surface roughness in machining: A review. *International Journal of Machine Tools and Manufacture* 43, 833–844.
- Beno, T., Hulling, U., 2012. Measurement of cutting edge temperature in drilling. *Procedia CIRP* 3, 531–536.
- Bhattacharyya, P., Sengupta, D., Mukhopadhyay, S., 2007. Cutting force-based real-time estimation of tool wear in face milling using a combination of signal processing techniques. *Mechanical Systems and Signal Processing* 21, 2665–2683.
- Bhuiyan, M.S.H., Choudhury, I.A., 2014. Review of Sensor Applications in Tool Condition Monitoring in Machining, in: *Comprehensive Materials Processing*. Elsevier, pp. 539–569.
- Binsaeid, S., Asfour, S., Cho, S., Onar, A., 2009. Machine ensemble approach for simultaneous detection of transient and gradual abnormalities in end milling using multisensor fusion. *Journal of Materials Processing Technology* 209, 4728–4738.
- Bonnet, C., Poulachon, G., Rech, J., Girard, Y., Costes, J.P., 2015. CFRP drilling: Fundamental study of local feed force and consequences on hole exit damage. *International Journal of Machine Tools and Manufacture* 94, 57–64.
- Braga, D.U., Diniz, A.E., Miranda, G.W.A., Coppini, N.L., 2002. Using a minimum quantity of lubricant (MQL) and a diamond coated tool in the drilling of aluminum-silicon alloys. *Journal of Materials Processing Technology* 122, 127–138.
- Brinksmeier, E., Fangmann, S., Rentsch, R., 2011. Drilling of composites and resulting surface integrity. *CIRP Annals - Manufacturing Technology* 60, 57–60.
- Brinksmeier, E., Janssen, R., 2002. Drilling of multi-layer composite materials consisting of carbon fiber reinforced plastics (CFRP), titanium and aluminum alloys. *CIRP Annals - Manufacturing Technology* 51, 87–90.
- Byrne, G., Dornfeld, D., Inasaki, I., Ketteler, G., König, W., Teti, R., 1995. Tool Condition Monitoring (TCM) - The Status of Research and Industrial Application. *CIRP Annals - Manufacturing Technology* 44, 541–567.
- Caggiano, A., Angelone, R., Napolitano, F., Nele, L., Teti, R., 2018a. Dimensionality Reduction of Sensorial Features by Principal Component Analysis for ANN Machine Learning in Tool Condition Monitoring of CFRP Drilling. *Procedia CIRP* 78, 307–312.

- Caggiano, A., Angelone, R., Teti, R., 2017. Image Analysis for CFRP Drilled Hole Quality Assessment. *Procedia CIRP* 62, 440–445.
- Caggiano, Alessandra, Centobelli, P., Nele, L., Teti, R., 2017. Multiple Sensor Monitoring in Drilling of CFRP/CFRP Stacks for Cognitive Tool Wear Prediction and Product Quality Assessment. *Procedia CIRP* 62, 3–8.
- Caggiano, A., Napolitano, F., Nele, L., Teti, R., 2019a. Study on thrust force and torque sensor signals in drilling of Al/CFRP stacks for aeronautical applications. *Procedia CIRP* 79, 337–342.
- Caggiano, A., Napolitano, F., Nele, L., Teti, R., 2018b. Multiple Sensor Monitoring for Tool Wear Forecast in Drilling of CFRP/CFRP Stacks with Traditional and Innovative Drill Bits. *Procedia CIRP* 67, 404–409.
- Caggiano, A., Nele, L., Teti, R., 2019b. Drilling of Fiber-Reinforced Composite Materials for Aeronautical Assembly Processes. *Characterizations of Some Composite Materials*.
- Caggiano, A., Rimpault, X., Teti, R., Balazinski, M., Chatelain, J.F., Nele, L., 2018c. Machine learning approach based on fractal analysis for optimal tool life exploitation in CFRP composite drilling for aeronautical assembly. *CIRP Annals* 67, 483–486.
- Chatha, S.S., Pal, A., Singh, T., 2016. Performance evaluation of aluminium 6063 drilling under the influence of nanofluid minimum quantity lubrication. *Journal of Cleaner Production* 137, 537–545.
- Chatterjee, S., Mahapatra, S.S., Abhishek, K., 2016. Simulation and optimization of machining parameters in drilling of titanium alloys. *Simulation Modelling Practice and Theory* 62, 31–48.
- Chen, W.-C.C., 1997. Some experimental investigations in the drilling of carbon fiber-reinforced plastic (CFRP) composite laminates. *International Journal of Machine Tools and Manufacture* 37, 1097–1108.
- Corne, R., Nath, C., El Mansori, M., Kurfess, T., 2017. Study of spindle power data with neural network for predicting real-time tool wear/breakage during inconel drilling. *Journal of Manufacturing Systems* 43, 287–295.
- Crocker, M.J., 2007. Handbook of Noise and Vibration Control. John Wiley & Sons.
- Cuesta, M., Aristimuño, P., Garay, A., Arrazola, P.J., 2016. Heat transferred to the workpiece based on temperature measurements by IR technique in dry and lubricated drilling of Inconel 718. *Applied Thermal Engineering* 104, 309–318.

- Cuka, B., Kim, D.-W., 2017. Fuzzy logic based tool condition monitoring for end-milling. *Robotics and Computer-Integrated Manufacturing* 47, 22–36.
- Denkena, B., Dahlmann, D., Brühne, T., Witt, M., 2016. Prozessbegleitende Werkstoffübergangsdetektion. *ZWF Innovative Fertigungsverfahren* 7–8, 407–410.
- Denkena, B., Flöter, F., 2012. Adaptive cutting force control on a milling machine with hybrid axis configuration. *Procedia CIRP* 4, 109–114.
- Desoutter Industrial Tools, 2020. L-EDU - Solutions for drilling applications . Available at: <https://www.desouttertools.com/tools/7/solutions-for-drilling-applications/71/electric-advanced-drilling-units-evo/711/evo-light/p/STSE5058/l-edu-motor> [accessed 8.4.20].
- Diadem, N., 2021. Basic Mathematics, in: Diadem Documentation.
- Dong, J., Subrahmanyam, K.V.R., Wong, Y.S., Hong, G.S., Mohanty, A.R., 2006. Bayesian-inference-based neural networks for tool wear estimation. *International Journal of Advanced Manufacturing Technology* 30, 797–807.
- Dornfeld, D.A., 1994. In process recognition of cutting states. *JSME International Journal* 37, 638–650.
- Dornfeld, D.A., DeVries, M.F., 1990. Neural Network Sensor Fusion for Tool Condition Monitoring. *CIRP Annals - Manufacturing Technology* 39, 101–105.
- Dornfeld, D.A., Kannatey-Asibu, E., 1980. Acoustic emission during orthogonal metal cutting. *International Journal of Mechanical Sciences* 22, 285–296.
- Elbestawi, M.A., Dumitrescu, M., Ng, E.G., 2006. Tool conditon monitoring in machining, in: Condition Monitoring and Control for Intelligent Manufacturing. pp. 55–82.
- Emel, E., Kannatey-Asibu, E., 1989. Acoustic emission and force sensor fusion for monitoring the cutting process. *International Journal of Mechanical Sciences* 31, 795–809.
- Eneyew, E.D., Ramulu, M., 2014a. On-Line Monitoring of Drill Wear Using Air-Coupled Audio Microphone when Drilling Composite Materials. *Applied Mechanics and Materials* 590, 645–650.
- Eneyew, E.D., Ramulu, M., 2014b. Multi-Sensor Detection and Estimation of Gaps When Drilling CFRP Composite Stacks, in: ASME 2014 International Mechanical Engineering Congress and Exposition. pp. 1–8.
- Eschelbacher, S., Duntschew, J., Möhring, H.-C.C., 2019. Recognition of wood and wood-based materials during machining using acoustic emission, Production at the leading edge of technology.

- Ezugwu, E.O., Wang, Z.M., 1997. Titanium alloys and their machinability. *Journal of Materials Processing Technology* 68, 262–274.
- Fallah, M., Moetakef-Imani, B., 2019. Adaptive inverse control of chatter vibrations in internal turning operations.
- Fang, Q., Pan, Z.M., Han, B., Fei, S.H., Xu, G.H., Ke, Y.L., 2015. A Force Sensorless Method for CFRP/Ti Stack Interface Detection during Robotic Orbital Drilling Operations. *Mathematical Problems in Engineering* 2015, 1–11.
- Faraz, A., Biermann, D., Weinert, K., 2009. Cutting edge rounding: An innovative tool wear criterion in drilling CFRP composite laminates. *International Journal of Machine Tools and Manufacture* 49, 1185–1196.
- Feito, N., Díaz-Álvarez, J., López-Puente, J., Miguelez, M.H., 2018. Experimental and numerical analysis of step drill bit performance when drilling woven CFRPs. *Composite Structures* 184, 1147–1155.
- Fernández-Pérez, J., Cantero, J.L., Díaz-álvarez, J., Miguélez, M.H., 2019. Hybrid composite-metal stack drilling with different minimum quantity lubrication levels. *Materials* 12.
- Fernández-Pérez, J., Cantero, J.L., Díaz-Álvarez, J., Miguélez, M.H., 2017. Influence of cutting parameters on tool wear and hole quality in composite aerospace components drilling. *Composite Structures* 178, 157–161.
- Fives, 2020. eADU® enhanced Automated Drilling Unit . Available at: <https://metal-cutting-composites.fivesgroup.com/products/drilling/eadur-elec.html> [accessed 9.2.20].
- Fleischer, J., Teti, R., Lanza, G., Mativenga, P., Möhring, H.C., Caggiano, A., 2018. Composite materials parts manufacturing. *CIRP Annals* 67, 603–626.
- Frederick, J.R., Felbeck, D.K., 1972. Dislocation Motion as a source of Acoustic Emission. *American Society for Testing and Materials* 129–139.
- Fu, R., Jia, Z., Wang, F., Jin, Y., Sun, D., Yang, L., Cheng, D., 2018. Drill-exit temperature characteristics in drilling of UD and MD CFRP composites based on infrared thermography. *International Journal of Machine Tools and Manufacture* 135, 24–37.
- Gao, Y., Wu, D., Nan, C., Ma, X., Dong, Y., Chen, K., 2015. The interlayer gap and non-coaxiality in stack drilling. *International Journal of Machine Tools and Manufacture* 99, 68–76.
- Geier, N., Szalay, T., 2017. Optimisation of process parameters for the orbital and conventional drilling



- of uni-directional carbon fibre-reinforced polymers (UD-CFRP). *Measurement: Journal of the International Measurement Confederation* 110, 319–334.
- Geng, D., Liu, Y., Shao, Z., Lu, Z., Cai, J., Li, X., Jiang, X., Zhang, D., 2019. Delamination formation, evaluation and suppression during drilling of composite laminates: A review. *Composite Structures* 216, 168–186.
- Ghosh, N., Ravi, Y.B., Patra, A., Mukhopadhyay, S., Paul, S., Mohanty, A.R., Chattopadhyay, A.B., 2007. Estimation of tool wear during CNC milling using neural network-based sensor fusion. *Mechanical Systems and Signal Processing* 21, 466–479.
- Gierlak, P., Burghardt, A., Szybicki, D., Szuster, M., Muszyńska, M., Muszy, M., 2017. On-line manipulator tool condition monitoring based on vibration analysis. *Mechanical Systems and Signal Processing* 89, 14–26.
- Gómez, M.P., Hey, A.M., Ruzzante, J.E., D’Attellisc, C.E., 2010. Tool wear evaluation in drilling by acoustic emission, in: *Physics Procedia*. Elsevier, pp. 819–825.
- Goodfellow, I., Bengio, Y., Courville, A., 2016. Deep Learning. *Nature* 521, 800.
- Griffin, R., Cao, Y., Peng, J.Y., Chen, X.B., 2016. Tool wear monitoring and replacement for tubesheet drilling. *International Journal of Advanced Manufacturing Technology* 86, 2011–2020.
- Guerin, S., 2018. Handheld machining device, particularly for drilling. US2013/0287509 A1.
- Guerin, S., da Costa, S., 2015. A Breakthrough in Handheld Smart Drilling Units : Material Detection with Advanced Electrical Drilling. *SAE Technical Papers*.
- Gutkin, R., Green, C.J., Vangrattanachai, S., Pinho, S.T., Robinson, P., Curtis, P.T., 2011. On acoustic emission for failure investigation in CFRP: Pattern recognition and peak frequency analyses. *Mechanical Systems and Signal Processing* 25, 1393–1407.
- Haber, R.E., Jiménez, J.E., Peres, C.R., Alique, J.R., 2004. An investigation of tool-wear monitoring in a high-speed machining process. *Sensors and Actuators, A: Physical* 116, 539–545.
- Hashmi, K., Graham, I.D., Mills, B., 2000. Fuzzy logic based data selection for the drilling process. *Journal of Materials Processing Technology* 108, 55–61.
- Heinemann, R., 2004. Improving the Performance of Small Diameter Twist Drills in Deep-Hole Drilling. PhD Thesis. The University of Manchester Institute of Science and Technology.
- Heinemann, R., Hinduja, S., 2012. A new strategy for tool condition monitoring of small diameter twist drills in deep-hole drilling. *International Journal of Machine Tools and Manufacture* 52, 69–76.

- Heinemann, R., Hinduja, S., Barrow, G., 2007. Use of process signals for tool wear progression sensing in drilling small deep holes. *International Journal of Advanced Manufacturing Technology* 33, 243–250.
- Heinemann, R.K., 2012. The effect of starting hole geometry on borehole quality and tool life of twist drills. *International Journal of Advanced Manufacturing Technology* 60, 519–526.
- Heisel, U., Pfeifroth, T., 2012. Influence of point angle on drill hole quality and machining forces when drilling CFRP. *Procedia CIRP* 1, 471–476.
- Hellstern, C., 2009. Investigation of Interlayer Burr Formation in the Drilling of Stacked Aluminum Sheets. Georgia Institute of Technology.
- Higo, Y., Inaba, H., 1991. The general problems of AE Sensors. *ASTM International* 7–24.
- Hoff, M., 1986. Analyse und Optimierung des Bohrprozesses. PhD Thesis. University of Aachen.
- Holman, J.P., 2011. Experimental Methods for Engineers - 8th edition. McGraw-Hill.
- Hong, S.Y., Ding, Y., 2001. Cooling approaches and cutting temperatures in cryogenic machining of Ti-6Al-4V. *International Journal of Machine Tools and Manufacture* 41, 1417–1437.
- Hsu, Y.-L., Lee, S.-T., Lin, H.-W., 2001. A Modular Mechatronic System for Automatic Bone Drilling. *Biomedical Engineering: Applications, Basis and Communications* 13, 168–174.
- Huang, N.E., Shen, Z., Long, S.R., Wu, M.C., Snin, H.H., Zheng, Q., Yen, N.C., Tung, C.C., Liu, H.H., 1998. The empirical mode decomposition and the Hubert spectrum for nonlinear and non-stationary time series analysis. *Proceedings of the Royal Society A: Mathematical, Physical and Engineering Sciences* 454, 903–995.
- Hussein, R., Sadek, A., Elbestawi, M.A., Attia, M.H., 2019. An investigation into tool wear and hole quality during low-frequency vibration-assisted drilling of CFRP/Ti6Al4V stack. *Journal of Manufacturing and Materials Processing* 3.
- Iliescu, D., Gehin, D., Gutierrez, M.E., Girot, F., 2010. Modeling and tool wear in drilling of CFRP. *International Journal of Machine Tools and Manufacture* 50, 204–213.
- Inasaki, I., 1998. Application of Acoustic Emission Sensor Machining Processes. *Ultrasonics* 36, 273–281.
- International Standards Organisation, 2017. ISO 13715:2017(en) Technical product documentation — Edges of undefined shape — Indication and dimensioning.

- Isbilir, O., Ghassemieh, E., 2013. Comparative study of tool life and hole quality in drilling of CFRP/titanium stack using coated carbide drill. *Machining Science and Technology* 17, 380–409.
- Isbilir, O., Ghassemieh, E., 2012. Delamination and wear in drilling of carbon-fiber reinforced plastic composites using multilayer TiAlN/TiN PVD-coated tungsten carbide tools. *Journal of Reinforced Plastics and Composites* 31, 717–727.
- Jantunen, E., 2002. A summary of methods applied to tool condition monitoring in drilling. *International Journal of Machine Tools and Manufacture* 42, 997–1010.
- Jemielniak, K., Kwiatkowski, L., Wrzosek, P., 1998. Diagnosis of tool wear based on cutting forces and acoustic emission measures as inputs to a neural network. *Journal of Intelligent Manufacturing* 9, 447–455.
- Jia, Z. yuan, Chen, C., Wang, F. ji, Zhang, C., Wang, Q., 2020. Analytical model for delamination of CFRP during drilling of CFRP/metal stacks. *International Journal of Advanced Manufacturing Technology* 106, 5099–5109.
- Jie, L., 2013. The formation and effect of interlayer gap in dry drilling of stacked metal materials. *International Journal of Advanced Manufacturing Technology* 69, 1263–1272.
- Jović, S., Arsić, N., Vukojević, V., Anicic, O., Vujičić, S., 2017. Determination of the important machining parameters on the chip shape classification by adaptive neuro-fuzzy technique. *Precision Engineering* 48, 18–23.
- Jun, M.B., Burak Ozdoganlar, O., DeVor, R.E., Kapoor, S.G., Kirchheim, A., Schaffner, G., 2002. Evaluation of a spindle-based force sensor for monitoring and fault diagnosis of machining operations. *International Journal of Machine Tools and Manufacture* 42, 741–751.
- Kakinuma, Y., Kamigochi, T., 2012. External sensor-less tool contact detection by cutting force observer. *Procedia CIRP* 2, 44–48.
- Kalvoda, T., Hwang, Y.-R., 2010. A cutter tool monitoring in machining process using Hilbert–Huang transform. *International Journal of Machine Tools and Manufacture* 50, 495–501.
- Kanish, T.C., Kuppan, P., Narayanan, S., Denis Ashok, S., 2014. A fuzzy logic based model to predict the improvement in surface roughness in magnetic field assisted abrasive finishing. *Procedia Engineering* 97, 1948–1956.
- Kao, Y.-T., Takabi, B., Tai, B.L., Hu, M., Takabi, B., Tai, B.L., 2017. Coolant Channel and Flow Characteristics of Mql Drill Bits: Experimental and Numerical Analyses. *Proceedings of the ASME 2017 12th International Manufacturing Science and Engineering Conference* 2, 1–7.

- Karimi, N.Z., Heidary, H., Najafabadi, M.A., Kianfar, P., Minak, G., Zucchelli, A., 2012. Online Monitoring of Drilling-Induced Delamination of Composite Materials by Acoustic Emission. *Proceedings of the ASME 2012 11th Biennial Conference on Engineering Systems Design and Analysis* 1–5.
- Karimi, N.Z., Minak, G., Kianfar, P., 2015. Analysis of damage mechanisms in drilling of composite materials by acoustic emission. *Composite Structures* 131, 107–114.
- Kelly, J.F., Cotterell, M.G., 2002. Minimal lubrication machining of aluminium alloys. *Journal of Materials Processing Technology* 120, 327–334.
- Kershaw, J., Yu, R., Zhang, Y., Wang, P., 2021. Hybrid machine learning-enabled adaptive welding speed control. *Journal of Manufacturing Processes* 71, 1526–6125.
- Kim, H.Y., Ahn, J.H., 2002. Chip disposal state monitoring in drilling using neural network based spindle motor power sensing. *International Journal of Machine Tools and Manufacture* 42, 1113–1119.
- Kim, S.-T., Lee, Y.-T., 1997. Characteristics of damage and fracture process of carbon fiber reinforced plastic under loading-unloading test by using AE method. *Materials Science and Engineering: A* 234–236, 322–326.
- Kimmelman, M., Duntschew, J., Schluchter, I., Möhring, H.-C.C., 2019. Analysis of burr formation mechanisms when drilling CFRP-aluminium stacks using acoustic emission. *Procedia Manufacturing* 40, 64–69.
- Kistler, 2015. Product Catalog - Sensors and solutions for cutting force measurements. Available at: [www.kistler.com](http://www.kistler.com) [accessed 5.18.18].
- Klocke, F., 2011. Manufacturing processes 1: Cutting. Springer.
- Klocke, F., Döbbeler, B., Pullen, T., Bergs, T., 2019. Acoustic emission signal source separation for a flank wear estimation of drilling tools. *Procedia CIRP* 79, 57–62.
- Ko, S.-L., Dornfeld, D.A., 1991. A Study on Burr Formation Mechanism. *Journal of Engineering Materials and Technology* 113, 75–87.
- König, W., Kutzner, K., Schehl, U., 1992. Tool monitoring of small drills with acoustic emission. *International Journal of Machine Tools and Manufacture* 32, 487–493.
- Korkut, I., 2003. A dynamometer design and its construction for milling operation. *Materials and Design* 24, 631–637.

- Krishnamoorthy, A., Lilly Mercy, J., Vineeth, K.S.M.M., Salugu, M.K., 2015. Delamination Analysis of Carbon Fiber Reinforced Plastic (CFRP) Composite plates by Thermo graphic technique. *Materials Today: Proceedings* 2, 3132–3139.
- Krishnaraj, V., Zitoune, R., Collombet, F., 2010. Comprehensive review on drilling of multi material stacks. *Journal of Machining and Forming Technologies* 2, 1–32.
- Kuo, C., Wang, C., Liu, M., 2017. Interpretation of force signals into mechanical effects in vibration-assisted drilling of carbon fibre reinforced plastic (CFRP)/aluminium stack materials. *Composite Structures* 179, 444–458.
- Kuo, C.L., Soo, S.L., Aspinwall, D.K., Carr, C., Bradley, S., M'Saoubi, R., Leahy, W., Saoubi, R.M., Leahy, W., 2018. Development of single step drilling technology for multilayer metallic-composite stacks using uncoated and PVD coated carbide tools. *Journal of Manufacturing Processes* 31, 286–300.
- Kuo, C.L., Soo, S.L., Aspinwall, D.K., Thomas, W., Bradley, S., Pearson, D., M'Saoubi, R., Leahy, W., 2014. The effect of cutting speed and feed rate on hole surface integrity in single-shot drilling of metallic-composite stacks. *Procedia CIRP* 13, 405–410.
- Lang, R.W., Manson, J.A., Hertzberg, R.W., 1987. Mechanisms of fatigue fracture in short glass fibre-reinforced polymers. *Journal of Materials Science* 22, 4015–4030.
- Lauro, C.H., Brandão, L.C., Baldo, D., Reis, R.A., Davim, J.P., 2014. Monitoring and processing signal applied in machining processes - A review. *Measurement: Journal of the International Measurement Confederation* 58, 73–86.
- Lazoglu, I., Poulachon, G., Ramirez, C., Akmal, M., Marcon, B., Rossi, F., Outeiro, J.C., Krebs, M., 2017. Thermal analysis in Ti-6Al-4V drilling. *CIRP Annals - Manufacturing Technology* 66, 105–108.
- Le Coz, G., Marinescu, M., Devillez, A., Dudzinski, D., Velnom, L., 2012. Measuring temperature of rotating cutting tools: Application to MQL drilling and dry milling of aerospace alloys. *Applied Thermal Engineering* 36, 434–441.
- Lee, D.E., Hwang, I., Valente, C.M.O., Oliveira, J.F.G., Dornfeld, D.A., 2006. Precision manufacturing process monitoring with acoustic emission, in: Condition Monitoring and Control for Intelligent Manufacturing. pp. 55–82.
- Lee, J.H., Lee, S.J., 1999. One-step-ahead prediction of flank wear using cutting force. *International Journal of Machine Tools and Manufacture* 39, 1747–1760.

- LEM, 2015. Current Transducer CASR series. Technical Specifications.
- Li, C., Xu, J., Chen, M., An, Q., El Mansori, M., Ren, F., El, M., Ren, F., 2019. Tool wear processes in low frequency vibration assisted drilling of CFRP/Ti6Al4V stacks with forced air-cooling. *Wear* 426–427, 1616–1623.
- Li, J., 2006. Signal processing in manufacturing monitoring, in: Condition Monitoring and Control for Intelligent Manufacturing. pp. 245–266.
- Li, R., Hegde, P., Shih, A.J., 2007. High-throughput drilling of titanium alloys. *International Journal of Machine Tools and Manufacture* 47, 63–74.
- Li, X., 2002. A brief review: Acoustic emission method for tool wear monitoring during turning. *International Journal of Machine Tools and Manufacture*.
- Li, X., Ouyang, G., Liang, Z., 2008. Complexity measure of motor current signals for tool flute breakage detection in end milling. *International Journal of Machine Tools and Manufacture* 48, 371–379.
- Li, Y., Hu, Y.X., Yao, Z.Q., 2012. Modeling and Analysis of the Effect of Preloaded Pressing Force on Gap Formation during the Drilling of Double-Layered Material. *Applied Mechanics and Materials* 217–219, 1541–1546.
- Liang, S.Y., Dornfeld, D.A., 1989. Tool Wear Detection Using Time Series Analysis of Acoustic Emission. *Journal of Engineering for Industry* 111, 199.
- Liu, L., Wu, F., Qi, C., Liu, T., Tian, J., 2018. High frequency vibration analysis in drilling of GFRP laminates using candlestick drills. *Composite Structures* 184, 742–758.
- Lübbering, 2020. Lübbering - L.ADU electronic. Available at: <https://www.luebbering.de/en/drilling/l-adu-electronic> [accessed 9.2.20].
- Lukyanov, A.D., Onoyko, T.S., Najafabadi, T.A., 2017. Optimization of Processing Conditions when Drilling Deep Holes: Twist Drills. *Procedia Engineering* 206, 427–431.
- Malchado, A.R., Wallbank, J., 1990. Machining of titanium and its alloys - a Review. *Proceedings of the Institution of Mechanical Engineers* 204, 53–60.
- Mallat, S.G., 1989. A Theory for Multiresolution Signal Decomposition: The Wavelet Representation. *IEEE Transactions on Pattern Analysis and Machine Intelligence* 11, 674–693.
- Martins de Carvalho, V.M., n.d. Tool Wear Detection through Optical Sensors 5–9.
- Mascaro, B., Gibiat, V., Bernadou, M., Esquerre, Y., 2005. Acoustic Emission of the drilling of Carbon

/ Epoxy composites. *Forum Acusticum Budapest*.

- Mathew, N.T., Vijayaraghavan, L., 2016. Drilling of titanium aluminide at different aspect ratio under dry and wet conditions. *Journal of Manufacturing Processes* 24, 256–269.
- Matsumura, T., Tamura, S., 2015. Cutting simulation of titanium alloy drilling with energy analysis and FEM. *Procedia CIRP* 31, 252–257.
- Matsushima, K., Sata, T., 1980. Development of intelligent machine tool 35, 395–405.
- Melkote, S.N., Newton, T.R., Hellstern, C., Morehouse, J.B., Turner, S., 2010. Interfacial burr formation in drilling of stacked aerospace materials, in: Aurich, J.C., Dornfeld, D. (Eds.), *Burrs – Analysis, Control and Removal*. Springer Berlin Heidelberg, Berlin, Heidelberg, pp. 89–98.
- Merino-Pérez, J.L., Royer, R., Merson, E., Lockwood, A., Ayvar-Soberanis, S., Marshall, M.B., 2016. Influence of workpiece constituents and cutting speed on the cutting forces developed in the conventional drilling of CFRP composites. *Composite Structures* 140, 621–629.
- Mikołajczyk, T., Nowicki, K., Bustillo, A., Yu Pimenov, D., 2018. Predicting tool life in turning operations using neural networks and image processing. *Mechanical Systems and Signal Processing* 104, 503–513.
- Miller, R.K., McIntire, P., 1987. Acoustic Emission Testing, in: *Nondestructive Testing Handbook*. Volume 5.
- Min, S., Lidde, J., Raue, N., Dornfeld, D., 2011. Acoustic emission based tool contact detection for ultra-precision machining. *CIRP Annals - Manufacturing Technology* 60, 141–144.
- Min, S., Sangermann, H., Mertens, C., Dornfeld, D., 2008. A study on initial contact detection for precision micro-mold and surface generation of vertical side walls in micromachining. *CIRP Annals - Manufacturing Technology* 57, 109–112.
- Möhring, H.-C., Kimmelman, M., Eschelbacher, S., Güzel, K., Gauggel, C., 2018. Process monitoring on drilling fiber-reinforced plastics and aluminum stacks using acoustic emissions. *Procedia Manufacturing* 18, 58–67.
- Möhring, H., Eschelbacher, S., Kimmelman, M., 2018. Material failure detection for intelligent process control in CFRP machining. *Procedia CIRP* 77 387–390.
- Moriwaki, T., 1983. Application of Acoustic Emission Measurement to Sensing of Wear and Breakage of Cutting Tool. *Bull Japan Soc Precis Eng* 17, 154–160.
- Mouritz, A., 2012. Fibre-polymer composites for aerospace structures and engines, in: *Introduction to*

- Aerospace Materials. pp. 338–393.
- Nandgaonkar, S., Gupta, T.V.K., Joshi, S., 2016. Effect of water oil mist spray ( WOMS ) cooling on drilling of Ti6Al4V alloy using Ester oil based cutting fluid. *Procedia Manufacturing* 6, 71–79.
- Nandi, A.K., Davim, P.J., 2009. A study of drilling performances with minimum quantity of lubricant using fuzzy logic rules. *Mechatronics* 19, 218–232.
- National Instruments, 2016. How to Choose the Right DAQ Hardware for Your Measurement System. Available at: <http://www.ni.com/white-paper/13655/en/> [accessed 1.6.18].
- Neugebauer, R., Ben-Hanan, U., Ihlenfeldt, S., Wabner, M., Stoll, A., 2012. Acoustic emission as a tool for identifying drill position in fiber-reinforced plastic and aluminum stacks. *International Journal of Machine Tools and Manufacture* 57, 20–26.
- Nordmann, 2020. Nordmann Tool Monitoring. Available at: <http://www.toolmonitoring.com/> [accessed 9.1.20].
- Nyquist, H., 1928. Certain topics in telegraph transmission theory. *Transactions AIEE (Reprinted by IEEE)* 26.
- Oyelola, O., Jackson-Crisp, A., Crawforth, P., Pieris, D.M., Smith, R.J., M’saoubi, R., Clare, A.T., 2020. Machining of directed energy deposited Ti6Al4V using adaptive control.
- Pande, S.S., Relekar, H.P., 1986. Investigations on reducing burr formation in drilling. *International Journal of Machine Tool Design and Research* 26, 339–348.
- Pani, A.K., Mohanta, H.K., 2015. Online monitoring and control of particle size in the grinding process using least square support vector regression and resilient back propagation neural network. *ISA Transactions* 56, 206–221.
- Park, S.S., 2003. High frequency bandwidth cutting force measurements in milling using the spindle integrated force sensor system. The University of British Columbia.
- Patne, H.S., Kumar, A., Karagadde, S., Joshi, S.S., 2017. Modeling of temperature distribution in drilling of titanium. *International Journal of Mechanical Sciences* 133, 598–610.
- Patra, K., 2011. Acoustic Emission based Tool Condition Monitoring System in Drilling. *Proceedings of the World Congress on Engineering III*, 5–9.
- Patra, K., Jha, A., Szalay, T., 2017. Tool Condition Monitoring in Micro-drilling Using Vibration Signals and Artificial Neural Network. *2017 International Conference on Industrial Engineering, Applications and Manufacturing (ICIEAM)*.



- Petueli, G., 2001. Wissensbasierte Prozessüberwachung. Shaker.
- Pezzullo, G., n.d. On-Line Monitoring of Grinding Machines 11–17.
- Phadnis, V.A., Makhadmeh, F., Roy, A., Silberschmidt, V. V., 2013. Drilling in carbon / epoxy composites : Experimental investigations and finite element implementation. *Loughborough University Institutional Repository* 47, 41–51.
- Portillo, E., Cabanes, I., Sánchez, J.A., Orive, D., Ortega, N., Marcos, M., 2012. A case study of a flexible software tool in the drilling process. *IFAC Proceedings Volumes* 333–338.
- Pv, A., Krishnaraj, V., Prabukarthi, A., Kumar, M.S., Elangovan, S., 2015. Study of Tool Condition Monitoring during Drilling of CFRP \ Ti Stacks under dry and wet Conditions. *Proceedings of International Conference on Advances in Materials, Manufacturing and Applications (AMMA)*.
- Qiu, K.X., Wang, C.D., An, Q.L., Chen, M., 2014. Defects Study on Drilling of Carbon Fiber Reinforced Polymer (CFRP) Laminates. *Materials Science Forum* 800–801, 61–65.
- Quinn, M., 2016. Basic Concepts and Measurements, in: Experimental Methods Course Notes. The University of Manchester. pp. 1–17.
- Rambabu, P., Prasad, N.E., Kutumbarao, V. V., 2017. Aluminium Alloys for Aerospace Applications, in: Aerospace Materials and Materials Technologies. Volume 1: Aerospace Materials. Springer.
- Ramirez, C., Poulachon, G., Rossi, F., M'Saoubi, R., 2014. Tool wear monitoring and hole surface quality during CFRP drilling. *Procedia CIRP* 13, 163–168.
- Ramulu, M., Branson, T., Kim, D., 2001. A study on the drilling of composite and titanium stacks. *Composite Structures* 54, 67–77.
- Rawat, S., Attia, H., 2009. Wear mechanisms and tool life management of WC-Co drills during dry high speed drilling of woven carbon fibre composites. *Wear* 267, 1022–1030.
- Renganathan, P., Karthi, P., Vijayan, K., Mouleeswaran, S., 2015. Identification of drill position in CFRP / Titanium alloy stacks using acoustic emission signals. *Proceedings of International Conference on Advances in Materials, Manufacturing and Applications (AMMA)*.
- Ripley, B.D., 1996. Pattern recognition and neural networks. Cambridge University Press.
- Robben, L., Rahman, S., Buhl, J.C., Denkena, B., Konopatzki, B., 2010. Airborne sound emission as a process monitoring tool in the cut-off grinding of concrete. *Applied Acoustics* 71, 52–60.
- Rubio, E.M., Teti, R., 2009. Cutting parameters analysis for the development of a milling process

- monitoring system based on audible energy sound. *Journal of Intelligent Manufacturing* 20, 43–54.
- Rumelhart, D.E., Hinton, G.E., McClelland, J.L., 1986. A General framework for Parallel Distributed Processing, in: *Parallel Distributed Processing: Explorations in the Microstructure of Cognition*, Vol. 1. pp. 45–76.
- Sakurai, K., Adachi, K., Kawai, G., Sawai, T., Ogawa, K., 2000. High Feed Rate Drilling of Aluminum Alloy. *Materials Science Forum* 331–337, 625–630.
- Salgado, D.R., Alonso, F.J., 2006. Tool wear detection in turning operations using singular spectrum analysis. *Journal of Materials Processing Technology* 171, 451–458.
- Sato, M., Aoki, T., Tanaka, H., Takeda, S., 2013. Variation of temperature at the bottom surface of a hole during drilling and its effect on tool wear. *International Journal of Machine Tools and Manufacture* 68, 40–47.
- Saw, L.H., Ho, L.W., Yew, M.C.K., Yusof, F., Pambudi, N.A., Ng, T.C., Yew, M.C.K., 2018. Sensitivity analysis of drill wear and optimization using Adaptive Neuro Fuzzy –Genetic Algorithm technique toward sustainable machining. *Journal of Cleaner Production* 172, 3289–3298.
- Scheffer, C., Heyns, P.S., 2004. An industrial tool wear monitoring system for interrupted turning. *Mechanical Systems and Signal Processing* 18, 1219–1242.
- Scheffer, C., Heyns, P.S., 2001. Wear monitoring in turning operations using vibration and strain measurements. *Mechanical Systems and Signal Processing* 15, 1185–1202.
- Schwarz, L., Pommer, B., Bijak, M., Watzek, G., Unger, E., 2015. Auto-stop Drilling Device for Implant Site Preparation: In Vitro Test of Eccentric Sensor Position. *The International journal of oral & maxillofacial implants* 30, 1041–1046.
- Seeholzer, L., Voss, R., Marchetti, L., Wegener, K., 2019. Experimental study: comparison of conventional and low-frequency vibration-assisted drilling (LF-VAD) of CFRP/aluminium stacks. *International Journal of Advanced Manufacturing Technology* 104, 433–449.
- Segreto, T., Simeone, A., Teti, R., 2013. Multiple sensor monitoring in nickel alloy turning for tool wear assessment via sensor fusion. *8th CIRP Conference on Intelligent Computation in Manufacturing Engineering Multiple* 85–90.
- Seti-tec Desoutter Industrial Tools, 2020. Electric Advanced Drilling Units - éVo . Available at: <https://www.desouttertools.com/tools/7/solutions-for-drilling-applications/71/electric-advanced->

drilling-units-evo [accessed 9.2.20].

- Shannon, C.E., 1949. Communication in the presence of Noise. *Proceedings of the IRE* 37, 10–21.
- Sharif, S., Rahim, E.A., 2007. Performance of coated- and uncoated-carbide tools when drilling titanium alloy-Ti-6Al4V. *Journal of Materials Processing Technology* 185, 72–76.
- Sharman, A.R.C., Amarasinghe, A., Ridgway, K., 2008. Tool life and surface integrity aspects when drilling and hole making in Inconel 718. *Journal of Materials Processing Technology* 200, 424–432.
- Shetty, P.K., Shetty, R., Shetty, D., Rehaman, N.F., Jose, T.K., 2014. Machinability Study on Dry Drilling of Titanium Alloy Ti-6Al-4V using L9 Orthogonal Array. *Procedia Materials Science* 5, 2605–2614.
- Shi, D., Gindy, N.N., 2007. Tool wear predictive model based on least squares support vector machines. *Mechanical Systems and Signal Processing* 21, 1799–1814.
- Shuaib, N.A., 2018. Design of a predictive tool condition monitoring system for micro drilling. PhD Thesis. The University of Manchester.
- Shunmugesh, K., Panneerselvam, K., 2016. Machinability study of Carbon Fiber Reinforced Polymer in the longitudinal and transverse direction and optimization of process parameters using PSO–GSA. *Engineering Science and Technology, an International Journal* 19, 1552–1563.
- Shyha, I., Soo, S.L., Aspinwall, D.K., Bradley, S., Dawson, S., Pretorius, C.J., 2010. Drilling of Titanium/CFRP/Aluminium Stacks. *Key Engineering Materials* 447–448, 624–633.
- Shyha, I.S.S., Soo, S.L.L., Aspinwall, D.K.K., Bradley, S., Perry, R., Harden, P., Dawson, S., 2011. Hole quality assessment following drilling of metallic-composite stacks. *International Journal of Machine Tools and Manufacture* 51, 569–578.
- Siddhpura, A., Paurobally, R., 2013. A review of flank wear prediction methods for tool condition monitoring in a turning process. *International Journal of Advanced Manufacturing Technology* 65, 371–393.
- Sobri, S.A., 2017. Mechanical and laser drilling of thick Carbon Fibre Reinforced Polymer Composites (CFRP). The University of Manchester.
- Sorrentino, L., Turchetta, S., Bellini, C., 2017. In process monitoring of cutting temperature during the drilling of FRP laminate. *Composite Structures* 168, 549–561.
- Sorrentino, L., Turchetta, S., Colella, L., Bellini, C., 2016. Analysis of Thermal Damage in FRP

- Drilling. *Procedia Engineering* 167, 206–215.
- Spur, G., 1961. Beitrag zur Schnittkraftmessung beim Bohren mit Spiralbohrern unter Berücksichtigung der Radialkräfte. Dr.-Ing. thesis. The University of Braunschweig.
- Stephenson, D.A., Agapiou, J.S., 2016. Metal Cutting Theory and Practice, Third edit. ed, Metal Cutting Theory and Practice. CRC Press.
- Strantz, M., Van Hemelrijck, D., Guillaume, P., Aggelis, D.G., 2017. Acoustic emission monitoring of crack propagation in additively manufactured and conventional titanium components. *Mechanics Research Communications* 84, 8–13.
- Sun, J., Hong, G.S., Rahman, M., Wong, Y.S., 2004. Identification of feature set for effective tool condition monitoring by acoustic emission sensing. *International Journal of Production Research* 42, 901–918.
- Sun, J., Hong, G.S., Wong, Y.S., Rahman, M., Wang, Z.G., 2006. Effective training data selection in tool condition monitoring system. *International Journal of Machine Tools and Manufacture* 46, 218–224.
- Sun, Q., Tang, Y., Yang Lu, W., Ji, Y., 2005. Feature Extraction with Discrete Wavelet Transform for Drill Wear Monitoring. *Journal of Vibration and Control* 11, 1375–1396.
- Suprock, C.A.C.A., Piazza, J.J.J., Roth, J.T.J.T., 2007. Directionally independent failure prediction of end-milling tools during pocketing maneuvers. *Journal of Manufacturing Science and Engineering* 129, 770–779.
- Tangjitsitharoen, S., 2009. In-process monitoring and detection of chip formation and chatter for CNC turning. *Journal of Materials Processing Technology* 209, 4682–4688.
- Techna-Tool, 2018. TC-USB. Available at: <http://www.techna-tool.com/techna-check-tc-usb/> [accessed 2.1.18].
- Teti, R., 2002. Machining of Composite Materials. *CIRP Annals - Manufacturing Technology* 46, 629–52.
- Teti, R., 1988. In-Process Monitoring of Cutting Conditions and Tool Wear Using Acoustic Emission. *XV Review of Progress in Quantitative NDE, University of California - San Diego, La Jolla, CA* 5, 2165–2172.
- Teti, R., Dornfeld, D., 1989. Modeling and Experimental Analysis of Acoustic Emission from Metal Cutting. *Journal of Engineering for Industry* 111, 229–237.

- Teti, R., Jemielniak, K., O'Donnell, G., Dornfeld, D., 2010. Advanced monitoring of machining operations. *CIRP Annals - Manufacturing Technology* 59, 717–739.
- Teti, R., Kumara, S.R.T., 1997. Intelligent computing methods for manufacturing systems. *CIRP Annals - Manufacturing Technology* 46, 629–652.
- Teti, R., La Commare, U., 1992. Cutting Conditions and Work Material State Identification through Acoustic Emission Methods. *CIRP Annals* 41, 89–92.
- Teti, R., Micheletti, G.F., 1989. Tool Wear Monitoring Through Acoustic Emission. *CIRP Annals - Manufacturing Technology* 38, 99–102.
- Teti, R., Segreto, T., Caggiano, A., Nele, L., 2020. Smart multi-sensor monitoring in drilling of CFRP/CFRP composite material stacks for aerospace assembly applications. *Applied Sciences (Switzerland)* 10, 1–16.
- Theobald, P., Zeqiri, B., Avison, J., 2008. Couplants and their influence on AE sensor sensitivity. *Journal of Acoustic Emission* 26, 91–97.
- Tian, W., Hu, J., Liao, W., Bu, Y., Zhang, L., 2016. Formation of interlayer gap and control of interlayer burr in dry drilling of stacked aluminum alloy plates. *Chinese Journal of Aeronautics* 29, 283–291.
- Totis, G., Wirtz, G., Sortino, M., Veselovac, D., Kuljanic, E., Klocke, F., 2010. Development of a dynamometer for measuring individual cutting edge forces in face milling. *Mechanical Systems and Signal Processing* 24, 1844–1857.
- Turrini, C.R.R., Zerrouki, V.J.S., Colin, C., Perrin, G.L., 2009. Method for detecting and quantifying drilling anomalies. US 7,523,678 B2.
- Wang, X., Kwon, P.Y., Sturtevant, C., Kim, D.D.W., Lantrip, J., 2014. Comparative tool wear study based on drilling experiments on CFRP/Ti stack and its individual layers. *Wear* 317, 265–276.
- Weinert, K., Kempmann, C., 2004. Cutting temperatures and their effects on the machining behaviour in drilling reinforced plastic composites. *Advanced Engineering Materials* 6, 684–689.
- Wertheim, R., Ben-Hanan, U., Ihlenfeldt, S., Stoll, A., Treppe, F., Wabner, M., 2012. Acoustic emission for controlling drill position in fiber-reinforced plastic and metal stacks. *CIRP Annals - Manufacturing Technology* 61, 75–78.
- Whiffen, R., 2018. Personal communication [conversation, 20 April 2018].
- Xie, Z., Lu, Y., Li, J., 2017. Development and testing of an integrated smart tool holder for four-

- component cutting force measurement. *Mechanical Systems and Signal Processing* 93, 225–240.
- Xu, J., An, Q., Chen, M., 2014. A comparative evaluation of polycrystalline diamond drills in drilling high-strength T800S/250F CFRP. *Composite Structures* 117, 71–82.
- Xu, J., El Mansori, M., 2016. Experimental study on drilling mechanisms and strategies of hybrid CFRP/Ti stacks. *Composite Structures* 157, 461–482.
- Xu, J., Li, C., Chen, M., El Mansori, M., Paulo Davim, J., 2020. On the analysis of temperatures, surface morphologies and tool wear in drilling CFRP/Ti6Al4V stacks under different cutting sequence strategies. *Composite Structures* 234, 111708.
- Xu, J., Mkaddem, A., El Mansori, M., 2016. Recent advances in drilling hybrid FRP/Ti composite: A state-of-the-art review. *Composite Structures* 135, 316–338.
- Yi, S., Li, G., Ding, S., Mo, J., 2017. Performance and mechanisms of graphene oxide suspended cutting fluid in the drilling of titanium alloy Ti-6Al-4V. *Journal of Manufacturing Processes* 29, 182–193.
- Yin, B., Wei, T., WenHe, L., Jian, H., Xin, S., 2015. Investigation of correlation between interlayer gap and burr height in drilling of stacked Al-7475 materials. *Proceedings of the Institution of Mechanical Engineers, Part B: Journal of Engineering Manufacture* 1–14.
- Zadeh, L. a., 1965. Fuzzy sets. *Information and Control* 8, 338–353.
- Zadeh, L.A., 2008. Is there a need for fuzzy logic? *Information Sciences* 178, 2751–2779.
- Zeilmann, R.P., Weingaertner, W.L., 2006. Analysis of temperature during drilling of Ti6Al4V with minimal quantity of lubricant. *Journal of Materials Processing Technology* 179, 124–127.
- Zhu, K., Wong, Y.S., Hong, G.S., 2009. Multi-category micro-milling tool wear monitoring with continuous hidden Markov models. *Mechanical Systems and Signal Processing* 23, 547–560.
- Zhu, Z., Guo, K., Sun, J., Li, J., Liu, Y., Zheng, Y., Chen, L., 2018. Evaluation of novel tool geometries in dry drilling aluminium 2024-T351/titanium Ti6Al4V stack. *Journal of Materials Processing Technology* 259, 270–281.
- Zhu, Z., Sui, S., Sun, J., Li, J., Li, Y., 2017. Investigation on performance characteristics in drilling of Ti6Al4V alloy. *The International Journal of Advanced Manufacturing Technology* 651–660.
- Zitoune, R., Krishnaraj, V., Collombet, F., Le Roux, S., 2016. Experimental and numerical analysis on drilling of carbon fibre reinforced plastic and aluminium stacks. *Composite Structures* 146, 148–158.

